UNIVERSITY OF BIRMINGHAM

STRUCTURAL BEHAVIOUR OF COLD-FORMED STEEL PURLIN-SHEETING SYSTEMS UNDER UPLIFT LOADING

CHONG REN

Doctor of Philosophy

School of Civil Engineering
College of Engineering and Physical Sciences
University of Birmingham
September 2012

ABSTRACT

Cold-formed steel sections are commonly used in a variety of ways such as for purlins, rails, sheeting, decking, mezzanine floor beams, lattice beams, wall studs, storage racking and shelving. Roof purlins and cladding rails are considered to be the most popular products and account for a substantial proportion of cold-formed steel usage in buildings. These members together are thus commonly treated as purlin-sheeting systems, in which the beams are either fully or partially restrained in their lateral and rotational directions by sheeting.

Cold-formed steel sections have been the subject of substantial experimental and theoretical research over the past 40 years. Most research on cold-formed steel sections only considers the purlins acting under pure bending or pure compression, and most studies of structural behaviour solely focus on cold-formed steel sections themselves. However, for an effective and practical design, the uniformly distributed load is considered as the main aspect of loading, in particular wind uplift load, and investigation into purlin-sheeting systems is significantly important for understanding the structural behaviour of cold-formed steel. Furthermore, due to the complex nature and the limitations of research, the interaction between distortional buckling and other failure modes such as local buckling, lateral torsional buckling and material yield is considered to be sufficiently important to warrant further investigation.

This thesis provides an investigation into the structural behaviour of cold-formed steel zed- and channel-section purlins when subjected to uplift loading in purlin-sheeting systems. The investigations are carried out in three steps, namely: pre-buckling, buckling and post-buckling. In pre-buckling, an analytical model is presented to describe the bending and twisting behaviour of partially restrained zed- and channel-section purlins when subjected to uplift loading. Formulae used to calculate the bending stresses of the roof purlins are derived by using the classical bending theory of thin-walled beams. Detailed comparisons are made between the present model and the simplified model proposed in Eurocode EN1993-1-3. To validate the accuracy of the present model, both available experimental data and finite element analysis results are used. In buckling, a numerical investigation is presented on the buckling behaviour of partially restrained cold formed steel zed- and channel-section purlins when subject to transverse distributed uplift loading. The buckling behaviour of zed- and channel-section purlins of different dimensions subjected to uplift loading under the influence of rotational spring stiffness applied on the middle line of the upper flange is examined. In the post-buckling, nonlinear finite element analysis models are created for the partially restrained cold-formed steel zed- and channel-section purlins subjected to transverse uniformly distributed uplift loading. The analyses are performed by considering both geometric and material nonlinearities, and corresponding design curves of zed- and channel-section purlins are established. The interactions of different failure modes are also discussed.

KEY WORDS: cold-formed steel sections; thin-walled structures; zed-section purlins; channel-section purlins; pre-buckling; buckling; post-buckling; local buckling; distortional buckling; lateral-torsional buckling; finite element method; analytical method; numerical modelling; purling-sheeting systems; interaction; uplift load.

ACKNOWLEDGEMENTS

I would like to express my sincere gratitude to my supervisor, Professor Long-Yuan Li for his persistent guidance, support and encouragement throughout the whole period of my PhD study, without him this thesis would never been completed.

I would also like to give massive thanks to Dr. Jian Yang for his friendship, patience and endless support.

Hugest thanks also to School of Civil Engineering, University of Birmingham, for providing such a great learning and research environment. My thanks go to everyone offering valuable advice and support during my study. I am incredibly lucky to work and study with such a superb group of people.

As ever, love and thanks to my expanding family: Chenxi Ren and Xuanyi Ren, and of course to my ever-fabulous and supportive wife, Ying Che. And finally, never enough thanks to my beloved parents, Yuqi Ren and Dongqin Mei who bring me to this wonderful world and keep me sane along the way.

CONTENTS

LIST OF FIGURES

LIST OF TABLES

NOMENCLATURE

a	the horizontal distance from the shear centre to the force line q_z
a'	the horizontal distance from the web line to the sheeting-purlin fixing
b	the width of the compression element
b_{mod}	$b_{mod}=a'$ is for cases where the equivalent lateral force ($-k_h q_z$) bringing the purlin into contact with the sheeting at the purlin web; or $b_{mod}=2a'+b$ is for cases where the equivalent lateral force ($-k_h q_z$) bringing the purlin into contact with the sheeting at the tip of the purlin flange
C_m	the constant to be determined
C_1	the factor depending on the loading condition (for uniformly distributed load $C_1=1$)
E	the modulus of elasticity
F_y	yield stress
G	the shear modulus
I_{fz}	the second moment of the cross-section area of the compression part about the z*-axis
I_T	the torsion constant

I_w the warping constant

I_y the second moments of the cross-sectional area about the *y*-axes

I_{yz} the product moment of the cross-sectional area

I_z the second moments of the cross-sectional area about the *z*-axes

k_R the correction factor for the largest moment of the beam bent about the z- axis. Eq. (3-21)

k_R^* the moment correction factor relating to the influence of the rotation restraint. Eq. (3-23)

k_σ the buckling coefficient

k_ϕ the per-unit length stiffness constant of the rotational spring

L,l the length of the beam

M_{cr} the critical elastic buckling moment

$M_{cr,d}$ the critical moment of distortional buckling

$M_{cr,l}$ the critical moment of local buckling

M_{nd} the design moment capacity for distortional buckling

M_{nl} the design moment capacity for local buckling

q_{cr} the critical uniformly distributed load obtained from the linear finite element analysis

q_y the densities of uniformly distributed loads in *y*-directions

q_z the densities of uniformly distributed loads in z-directions

S_f the gross section modulus referenced to the extreme fiber in first yield

t the thickness

v the y- components of displacement of the cross-section at the shear centre

w the z- components of displacement of the cross-section at the shear centre

$\bar{y}$ the horizontal distance between the z*-axis and the z-axis

z_k the vertical distance from the shear centre to the force line q_y

$\sigma_{cr,l}$ the critical stress of local buckling

σ_y the yield stress which is taken as 390 N/mm^2 in this case

ν Poisson's ratio

ϕ the angle of twisting

ω the sectorial coordinate with respect to the shear centre

$\overline{\omega}$ the average value of ω

ω_{cr} the ultimate load obtained from the nonlinear finite element analysis

CHAPTER 1 INTRODUCTION

1.1 What is a cold-formed steel section

Thin-walled, cold-formed steel sections are commonly used in the construction of modern industrial and residential buildings as sheeting and decking, purlins and sheeting rails, wall studs, storage racking and shelving. The most popular products are roof purlins and sheeting rails which account for a considerable proportion of cold-formed steel usage in buildings.

Cold-formed roof purlins and sheeting rails are usually used as the intermediate members between the main structural frame and the corrugated roof or wall sheeting in buildings. Trapezoidal sheeting is usually fixed to these members in order to enclose the building. The most common sections are the zed, channel and sigma shapes, which may be plain or have stiffened lips. The lips are small additional elements provided to a section to improve its efficiency under compressive loads. The popularity of cold-formed steel sections has dramatically increased in recent years (100,000 tonnes/year in the UK) due to advantages such as consistency and accuracy of profile, ease of fabrication, high strength-to-weight ratios, lightness (which can save costs on transport, erection and the construction of foundation), and flexibility which allows the sections to be produced in a wide variety of section profiles resulting in more cost-effective designs and waste reduction. However, cold formed steel cannot be compared with the usage of the hot-

rolled sections, because cold-formed sections are normally thin-wall, and special care must be given to design, which increases the cost. Furthermore, the complex mechanical properties may reduce the usage of cold-formed steel.

1.2 How is cold-formed steel manufactured

Thin cold-formed steel members begin as thick, molten, hot steel slabs. Each slab is typically hot-rolled, cold-reduced, and annealed before coiling and shipping the thin steel sheet to roll-forming producers (Moen et al., 2008). Once at a plant, the sheet is unwound through a production line and then it is plastically formed by means of folding, press-braking or cold rolling to the final shape of a structural member (see Figure 1.1). Folding has simple process for manufacturing but has limitations such as simple geometry and short length. Press-braking is more commonly used and can make variety of cross-sectional shapes. However, like folding, press-braking also has limitations on the profile geometry, and more importantly, on the section lengths (which are generally not longer than 8000 mm). Cold rolling is widely used for large volume production. In cold rolling, strip material is formed progressively into the desired profile shape by continuously feeding it through successive pairs of rollers. The needed number of pairs of rollers is determined by the thickness of the material and the complexity of the required profile shape. Production of cold-formed steel members by rolling requires a substantial capital outlay for tooling in comparison with press braking, but after the initial outlay the costs reduce as production volume increases, so that the rolling process is ideally suited to large volume production. Many large volume rolling mills nowadays are highly

automated and computer controlled to ensure profile accuracy and precision of length. Holes, notches and cutouts can be produced in a member during the rolling process. Pregalvanised or precoated steel strip is often used to eliminate corrosion and to produce aesthetically pleasing finished products.

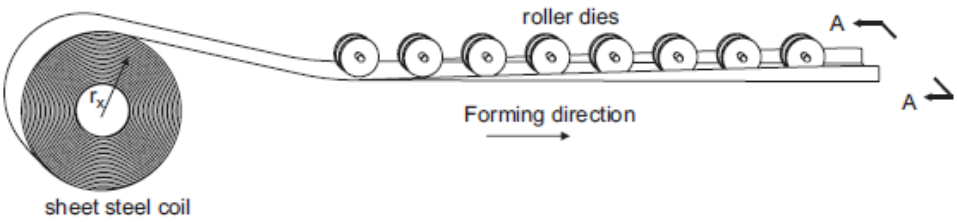

(a)

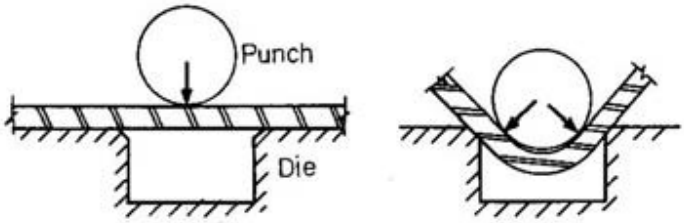

(b)

Figure 1.1 Forming methods for cold-formed steel members (a) Cold rolling (Moen et al., 2008) (b) Press-braking (Yu, 2000).

The cold forming process introduces local work hardening in the strip being formed in the vicinity of the formed corners. This local work hardening results in the yield strength and ultimate strength being increased at the corners. Due to the local increase in yield strength the average yield strength of the formed section can be as much as 25% greater than the virgin yield strength of the flat strip. Under favourable conditions this produces a

'bonus' load-carrying capacity which can be used in the assessment of design strength. With the advance of science and material processing technology, the yield strength of cold formed steel can now reach to as high as 550 MPa. This makes cold-formed steel even more competitive compared with hot-rolled steel.

1.3 Research background on cold-formed steel sections

The use of cold-formed steel sections in buildings as load-bearing structural components dates from about the end of the Second World War. The first systematic and thoroughly documented research into the behaviour of cold-formed steel sections was carried out by Winter at Cornell University during the period of the Second World War (Winter, 1947; 1949). This resulted in the first design specification dealing with cold-formed steel sections in 1946 (AISI, 1946). In the UK, research into this field began in the early 1950s (for example, Chilver, 1953a; 1953b; Kenedi and Harvey, 1951; Harvey, 1952; 1953). The first British Specification was published in 1959 (BSI, 1959), although the proposal for the design specification had been made eight years earlier (Shearer, 1951).

Since the 1950s, extensive research of cold-formed structures has been carried out, and several international conferences for cold-formed steel have been established to disseminate the most recent research findings. Additionally, there are number of books for the analysis and design of cold-formed steel sections (Walker, 1975; Rhodes, 1991; Rhodes and Lawson, 1992; Yu, 2000; Li and Chu, 2007, Hancock, 2008).

1.4 Brief history of buckling

Buckling of structural members is an important branch of solid mechanics. The simplest examples are the buckling of the strut, studied first by Euler in 1757 (Timoshenko, 1953), and the buckling of the flat plate studied by Navier in 1823 (Timoshenko, 1953) and later by Bryan in 1891 (Timoshenko, 1953). For thin-walled columns and thin-walled beams, since they are formed by folding a flat plate into a section, it is conceivable that when they are subjected to compression loads they may buckle either locally - like the buckling of the plate if the member is very short, or globally - like the buckling of the strut if the member is very long. In addition to local and global buckling, a thin-walled member of an open cross section may also exhibit buckling involving a "distortion" of the cross section. Compared to local and global buckling, distortional buckling was not very familiar and was discovered only in thin-walled members of open cross sections such as cold-formed steel section columns and beams.

It was perhaps Lundquist and Stowell (1943) who first detected the distortional-like buckling mode when they investigated the buckling of a restrained flat plate with a sturdy stiffener along an edge of the plate. Later, Gallaher and Boughan (1947) also discovered a similar distortional buckling mode in zed-stiffened panels.

Distortional buckling in cold-formed steel sections was first discovered by Van der Maas (1954) and reported the occurrence of "another kind" of local buckling phenomenon involving flange-stiffener rotations. In the next couple of decades, researcher (Dwight,

1963, Sharp, 1966) continued to develop some methods to understand this buckling. In the late 1970s and early 1980s, Desmond (1977, 1981a and 1981b) presented some findings on the distortional buckling behaviour of lipped channel beams and columns. At the same time, Thomasson (1978) also provided results to reveal the existence of distortional buckling in lipped channel columns.

In spite of these publications mentioned above, which reported the occurrence of "flange-stiffener" buckling observed in stiffened-section members, the expression "distortional buckling" was first coined by Hancock (1978) to distinguish it from local and lateral-torsional buckling. Later on, Hancock (1985) published the first numerical study on the distortional buckling of columns with edge stiffened cross-sections (lipped channel and racks). He showed that the corresponding buckling curves display two local minima, associated with local buckling for short columns and distortional buckling for intermediate columns. Furthermore, he showed that for some cases the distortional buckling may be critical. It is fair to say that Hancock was probably the first person who recognised the importance of taking into account distortional buckling in the design of thin-walled members with edge stiffened cross-sections.

1.5 Main features of cold-formed steel sections

The prime difference between the behaviour of cold-formed sections and hot rolled structural sections is that the cold-formed members involve thin-walled plate elements which tend to buckle locally under compression. Cold-formed cross-sections are

therefore usually classified as slender sections because they cannot generally reach their full strength based on the amount of material in the cross-section due to premature buckling failure (Li and Chu, 2007). The secondary difference is that the cold-formed members have low lateral bending stiffness and low torsional stiffness because of their open, thin, cross-sectional geometry, which gives great flexural rigidity about one axis at the expense of low torsional rigidity and low flexural rigidity about a perpendicular axis. This leads the cold-formed members to also be susceptible to distortional buckling and lateral-torsional buckling.

1.6 Objectives of this study

The purpose of this thesis is to investigate the structural behaviour of cold-formed zed- and channel-sections in purlin-sheeting systems using both analytical (closed-form solutions) and numerical methods (finite element methods). The individual measurable objectives are listed below:

1. To develop an analytical model based on the classical bending theory of thin-walled beams for the stress analysis of cold-formed zed- and channel-sections when subjected to uniformly distributed uplift load and which are fully laterally restrained and partially rotationally restrained by the sheeting.

2. To examine the applicability of Eurocodes (EN1993-1-3) in predicting the stress distribution of cold-formed zed- and channel-sections when subjected to

uniformly distributed uplift load and which are fully laterally restrained and partially rotationally restrained by the sheeting.

3. To investigate the pre-buckling behaviour of cold-formed zed- and channel-sections when subjected to uniformly distributed uplift load and which are fully laterally restrained and partially rotationally restrained by the sheeting.
4. To investigate the buckling behaviour of cold-formed zed- and channel-sections when subjected to uniformly distributed uplift load and which are fully laterally restrained and partially rotationally restrained by the sheeting.

5. To investigate the post-buckling and failure mode behaviour of cold-formed zed- and channel-sections when subjected to uniformly distributed uplift load and which are fully laterally restrained and partially rotationally restrained by the sheeting.

6. To study the influence of span lengths, dimensions of cross section and rotational spring stiffness on the behaviour of cold-formed zed- and channel-sections when subjected to uniformly distributed uplift load within purlin-sheeting systems.

7. To establish the design curve of cold-formed zed- and channel-sections when subjected to uniformly distributed uplift load within purlin-sheeting systems.

1.7 Order of this thesis

Chapter 1 presents an introduction to cold-formed steel sections, the manufacturing procedure of cold-formed steel, the research background and a brief history of cold-formed steel, design codes and specifications and main features of cold-formed steel sections. Additionally, the objectives are highlighted in this chapter.

Chapter 2 provides a literature review of the characteristics of cold-formed steel sections, including aspects such as the buckling behaviour of cold-formed steel sections, the buckling analysis methods, the interaction of different buckling modes and a review of purlin-sheeting systems. Importantly, the knowledge gap and methodology are contained in this chapter.

Chapter 3 describes the analysis of pre-buckling stress for both zed- and channel-section beams with partial restraints. An analytical method is produced to describe the bending and twisting behaviour of the partially restrained cold-formed steel purlins when subjected to uplift loading for zed- and channel-sections. Detailed comparisons are made between finite element method, the present model and the simplified model proposed in Eurocodes (EN1993-1-3). The validation and comparison of boundary conditions are examined in this chapter.

Chapter 4 shows the analysis of buckling behaviour for both zed- and channel-section beams with partial restraints. The studies are carried out based on the elastic linear

buckling analysis which governs the buckling behaviour of purlin-sheeting systems. The validation and comparison of boundary conditions are detailed in this chapter.

Chapter 5 demonstrates the post-buckling analysis of zed- and channel-section beams with partial restraints. The investigations are focused on the ultimate strength and failure mode by using a finite element method and considering both geometrical and material nonlinearities to study the post-buckling structural behaviour of purlin-sheeting systems. The validation and comparison of boundary conditions are discussed in this chapter.

Chapter 6 summaries the conclusions drawn from pre-buckling, buckling and post-buckling analyses, and future work is also presented in this chapter.

CHAPTER 2 LITERATURE REVIEW

2.1 Introduction

The popularity of cold-formed steel sections has dramatically increased in recent years due to advantages such as consistency and accuracy of profile, ease of fabrication, high strength to weight ratios and lightness. Another advantage is flexibility, in that the sections can be produced in a wide variety of sectional profiles resulting in more cost-effective designs and waste reduction. The rising demand of cold-formed steel in the industry necessitates simple and reliable design methods and attracts much more research about structural behaviour. Over recent years, researchers have published a number of journal articles which reviewed and summarised the development of cold-formed steel, such as Hancock (1997 & 2003), Rondal (2000), Davies (2000), Schafer (2008) and Li (2011). In the past few years, the developed design standards of cold-formed steel in North America (AISI, 2005), Australia and New Zealand (AS/NZS, 2005) and Europe (EN1993-1-3, 2006) have also been established.

This chapter provides an overview of the development of cold-formed steel including the behaviour of local, distortional and lateral-torsional buckling, the methods of analysing buckling, the interactions of different buckling modes and the structural behaviour of purlin-sheeting systems. Moreover, knowledge gap and methodology are also discussed in this section.

2.2 Local, distortional and lateral-torsional buckling

2.2.1 Local buckling

Local, distortional and lateral-torsional/Euler buckling are three different types of buckling (Hancock, 1978). Local buckling (see Figure 2.1) is characterised by ripples of relatively short half-wavelength of the order of magnitude of individual plate elements and the displacements are only perpendicular to plate elements while the fold lines remain straight. When a thin plate is loaded in compression the possibility of local buckling arises. This type of buckling is so called because the length of the buckles which form is similar to the dimensions of the cross-section rather than the length of the structural member. When an element buckles locally it does not necessarily mean that this element will collapse or loss its ability to carry loads. In fact, a plate can be allowed to take a considerably increased load beyond initial buckling before any danger of collapse occurs. This is because the deflections due to buckling are accompanied by stretching of the middle surface of the plate. It is not always possible for practical reasons to allow some elements of a structure to buckle, but if stable buckles can be tolerated, a considerable gain follows in structural efficiency. To account for the load-carrying capacity of a locally buckled plate one has to know the post-buckling behaviour of the plate. Considerable efforts were made to investigate the post-buckling behaviour of plates in the 1930s (von Karman et al., 1932) and of cold-formed steel sections in the 1960s (Winter, 1968). In Winter's method, the load-carrying capacity of a plate element in a cold-formed steel section was calculated based on the effective width of the plate. The effective width of a plate element is the function of the ratio of yield strength to the

critical stress of local buckling. The effective width method (EWM) is extensively discussed in section 2.3.1. The design specifications currently used in North America (AISI, 2005), Australia (AS/NZS, 2005) and Europe (EN1993-1-3, 2006) utilise Winter's method.

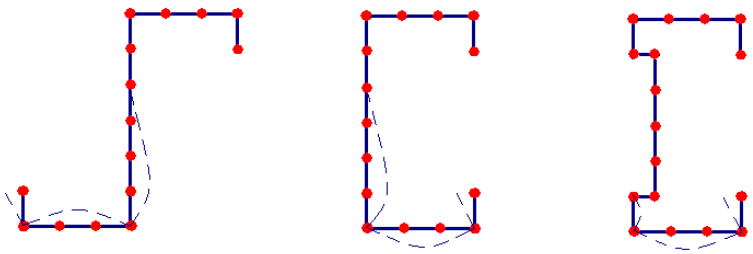

Figure 2.1 Local buckling.

2.2.2 Distortional buckling

Distortional buckling (see Figure 2.2) occurs only in the structural members of open cross-sections. This buckling is characterised by the distortion of the cross-section of the structural member. The half-wavelength of the distortional buckling mode is typically several times larger than the largest characteristic dimension of the cross-section. Local buckling may interacts with the distortional mode, and the interaction reduces the capacity of cold-formed steel member. The reason for the interaction of the distortional and local buckling is that the behaviour of post-distortional buckling is normally stable and in-plane deformations leads to membrane stresses becoming yield and failure in the member. Once local buckling has occurred before distortional buckling, the interaction of

the distortional and local buckling promotes quick failure in the cold-formed steel member. Distortional buckling has received the attention of a number of researchers in the last 20 years but its interaction with local or lateral-torsional mode has not yet been developed (see, Hancock, 2008; Camotim et al, 2008a, for example).

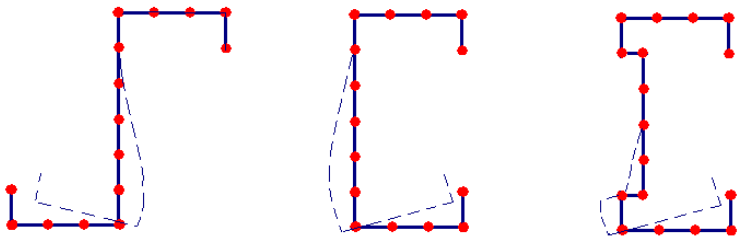

Figure 2.2 Distortional buckling.

2.2.3 Lateral-torsional buckling

The buckling of a strut in compression or a beam in bending is called Euler buckling or lateral-torsional buckling (see Figure 2.3). Lateral-torsional buckling usually occurs when a rigid body is bent to twist and translate to have lateral movements but do not have deformation in shape of cross-section. Roof purlins and sheeting rails, in most cases, are restrained against lateral movement by roof or wall cladding, which reduce the possibility of lateral-torsional buckling, but do not necessarily eradicate the problem. For example, under wind uplift, the unrestrained flange still has compression to produce lateral-torsional buckling. For short lengths of the member the first buckling mode is local, but for longer members lateral-torsional buckling occurs first. In cases of members with continuous restraint, the lateral-torsional buckling capacity reaches a minimum value

over the finite length of the beam, whereas in the absence of restraint the buckling capacity decreases indefinitely with length. A method to determine the elastic critical stress of lateral-torsional buckling of cold-formed steel sections under transverse distribution loads with or without restraints was developed by Li (2004).

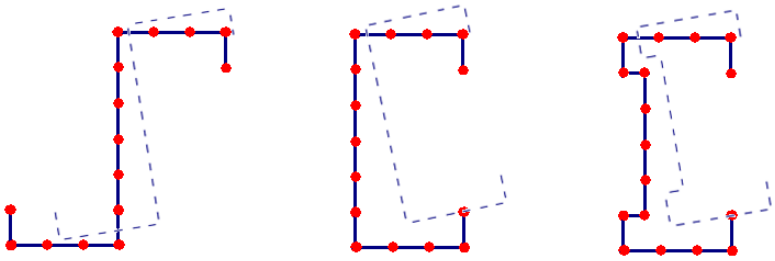

Figure 2.3 Lateral-torsional buckling.

2.3 Methods of analysing buckling

2.3.1 Analytical methods

Local buckling of cold-formed steel sections has been known for many years and is well understood, and some analytical methods have been developed by researchers. Li and Chu (2007) used the Eq.(2-1) to calculate the critical stress to cause local buckling in a compression element.

$$\sigma_{cr,l} = \frac{k_\sigma \pi^2 E}{12(1-v^2)}\left(\frac{t}{b}\right)^2 \qquad (2\text{-}1)$$

where $\sigma_{cr,l}$ = the critical stress of local buckling;

k_σ = the buckling coefficient which is 4 for a simply supported plate in uniform compression and 0.43 for an outstand plate element with one edge free;

E = the modulus of elasticity;

ν = Poisson's ratio;

t = the thickness;

b = the width of the compression element.

The effective width method (EWM) and the direct strength method (DSM) are two basic design methods available in design specifications of cold-formed steel zed- and channel-sections. EWM is adopted in the current design codes including Eurocodes (EN1993-1-3, 2006), North American Specification (AISI, 2005) and Australian/New Zealand Standard (AS/NZS, 2005). The EWM was initially proposed by von Karman and was calibrated for cold-formed steel by Winter. The theory of the EWM is to calculate the design stress by using a reduced plate width which is due local plate buckling to the redistribution of compression stress within the plate. Each plate with compression stresses in a cross-section is reduced to its effective width although the calculation of effective widths of individual plate elements that form the cross-section is dependent on their slenderness and position in the cross-section (Li, 2011). Figure 2.4 shows the reduction of compression plate elements from the gross cross-section to the effective cross-section of zed-section beam. It can be seen in this figure that the effective cross-section demonstrates the ineffective areas of carrying loads, and shows how to include the effect of local buckling in the calculations of beam deflection and lateral-torsional buckling.

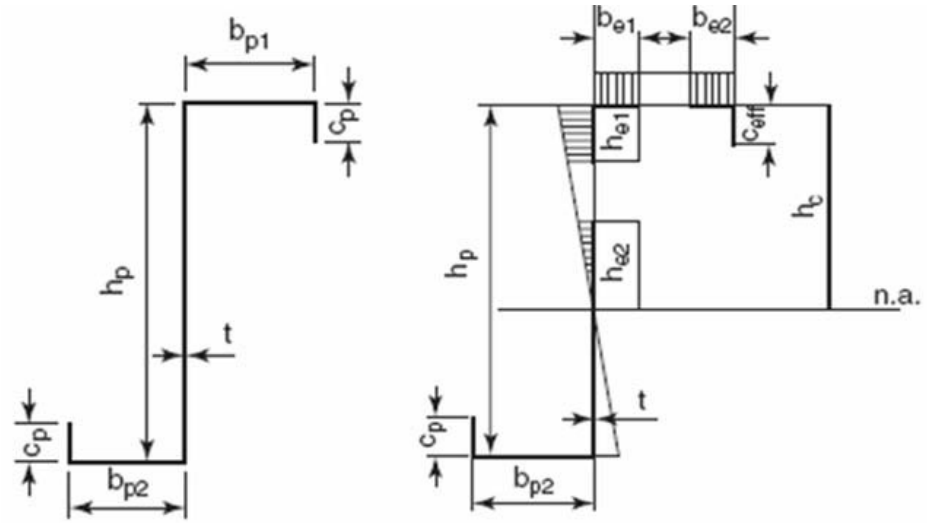

(a) (b)

Figure 2.4 (a) Gross and (b) effective cross-sections of a CFS zed member (Li, 2011).

The disadvantage of EWM is that it is an elemental method that only accounts for an individual element and thus the interaction between elements is not taken into account. The EWM is not accurate when sections become more complex, or if sections have an additional edge and intermediate stiffener which leads to the interaction of elements becoming more significant. To overcome this problem, Schafer and Pekoz (1998) developed the DSM method which is based on the results obtained from numerical methods. For any cross-section of member, the initial buckling load and the capacity of the section member can be evaluated by using empirical formulae, and the moment capacity for lateral-torsional buckling of beams is determined by Eq.(2-2) (Schafer and Pekoz, 1998),

$$M_{ne} = \begin{cases} M_{cre} & if \quad M_{cre} < 0.56M_y \\ \frac{10}{9}M_y(1-\frac{10M_y}{36M_{cre}}) & if \ 2.78M_y \geq M_{cre} \geq 0.56M_y \\ M_y & if \quad M_{cre} > 2.78M_y \end{cases} \tag{2-2}$$

Where M_{ne} = the design moment capacity for lateral-torsional buckling;

M_{cre} = critical elastic lateral-torsional buckling moment;

$M_y = S_f F_y$ the yield moment;

S_f = the gross section modulus referenced to the extreme fiber in first yield;

F_y = yield stress.

The moment capacity for local buckling of beams is determined by Eq.(2-3) (Schafer and Pekoz, 1998),

$$\frac{M_{nl}}{M_{ne}} = \begin{cases} 1 & \sqrt{M_{ne}/M_{cr,l}} \leq 0.776 \\ \left[1-0.15\left(\frac{M_{cr,l}}{M_{ne}}\right)^{0.4}\right]\left(\frac{M_{cr,l}}{M_{ne}}\right)^{0.4} & \sqrt{M_{ne}/M_{cr,l}} > 0.776 \end{cases} \tag{2-3}$$

where M_{nl} = the design moment capacity for local buckling;

$M_{cr,l}$ = the critical moment of local buckling.

Furthermore, the moment capacity for distortional buckling of a cold-formed steel member is determined by Eq.(2-4)) (Schafer and Pekoz, 1998),

$$\frac{M_{nd}}{M_y} = \begin{cases} 1 & \sqrt{M_y/M_{cr,d}} \leq 0.673 \\ \left[1-0.22\left(\frac{M_{cr,d}}{M_y}\right)^{0.5}\right]\left(\frac{M_{cr,d}}{M_y}\right)^{0.4} & \sqrt{M_y/M_{cr,d}} > 0.673 \end{cases} \tag{2-4}$$

where M_{nd} = the design moment capacity for distortional buckling;

$M_{cr,d}$ = the critical moment of distortional buckling.

Schafer (2008) presented an accurate calculation of member elastic buckling behaviour, such as the finite strip method or generalised beam theory, is necessarily considered to calculate the stability for gross cross-section properties of DSM and claimed the DSM is on path to be a completely viable alterative design procedure for cold-formed steel member design.

An analytical solution for the distortional buckling of thin walled sections subjected to axial compression was derived first by Law and Hancock (1987). The analytical model proposed by Law and Hancock (1987) is shown in Figure 2.5, in which the rotational spring and the translational spring applied at the web-flange junction represent the restraints of the rest part of the section to the buckled compression flange and lip system. The flange and lip system shown in Figure 2.5 can be treated as a thin walled beam under axial compression and thus the critical stress of the beam can be obtained by solving the three simultaneous buckling equations of beams involving torsion and bending about two axes (Law and Hancock, 1987) if the two spring constants are known. The smallest critical stress of the beam represents the critical stress of the distortional buckling of the section. Law and Hancock (1987) found that the translational spring has very little influence on the obtained critical stress and thus it was suggested to be neglected. For the rotational spring, its stiffness was found to be dependent on not only the web geometry but also the stress in the web when the compression flange and lip system buckles. A

model to determine the rotational spring stiffness was also proposed in the Law and Hancock paper (1987).

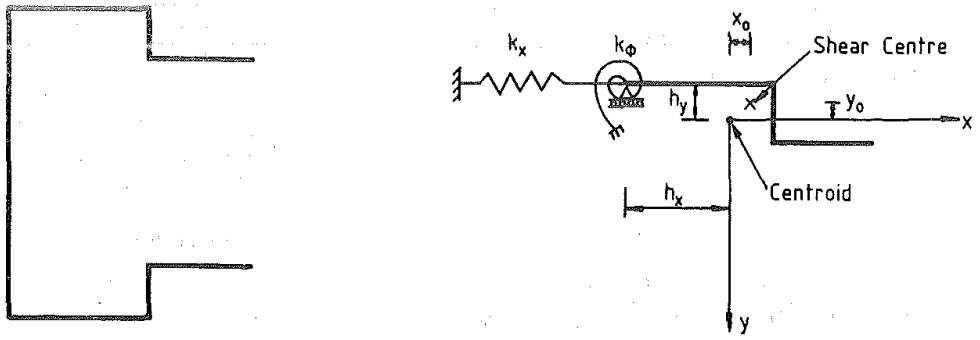

(a) Original column section (b) isolated flange

Figure 2.5 Flange elastically restrained along the flange/web junction (Lau and Hancock, 1987).

Later, Hancock (1995 and 1997) applied the above model further by modifying the rotational spring stiffness, which was obtained by assuming the tension end of the web to be fixed. Davies and Jiang (1996 and 1997) developed a similar model to investigate the distortional buckling behaviour by using rotational spring. Teng et al (2003) also presented a closed-form solution to study the distortional buckling of channel-sections, and the solution can be considered to be a solution extension of Lau and Hancock. An alternative distortional buckling model is provided in the recently published Eurocode (EN 1993-1-3, 2006). In this model (see Figure.2.6), the distortional buckling of the compression flange and lip system was simulated by a stiffener on an elastic foundation, in which the stiffener contains the half flange plus the lip adjacent to the flange and the elastic foundation represent the restraint of the rest part to the stiffener. The critical stress

of the stiffener on the elastic foundation under axial compression is obtained by solving the buckling equation of beams involving bending about an axis parallel to the flange. The obtained critical stress for the stiffener is the critical stress of the distortional buckling of the section. The stiffness of the elastic foundation was obtained by using the unit load method in which the two ends of the web were assumed to be simply supported and the unit load was applied at the centroid of the stiffener (EN 1993-1-3, 2006).

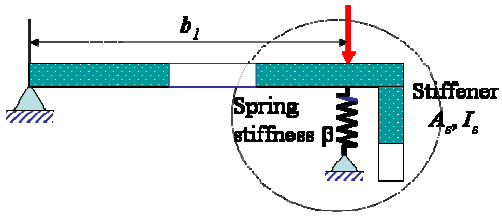

Figure 2.6 The analytical model used to analyse distortional buckling (EN 1993-1-3, 2006).

More recently, Li and Chen (2008) modified Hancock's model by adding the influence of flexure of the compression flange on the distortional buckling of the compression flange and lip system. In Li and Chen's model, the rotational spring at the flange-web junction was substituted by a vertical spring, and the vertical spring was at the centroid of the compression flange and lip system (see Figure.2.7). Li and Chen's model is almost the same as Hancock's model (1995 and 1997) if the compression flange is rigid, and the only difference between these two models is the stiffness expression of the spring. Li and Chen used finite strip method to demonstrate that their model is more accurate for most zed-, channel- and sigma-sections. It should be pointed out that all of the analytical

models mentioned above do not consider the variation of the pre-buckling stress along the longitudinal axis of the beam. In other words, these models can only deal with the distortional buckling of sections subjected to either pure compression or pure bending. They cannot be used to analyse the distortional buckling of sections subjected to transverse loading because the pre-buckling stress for the transversely loaded beam involves a stress gradient along the longitudinal axis.

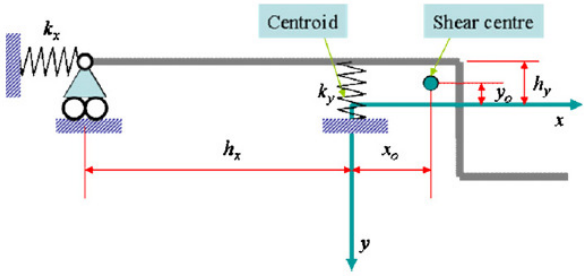

Figure 2.7 Analytical model for the distortional buckling of a lipped flange (Li and Chen, 2008).

Ings and Trahair (1984) presented a simple model for the elastic lateral buckling of a continuous cold-formed roof purlin. The model was analysed by using a finite element method, and predictions of the maximum moment in a segment at elastic buckling under uplift and gravity load were presented. However, in this model, the effects of cross-section distortion and local buckling were ignored.

2.3.2 Generalised beam theory

The Generalised Beam Theory (GBT) is a method of analysis originally developed by Schardt (1989), which was used to calculate a number of section properties, some related to rigid body deformation modes and others related to cross section distortion modes. Subsequently, a calculation method for the critical stress which takes account of distortional effects was presented by Schardt (1994).

Also in 1994, Davies and Leach introduced the first-order and second-order GBT. The first-order GBT showed how this theory may be used to analyse cold-formed sections in which distortion of the cross-section is significant (Davies and Leach, 1994a), while the second-order GBT was associated with geometric nonlinearity (Davies and Leach, 1994b). The success of GBT for a wide range of situations was demonstrated by comparing the results obtained with both test results and other analyses. Leach and Davies (1996) compared the critical buckling predictions of GBT with the results obtained in two series of tests carried out on lipped and unlipped channels subjected to a major axis bending moment. They concluded that GBT is a powerful and effective analysis tool for the solution of interactive buckling problems where both local and overall buckling can occur. Davies et al (1997) also carried out an investigation into how perforated cold-formed steel sections subjected to axial load and bending can be designed analytically using GBT. They believed that GBT could be modified to take account of perforations so that the lower bound results give a sufficiently accurate column design curve, which takes account of local, distortional and global buckling, thus making extensive testing unnecessary. Davies and Jiang (1998) believed that GBT offered by far

the best vehicle for a fundamental understanding of the subject of distortional buckling and offered a yardstick by which other approaches may be evaluated. They emphasised a particular advantage of GBT was that it allowed individual buckling modes to be isolated and considered either separately or in selected combinations. It also allowed explicit expressions to be derived for the critical stress and wavelength for distortional buckling.

Silvestre and Camotim (2002a) introduced the formulation of GBT developed by Davies and Jiang and analysed the structural behaviour of composite thin-walled members made of laminated plates and displaying arbitrary orthotropy. The main concepts and procedures involved in the available isotropic first-order GBT were revisited and adapted to account for the specific aspects related to the member orthotropy. Moreover, they investigated different laminated plate material behaviours and their influence on the GBT equations. The application and capabilities of the formulated first-order GBT were illustrated. Later, Silvestre and Camotim (2002b) presented the formulation of the second-order GBT and analysed the buckling behaviour of composite thin-walled members made of laminated plates and displaying arbitrary orthotropy. They also clarified a few ambiguous aspects related to the structural meaning of the results yielded by member linear stability analyses. Later in 2002, Silvestre and Camotim (2002c) further explained the main concepts and steps involved in the derivation of GBT based fully analytical formulae. Such formulae provided distortional bifurcation stress estimates in cold-formed steel channel columns and beams with arbitrary sloping single-lip edge stiffeners and pinned/free-to-warp or fixed/warping-free end sections.

Silvestre and Camotim have developed several GBT based distortional buckling formulae for cold-formed steel sections over the past few years. In 2003, they addressed a GBT-based general approach to derive "quasi-analytical" distortional buckling formulae for cold-formed steel members with arbitrary cross-section shapes and four end conditions (Silvestre and Camotim, 2003). A year later, they presented the derivation of GBT based fully analytical formulae to provide distortional critical lengths and bifurcation stress resultant estimates in cold-formed steel channel- and zed-section members (Silvestre and Camotim, 2004). Furthermore, they described the main steps involved in the derivation of a GBT formulation to analyse the buckling and vibration behaviour of loaded cold-formed steel members (Silvestre and Camotim, 2006).

The GBT method also contributed to the investigation concerning the local-plate and distortional post-buckling behaviour of cold-formed steel lipped channel columns with web and flange intermediate stiffeners. It provided the explanations for the qualitative differences existing between the local-plate and distortional post-buckling behaviour of lipped channel columns with and without intermediate stiffeners (Silvestre and Camotim, 2005).

More recently, Camotim et al. (2008b) provided a general procedure on the use of the GBT they developed and corresponding finite element implementation, to analyse the local and global buckling behaviour of thin-walled members with arbitrary loading and support conditions.

2.3.3 Finite element methods

The finite element method (FEM) is a general analysis method, which can provide solutions to any governing differential equations. In principle, all of the required phenomena can be modelled using appropriate finite element techniques. The advantage of using FEM is the availability of various commercial software packages, although considerable time may be required on data preparation, post-processing and validation of obtained results, particularly when geometrical and/or material nonlinearities are involved, and some commercial software can be expensive to employ. It should be noted that great care is needed in formulating the correct boundary conditions and loading conditions to ensure the model is consistent with the problem to be investigated. Any change in either loading or boundary conditions may lead to the solution being not only quantitatively inaccurate but also qualitatively incorrect.

Two types of finite element analyses can be conducted for analysing the buckling of cold-formed steel sections. One is the linear buckling analysis in which only critical loads and corresponding buckling modes are obtained; the other is the nonlinear analysis in which nonlinear load-displacement response curves are obtained. Lucas et al. (1997a and 1997b) presented a full model and a simplified model to investigate the influence of sheeting on the performance of cold-formed steel sections using the finite element method.

Therefore most existing finite element analyses have used the nonlinear model to investigate the behaviour of cold-formed steel sections when they exhibit distortional

buckling. Pi et al. (1997 and 1999) analysed the buckling behaviour of cold-formed channel- and zed-section beams. The model was used to investigate elastic lateral-distortional buckling, inelastic behaviour, and strengths of channel- and zed-section beams with residual stresses and initial imperfections. Dinis et al. (2007) investigated the elastic and elastic-plastic post-buckling behaviour of cold-formed steel lipped channel columns affected by distortional and flexural-torsional buckling mode interaction. Yu and Schafer (2007) used the finite element method to simulate local and distortional buckling of cold-formed steel beams. More recently, Yin et al. (2011) investigated the distortional and post-distortional buckling behaviour of the compression flange and lip system in channel- and zed-section beams using ABAQUS.

2.3.4 Finite strip methods

The Finite Strip Method (FSM) is applicable to elastic local, distortional and global buckling of structures with uniform stress distribution along the longitudinal axis of the member. The FSM falls within the category of numerical methods, which are specifically designed for prismatic members. The difference between the FSM and the FEM is that in the FSM the piece-wise displacement interpolation functions are used only within the cross-section of the prismatic member, while along the axis of the member analytical displacement functions, usually *sine* or *cosine* series are employed (see Figure.2.8). Thus the FSM has the advantage of few degrees of freedom and requiring less computing time and memory, Finite Strip method can deal with nonlinear but it may not be efficient and not particular suitable to deal with material nonlinear or collapse type problems. (Chin et al, 1993; Friedrich, 2000).

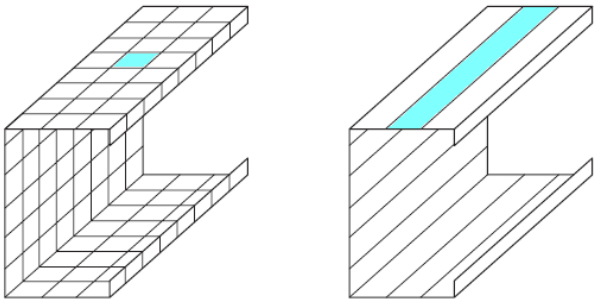

(a) (b)

Figure 2.8 The finite element (a) and finite strip (b) methods.

The FSM was first proposed by Cheung (1976) and was promoted by Lau and Hancock (1986 and 1989), Loughlan (1993) and Schafer (1997) to analyse cold-formed steel sections for understanding and predicting the buckling behaviour of cold-formed steel members. A basic introduction to the FSM employed in a finite strip analysis program called CUFSM was presented by Schafer (1997, 2001 and 2003), which includes the theoretical development and derivation of the initial stiffness and geometric stiffness matrices. CUFSM is free to access, and is available on the internet (http: //www. ce.jhu.edu/bschafer/cufsm). Nowadays, CUFSM has been used not only in the USA but also in many other countries.

Hancock was the first to use the FSM to analyse the distortional buckling problem of prismatic members with both ends simply supported (1978, 1985). Lau and Hancock (1988) provided a finite strip buckling analysis method to predict the inelastic distortional buckling strengths of columns, in which the analysis provided precise estimates of the test failure loads and modes. Later, Lau and Hancock (1990) extended the finite strip

buckling capabilities to the spline finite strip method to allow for other types of boundary conditions. Lindner and Guo (1994) also presented an inelastic spline finite strip analysis and introduced the concept of the cold-formed section being divided into two different types of strips, and consequently revealed that the inelastic distortional buckling behaviour was very important.

Ye et al. (2002 and 2004) investigated the influence of the cladding restraints on the pre-buckling stress and corresponding buckling behaviour of cold-formed steel channel- and zed-section members by using the FSM. They found that for both local and distortional buckling the restraints had significant influence on the critical loads through their influence on the pre-buckling stress rather than directly on the buckling modes, and for lateral-torsional buckling, the influence of the restraints on the critical loads was mainly due to their influence on the buckling modes rather than the pre-buckling stress.

Chu et al. (2005 and 2006) extended the FSM into a semi-analytical finite strip method and investigated the local and distortional buckling behaviour of cold-formed steel channel- and zed-section beams subjected to uniformly transverse distributed loads. They found the critical stress of the distortional buckling decreases with the increase in beam length until the beam reaches a certain length. This indicated that the design load for the distortional buckling may need to involve the member length.

More recently, Adany and Schafer (2006a, 2006b and 2008) developed a mode-restrained finite strip method which can be used to predict the critical loads of various individual

buckling modes in single-branched open cross-section members. The mode-restrained FSM is essentially similar to the GBT method but is mathematically simpler.

2.3.5 Experimental methods

Experiments are suitable for the determination of design strength of all kinds of cold-formed steel structures. There have been a large number of experimental studies on cold-formed steel sections (Mahendran and Avery, 1997; Schafer, 2001; Yap and Hancock, 2008; Moen and Schafer, 2008b). Most of these tests were conducted in Cornell University in USA, the University of Sydney in Australia, and the University of Strathclyde in the UK.

Hancock et al. (1990) presented some tests to investigate purlins connect with sheeting under wind uplift loading, and Put et al. (1999a and 1999b) provided some tests to study the lateral-torsional buckling on braced channel- and zed-section purlins. Laine and Tuomala (1999) studied experimentally on the influence of internal supports and sheeting on the top flange for purlins under gravity load. Beshara and La Boube (2001) provided a study of laterally braced channel-section wall studs and presented the experimental investigation of the rotational restraint influence of laterally braced channel-section. Yap and Hancock (2006) performed an experimental investigation of a series of compressive tests on a stiffened-cross shaped section fabricated from cold-formed high strength steel of thickness 0.42 mm and nominal yield stress of 550 MPa. They found that the interaction of local and distortional buckling has a significant influence on the strength of intermediate and longer member. Liu et al. (2011a and 2011b) presented an experimental

study and a numerical study on the pre-buckling, buckling, post-buckling and post-failure behaviours of continuous beams with cold-formed sigma sections near internal supports, based on which the pseudo-plastic moment resistance (PPMR) was derived.

2.4 Interactions of different buckling modes

It is well known that for a column subjected to compression loads its failure can be due to its strength if the compression stress is greater than its material strength, or due to the buckling if the compression stress is greater than the critical buckling stress of the column. The design curve for cold-formed steel sections recommended in EN1993-1-3 is plotted in Figure 2.9, in which the theoretical buckling curve calculated from the Euler formula and the theoretical strength line based on the material yield strength are superimposed. It can be seen from the figure that the design curve for the lateral-torsional buckling coincides with the buckling curve for long columns and with the strength line for short columns. For intermediate columns, however, the design curve is below the two theoretical lines. The reason for this is partly due to the imperfection of the columns in geometry and/or material, and partly due to the interaction between buckling and material yield. The latter implies that when the column fails it involves not only buckling but also material yield. Unlike elastic buckling, loss of stability due to yielding and plastic deformation is very difficult to formulate. This is because when a column buckles, it usually changes from a state of compression to a combined state of compression and bending, in which case the stress in some parts of the material increases (where the material becomes plastic), while in other parts the stress may reduce (where the material

remains elastic). Thus, it is impossible to use a single formula to describe the behaviour of plastic buckling. The formulae recommended in design standards such as EN1993-1-3 were developed purely based on the large number of experiments and thus they are empirical formulae.

In contrast, the design curves for local and distortional buckling are below the buckling curve when the critical stress is close to the yield stress and above the buckling curve when the critical stress is far less than the yield stress. The former is due to the interaction between buckling and material yield. The latter takes account of the post-buckling capacity of the section.

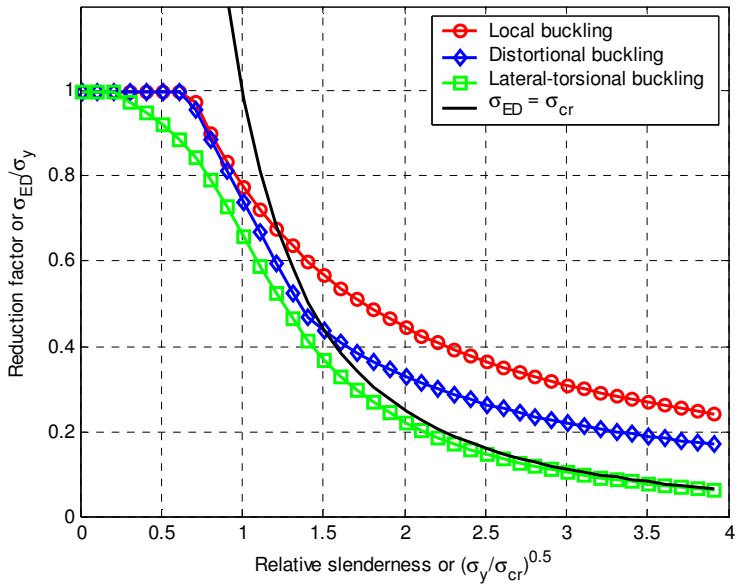

Figure 2.9 Design curves for members subjected to compression loads (EN1993-1-3, 2006).

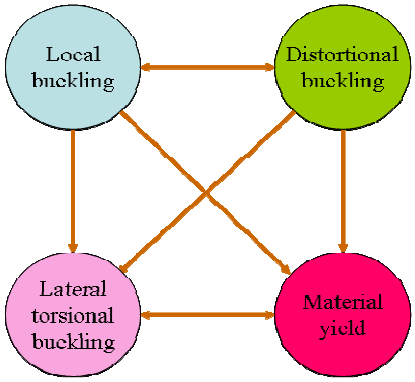

Figure 2.10 Interaction between different buckling and failure modes.

Cold-formed steel sections may have local, distortional, and lateral-torsional buckling modes. The interactions between different buckling modes and between buckling and material yield are summarised in Figure 2.10.

The interaction between local buckling and material yield was investigated by Winter (1968) and many others (Kwon et al., 2009, Camotim et al., 2008b). Empirical formulae were developed and utilised in design standards (EN1993-1-3, 2006; North American, 2005; Australia/New Zealand, 2005).

The interaction between local and lateral-torsional buckling modes was investigated by Becque and Rasmussen (2006). The interaction between lateral-torsional buckling and material yield was investigated experimentally by Moen and Schafer (2008b). The empirical formulae developed for cold-formed steel sections were very similar to those for hot-rolled steel sections.

Research on interactions involving distortional buckling has been carried out very recently. Dinar and Camotim (2008a) investigated the interaction between local and distortional buckling using the finite element method. Kwon et al. (2008) experimentally investigated the interaction between distortional buckling and material yield. Nandini and Kalyanaraman (2008) investigated the interaction between distortional buckling and lateral-torsional buckling also using the finite element method. Yin et al. (2011) investigated the interaction between local and distortional buckling of a compression flange and lip system. However, all of these studies were limited to the cases where the cold-formed steel sections were subjected to pure compression or pure bending.

2.5 Purlin-sheeting systems

Lateral movements of roof purlins and sheeting rails are usually eliminated by the restraint of the supported roof or wall cladding. Lateral buckling of the whole section could be potentially reduced by such restraints. However, this does not necessarily eradicate the possibility of failure. For example, roof purlins are normally restrained against lateral displacement by cladding. For a simply supported purlin under a gravity load, its upper flange is in compression. Thus, the purlin will not buckle lateral-torsionally. However, when wind uplift occurs and induces compression in the unrestrained flange, there is potential risk of causing lateral-tensional buckling, and wind uplift is an important design condition for roof purlins. This occurs due to the flexibility of the restraining cladding and the distortional flexibility of the section itself, which permits lateral movement to occur in the compression flange even if the other flange is

restrained. Previous studies have reported that lateral and rotational restraints play an important role in the buckling behaviour of the attached purlin. Katnam et al. (2007a and 2007b) addressed a non-linear finite element model to estimate the rotational restraint provided by the first and second generation trapezoidal sheeting and the sandwich panels to the attached purlin.

Numerical investigations into the influence of sheeting restraints on purlin lateral-torsional buckling as proposed by Li (2011) are shown in Figure 2.11. These investigations showed that the twisting restraint has significant influence and the translational restraint has almost no influence on the lateral-torsional buckling of the purlin.

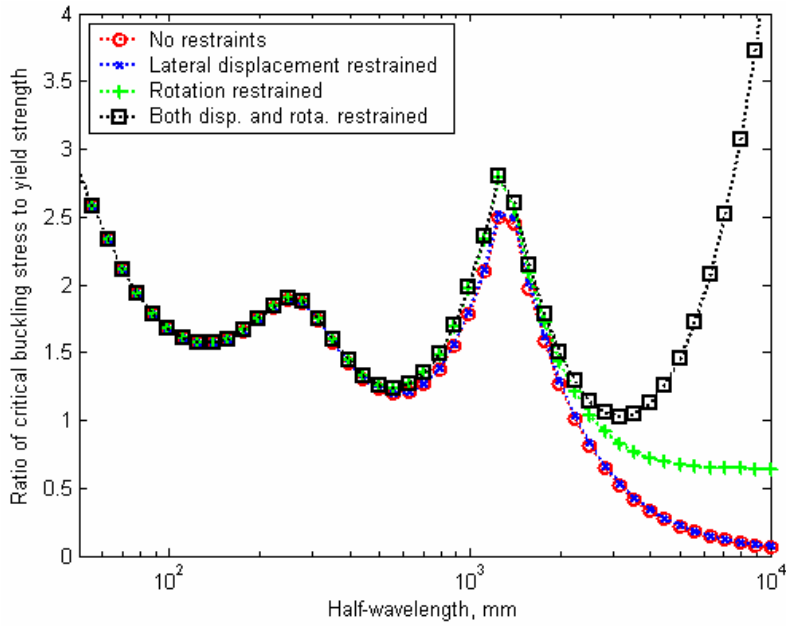

Figure 2.11 Buckling curves of a simply supported zed-section beam (web depth 240 mm, flange width 75 mm, lip length 20 mm, thickness 2.0 mm) with different restraints at web-flange junction (tension side) subjected to pure bending (Li, 2011) .

For purlin-sheeting systems, the rotational and/or translational restraints have been considered by researchers and there are different methods to analyse pre-buckling stress distribution, buckling behaviour and post-buckling load resistance. Considerable research of analytical methods has been conducted over many years. Ye et al. (2002 and 2004) presented an analytical model on the buckling behaviour and pre-buckling stress analysis of purlin-sheeting systems under uniformly distributed uplift loads. Two springs were used to represent the translational and rotational restraints provided by the sheeting, in which the partial lateral and rotational restraints have effects on the results of stresses and buckling modes. Li (2004) presented an analytical model and used energy methods to study the lateral-torsional buckling of cold-formed zed-sections, partial laterally restrained by anti-sag bars and sheeting with various boundary conditions under uniformly distributed gravity or uplift loads. Chu et al. (2005 and 2006) modified Li's model to predict the critical loads of zed- and channel-sections. Recent reports (Li et al. 2012 and Ren et al 2012) described the bending and twisting behaviour of partially restrained zed- and channel-section purlins when subjected to uniformly distributed uplift loads. Formulae used to calculate the bending stresses of the roof purlins were derived by using the classical bending theory of thin-walled beams, and finite element analysis results were used for validation.

The analytical model of Eurocode 3 (EN1993-1-3, 2006) to obtain the critical stress of the member under various loading combinations was based on the concept of Sokol's model (1996). The approach used an energy method and assumed the behaviour of a compressed free flange and a single compressed member on elastic foundation (see

Figure 2.12). The former was equivalent to the compression free flange and lip plus 1/5 of the web length with a lateral spring replacing the rotational spring of the purlin fixed to the sheeting. The latter corresponded to the effect of torsion and lateral bending (including cross section distortion) on a single span with uplift loading.

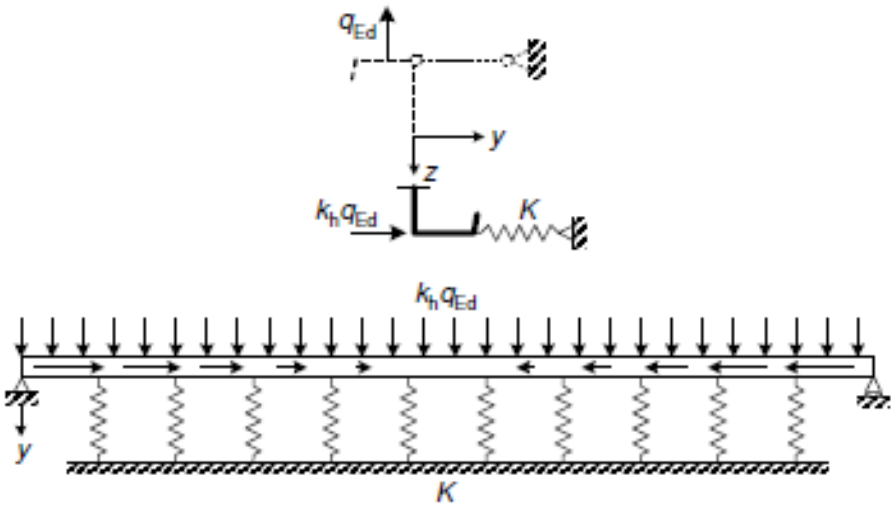

Figure 2.12 Modelling laterally braced purlins rotationally restrained by sheeting (EN1993-1-3, 2006).

Pekoz and Soroushian (1982) presented an analytical approach to develop purlin-sheeting models to study the bending and torsion of zed- and channel-section purlins under uplift loads. Several design conditions were considered in the analytical method and parametric studies were carried out in the paper. Consequently, the ultimate loads were predicted for zed- and channel-section purlin-sheeting models under uplift loads and the experimental and analytical results were compared with each other.

In the past few decades, there have been many experimental studies of purlin-sheeting systems. Wills and Wallace (1990) carried out full-scale tests of cold-formed steel channel- and zed-section purlins with metal-building roof panels under gravity loading and presented the influence of gravity load on the fastener location of a channel-section. Test data illustrated that the current edition of the AISI specification (AISI: Specification 1986) over predicts the capacity of purlins with wide compression-flange-stiffener lips. Toma and Wittemann (1994) discussed the calculation model which was the basis of Eurocode (EN 1993-1-3, 2006). They compared the results of the calculation model and test for single span beams subject to both downward and uplift loads, and found the ultimate load was generally limited by lateral-torsional buckling of the free flange with uplift loading. Additionally, the report showed the conservatism of the Eurocode to predict ultimate loads for both gravity and uplift. Rousch and Hancock (1997) developed experimental tests which were performed on both bridged and unbridged purlins under uplift loadings. The test on the simply supported channel- and zed-section purlins with screw fastened sheeting has been performed in a vacuum test to simulate the uniformly distributed load by wind uplift loading. The test results contain the comparison of pre-buckling stress and lateral deflections. Moreover, the failure loads and failure modes were also compared. Rogers and Schuster (1997) identified the flange/web distortional buckling of cold-formed steel channel- and zed-sections by using experimental tests to reveal the prediction of bending resistance. This report recommended the use of the modified Lau and Hancock's model, with S136-94 Standard calculated effective sections modulus, as the North American predictor model for the flange/web distortional buckling moment resistance of cold-formed steel section in bending. Laterally braced cold-formed

steel beams generally fail due to local or distortional buckling. Yu and Schafer (2003 and 2006) investigated local and distortional buckling tests and corresponding finite element analysis to provide upper and lower bounds for the capacity of laterally braced cold-formed steel beams in common use in North America.

The recently developed numerical methods in purlin-sheeting systems aimed to be more accurate and simpler than the analytical methods, and to be more economical and efficient than experimental testing. Ings and Trahair (1984) developed a simple model by using the finite element method to predict the maximum moment in a segment at elastic buckling under uplift and gravity load. In the simple model, the lateral and rotational movements were braced with the effects of cross-section distortion and local buckling being ignored. The results obtained from this study highlight that the simple model has an advantage when the design of a roof purlin is governed by lateral buckling considerations. Lucas et al. (1997a and 1997b) established a full model and a simplified model by using the nonlinear elasto-plastic finite element method to predict the structural behaviour of purlin-sheeting systems. The full model contained both purlin and sheeting to merge the interaction between the two components of the system. The simplified model included only purlin and replaced sheeting by linear elastic spring as the effects of lateral and rotational restraints at purlin-sheeting connections. These two models were both able to account for cross-section distortion of purlin and ultimate failure load of purlin by local buckling or yielding. Lucas et al. claimed that the full model and the simplified model were able to predict the failure load of the purlin within respective five percent and ten percent differences from the experimental results. Yu and Schafer (2007)

produced a nonlinear finite element model for laterally braced beams to simulate local buckling and distortional buckling failures. The model was also applied to analyse the effect of moment gradient on distortional buckling. Yu and Schafer stated that the moment gradient effect on distortional buckling failures can be conservatively accounted for in the Direct Strength Method by using an elastic buckling moment to account for the moment gradient. Vieira et al. (2010) used numerical methods to study the longitudinal stress distribution on the cross-section of purlin-sheeting systems, and four cases of lateral and rotational restraints were compared. More recently, Zhu el at. (2012) developed a geometrical and material nonlinear finite element analysis model for cold-formed steel zed-section purlins subjected to uplift loading. In the model, the lateral and rotational restraints provided by the sheeting to the purlin were simplified as a lateral rigid restraint imposed at the upper flange-web junction and a rotational spring restraint applied at the mid of the upper flange where the sheeting was fixed. It was found that the rotational spring stiffness has significant influence on the purlin performance.

2.6 Knowledge gap

The structural behaviour of cold-formed steel is presented in this chapter. The review discusses buckling, the analysis methods, the interaction of buckling modes and purlin-sheeting systems. Although there has been substantial research on various section members, there are still some problems which are not fully understood and require further investigation, particularly in the following aspects:

1. Most researches and design codes provide the critical stress for the purlins with pure bending or pure compression. However, for an effective and practical design, the moment gradient along the longitudinal axis of the purlin needs to be considered. The uniformly distributed load is considered as the main aspect of loading in the next three chapters. Furthermore, the ultimate strength from geometrically and materially nonlinear analysis is a critical part of the research.

2. Sheeting provides lateral and rotational restraints which reduce the potential of lateral buckling of the whole section, but do not necessarily eradicate the problem. Under wind uplift, which induces compression in the unrestrained flange, lateral-torsional buckling is still a common cause of failure. This occurs due to the flexibility of the restraining cladding and to the distortional flexibility of the section itself which permits lateral movement to occur in the compression flange even if the other flange is restrained. Some publications mentioned this issue but not comprehensively. The present research work will concentrate on uplift loading and the corresponding analyses related to pre-buckling, buckling and post-buckling.

3. There is very limited research being carried out on the interaction between distortional buckling and other failure modes such as local buckling, lateral torsional buckling and material yield. How their interaction affects the design load that needs to be investigated for various types of sections.

4. Most research on structural behaviour solely focuses on cold-formed steel sections themselves. However, in practice, most sections are used to support the roof or wall sheeting which will provide lateral restraints to the sections. There is experimental evidence that shows different influences of the sheeting on the local, distortional and lateral-torsional buckling. The investigation into purlin-sheeting systems is significantly important for understanding the structural behaviour of cold-formed steel sections.

The present study will address the above problems. By using analytical (the classical bending theory) and numerical (finite element method) methods, the structural behaviour of cold-formed steel zed- and channel-section purlins under uniformly distributed uplift loads will be investigated. Interactions of different buckling modes will also be examined in detail.

2.7 Summary

This chapter has presented a literature review of the structural behaviour of cold-formed steel sections. The literature review has focused on the development of cold-formed steel, buckling behaviour, methods of analysing buckling, the interactions of different buckling modes and the structural behaviour of purlin-sheeting systems. Some important conclusions drawn from the literature review are summarised as follows:

1. The buckling behaviour of cold-formed steel is listed and the characteristics of buckling are discussed, including local, distortional and lateral-torsional buckling modes.

2. The methods of analysing buckling of cold-formed steel are summarised, including the advantages and disadvantages of analytical methods, Generalised Beam Theory (GBT), finite element methods, finite strip methods and experimental methods.

3. The importances of the interactions between different buckling modes are demonstrated and the characteristics of the interactions are addressed.

4. The structural behaviour of purlin-sheeting systems is presented, the importance of purlin-sheeting systems in the cold-formed steel structure is demonstrated and the analysis methods of purlin-sheeting systems are reviewed.

5. The knowledge gap are summarised and the methodology for research and development are described.

CHAPTER 3 PRE-BUCKLING STRESS ANALYSIS OF PURLIN-SHEETING SYSTEMS

3.1 Introduction

Thin-walled, cold-formed steel sections are widely used as purlins and rails; the intermediate members between the main structural frame and the corrugated roof or wall sheeting in farming and industrial buildings. The most common sections are the zed, channel and sigma shapes, and trapezoidal sheeting is usually fixed to these members in order to enclose the building. Lateral movements of roof purlins and sheeting rails are usually eliminated by the restraint of the supported roof or wall cladding. Lateral buckling of the whole section could be potentially reduced by such restraints. However, this does not necessarily eradicate the possibility of failure. For example, roof purlins are normally restrained against lateral displacement by cladding, but if wind uplift occurs and induces compression in the unrestrained flange, there is potential risk of lateral-torsional buckling. This occurs due to the flexibility of the restraining cladding and the distortional flexibility of the section itself, which permits lateral movement to occur in the compression flange even if the other flange is restrained.

In this chapter, an analytical model is presented to describe the bending and twisting behaviour of the partially restrained cold-formed steel purlins when subjected to uplift

loading for zed- and channel-sections. Formulae used to calculate the bending stresses of the roof purlins are derived using the classical bending theory of thin-walled beams. Detailed comparisons are made between the present model and the simplified model proposed in Eurocode (EN1993-1-3). Furthermore, to validate the present model, finite element analysis is also conducted and the bending stress distribution along the lip, flange and web lines obtained from the finite element analysis is compared with that obtained from the present and EN1993-1-3 models. The comparisons of cleat bolted supported and web simply supported for zed- and channel-sections are also presented.

3.2 The influence of boundary conditions

In practice, purlins are supported by cleats through two bolts on each side. To model the bolt connections one has to use irregular meshes in the zones near the ends, which makes the analysis inefficient. To make the analysis more efficient but without loss of accuracy, an equivalent boundary condition to the cleat bolted supported boundary condition has been identified, which is to simply support the web. In this section, a comparison of bending stresses of zed- and channel-sections subjected to uplift loading between the cleat bolted supported boundary condition and the web simply supported boundary condition is presented.

The boundary condition of long beam is assumed to be the simply support applied by restraining the lateral and tangential displacements of the web lines at the two ends of the section are zero. In order to eliminate the rigid displacement in the longitudinal direction, the coordinate original point in one of the two end sections is also restrained in the longitudinal axis of the member. For cleat bolted supported, the boundary condition is assumed to be that in which the lateral and normal displacements of the lines along the bolted holes are zero, plus a zero tangential displacement applied at a lower point at each hole. In addition, for both types of boundary conditions, the member is laterally restrained at the upper flange-web junction to represent the sheeting restraint, and a uniformly distributed rotational spring is applied at the middle line of the upper flange to simulate the rotational restraint provided by the sheeting. According to the experiment of Zhao et al (2012), the value of rotational spring stiffness is about 400 N to 770 N for

different dimensions of cross-section. The material properties of the purlin analysed are assumed to be linear elastic with Young's modulus, E=210 GPa and Poisson's ratio, ν=0.3. Material yield will not be considered in this case. The four-node shell element of reduced integration scheme and the chosen element has one point integration with hourglass mode stabilisation (ABAQUS standard user's manual—version 6.3, 2002). The S4R is employed for analysing both web simply supported and cleat bolted supported boundary conditions. For the cleat bolted supported purlin, local fine meshes are used to avoid possible stress concentration (see Figure 3.1).

Figures 3.2 and 3.3 show the detailed comparisons of the total bending stresses obtained from the finite element analysis for both web simply supported and cleat bolted supported boundary conditions of a small (Z12515) and a large (Z40132) zed-sections. The comparison of total bending stress for web simply supported and cleat bolted supported boundary conditions for a small and a large channel-sections (C12515 & C40132) is shown in Figures 3.4 and 3.5, respectively. It can be seen from these figures that for k_ϕ=0 N and k_ϕ=750 N, the results predicted by the web simply supported boundary condition agree very well with the cleat bolted supported boundary condition results. The stresses of web simply supported and cleat bolted supported along the web are very close in value. However, it can be found in a few cases that, at the flange and the lip, the stresses obtained by web simply supported boundary condition are slightly higher. This is probably due to the boundary condition for the cleat bolted supported being located at the hole in the web which is 29 mm away from the edge of the web, leading the actual beam length from support to support to be slightly shorter. Nevertheless, the FE simulations are

in good agreement with the two different types of boundary conditions for zed- and channel- sections, indicating that the web simply supported boundary condition proposed in the present study are able to represent the commonly used standard two-hole cleat bolted supported boundary condition used in practice.

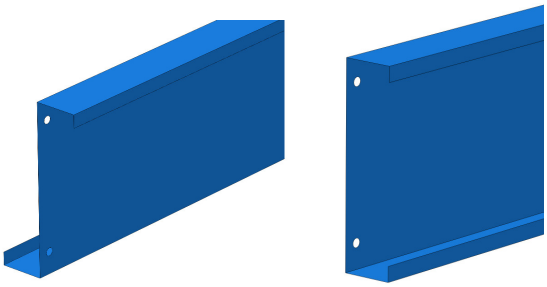

(a)

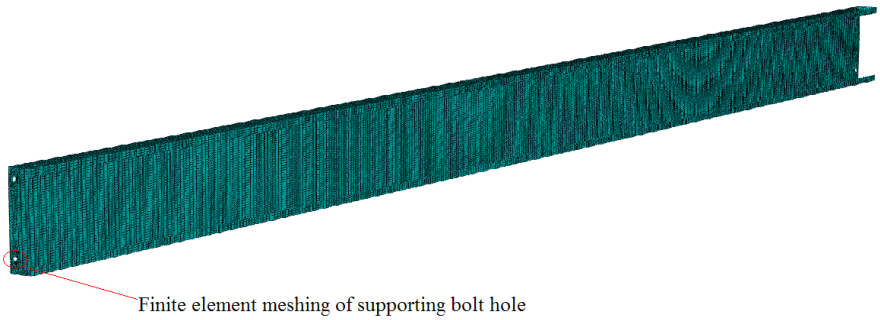

(b)

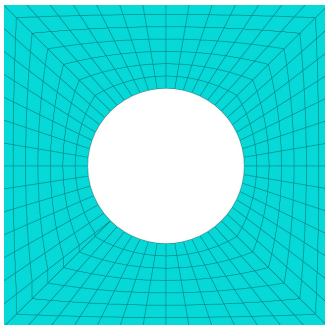

(c)

Figure 3.1 (a) Cleat bolted supported boundary condition of zed- and channel-sections (b) Finite element mesh and (c) zoom of local mesh in the region near the bolt hole.

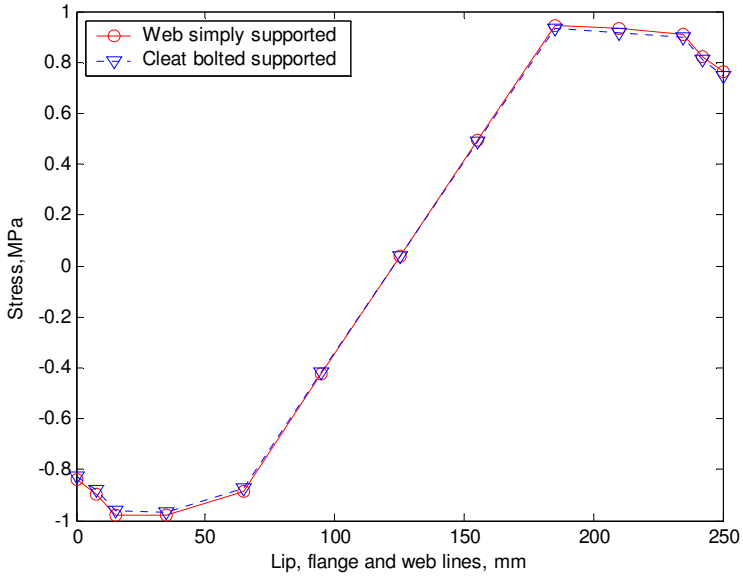

(a) k_{ϕ} =0 N

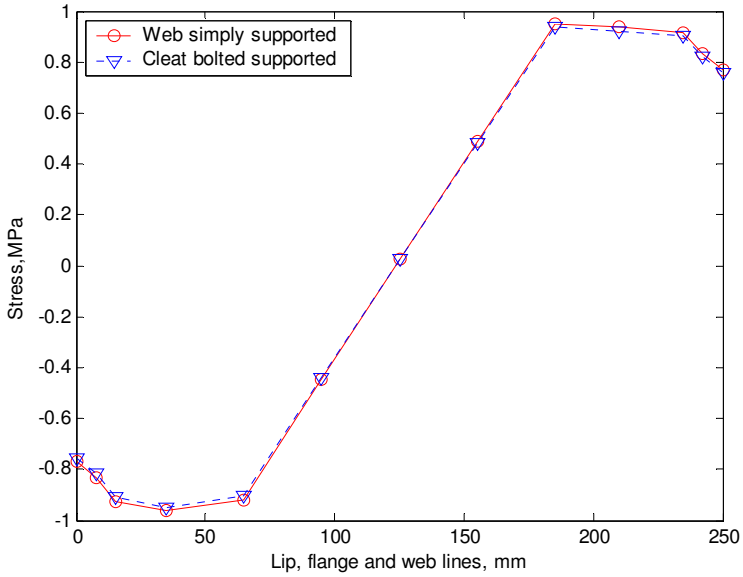

(b) k_{ϕ} =750 N

Figure 3.2 Bending stress distribution of zed-section along the lip, flange and web lines (abscissa starts from the tip of lower lip and ends at the tip of upper lip) (Z12515, L=7000 mm).

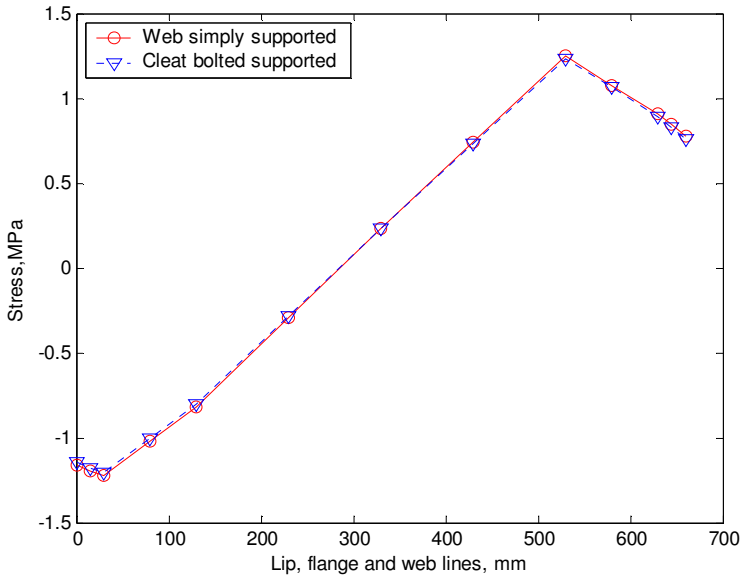

(a) k_{ϕ} =0 N

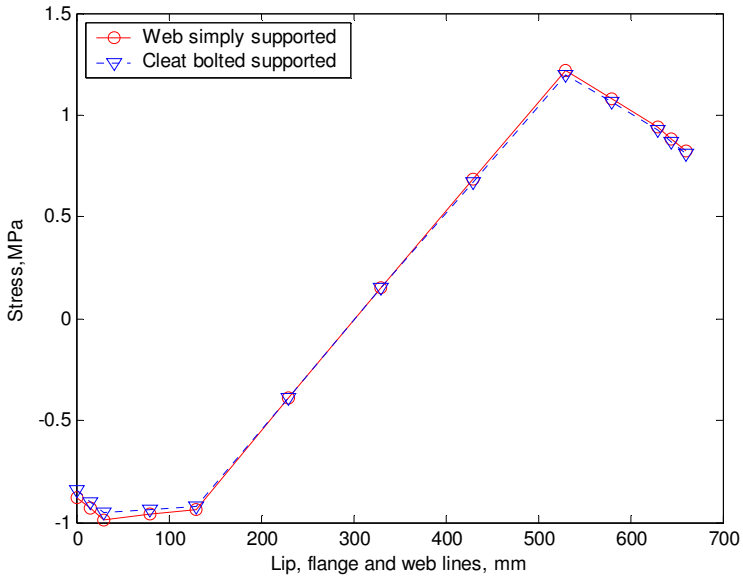

(b) k_{ϕ} =750 N

Figure 3.3 Bending stress distribution of zed-section along the lip, flange and web lines (abscissa starts from the tip of lower lip and ends at the tip of upper lip) (Z40132, L=7000 mm).

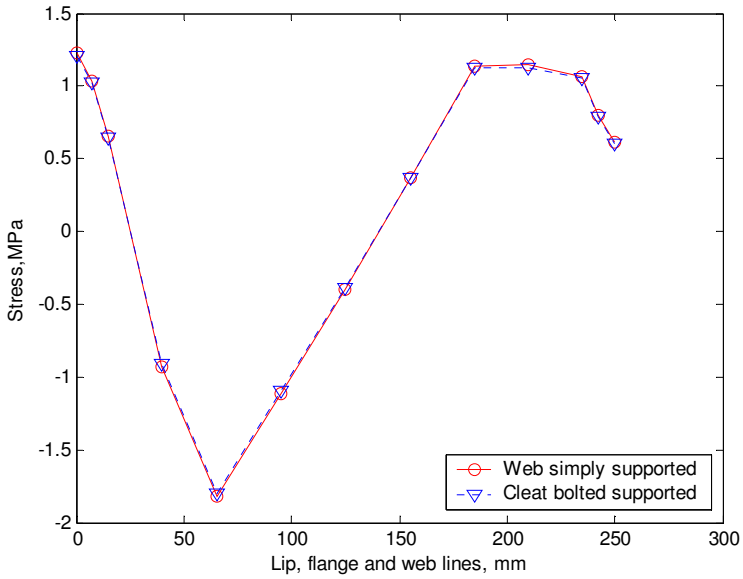

(a) k_ϕ =0 N

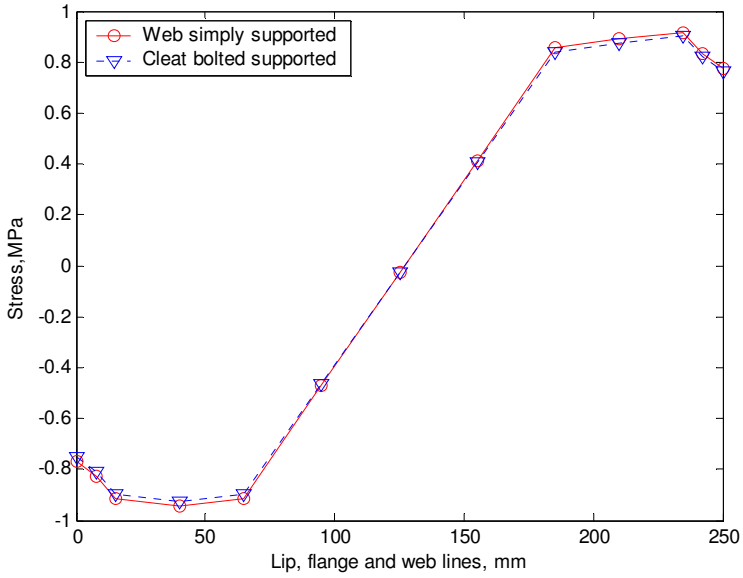

(b) k_ϕ =750 N

Figure 3.4 Bending stress distribution of channel-section along the lip, flange and web lines (abscissa starts from the tip of lower lip and ends at the tip of upper lip) (C12515, L=7000 mm).

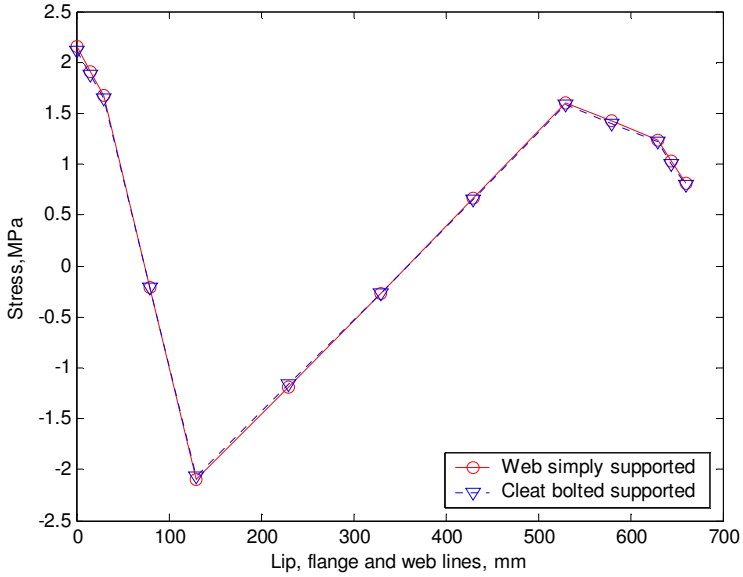

(a) k_ϕ =0 N

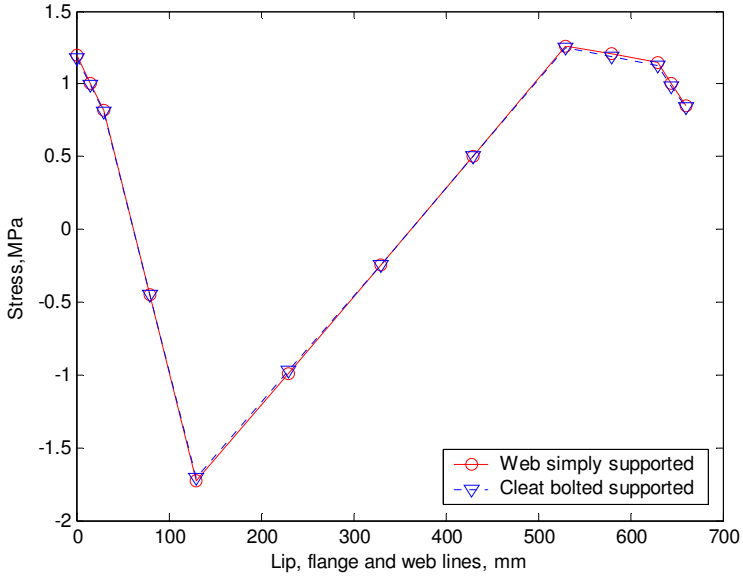

(b) k_ϕ =750 N

Figure 3.5 Bending stress distribution of channel-section along the lip, flange and web lines (abscissa starts from the tip of lower lip and ends at the tip of upper lip) (C40132, L=7000 mm).

3.3 Pre-buckling stress analysis of zed-sections

3.3.1 Analytical model and calculation

Consider a purlin-sheeting system in which the upper flange of the section is connected to the sheeting by self-drilling or self-tapping screw fasteners, while the lower flange remains free. The attached sheeting provides lateral and rotational restraints to the upper flange, which can influence both the bending and buckling behaviour of the section. The lateral restraint is due to the membrane stiffness of the sheeting, whereas the rotational restraint is provided by a resisting couple produced by the contact stresses between the flange and the sheeting. For most types of sheeting, the lateral restraint is sufficient and therefore the lateral displacement at the upper flange-web junction may be assumed to be fully restrained. The rotational restraint, however, is dependent on several factors. These include the dimensions of sheeting and purlin, and the number, type and position of the screws. If the stiffness of the rotational restraint provided by the sheeting is known, then the purlin-sheeting system may be idealised as a purlin with lateral displacement fully restrained, and rotation partially restrained, at its upper flange-web junction as shown in Figure 3.6.

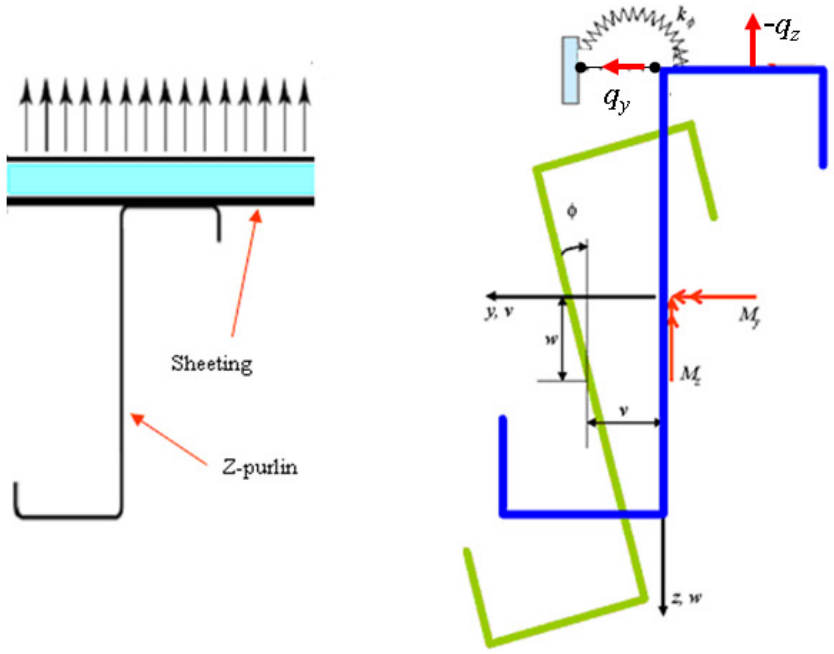

Figure 3.6 Analytical model used for a zed-section purlin-sheeting system.

Let the origin of the coordinate system (x,y,z) be the shear centre of the cross-section, with the x-axis being along the longitudinal direction of the beam, and the y- and z-axes taken in the plane of the cross-section, as shown in Figure 3.6. According to the bending theory of asymmetric beams from Timoshenko and Gere (1961), and noting that for a zed-section the shear centre and centroid of the cross-section are at the same point, the equilibrium equations, expressed in terms of displacements, are given as follows,

$$EI_z \frac{d^4 v}{dx^4} + EI_{yz} \frac{d^4 w}{dx^4} = q_y \tag{3-1}$$

$$EI_{yz} \frac{d^4 v}{dx^4} + EI_y \frac{d^4 w}{dx^4} = q_z \tag{3-2}$$

$$EI_w \frac{d^4 \phi}{dx^4} - GI_T \frac{d^2 \phi}{dx^2} + k_\phi \phi = z_k q_y - a q_z \tag{3-3}$$

Where v = the y- components of displacement of the cross-section at the shear centre;

w = the z- components of displacement of the cross-section at the shear centre;

ϕ = the angle of twisting;

G = the shear modulus;

I_y = the second moments of the cross-sectional area about the y-axes;

I_z = the second moments of the cross-sectional area about the z-axes;

I_{yz} = the product moment of the cross-sectional area;

I_w = the warping constant;

I_T = the torsion constant;

k_ϕ = the per-unit length stiffness constant of the rotational spring;

q_y = the density of uniformly distributed load in y-direction;

q_z = the density of uniformly distributed load in z-directions;

z_k = the vertical distance from the shear centre to the force line q_y;

a = the horizontal distance from the shear centre to the force line q_z.

Note that the governing equations (3-1) to (3-3) are only valid for long beam due to the assumption that the shape of the cross section remains the same after deformation. For short beam, these governing equations would become unsuitable. Using Eq.(3-1) to eliminate q_y and Eq.(3-2) to eliminate w in Eq.(3-3), it yields,

$$EI_w \frac{d^4\phi}{dx^4} - GI_T \frac{d^2\phi}{dx^2} + k_\phi \phi - z_k \left[EI_z \frac{d^4 v}{dx^4} + \frac{I_{yz}}{I_y} \left(q_z - EI_{yz} \frac{d^4 v}{dx^4} \right) \right] = -aq_z \tag{3-4}$$

Note that the lateral displacement restraint applied at the upper flange-web junction requires,

$$z_k \phi + v = 0 \tag{3-5}$$

Using Eq.(3-5) to eliminate the angle of twisting, ϕ, in Eq.(3-4), it yields,

$$\left(EI_z - \frac{EI_{yz}^2}{I_y} + \frac{EI_w}{z_k^2} \right) \frac{d^4 v}{dx^4} - \frac{GI_T}{z_k^2} \frac{d^2 v}{dx^2} + \frac{k_\phi}{z_k^2} v = q_z \left(\frac{a}{z_k} - \frac{I_{yz}}{I_y} \right) \tag{3-6}$$

Let

$$I_{eq} = \frac{1}{4} \left(I_z - \frac{I_{yz}^2}{I_y} + \frac{I_w}{z_k^2} \right) \tag{3-7}$$

$$k_h = \frac{1}{2} \left(\frac{I_{yz}}{I_y} - \frac{a}{z_k} \right) \tag{3-8}$$

Note that z_k=h/2 for zed-sections of equal flanges where h is the web depth. Then Eq.(3-6) can be rewritten as,

$$EI_{eq} \frac{d^4 v}{dx^4} - \frac{GI_T}{h^2} \frac{d^2 v}{dx^2} + \frac{k_\phi}{h^2} v = -\frac{k_h q_z}{2} \tag{3-9}$$

The solution of Eq.(3-9) for a simply supported beam in both y- and z-directions can be approximately expressed as follows,

$$v(x) = \sum C_m \sin \frac{m\pi x}{l} \tag{3-10}$$

where l = the length of the beam;

C_m = the constant to be determined.

Substituting Eq.(3-10) into (3-9), it yields,

$$C_m = \frac{\frac{-k_h q_z}{m\pi}\left[1-(-1)^m\right]}{EI_{eq}\left(\frac{m\pi}{l}\right)^4 + \left(\frac{GI_T}{h^2}\right)\left(\frac{m\pi}{l}\right)^2 + \frac{k_\phi}{h^2}} \tag{3-11}$$

Thus the horizontal component of the displacement of the cross-section at the shear centre due to the uniformly distributed vertical load can be expressed as follows,

$$v(x) = -\sum_{m-1,3,5} \frac{2k_h q_z l^4}{m\pi^5 EI_{eq}} \frac{1}{m^4 + \left(\frac{GI_T}{EI_{eq}}\right)\left(\frac{ml}{\pi h}\right)^2 + \frac{k_\phi l^4}{\pi^4 EI_{eq} h^2}} \sin\frac{m\pi x}{l} \tag{3-12}$$

The bending stress generated by the displacements can be calculated as follows,

$$\sigma_x(x,y,z) = -Ey\frac{d^2v}{dx^2} - Ez\frac{d^2w}{dx^2} + E(\overline{\omega}-\omega)\frac{d^2\phi}{dx^2} \tag{3-13}$$

where ω = the sectorial coordinate with respect to the shear centre;

$\overline{\omega}$ = the average value of ω.

The first term on the right hand side of Eq.(3-13) is the stress generated by the deflection of the beam in vertical direction, the second term is the stress generated by the deflection of the beam in horizontal direction, and the third term is the warping stress. For convenience of comparison, the displacement component w is now split into two parts, that is, $w=w_o+w_1$, where w_o is the displacement generated by the load q_z when the beam is fully restrained in rotation (that is, the beam is bent only in the plane of the web) and w_1 is the displacement due to the compatibility with the displacement component v when the

beam is not fully restrained in rotation. Hence, according to Eq.(3-2), these two parts of w can be calculated as follows,

$$EI_y \frac{d^4 w_o}{dx^4} = q_z \tag{3-14}$$

$$EI_{yz} \frac{d^4 v}{dx^4} + EI_y \frac{d^4 w_1}{dx^4} = 0 \tag{3-15}$$

With the use of Eqs.(3-5), (3-14) and (3-15), Eq.(3-13) can be rewritten as,

$$\sigma_x(x, y, z) = -Ez \frac{d^2 w_o}{dx^2} - E\left(y - \frac{zI_{yz}}{I_y} + \frac{\overline{\omega} - \omega}{z_k} \right) \frac{d^2 v}{dx^2} \tag{3-16}$$

Eq.(3-16) indicates that the total bending stress can be decomposed into two parts. One is the stress that is generated by the load q_z when the beam is considered to be fully restrained in rotation and can be calculated as follows,

$$\sigma_{x1}(x, y, z) = -Ez \frac{d^2 w_o}{dx^2} \tag{3-17}$$

The other is the stress that is generated by the deflection of the beam in a horizontal direction v due to the lateral load $-k_h q_z$ as shown in Eq.(3-9) and can be calculated as follows,

$$\sigma_{x2}(x, y, z) = -E\left(y - \frac{zI_{yz}}{I_y} + \frac{\overline{\omega} - \omega}{z_k} \right) \frac{d^2 v}{dx^2} \tag{3-18}$$

For a simply supported beam the bending stress σ_{x1} can be expressed as follows,

$$\sigma_{x1}(\frac{l}{2}, y, z) = \frac{zM_{y,\max}}{I_y} \tag{3-19}$$

where under simply supported boundary condition, $M_{y,\max} = \frac{q_z l^2}{8}$ is the largest moment of the beam bent about y-axis. The bending stress σ_{x2} is obtained by substituting Eq.(3-12) into (3-18), that is,

$$\sigma_{x2}(\frac{l}{2}, y, z) = -\frac{k_R k_h M_{y,\max}}{I_{eq}}\left(\frac{y}{2} - \frac{zI_{yz}}{2I_y} + \frac{\overline{\omega} - \omega}{h}\right) \tag{3-20}$$

where k_R = the correction factor for the largest moment of the beam bent about the z-axis, considering the influence of the rotational spring and torsional rigidity of the section on the maximum moment, which is defined as follows,

$$k_R = \frac{32}{\pi^3}\sum_{m=1,3,5}\frac{(-1)^{\frac{m-1}{2}} m}{m^4 + \left(\frac{GI_T}{EI_{eq}}\right)\left(\frac{ml}{\pi h}\right)^2 + \frac{k_\phi l^4}{\pi^4 h^2 EI_{eq}}} \tag{3-21}$$

It is obvious from Eq. (3-21) that, if $k_\phi = 0$ and $I_T = 0$ then $k_R = 1$, otherwise, if $k_\phi = \infty$ or $I_T = \infty$ then $k_R = 0$. The latter represents the case where the purlin is fully restrained in rotation or has an infinitely large torsion constant, in which case $\sigma_{x2} = 0$.

3.3.2 Comparison with EN1993-1-3

In Eurocode (EN1993-1-3, 1993), the bending stress of a zed-section purlin of web depth *h*, flange width *b*, lip length *c* and thickness *t*, with lateral displacement fully restrained

and rotation partially restrained at the upper flange-web junction is calculated based on two types of bending. One is where the beam is bent only in the plane of the web, in which case the stress is calculated in exactly the same way as that shown in Eq.(3-17). The other is in the compression part of the section, consisting of the lip and flange plus 1/5 of the web height from the flange, bent about an axis parallel to the z-axis, in which case the stress is calculated as follows,

$$\sigma_{x2}(\frac{l}{2}, y, z) = -\frac{k_R^* k_h M_{y,\max}}{I_{fz}}(y - \bar{y}) \tag{3-22}$$

where k_R^* = the moment correction factor relating to the influence of the rotation restraint;

I_{fz} = the second moment of the cross-section area of the compression part about the z*-axis for the zed-section as defined in Figure 3.7;

$\bar{y}$ = the horizontal distance between the z*-axis and the z-axis.

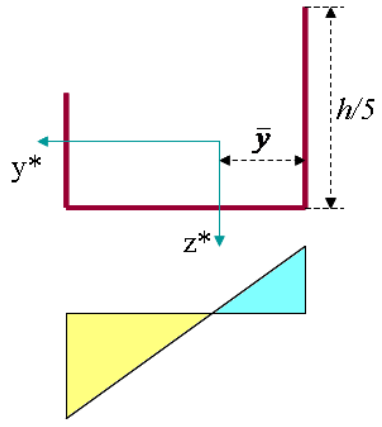

Figure 3.7 Bending stress calculated in EN1993-1-3.

Upper: Compression part consisting of lip and flange plus 1/5 of web length.

Lower: Stress distribution due to the bending about z* axis.

Table 3.1 lists the differences between Eqs.(3-20) and (3-22). In the Eurocode, the moment correction factor for a simply supported purlin with no anti-sag bar is given as,

$$\kappa_R^* = \frac{1-0.0225R}{1+1.013R} \tag{3-23}$$

$$R = \frac{Kl^4}{\pi^4 E I_{fz}} \tag{3-24}$$

$$K = \left(\frac{4(1-\nu^2)h^2(h+b_{\mathrm{mod}})}{Et^3} + \frac{h^2}{k_\phi} \right)^{-1} \tag{3-25}$$

where $b_{mod}=a'$ is for cases where the equivalent lateral force ($-k_h q_z$) bringing the purlin into contact with the sheeting at the purlin web; or

$b_{mod}=2a'+b$ is for cases where the equivalent lateral force ($-k_h q_z$) bringing the purlin into contact with the sheeting at the tip of the purlin flange;

a' = the horizontal distance from the web line to the sheeting-purlin fixing.

Table 3.1 List of differences between the present and EN1993-1-3 models

Models	Present model	EN1993-1-3
Formula used for calculating moment correction factor	Eq.(3-21)	Eq.(3-23)
Definition of the second moment used for calculating bending stress	I_{eq} Eq.(3-7)	I_{fz} Figure 3.7
Coordinate used for calculating bending stress	$\frac{y}{2} - \frac{zI_{yz}}{2I_y} + \frac{\overline{\omega}-\omega}{h}$	$y-\overline{y}$

Figure 3.8 shows the comparisons of the moment correction factors calculated from the present and EN1993-1-3 models. It can be seen from the figure that the moment correction factor decreases with the increase of either beam length or the stiffness of the rotational spring. The rate of decrease is found to be fast in a small section than in a large section. It can also be observed from the figure that the moment correction factor calculated using the EN1993-1-3 model is higher than that calculated using the present model, particularly when the stiffness of the rotational spring is very small or very large. Note that the main difference in the moment correction factors between the present and EN1993-1-3 models is the torsional rigidity. In the present model the torsional rigidity is included, which makes the moment correction factor smaller, particularly for cases where the stiffness of the rotational spring is small. In the EN1993-1-3 model, the torsional rigidity is not included. However, its spring stiffness, calculated using Eq.(3-25), takes into account the influence of the section distortion, which makes the moment correction factor larger, particularly for cases where the stiffness of the torsional spring is large. This is why a greater difference in the moment correction factors between the two models is found in the case where the stiffness of rotational spring is either very large or very small. If the section distortion is ignored in the spring stiffness in the EN1993-1-3 model (that is, EN1993-1-3* plotted in Figure 3.8 and the corresponding results are represented by the plus, x-mark, and star symbols), then the moment correction factor predicted by the EN1993-1-3 model is found to be higher for the small stiffness of rotational spring but lower for the large stiffness of rotational spring than that calculated using the present model.

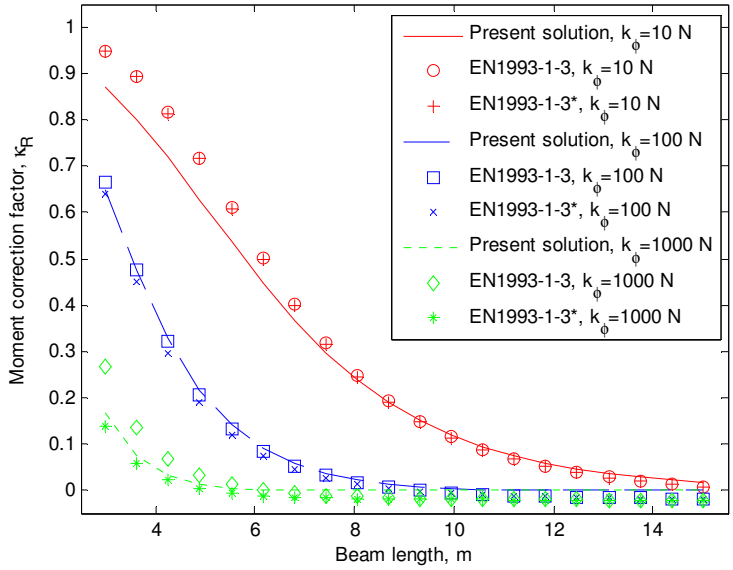

(a) h=120 mm, b=50 mm, c=15 mm, t=1.5 mm, a=b/2.

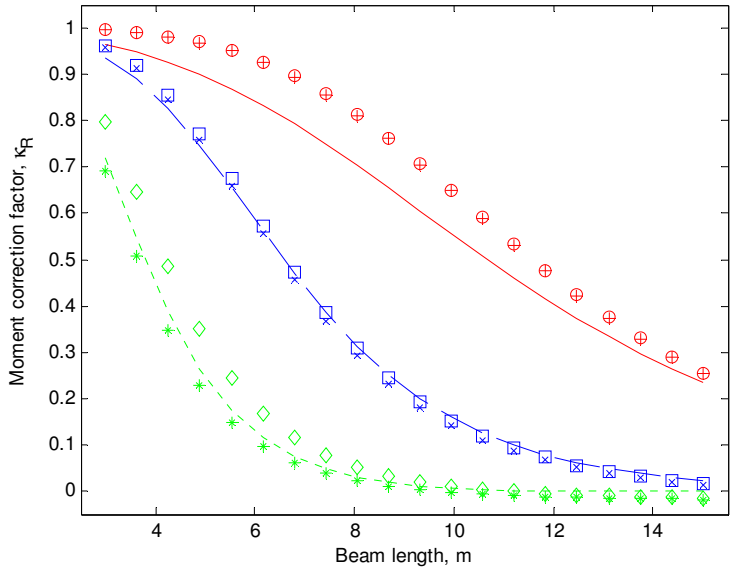

(b) h=200 mm, b=75 mm, c=20 mm, t=2 mm, a=b/2.

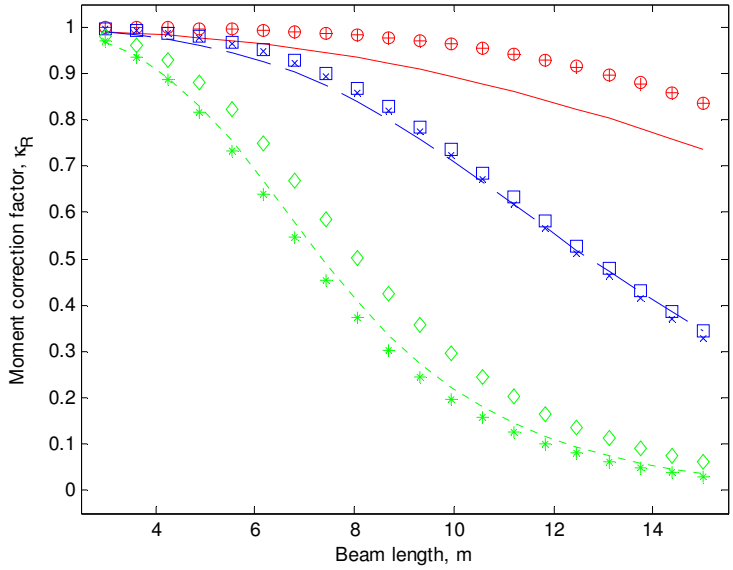

(c) h=400 mm, b=100 mm, c=30 mm, t=2.5 mm, a=b/2.

Figure 3.8 Comparison of moment correction factors between the present and EN1993-1-3 models. In EN1993-1-3, K is calculated using Eq.(3-25), while in EN1993-1-3*, $K=k_\phi/h^2$ is used.

In the EN1993-1-3 model, the bending stress σ_{x2} is calculated based on a simplified beam model on an elastic foundation. The lateral displacement of the simplified beam is twice the lateral displacement of the purlin defined by Eq.(3-12) because of the lateral restraint applied at the upper flange-web junction. By using the lateral displacement derived in the present model, the bending stress σ_{x2} based on the simplified beam model can be expressed as follows,

$$\sigma_{x2}(x,y,z) = -E\frac{d^2(2v)}{dx^2}(y-\bar{y}) \tag{3-26}$$

Substituting Eq.(3-12) into (3-26), it yields,

$$\sigma_{x2}(\frac{l}{2}, y, z) = -\frac{k_R k_h M_{y,\max}}{I_{eq}}(y - \bar{y}) \tag{3-27}$$

Comparison of Eqs.(3-22) and (3-27) indicates that, apart from the difference in the moment correction factors, the second moments of cross-section area used to calculate the bending stress in the present and the EN1993-1-3 models are also different. Figure 3.9 shows the variation of the ratio of the equivalent second moment of cross-section area I_{eq} used in the present model and that I_{fz} used in the EN1993-1-3 model for 60 zed-sections of different sizes (see Appendix A) produced by a UK manufacturer (Albion Section Ltd, 2008). The figure shows that for all sections the second moment of cross-section area employed in the EN1993-1-3 model is smaller than the equivalent second moment used in the present model. This indicates that the bending stress calculated using the EN1993-1-3 model will be higher. Note that the increase in web length involved in I_{fz} does not simply scale down or scale up the bending stress in the flange. This is because although it increases the value of I_{fz}, it also changes the position of the neutral axis and thus alters the stress distribution pattern in the flange. In the literature there is some argument about how to choose a suitable web length to be included in the beam-column model for calculating the out-of-plane bending stress. In the Australian design codes (AS/NZS, 2005), for example, it is suggested that 35% of the total web length is used, instead of the 20% of the total web length used in EN1993-1-3, in the beam-column model.

The third difference between the present and the EN1993-1-3 models is the coordinates used to calculate the bending stress in Eqs. (3-20) and (3-22). The EN1993-1-3 model

does not take into account the warping stress, whereas the present model does. Figure 3.10 shows a comparison of the bending stresses generated by the lateral displacement v due to the lateral load $-k_h q_z$ along the lip, flange and web lines, obtained from the two models. It also shows a combined influence of the second moment of cross-section area and the coordinate employed in the model. For simple comparison purposes, the correction factor in both models is not applied (that is, $k_R = k_R^* = 1$) and the stresses are normalised by using the maximum value of σ_{x1}. It can be seen from the figure that the EN1993-1-3 model predicts higher stresses in the flange, web and most part of the lip than the present model does. It is only in the small part of the lip where the stresses predicted by the EN1993-1-3 are lower than those predicted by the present model. It should be noted that the safety factor is not applied for the present and EN1993-1-3 models when consider the comparison of analysis. However, in practice the safety factor is needed for design purpose.

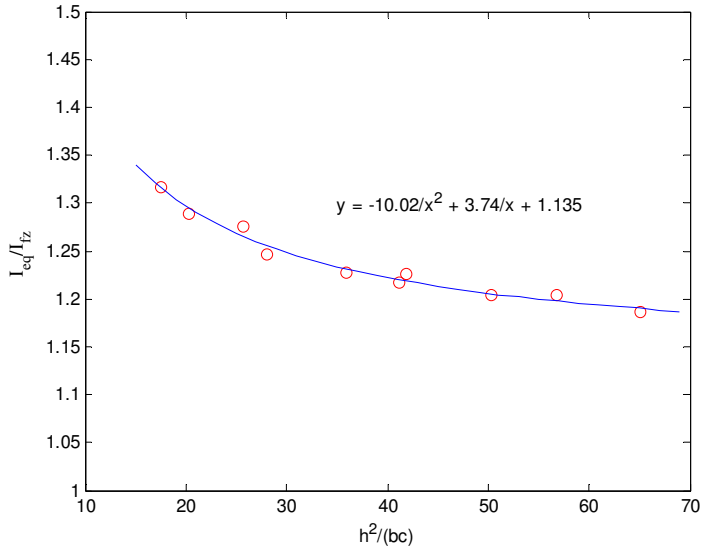

Figure 3.9 Ratio of the equivalent second moments of cross-section area used in the present (I_{eq}) and the EN1993-1-3 (I_{fz}) models for 60 zed-sections.

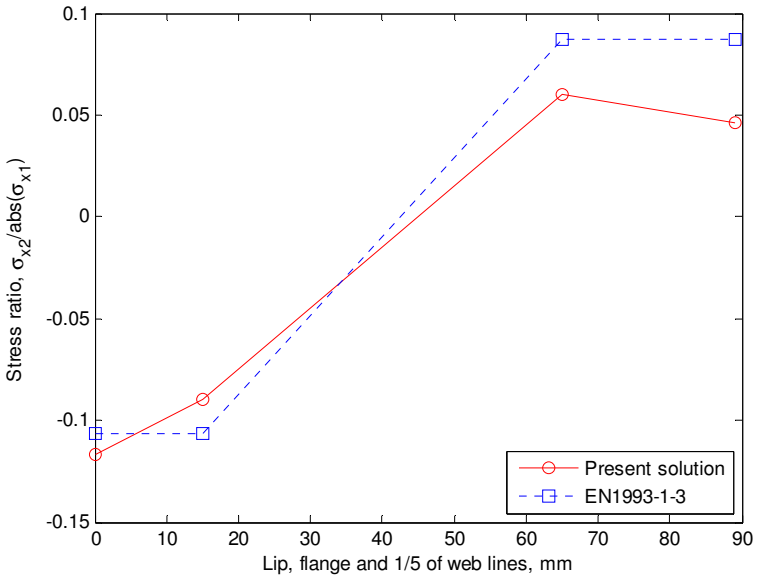

(a) h=120 mm, b=50 mm, c=15 mm, t=1.5 mm and a=b/2.

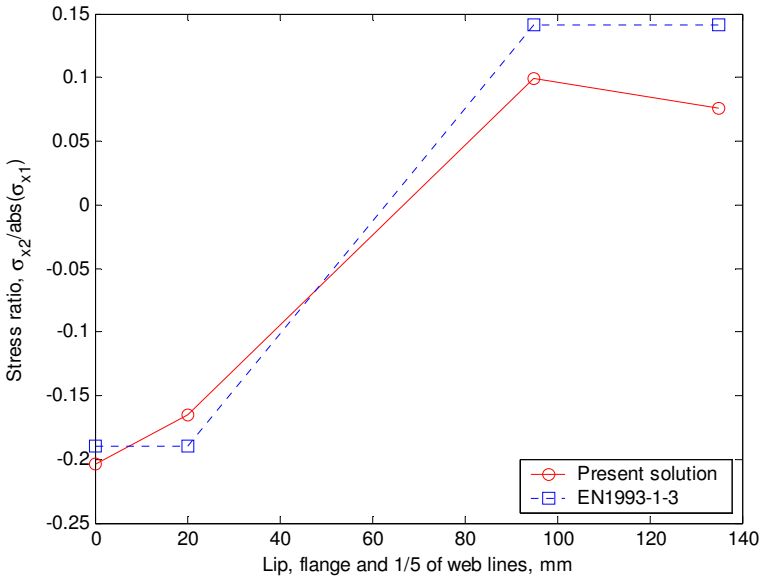

(b) h=200 mm, b=75 mm, c=20 mm, t=2 mm, and a=b/2.

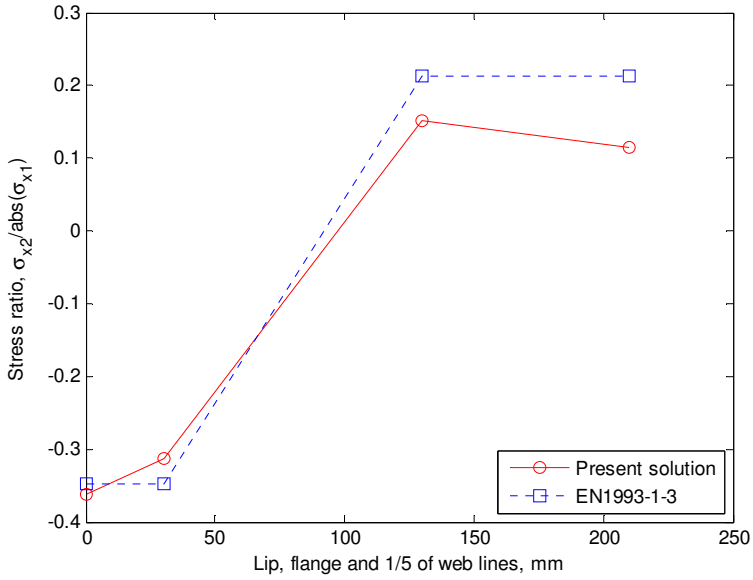

(c) h=400 mm, b=100 mm, c=30 mm, t=2.5 mm, and a=b/2.

Figure 3.10 Bending stress distribution along the lip, flange and web lines (abscissa starts from the tip of lip and ends at 1/5 of the web length).

3.4 Pre-buckling stress analysis of channel-sections

3.4.1 Analytical model and calculation

Consider a channel-section purlin that is subjected to a uniformly distributed uplift load acting on the middle line of the upper flange and is partially restrained by the sheeting which is simplified as a lateral restraint and a rotational restraint on its upper flange. For most types of sheeting the lateral restraint is sufficiently large and therefore the lateral displacement at the upper flange-web junction may be assumed to be fully restrained. The

rotational restraint, however, is dependent on the dimensions of sheeting and purlin, and on the number, type and position of the screws used in the fixing. The rotational spring is created to simulate the stiffness of the rotational restraint by the sheeting. Consequently, the purlin-sheeting system may be idealised as a purlin with lateral displacement fully restrained and rotation partially restrained at its upper flange-web junction. Figure 3.11 shows an analytical model for a channel-section purlin-sheeting system.

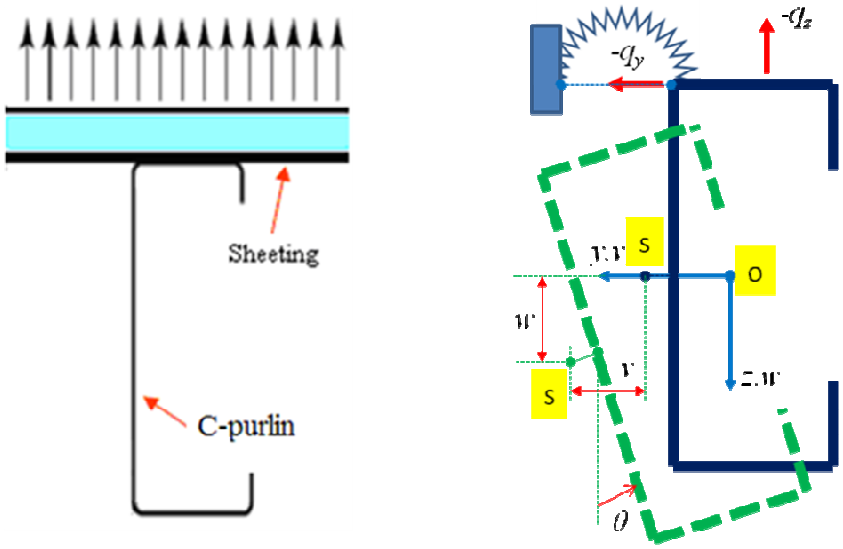

Figure 3.11 Analytical model used for a channel-section purlin-sheeting system.

Let the origin of the coordinate system (x,y,z) be the centroid of the channel cross-section, with the x-axis being along the longitudinal direction of the beam, and the y- and z-axes taken in the plane of the cross-section, as shown in Figure 3.11. According to the classical bending and torsion theory of beams, the equilibrium equations, expressed in terms of displacements, are given as follows,

$$EI_z \frac{d^4 v}{dx^4} = q_y \tag{3-28}$$

$$EI_y \frac{d^4 w}{dx^4} = q_z \tag{3-29}$$

$$EI_w \frac{d^4 \phi}{dx^4} - GI_T \frac{d^2 \phi}{dx^2} + k_\phi \phi = z_k q_y - y_q q_z \tag{3-30}$$

Using Eq.(3-28) to eliminate q_y and Eq.(3-29) to eliminate w in Eq.(3-30), it yields,

$$EI_w \frac{d^4 \phi}{dx^4} - GI_T \frac{d^2 \phi}{dx^2} + k_\phi \phi - z_k EI_z \frac{d^4 v}{dx^4} = -y_q q_z \tag{3-31}$$

Note that the lateral displacement restraint applied at the upper flange-web junction requires as shown in Eq.(3-5).

Using Eq.(3-5) to eliminate the angle of twisting, ϕ, in Eq.(3-31), it yields,

$$\left(I_z + \frac{I_w}{z_k^2} \right) \frac{d^4 v}{dx^4} - \frac{GI_T}{Ez_k^2} \frac{d^2 v}{dx^2} + \frac{k_\phi}{Ez_k^2} v = \frac{y_q q_z}{Ez_k} \tag{3-32}$$

Let

$$a_0 = \frac{k_\phi}{Ez_k^2} \tag{3-33}$$

$$a_1 = \frac{GI_T}{Ez_k^2} \tag{3-34}$$

$$a_2 = I_z + \frac{I_w}{z_k^2} \tag{3-35}$$

With the use of Eqs.(3-33), (3-34) and (3-35), Eq.(3-32) can be rewritten into,

$$a_2 \frac{d^4 v}{dx^4} - a_1 \frac{d^2 v}{dx^2} + a_0 v = \frac{y_q q_z}{E z_k} \tag{3-36}$$

Eq.(3-36) is a fourth-order differential equation, which, under the boundary condition for simply supported beams, can be solved analytically.

The longitudinal stress at any point on the cross-section generated by the two displacement components and warping can be calculated using Eq.(3-13). The first term in the right hand side of Eq.(3-13) is the stress generated by the deflection of the beam in horizontal direction, the second term is the stress generated by the deflection of the beam in vertical direction, and the third term is the warping stress.

Using Eq.(3-5) to eliminate ϕ, Eq.(3-13) can be rewritten into,

$$\sigma_x(x, y, z) = -Ez \frac{d^2 w}{dx^2} - E\left(y + \frac{\overline{\omega} - \omega}{z_k} \right) \frac{d^2 v}{dx^2} \tag{3-37}$$

Eq.(3-37) indicates that the total longitudinal stress in the beam can be split into two parts. One is the stress that is generated by load q_z when the beam is considered to be fully restrained in rotation and can be calculated using Eq.(3-17). The other is the stress that is generated by the lateral deflection of the beam and can be calculated as follows,

$$\sigma_{x2}(x, y, z) = -E\left(y + \frac{\overline{\omega} - \omega}{z_k} \right) \frac{d^2 v}{dx^2} \tag{3-38}$$

For a simply supported beam in both the *y*- and *z*-directions, the bending stress σ_{x1} can be expressed as Eq.(3-19), and by solving the differential Eq.(3-36) analytically and then substituting the solution into Eq.(3-38). This yields,

(1) Rotation partially restrained case, when $k_\phi \neq 0$

$$\sigma_{x2}(\frac{l}{2}, y, z) = \left(y + \frac{\omega - \overline{\omega}}{z_k} \right) \left(\frac{A(\beta_1^{\,2} + \beta_2^{\,2})^2}{\beta_1 \beta_2 (A^2 + B^2)} \right) \frac{y_q q_z}{2 z_k a_0} \tag{3-39}$$

(2) Rotation free case, when $k_\phi = 0$

$$\sigma_{x2}(\frac{l}{2}, y, z) = \left(y + \frac{\omega - \overline{\omega}}{z_k} \right) \frac{8 y_q z_k E M_{y,\max}}{l^2 G I_T} \left[\sec h \left(\frac{l}{2} \sqrt{\frac{a_1}{a_2}} \right) - 1 \right] \tag{3-40}$$

where *A*, *B*, β_1 and β_2 are the constants defined as follows,

$$A = \sin \frac{\beta_2 l}{2} \sinh \frac{\beta_1 l}{2} \tag{3-41}$$

$$B = \cos \frac{\beta_2 l}{2} \cosh \frac{\beta_1 l}{2} \tag{3-42}$$

$$\beta_1 = \left(\frac{1}{2} \sqrt{\frac{a_0}{a_2}} + \frac{1}{4} \frac{a_1}{a_2} \right)^{\frac{1}{2}} \tag{3-43}$$

$$\beta_2 = \left(\frac{1}{2} \sqrt{\frac{a_0}{a_2}} - \frac{1}{4} \frac{a_1}{a_2} \right)^{\frac{1}{2}} \tag{3-44}$$

For given dimensions of a section, one can use Eq.(3-39) or (3-40) to calculate the longitudinal stress at any coordinate point (y, z).

3.4.2 Comparison with EN1993-1-3

As described in section 3.4.2, in the Eurocode (EN1993-1-3, 2006), Eqs.(3-19) and (3-22) represent the bending stress of the channel-section purlin with lateral displacement fully restrained and rotation partially restrained at the upper flange-web junction, in which the bending stress is calculated from the combination of the beam bent only in the plane of the web, and the bending consisting of the lip and flange plus 1/5 of web height bent about an axis parallel to the z-axis, and k_R^* is the moment correction factor considering the influence of the rotation restraint, defined as Eqs.(3-23), (3-24), (3-25) and (3-45),

$$k_h = -\frac{y_q}{2z_k} \tag{3-45}$$

The nomenclature has already been defined in section 3.4.1. However, for a channel-section, the shear centre and the centroid are not in the same position and therefore it should be noted that $I_{fz\_Channel}$ is the second moment of the cross-section area of the compression part about the z*-axis, and $\bar{y}'$ is the horizontal distance between the z- and z*-axes as defined in Figure 3.12,

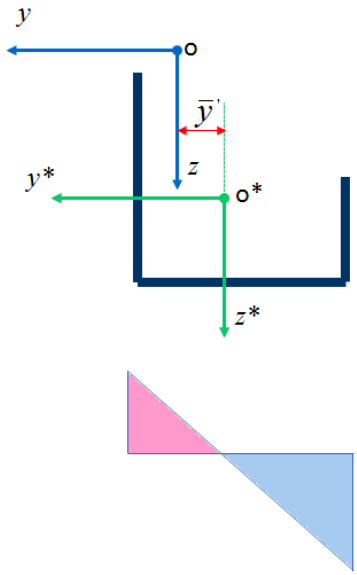

Figure 3.12 Bending stress calculated in accordance with EN1993-1-3.

Upper: Compression part consisting of lip and flange plus 1/5 of web length.

Lower: Stress distribution due to the bending about the z* axis.

For the convenience of comparison, Eq.(3-39) is now rewritten into the following format:

$$\sigma_{x2}(\frac{l}{2}, y, z) = \frac{k_R k_h M_{y,\max}}{I_{eq}}\left(y + \frac{\omega - \overline{\omega}}{z_k}\right) \tag{3-46}$$

in which,

$$k_R = \frac{8 I_{eq}}{a_0 l^2}\left(\frac{A(\beta_1^{\ 2} + \beta_2^{\ 2})^2}{\beta_1 \beta_2 (A^2 + B^2)}\right) \tag{3-47}$$

$$I_{eq} = \frac{1}{4}\left(I_z + \frac{I_w}{z_k^2}\right) \tag{3-48}$$

The comparison of Eqs.(3-22) and (3-46) shows that there are three differences between the present model and the EN1993-1-3 model for calculating the longitudinal stress. The first is the moment correction factor used in calculating the lateral bending moment. The second is the second moment of cross-section area used to calculate the bending stress. The third is the lateral coordinate used to calculate the lateral bending stress (or the position of the neutral axis). Figure 3.13 shows the comparisons of the moment correction factors for channel-sections calculated from the present and EN1993-1-3 models. The main features of this figure are similar to those shown in Figure 3.8 and therefore are not discussed further.

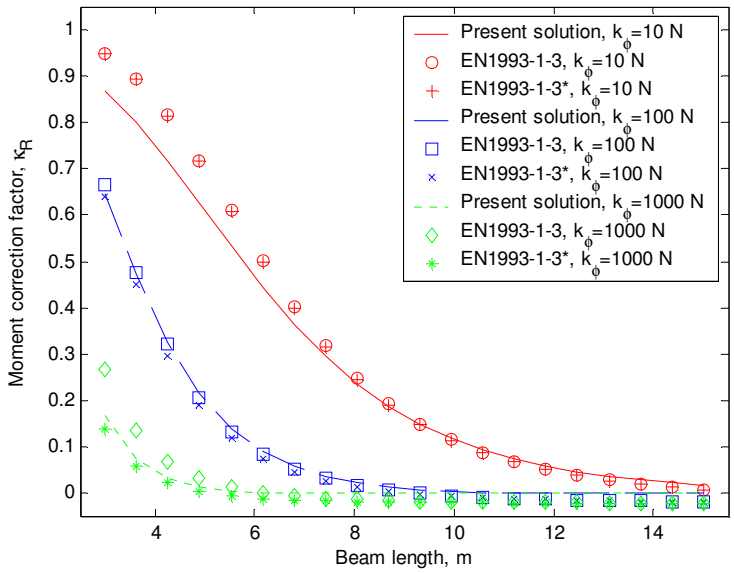

(a) h=120 mm, b=50 mm, c=15 mm, t=1.5 mm, a=b/2.

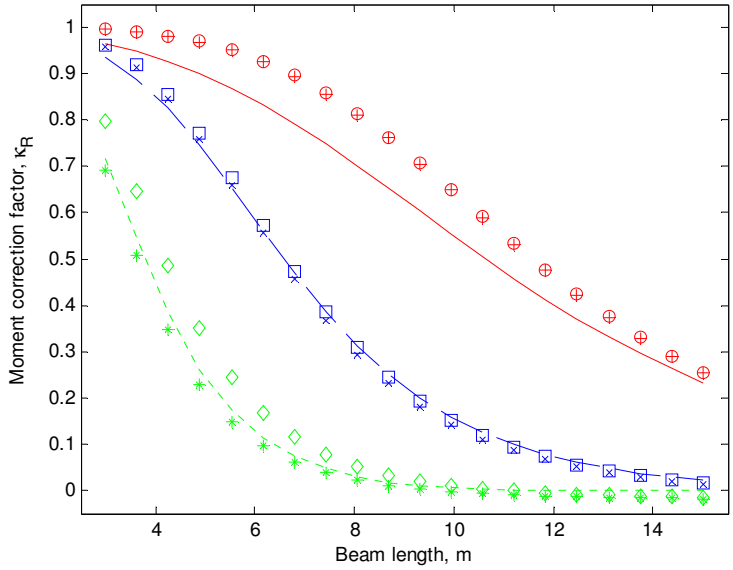

(b) h=200 mm, b=75 mm, c=20 mm, t=2 mm, a=b/2.

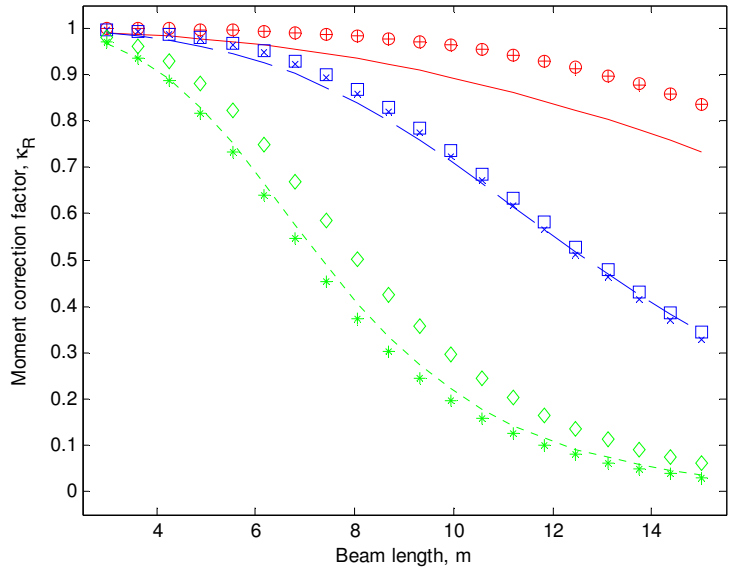

(c) h=400 mm, b=100 mm, c=30 mm, t=2.5 mm, a=b/2.

Figure 3.13 Comparison of moment correction factors between the present and EN1993-1-3 models. In EN1993-1-3 K is calculated using Eq.(3-25), while in EN1993-1-3* (the section distortion is ignored), K= k_ϕ/h^2 is used.

Figure 3.14 shows the variation of the ratio of the equivalent second moment of cross-section area I_{eq} used in the present model and that I_{fz} used in the EN1993-1-3 model for 60 channel-sections of different sizes (see Appendix A) produced by a UK manufacturer (Albion Section Ltd, 2008). Again, as with the zed-section, the equivalent second moment I_{eq} used in the present model is greater than the second moment I_{fz} of cross-section used in the EN1993-1-3 model, indicating that the bending stress calculated using EN1993-1-3 model will be higher.

Another difference between the present and the EN1993-1-3 models is that the EN1993-1-3 model does not take into account the warping stress, whereas the present model does. Figure 3.15 shows a comparison of the bending stresses generated by the lateral displacement due to the lateral load $-k_h q_z$ along the lip, flange and web lines, obtained from the two models. The figure shows a combined influence of the second moment of cross-section area and coordinates used to calculate the bending stress in Eqs.(3-22) and (3-46). For comparison purposes, the correction factor in both models is not applied (that is, $k_R = k_R^* = 1$) and the stresses are normalised by using the maximum value of σ_{x1}. It can be seen from the figure that in the small section (C12515) and the intermediate section (C20720), the EN1993-1-3 model predicts higher stresses in the lip, web, and flange than the present model does. It is in the large section (C40125), only small part near the flange–web junction of the section where the stress predicted by the EN1993-1-3 is slightly lower than that predicted by the present model. This reveals that the EN1993-1-3 model is more conservative in predicting the bending stresses.

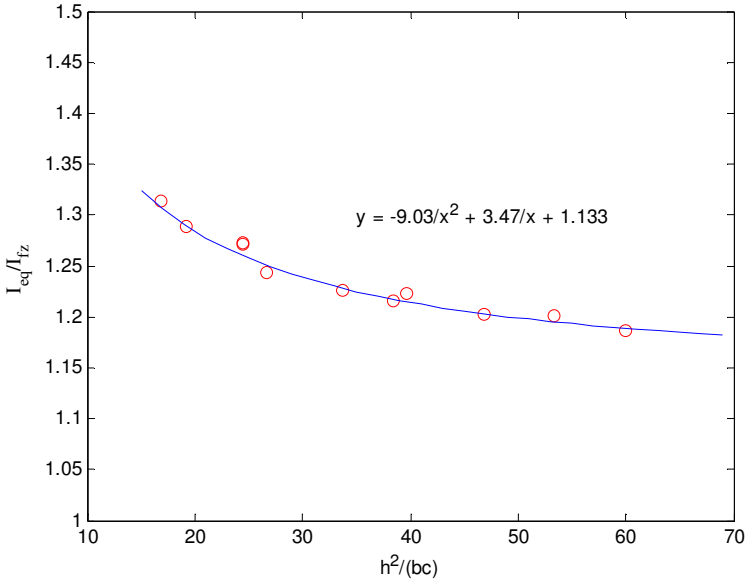

Figure 3.14 Ratio of the equivalent second moments of cross-section area used in the present (I_{eq}) and EN1993-1-3 (I_{fz}) models for 60 channel-sections.

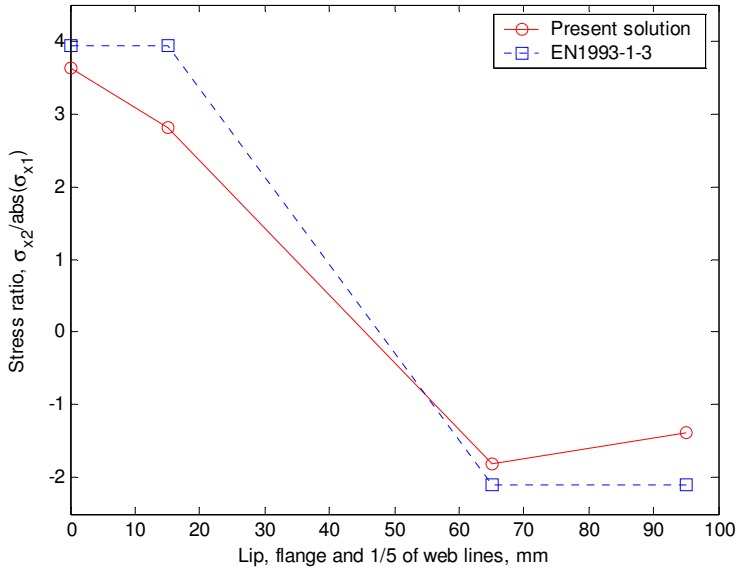

(a) h=120 mm, b=50 mm, c=15 mm, t=1.5 mm and a=b/2.

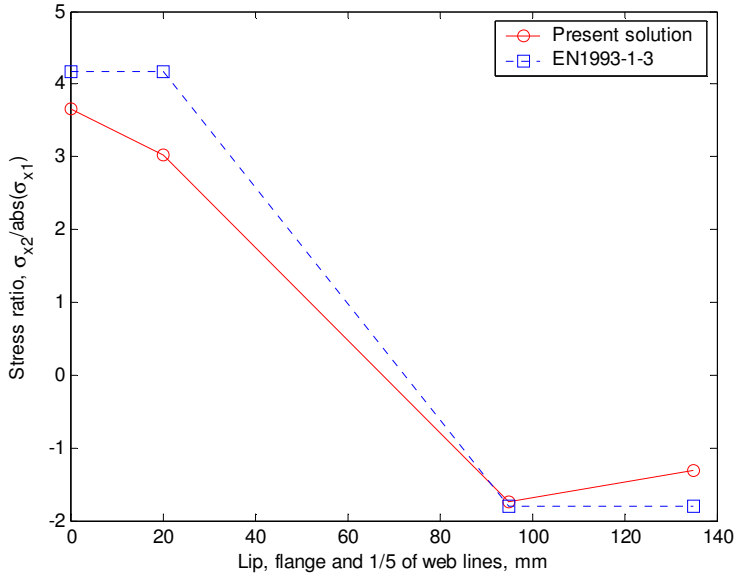

(b) h=200 mm, b=75 mm, c=20 mm, t=2 mm, and a=b/2.

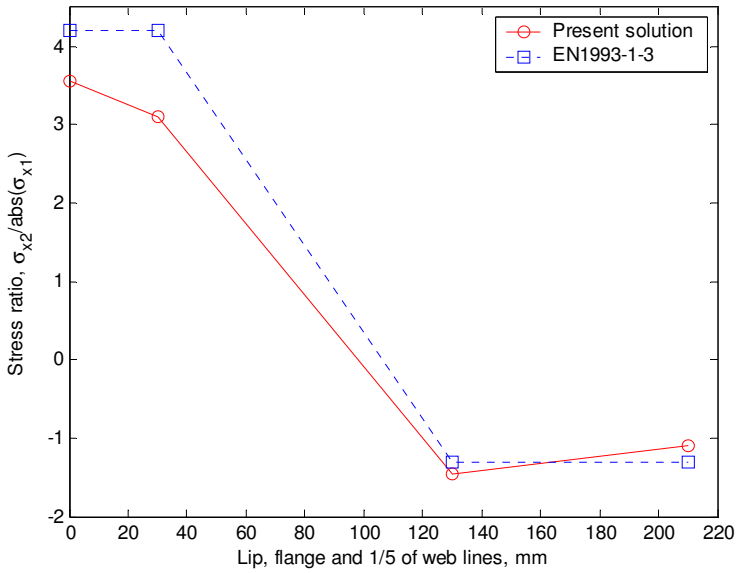

(c) h=400 mm, b=100 mm, c=30 mm, t=2.5 mm, and a=b/2.

Figure 3.15 Bending stress distribution along the lip, flange and web lines (abscissa starts from the tip of lip and ends at 1/5 of the web length).

3.5 Finite element model and analysis

The analysis of pre-buckling stress of cold-formed steel members involves the use of linear finite element analysis. The purpose of the analysis is to investigate the pre-buckling stress distribution of the zed- or channel-section purlins when subjected to uniformly distributed uplift loads, and to examine the pre-buckling structural behaviour of the cold-formed steel purlins. The analysis was performed using a commercial finite element package – ABAQUS.

3.5.1 Geometry

In order to simulate the model proposed herein, finite element analysis of a zed- (see Figure 3.16) or channel-section (see Figure 3.17) purlin beam of length *L*, web depth *h*, flange width *b*, lip length *c* and thickness *t* is performed for different values of rotational spring stiffness in several different beam lengths.

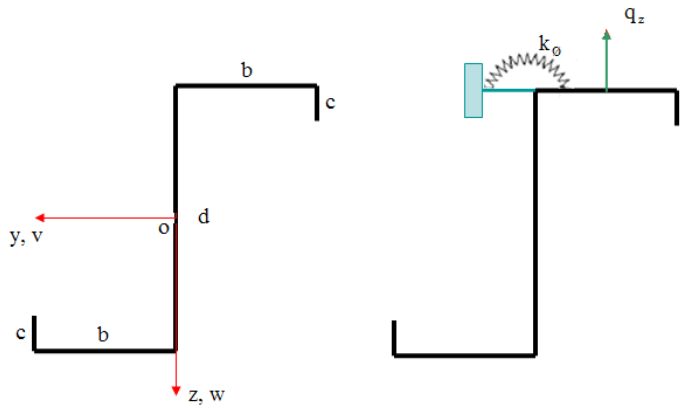

(a) Section dimensions (b) Uplift loading

Figure 3.16 Zed-section.

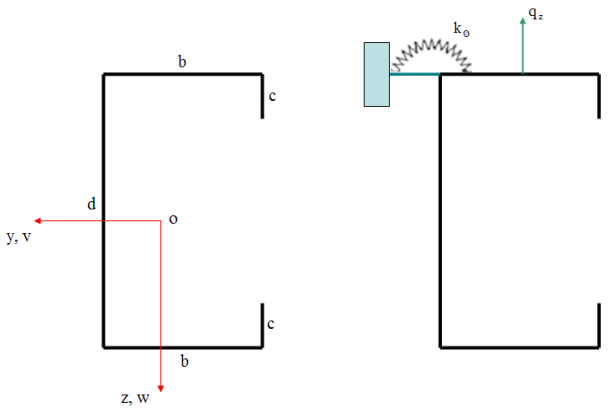

(a) Section dimensions (b) Uplift loading

Figure 3.17 Channel-section.

3.5.2 Material properties

The material properties of the purlin are assumed to be linear elastic with Young's modulus E=210 GPa and Poisson's ratio □=0.3. No plastic deformation is considered in the pre-buckling analysis.

3.5.3 Loads and boundary conditions

In reality, the wind pressure is transferred to the purlin flange via screw connections, and as the screw spacing is much smaller than the purlin span, it is rational to assume a line load acting on the middle of upper flange. Therefore, the member is assumed to be subjected to a transverse uniformly distributed uplift loading. Because of the symmetry, only half of the length of the beam is modelled. The boundary conditions at one end of the beam are assumed to be simply supported, in which the lateral and vertical components of the displacement of the web line are assumed to be zero. The boundary

conditions at the other end are assumed to have symmetric boundaries (i.e. $u=\phi_y=\phi_z=0$) about both vertical and lateral axes (see Figure 3.18).

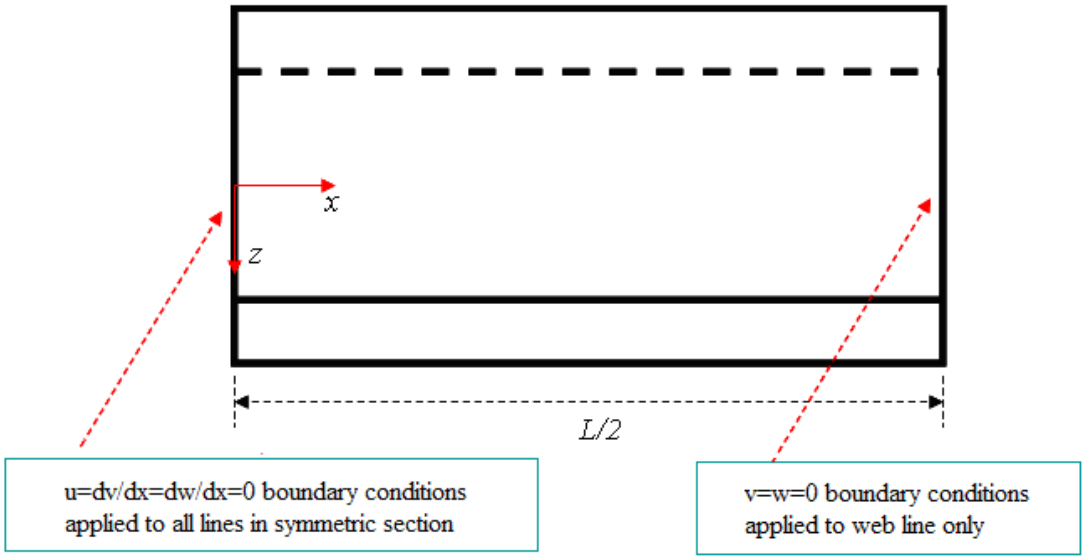

Figure 3.18 The boundary condition of half length of the beam model.

3.5.4 Restraints

Roof purlins and sheeting rails are usually restrained against lateral and rotational movement by their supported roof or wall cladding. The lateral component of the displacement at the line of the upper flange-web junction is assumed to be zero to simulate the lateral restraint provided by the sheeting. In addition, a uniformly distributed rotational spring is applied at the middle line of the upper flange to simulate the rotational restraint provided by the sheeting. Consider a zed- or channel-section that is partially restrained by the sheeting on its upper flange, several different rotational stiffnesses (k_ϕ=0, k_ϕ=300 N, and k_ϕ=750 N) are used in the analysis. These three stiffnesses represent the sheeting of weaker, normal and stronger rotational rigidity, respectively.

3.5.5 Finite element and corresponding element mesh

The finite element program ABAQUS is used to perform elastic linear buckling analysis for pre-buckling analysis, which is to determine the pre-buckling stress distribution along the lip, flange and web lines of the cross section. The four-node shell element of reduced integration scheme built in ABAQUS is employed to carry out the static linear analysis. The element used is a thin, shear flexible, isometric quadrilateral shell element. In order for the results obtained from the finite element analysis to be accurate enough, the element size used in the finite element mesh is kept to be 10 mm. Figure 3.19 shows the zed- and channel-section purlin typical meshes used in the analysis. In tests of numerical models with different meshes, it can be shown that this kind of mesh is accurate enough as any further reduction in element size (i.e. 5 mm) has negligible influence on the obtained results.

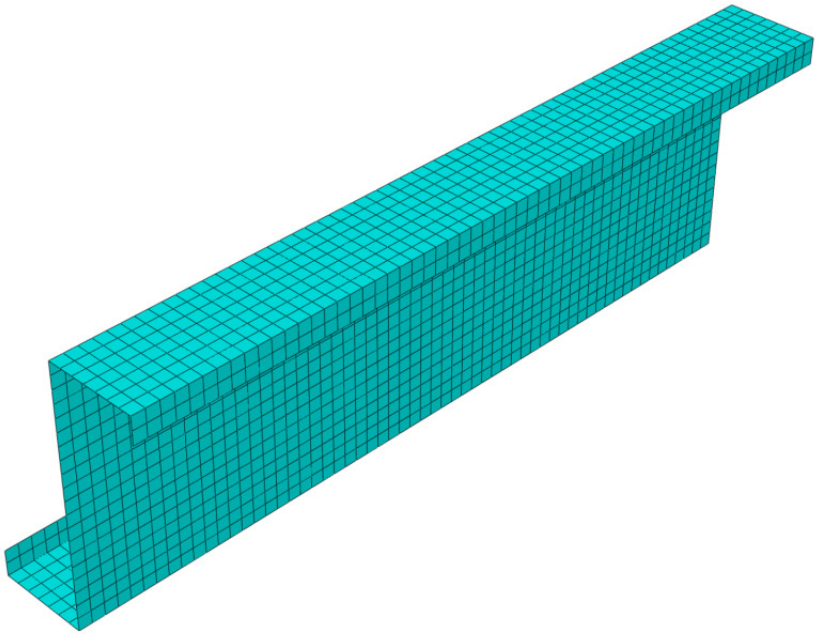

(a) Zed-section

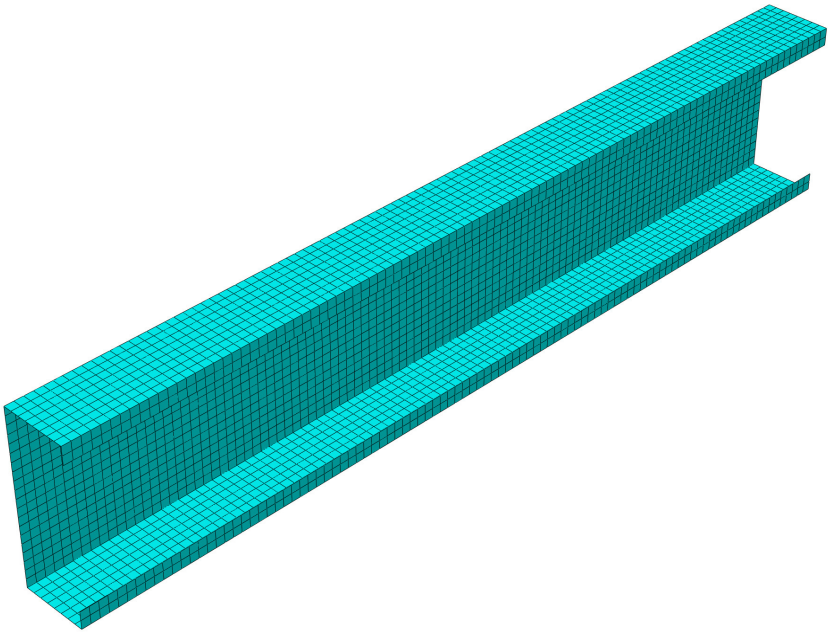

(b) Channel-section

Figure 3.19 Finite element mesh employed for the analysis of zed- and channel-section purlins.

3.5.6 Finite element analysis of zed-section

In order to validate the model proposed herein, finite element analysis of a zed-section purlin beam of web depth h=200 mm, flange width b=75 mm, lip length c=20 mm, and thickness t=2.0 mm is performed for three different values of rotational spring stiffness in four different beam lengths. Figure 3.20 shows the undeformed and deformed shapes of the partially restrained zed-section purlin under a uniformly distributed uplift load. The boundary condition of the half length beam model takes symmetry into account. Figure 3.21 shows a comparison of the total bending stresses obtained from the finite element analysis, the present and the EN1993-1-3 models. It can be seen from the figure that the total bending stresses are very close between the present and the EN1993-1-3 models.

The difference in the total bending stresses between the present model and the finite element analysis is mainly found in cases where the beam is short and the stiffness of the rotational spring is large. The former is because the overall bending stress of the beam is dominated by the bending stress σ_{x1}. The bending stress, σ_{x2} is only a small portion of the overall bending stress and thus the difference between the two models becomes unnoticeable when the stress is plotted as total stress ($\sigma_{x1}+\sigma_{x2}$). The latter is due to the use of the bending theory of beams in the present and the EN1993-1-3 models. For the short beam, the bending stresses calculated based on the classical bending theory of beams do not provide accurate stress distribution in the beam. This kind of inaccuracy is likely to be amplified by the involvement of the lateral displacement restraint and the rotational spring applied on the upper flange. The difference in the total bending stresses between the present model and the finite element analysis for long beams can be observed at the lip-flange junction but appears insignificant.

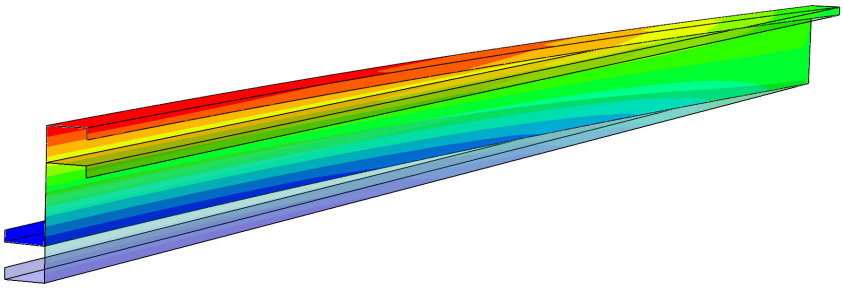

Figure 3.20 The undeformed and deformed shapes of the partially restrained purlin under uplift loading (Z20720, k_ϕ=300 N).

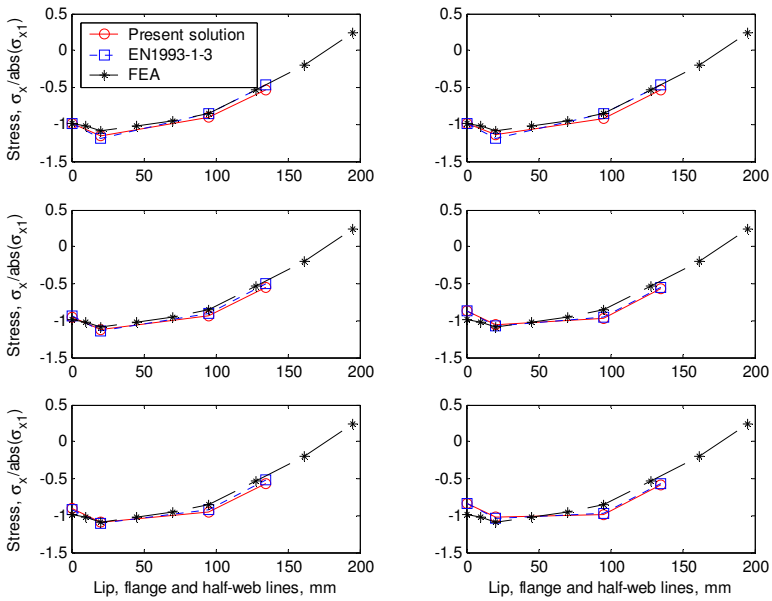

(a) L=4000 mm (b) L=6000 mm

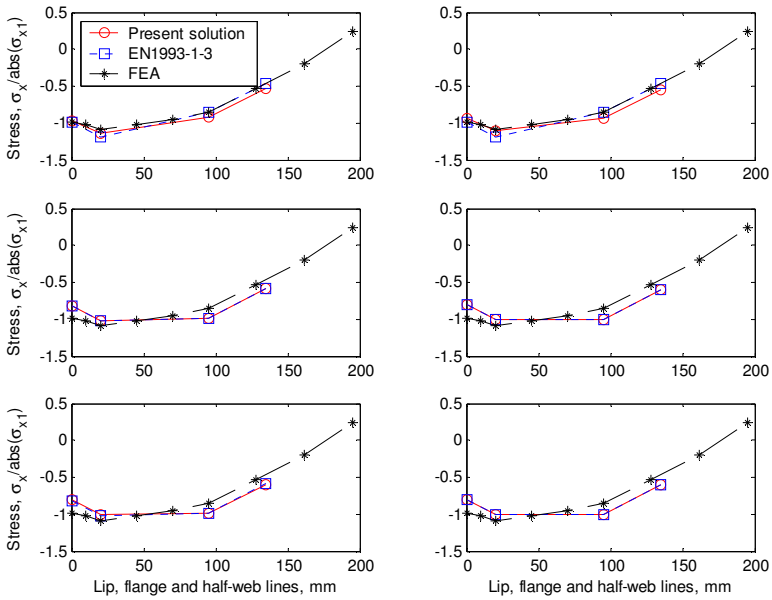

(a) L=8000 mm (b) L=12000 mm

Figure 3.21 Bending stress distribution along the lip, flange and web lines (abscissa starts from the tip of lip and ends at the half of web length, h=200 mm, b=75 mm, c=20 mm, t=2.0 mm, a=b/2). Top: k_ϕ=0. Middle: k_ϕ=300 N. Bottom: k_ϕ=750 N.

3.5.7 Finite element analysis of channel-section

The present model is validated by using both finite element analysis results and available experimental data. The experimental data are taken from Hancock and his colleagues' reports (Rousch and Hancock, 1997), which described a series of tests on simply supported channel-section purlins with screw-fastened sheeting under wind uplift loading, performed in a vacuum test rig. The section dimensions, material properties, loading conditions and boundary conditions employed are exactly the same as those used in the preceding sections. Figure 3.22 shows the comparison of total bending stresses and lateral deflections of the compression flange obtained from different models. Again, good agreement of the present model with the experimental data demonstrates that using the linear bending model and taking into account the warping torsion can provide a good prediction of the bending stresses of partially restrained channel-section purlins subjected to uplift loading. In contrast, the bending stress provided by the EN1993-1-3 model is likely to be over-predicted. Figure 3.23 shows the undeformed and deformed shape of a partially restrained channel-section purlin under a uniformly distributed uplift load (for a half-length of beam).

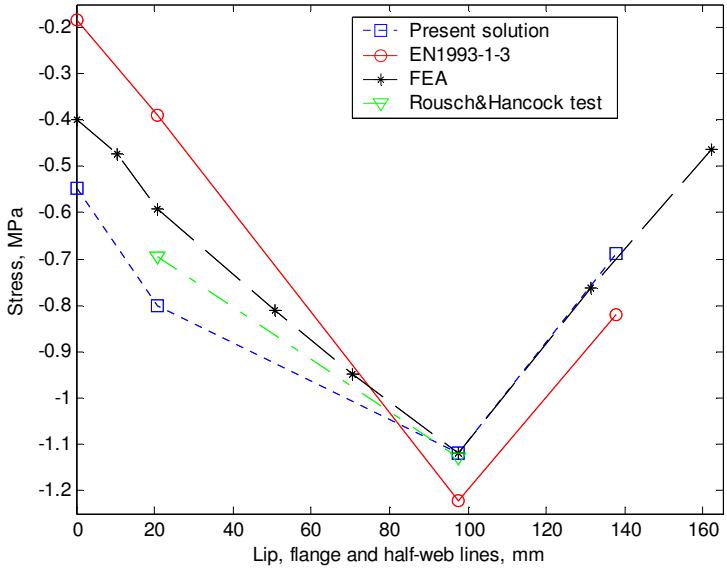

(a)

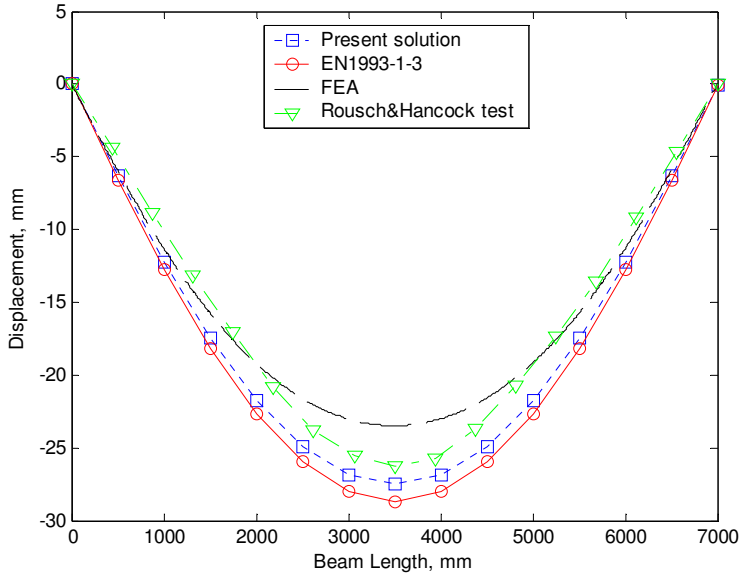

(b)

Figure 3.22 (a) Bending stress distribution along the lip, flange and web lines (abscissa starts from the tip of lip and ends at the half of the web length). (b) Lateral deflection at lower flange-web junction (h=202 mm, b=76.7 mm, c=20.8 mm, t=1.51 mm).

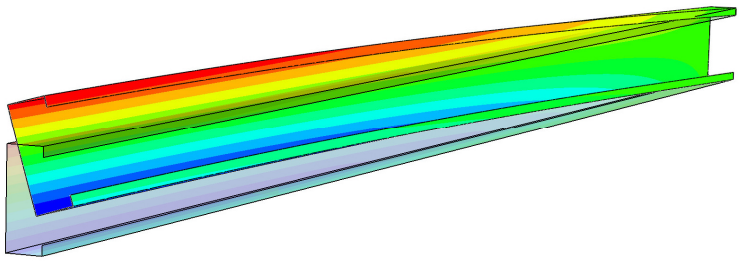

Figure 3.23 The undeformed and deformed shape of the partially restrained purlin under uplift loading (C20720, k_ϕ=300 N).

Figure 3.24 shows the detailed comparison of the total bending stresses obtained from the finite element analysis, the present model and the EN1993-1-3 model. It can be seen from the figure that the results predicted by the present model agree very well with the finite element analysis results. However, in most of the cases the results provided by the EN1993-1-3 model are over-conservative, particularly when the stiffness of the rotational spring is very small. Since the stresses plotted in Figure 3.24 are normalised by the maximum bending stress in the web plane, the variation of the stress along the compression flange reflects the contribution of the bending stress due to lateral deflection. It can be found from the figure that the lateral bending reduces the bending stress (or alters the stress direction from compression to tension) near the flange and lip junction, but increases the bending stress near the flange and web junction. The extent of the reduction or increase in stresses is dependent on the stiffness of the rotational spring. The greater the stiffness of the rotational spring, the smaller the stress contributed by the lateral bending. It is noticed from Figure 3.24 that the contribution of the lateral bending is very significant to the total longitudinal bending stress, particularly when the stiffness of the rotational spring is small.

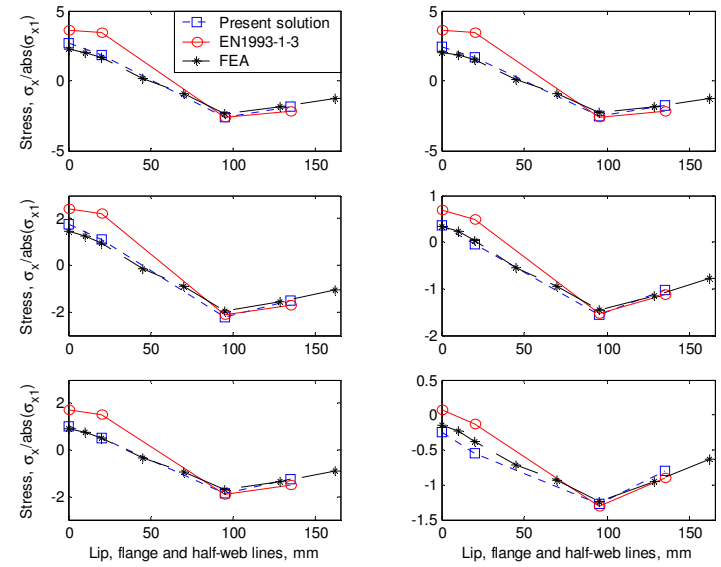

(a) L=4000 mm (b) L=6000 mm

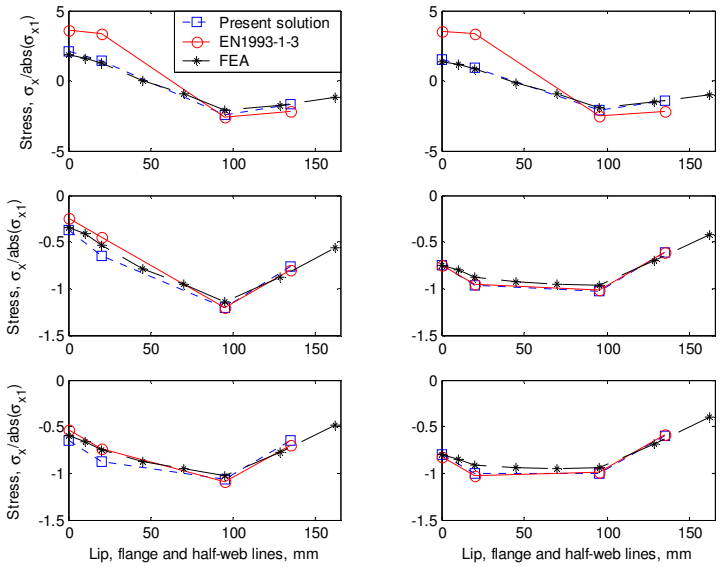

(c) L=8000 mm (d) L=12000 mm

Figure 3.24 Bending stress distribution along the lip, flange and web lines (abscissa starts from the tip of lip and ends at the half of web length, h=200 mm, b=75 mm, c=20 mm, t=2.0 mm, a=b/2). Top: k_ϕ=0. Middle: k_ϕ=300 N. Bottom: k_ϕ=750 N.

3.6 Summary

This chapter has presented an analytical model which describes the bending and twisting behaviour of partially restrained cold-formed steel purlins when subjected to uplift loading. Formulae to calculate the bending stresses of roof purlins have been derived using the classical bending theory of thin-walled beams. Some important conclusions drawn from the study shown in this chapter can be summarised as follows:

1. For zed- and channel-sections, comparisons of the results show good agreement between cleat bolted supported and web simply supported boundary conditions. The idealised boundary conditions proposed in the present study represent the standard two-hole cleat support conditions used for pre-buckling stress analysis.

2. Detailed comparisons of zed- and channel-section have been made between the present model and the simplified model proposed in Eurocode (EN1993-1-3), and have shown that, although the bending stresses in the compression flange for the lateral bending are over-predicted by EN1993-1-3, the total bending stresses are still accurate enough, due to the bending stresses being dominated by the bending in the plane of the web rather than by lateral bending.

3. For zed-sections, the finite element analysis results have demonstrated that the total bending stresses predicted using the present and the EN1993-1-3 models are accurate for medium and long beams. Only for short beams with a high stiffness

of rotational spring, are the bending stresses in lip and part of the flange over-predicted by the two analytical models.

4. The results obtained from the present model have also shown that the longitudinal stress induced by lateral bending is significant for channel-section purlins. This additional stress may change the failure modes from lateral-torsional buckling to local or distortional buckling.

5. For channel-sections, detailed comparisons of bending stresses obtained from the finite element analysis, available experimental data, the present model and the EN1993-1-3 model are provided, which demonstrate that the linear bending model, taking into account warping torsion, can provide good predictions for the bending stresses of the sheeting-purlin system. However, for most cases, the results provided by the EN1993-1-3 model are over-conservative, particularly when the stiffness of the rotational spring is very small.

CHAPTER 4 BUCKLING ANALYSIS OF PURLIN-SHEETING SYSTEMS

4.1 Introduction

Local, distortional and lateral-torsional buckling are three different types of buckling mode which may occur in a cold-formed steel member. Local buckling is characterised by the plate-like flexural buckling of individual elements in the section. Distortional buckling is represented by the change of cross-sectional shape excluding local buckling. For a channel- or a zed-section this usually involves the rotation of the compression flange and lip about the flange-web junction. In lateral-torsional buckling, individual cross-sections rotate and translate but do not distort in shape. Since the 1970s there has been substantial research activity in the field of cold-formed structures which has led to much published work on the local, distortional and lateral-torsional buckling of cold-formed steel sections (see LaBoube (1986), Rhodes (1991), Yu (2000) and Hancock (2003) for example). The outcome of this has also led to new design specifications being developed recently in EN 1993-1-3 (2006), AISI (2005) and AS/NZS (2005).

In this chapter a numerical investigation is presented on the buckling behaviour of partially restrained cold formed steel zed- and channel-section purlins when subject to transverse distributed uplift loading. The investigation is performed numerically using

linear finite element methods. The buckling behaviour of zed- and channel-section purlins of different dimensions subjected to uplift loading under the influence of rotational spring stiffness applied on the middle of upper flange is examined. The finite element analysis model and results are validated with available experimental data.

4.2 Finite element analysis model and validation

4.2.1 *Finite element model validation*

In order to ensure the model chosen here is appropriate, analysis of an example for which experimental data are available is performed. The example analysed is a channel-section, which has web depth *d*, flange width *b*, lip length *c* and thickness *t* (see Figure 4.1 and Table 4.1). The channel-section member is fixed at both ends and subjected to pure compression. The experimental results of the channel-section were provided by Young et al. (1992). Table 4.2 provides a detailed comparison of the critical buckling stresses and buckling modes obtained from the experimental method and the present finite element analysis model. It can be seen from the table that the finite element analysis results are in good agreement with those obtained from experiments.

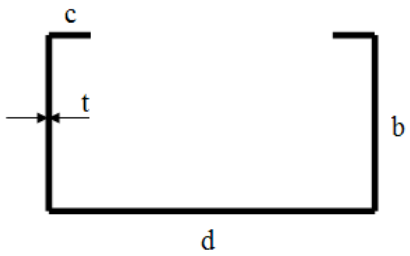

Figure 4.1 Simple lipped channel-section (Young et al., 1992).

Table 4.1 Measured test specimen dimensions simple lipped channel (Young et al., 1992).

Section	Web (mm)	Flange (mm)	Lip (mm)	Thickness (mm)	Length (mm)
CH1-5-800	119.55	89.65	4.8	1.085	800
CH1-6-800	119.80	89.75	6.0	1.085	800
CH1-7-800	120.50	89.50	7.0	1.100	800
CH1-7-600	120.40	89.55	7.0	1.095	600
CH1-7-400	120.80	89.70	7.0	1.095	400

Table 4.2 Comparison of buckling stress and buckling mode of simple lipped channel between experiment and finite element analysis.

Section	Buckling Stress		Buckling Mode	
	Test (MPa)	FEA (MPa)	Test	FEA
CH1-5-800	45.0	43.48	D(2)	D(2)
CH1-6-800	55.5	52.84	D(2)	D(2)
CH1-7-800	68.6	62.12	D(2)	D(2)
CH1-7-600	75.8	63.80	D(1)	D(1)
CH1-7-400	88.8	75.41	D(1)	D(1)

Note: D = Distortional buckling mode; ( ) = numbers of buckle half-wavelength.

4.2.2 *Influence of boundary conditions*

As described in chapter three that cleat bolted supported boundary condition has to use irregular meshes in the zones near the ends, which makes the analysis inefficient, an equivalent analytical boundary condition to the cleat bolted supported boundary condition has been established, which is the web simply supported boundary condition. The finite element model, material properties, loading conditions, shell element and size are the same with those used in chapter three and thus are not provided here again (see Figure 3.1).

Table 4.3 shows the detailed comparison of critical load factors and buckling modes of two zed-section purlins obtained from the web simply supported and cleat bolted supported boundary conditions. It can be seen from this table that the critical load factors are very close and the buckling modes are almost identical between these two boundary conditions. This suggests that the web simply supported boundary condition can be used to model the cleat bolted supported boundary condition for the buckling analysis due to

its convenience in mesh generation and its efficiency in analysis. Table 4.4 shows the similar comparison of results of channel-section purlins between these two boundary conditions. Again, good agreement in critical buckling loads and buckling modes is found between these two boundary conditions.

Table 4.3 Comparison of critical loads and buckling modes of zed-section purlins between two different boundary conditions

Section	Boundary Condition	Critical Load Factor	Buckling Mode
Z12515 $k_\phi = 0\,\mathrm{N}$	Web simply supported	1.471	LTB
	Cleat bolted supported	1.543	LTB
Z12515 $k_\phi = 750\,\mathrm{N}$	Web simply supported	10.542	LTB*
	Cleat bolted supported	10.777	LTB*
Z40132 $k_\phi = 0\,\mathrm{N}$	Web simply supported	0.087	LTB
	Cleat bolted supported	0.091	LTB
Z40132 $k_\phi = 750\,\mathrm{N}$	Web simply supported	5.501	LTB
	Cleat bolted supported	5.656	LTB

Note: LTB - Lateral-torsional buckling; LTB* - Secondary lateral-torsional buckling.

Table 4.4 Comparison of critical loads and buckling modes of channel-section purlins between two different boundary conditions

Section	Boundary Condition	Critical Load Factor	Buckling Mode
C12515 $k_\phi = 0\,\mathrm{N}$	Web simply supported	3.043	LTB
	Cleat bolted supported	3.132	LTB
C12515 $k_\phi = 750\,\mathrm{N}$	Web simply supported	11.631	LTB*
	Cleat bolted supported	11.891	LTB*
C40132 $k_\phi = 0\,\mathrm{N}$	Web simply supported	2.852	LB
	Cleat bolted supported	2.931	LB
C40132 $k_\phi = 750\,\mathrm{N}$	Web simply supported	3.779	LB
	Cleat bolted supported	3.854	LB

Note: LTB - Lateral-torsional buckling; LTB* - Secondary lateral-torsional buckling; LB – Local buckling.

4.3 Buckling analysis of zed-sections

4.3.1 Finite element model

For both zed- and channel-section purlins, the finite element model used for linear buckling analysis is similar to that used in the previous chapter for pre-buckling stress analysis. However, to examine both symmetric and asymmetric buckling modes, the full length of the beam needs to be considered. Hence, the boundary conditions used for buckling analysis are that the normal and tangential displacements of the web at each end of the member are zero, and the coordinate original point in one of the two end sections is restrained in the longitudinal axis of the member in order to eliminate the axial rigid displacement (see Figure 4.2). The other difference is that the option for analysis in ABAQUS buckling is chosen as the eigen-value analysis for linear analysis to determine the critical load at which the member has a bifurcation buckling, which is the first positive eigen-value times the applied load. The buckling mode is the corresponding eigenvector.

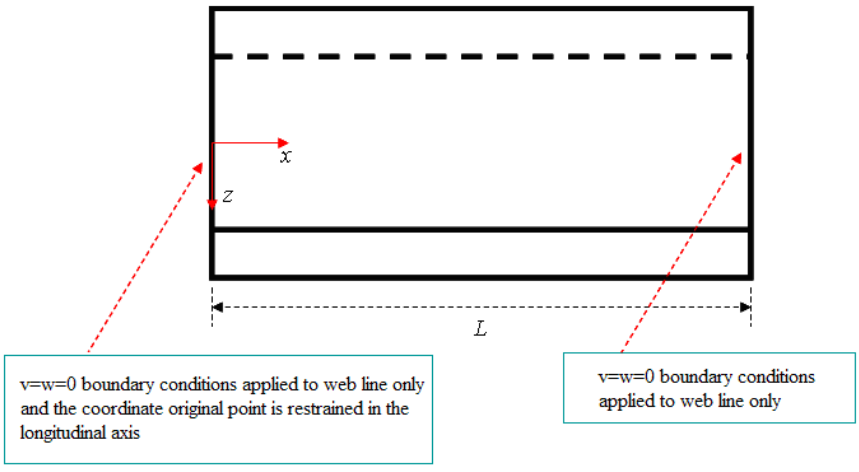

Figure 4.2 The boundary condition of full length of the beam model.

4.3.2 Influence of spring stiffness

For a given beam length, linear finite element analysis is performed from which the critical load of bifurcation buckling is obtained. Eq.(4-1) shows the critical load factor used for a beam.

$$\text{Critical load factor} = \frac{M_{cr}}{M_y} = \frac{q_{cr} L^2 d}{16 \sigma_y I_y} \tag{4-1}$$

where M_{cr} = the critical elastic buckling moment;

q_{cr} = the critical uniformly distributed load obtained from the linear finite element analysis;

σ_y = the yield stress which is taken as 390 N/mm^2 in this case;

L = the length of the beam.

It is seen from Figure 4.3 that, the critical load factor decreases with the increase of beam length when the rotation is unrestrained or partially restrained. However, when the rotation is fully restrained, the critical load factor increases with the member length until it reaches a certain length and then it decreases with increasing member length. The examination of the buckling modes reveals that there are several types of buckling. When the rotation is unrestrained, the buckling mode is only dominated by the lateral-torsional buckling of the free flange. However, when the rotation is fully restrained, the buckling mode is mainly controlled by distortional buckling of the compression flange and lip system where the member is longer than 6000 mm, and local buckling is occurring mainly where the member is shorter than 6000 mm. When the rotational spring provides

partial restrained, the main buckling is the lateral-torsional buckling, and a secondary lateral-torsional buckling also occurs largely in the members longer than 8000 mm for k_ϕ=300 N and 7000 mm for k_ϕ=750 N. This indicates that for zed-section purlins the rotational spring of the member has a significant influence on their buckling behaviour. Figure 4.4 shows typical buckling modes of members of different lengths, with different rotational spring stiffness values.

It should be mentioned here that secondary lateral-torsional buckling has a lower half-wavelength compared to the high half-wavelength found in lateral-torsional buckling. For lateral-torsional buckling, the half-wavelength is generally over 3000 mm, and buckling mode involves only one half-wavelength in the length of beam. Buckling mode is characterised by the rotation and translation of the section but no shape distortion. For secondary lateral-torsional buckling, the half-wavelength is just over 1000 mm, which is less than the length of beam. In general, secondary lateral-torsional buckling involves several half-wavelengths in the length of the beam. The former can be explained by the geometry of the cross section, which gives good flexural rigidity about one axis at the expense of low torsional rigidity and low flexural rigidity about a corresponding perpendicular axis. The latter is due to the flange distortional buckling and its interaction with lateral-torsional buckling. Figure 4.5 displays some typical modes of the secondary lateral-torsional buckling in beams of different lengths.

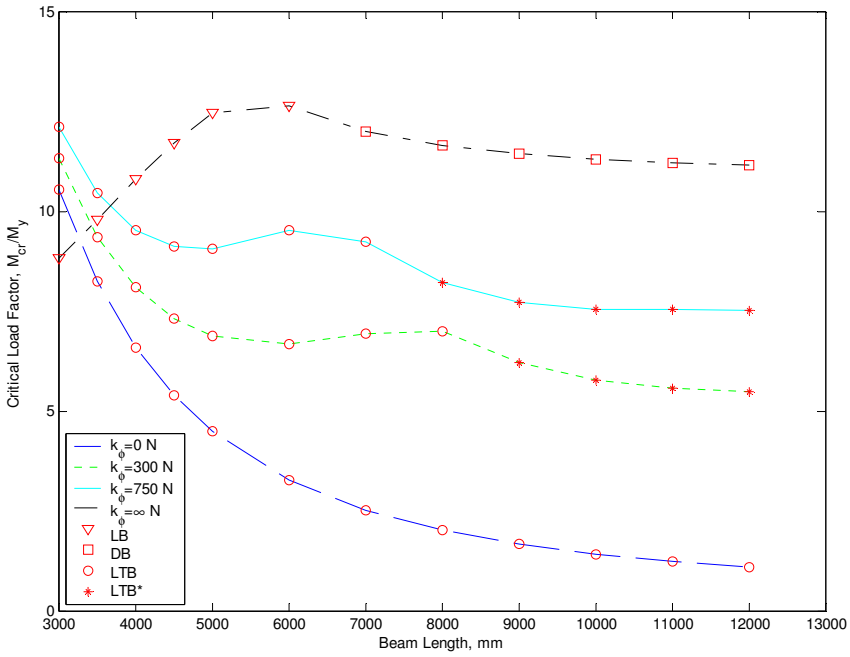

Figure 4.3 Critical load curve of simply supported zed-section with different rotational spring stiffness under uniformly distributed uplift loading (d=200 mm, b=75 mm, c=20 mm, t=2 mm) (LB = Local Buckling. DB = Distortional Buckling. LTB = Lateral-torsional Buckling. LTB* = Secondary Lateral-torsional Buckling).

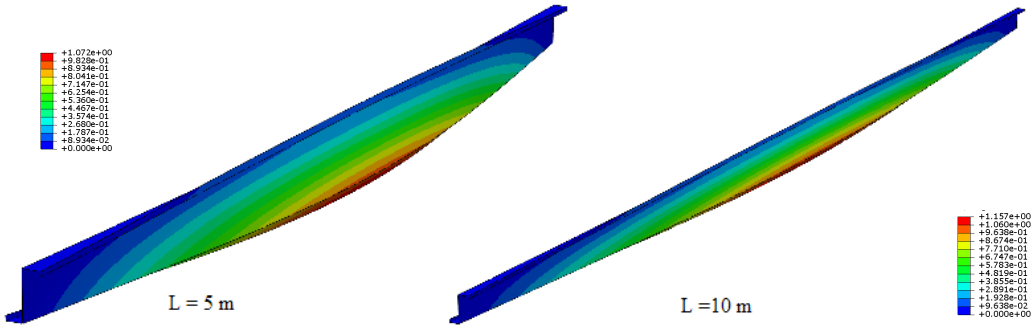

(a) k_ϕ =0 N

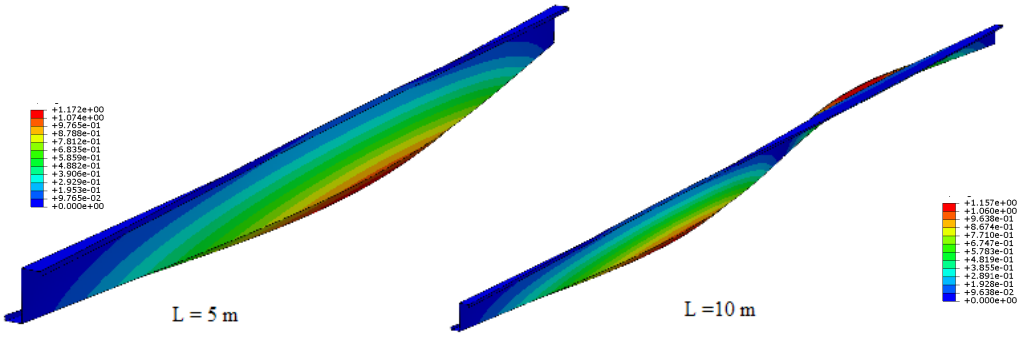

(b) k_ϕ =300 N

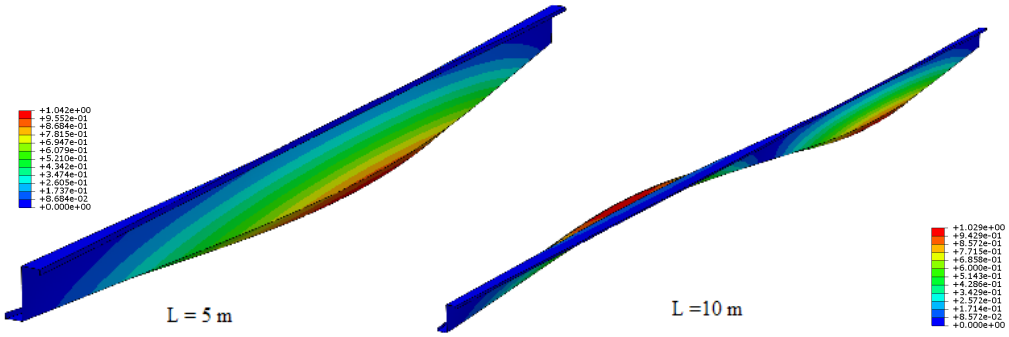

(c) k_ϕ =750 N

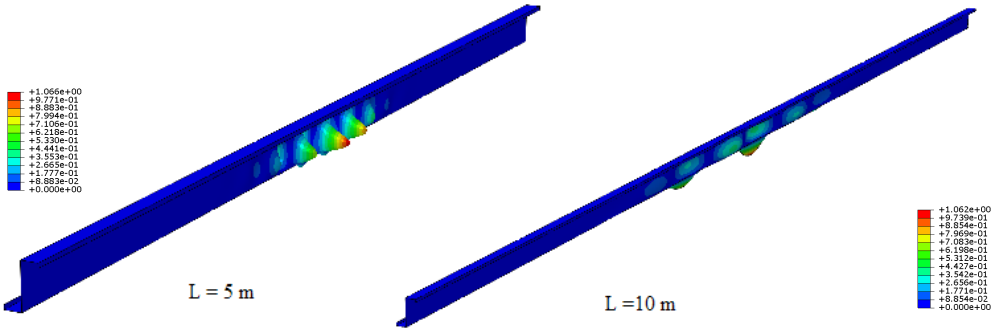

(d) k_ϕ =∞ N

Figure 4.4 Buckling modes of cold-formed steel members under four different rotational spring stiffness values

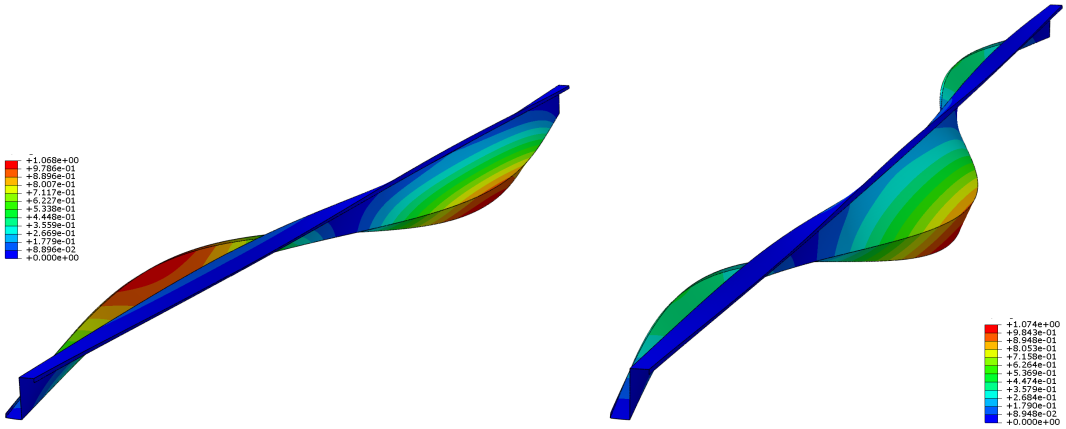

(a) L=8000 mm (b) L=12000 mm

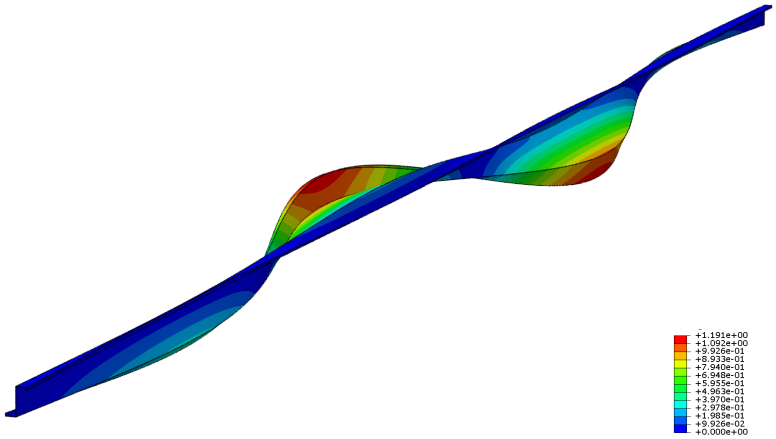

(b) L=18000 mm

Figure 4.5 Buckling modes of secondary lateral-torsional buckling in different beam lengths (d=200 mm, b=75 mm, c=20 mm, t=2 mm, k_ϕ =750 N).

4.3.3 Influence of the dimensions of cross section

In this section the influence of the section dimensions on the buckling behaviour of purlins with partial restraint, subjected to a uniformly distributed uplift load is investigated. Figure 4.6 shows the critical loads of purlins with three different dimensions

of cross sections (Z12515, Z20720 and Z40132). It can be seen from the figure that the critical load factor decreases with the increase of either beam length or the dimension of cross section. For the small section (Z12515), the first buckling mode is lateral-torsional buckling of the free flange. This buckling occurs mainly in the member whose length is less than 3500 mm. The second buckling mode is secondary lateral-torsional buckling, which occurs largely in members longer than 3500 mm. For the intermediate section (Z20720), the beam length between the lateral-torsional buckling and the secondary lateral-torsional buckling is 7000 mm. For the large section (Z40132), the main buckling mode is lateral-torsional buckling. Typical buckling modes of members of different dimensions are plotted in Figure 4.7.

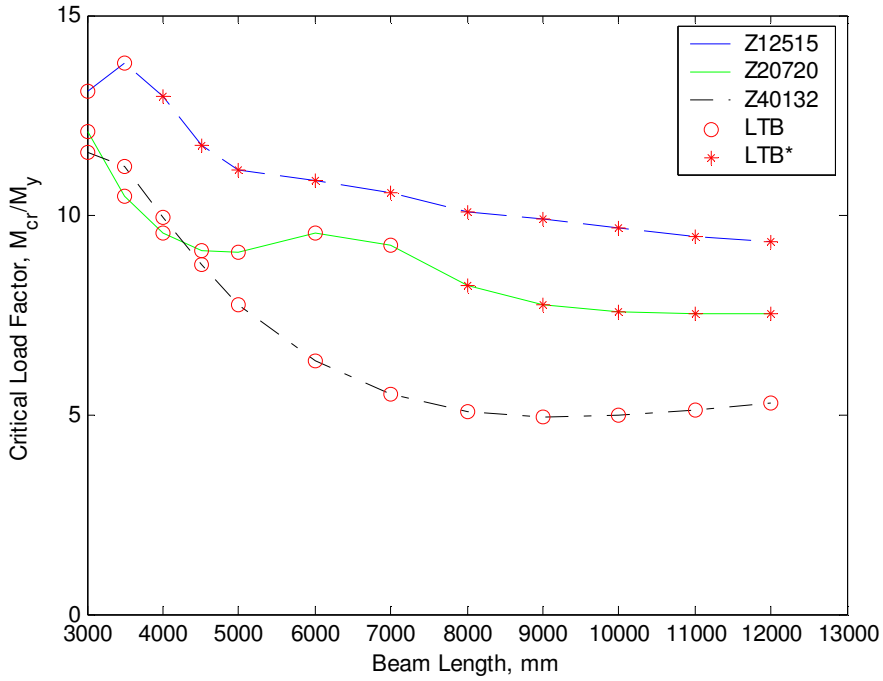

Figure 4.6 Critical load curve of simply supported zed-section with different section dimensions under uniformly distributed uplift loading (k_ϕ =750 N) (LTB = Lateral-torsional Buckling. LTB* = Secondary Lateral-torsional Buckling).

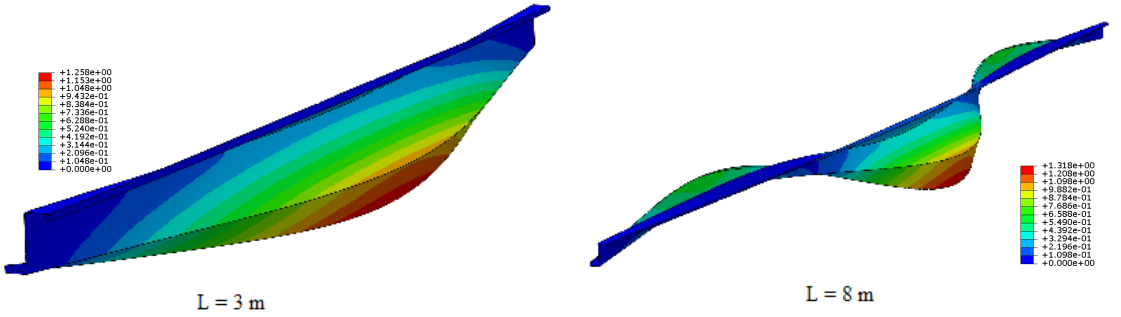

(a) Z12515

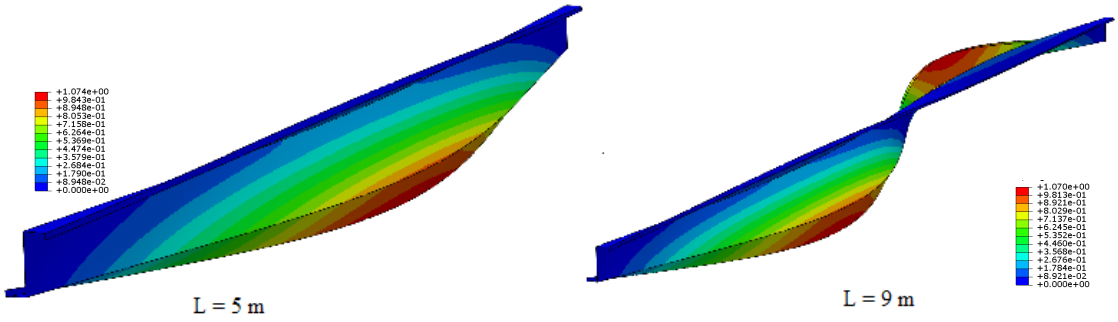

(b) Z20720

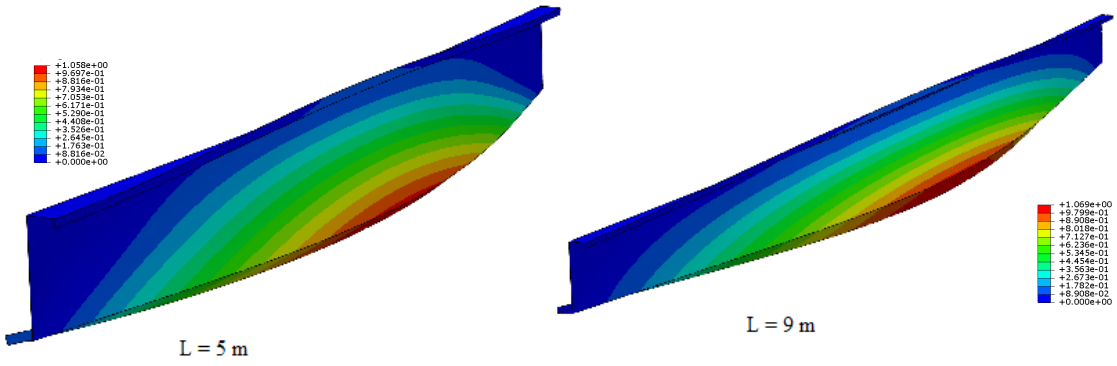

(c) Z40132

Figure 4.7 Buckling modes of cold-formed steel members of different beam length, with different cross section dimensions.

The parametric distribution of different buckling modes obtained from the finite element analysis for zed-section purlins with web depth to length ratio against different rotational spring stiffness values is shown in Figure 4.8. It is seen from this figure that, when k_ϕ=0, the buckling mode is dominated by lateral-torsional buckling. When k_ϕ=300 N or k_ϕ=750 N, for members low ratio of web depth to length, the buckling mode is dominated by secondary lateral-torsional buckling, whereas for members of intermediate and high ratio of web depth to length, the buckling modes are mainly controlled by lateral-torsional buckling. When k_ϕ=∞ N, the lateral-torsional buckling is prevented by the restraint, and secondary lateral-torsional buckling, distortional buckling and local buckling separate the ratio of web depth to length. This figure reveals that not only rotational spring stiffness has significant influence, but also the web depth and length has important impact on the buckling mode. It should be pointed out that, when purlin is under rotational restraint, secondary lateral-torsional buckling only appears at lower ratio of web depth to length. This can be explained by the interactions among rotational restraint, web depth and member length have influence on the half-wavelength of the purlin and also the compressive stress distribution at free flange.

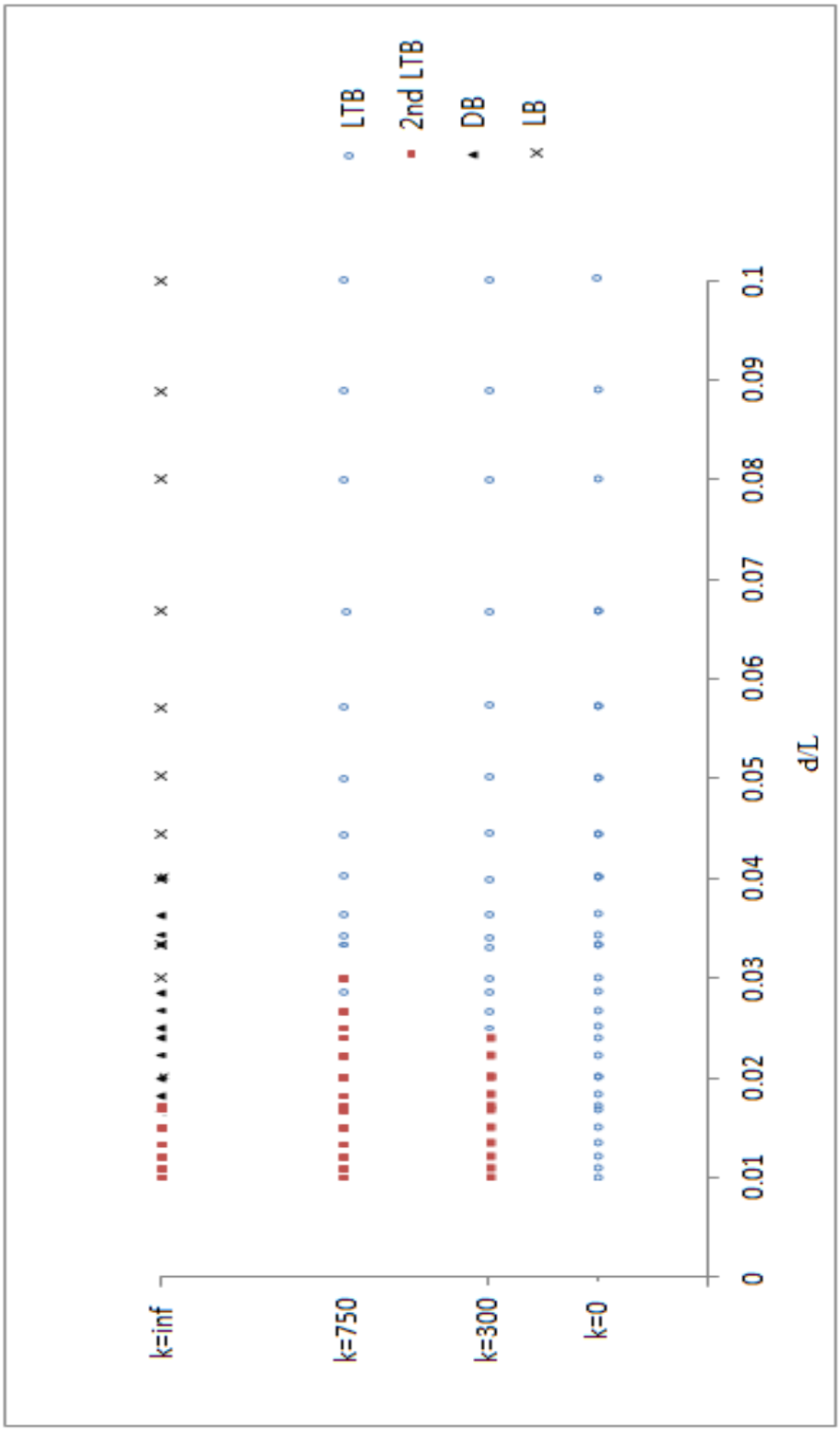

Figure 4.8 Parametric distribution of different buckling modes.

4.4 Buckling analysis of channel-sections

4.4.1 Influence of spring stiffness

For a channel-section beam with simply supported boundary conditions, the elastic critical moment, M_{cr}, of lateral-torsional buckling can be expressed as Eq.(4-2) (Laurence and Purkiss, 2007),

$$M_{cr} = C_1 \frac{\pi^2 EI_z}{L^2} \sqrt{\frac{I_w}{I_z} + \frac{(kL)^2 GI_t}{\pi^2 EI_z}} \tag{4-2}$$

where C_1 = the factor depending on the loading condition (for uniformly distributed load C_1=1).

Figure 4.9 shows the critical load curves obtained from the finite element analysis for a channel-section purlin with different rotational spring stiffness values. It can be seen from the figure that for all rotational spring stiffness values, the critical load increases with either beam length or the stiffness of rotational spring until it reaches a certain length and then it decreases with increasing member length. Examination of the buckling modes reveals that there are two different types of buckling modes in each curve. For short members, the buckling mode is dominated by local buckling of the web, whereas for long members, the buckling modes are mainly controlled by the distortional buckling of the lower flange and lip system when the rotation is fully restrained, and lateral-torsional buckling of the free flange when there is no rotational restraint. Again, the buckling modes of the secondary lateral-torsional buckling are also involved in the long members when the rotational spring stiffness is 300 N and 750 N, respectively. This

indicates that the rotational spring stiffness has significant influence on the buckling behaviour of long length purlins.

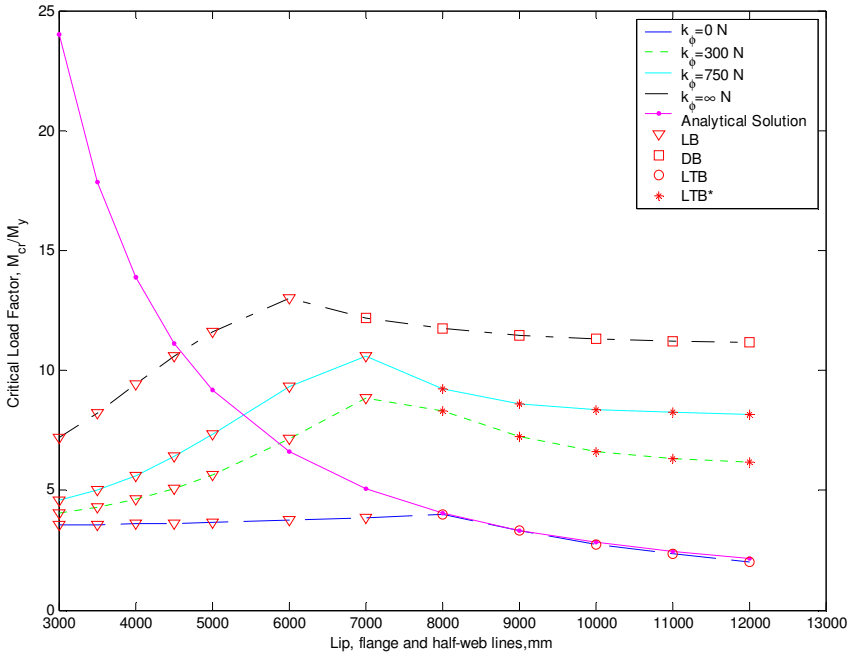

Figure 4.9 Critical load curve of simply supported channel-section with different rotational spring stiffness values under uniformly distributed uplift loading (d=200 mm, b=75 mm, c=20 mm, t=2 mm) (LB = Local Buckling. DB = Distortional Buckling. LTB = Lateral-torsional Buckling. LTB* = Secondary Lateral-torsional Buckling).

It can also be observed from Figure 4.9 that the numerical solution of k_ϕ=0 and the analytical solution provide an almost identical critical load for purlins greater than 8000 mm, but for purlins shorter than 8000 mm the results are different. The reason for this is that the analytical solution only provides the critical load of lateral-torsional buckling of the member. For purlins shorter than 8000 mm, the lowest buckling modes are not lateral torsional buckling, but local or distortional buckling modes. This is demonstrated by the buckling modes shown in Figure 4.10.

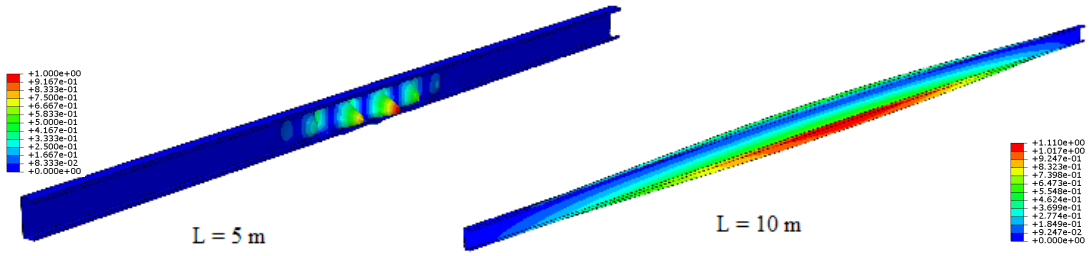

(a) k_ϕ =0 N

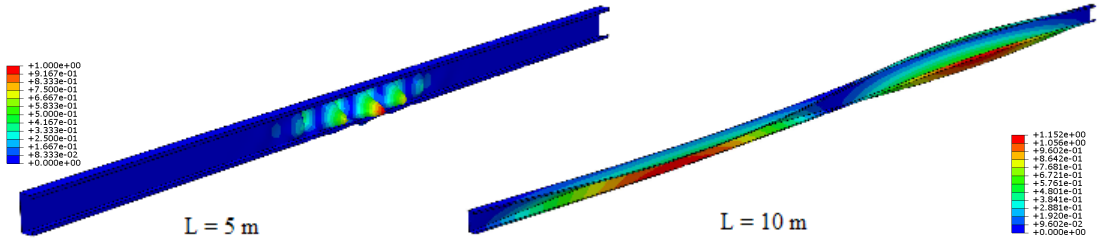

(b) k_ϕ =300 N

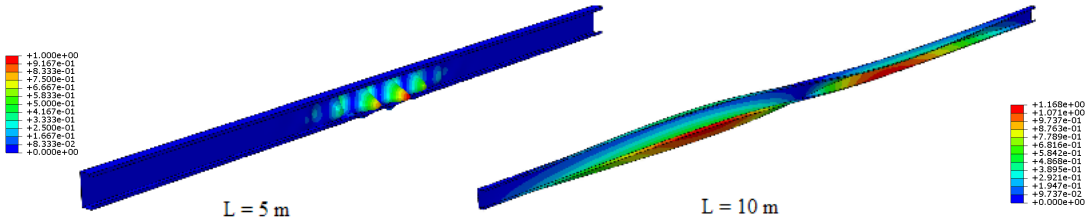

(c) k_ϕ =750 N

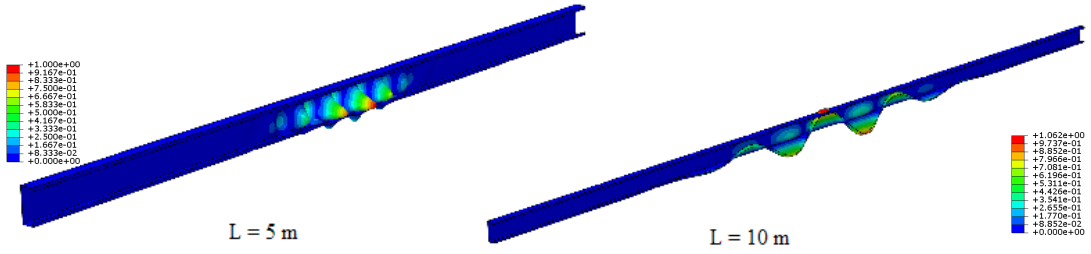

(d) k_ϕ =∞ N

Figure 4.10 Buckling modes of cold-formed steel members under four different rotational spring stiffness values.

Figure 4.11 shows the buckling modes of the secondary lateral-torsional buckling of the simply supported channel-section purlin under a uniformly distributed uplift load. Again, like the zed-section purlins, the secondary lateral-torsional buckling in channel-section purlins also exhibits more than two half-wavelengths, which depend on the length of the member.

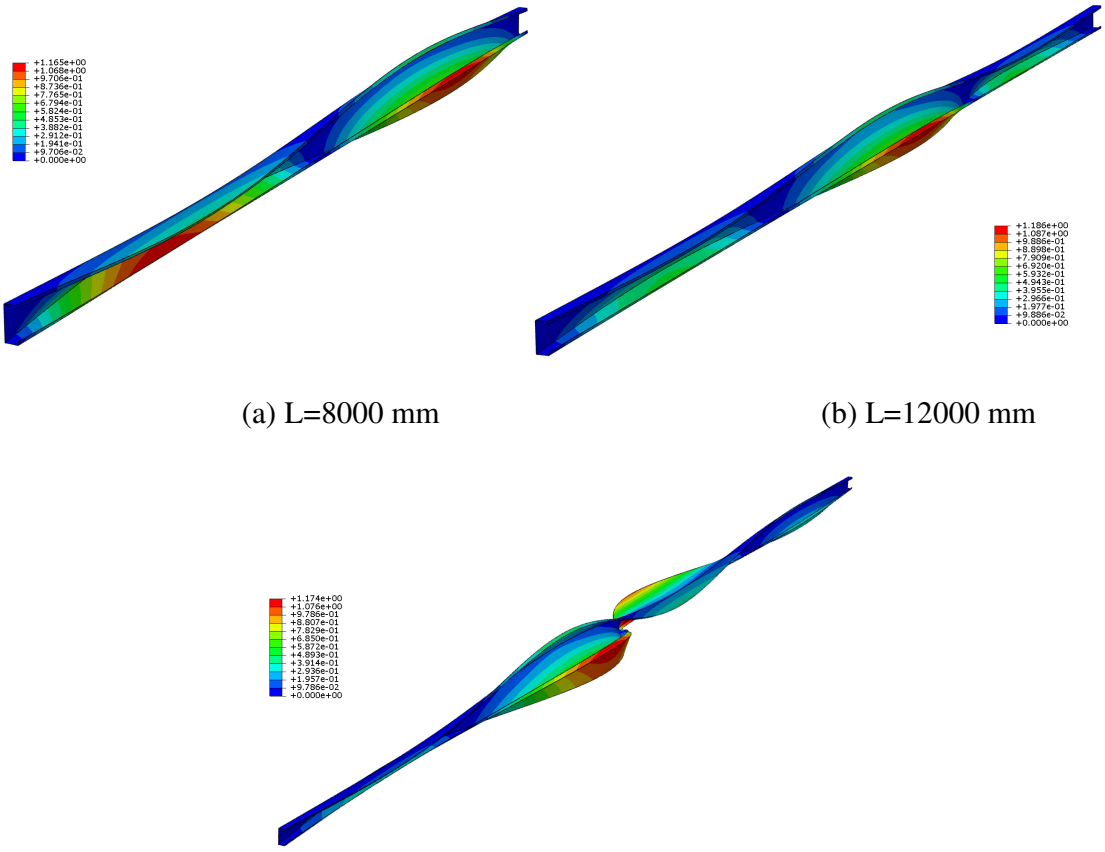

(a) L=8000 mm

(b) L=12000 mm

(c) L=18000 mm

Figure 4.11 Buckling modes of secondary lateral-torsional buckling in different beam lengths (d=200 mm, b=75 mm, c=20 mm, t=2 mm, k_{ϕ}=750 N).

Figure 4.12 shows a comparison of pre-buckling bending stresses for the channel-section purlins with different rotational spring stiffness values. It can be seen from the figure that, except for the case of k_ϕ=0, all other cases have very similar bending stresses. This indicates that the rotational spring stiffness has a two-fold influence on the critical buckling load. One of those influences is on pre-buckling stress, which only applies where the spring stiffness is very small. The other is on buckling mode. It can be seen from the figure that the pre-buckling bending stresses in most parts of the flange and web are higher when k_ϕ=0 than when k_ϕ≠0. This indicates that for small rotational spring stiffness, the lateral bending makes an important contribution to the longitudinal bending stress, which may change the buckling behaviour of the purlin.

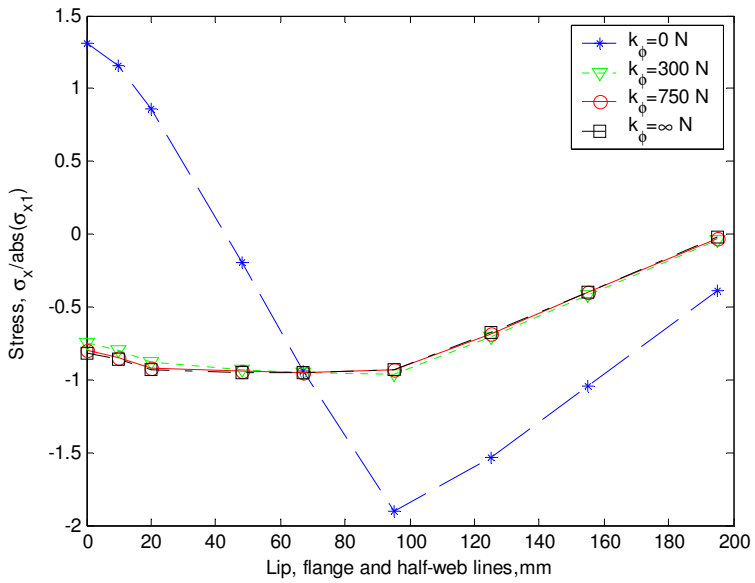

Figure 4.12 Bending stress distribution along the lip, flange and web lines (abscissa starts from the tip of lip and ends at half web length, h=200 mm, b=75 mm, c=20 mm, t=2.0 mm, L=12000 mm).

4.4.2 Influence of the dimensions of cross section

Figure 4.13 shows the critical load curves of simply supported channel-section purlins with different section dimensions (C12515, C20720 and C40132) under uniformly distributed uplift loading. It can be seen from the figure that for small and intermediate sections (C12515 & C20720), the critical load increases with the member length until it reaches a certain length and then it decreases with increasing member length. But for the large section (C40132), the critical load factor increases until the length reaches 12000 mm. Examination of the buckling modes reveals that for the small and intermediate sections, the buckling mode is dominated by local buckling of the lower flange and web at the point where the critical load rises. However, where the critical load reduces, the main buckling mode is secondary lateral-torsional buckling of the free flange. For the large section, the buckling mode is mainly controlled by local buckling of the lower flange and web if the purlin length is less than 10000 mm. For purlins longer than 10000 mm, lateral-torsional buckling is the dominant buckling mode. This may indicate that for channel-section purlins used in practice, secondary lateral-torsional buckling would not occur in the deep web section. This is probably due to the web-length ratio used. Figure 4.14 shows some typical buckling modes of purlins with different lengths and different section dimensions.

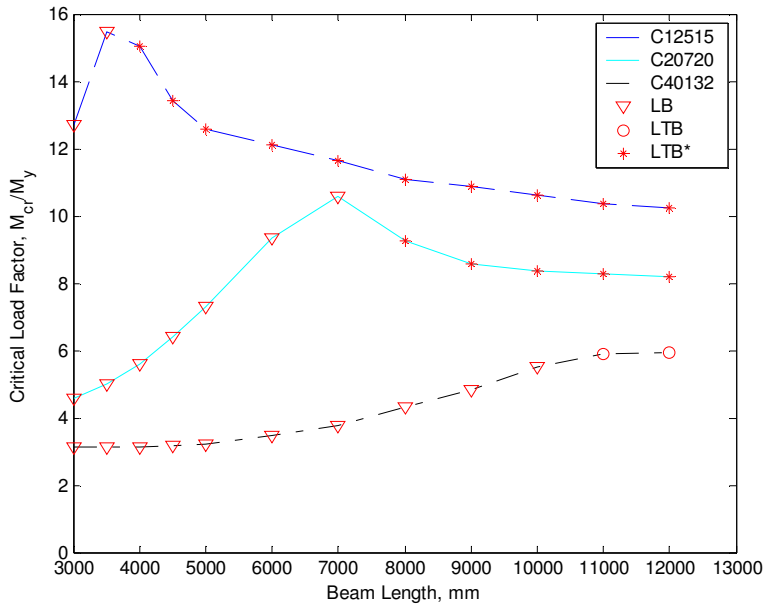

Figure 4.13 Critical load curve of simply supported channel-section with different section dimensions under uniformly distributed uplift loading (k_ϕ =750 N). (LB = Local Buckling. LTB = Lateral-torsional Buckling. LTB* = Secondary Lateral-torsional Buckling).

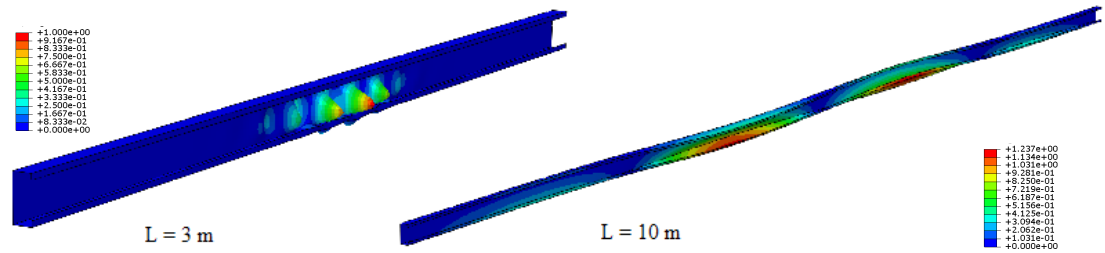

(a) C12515

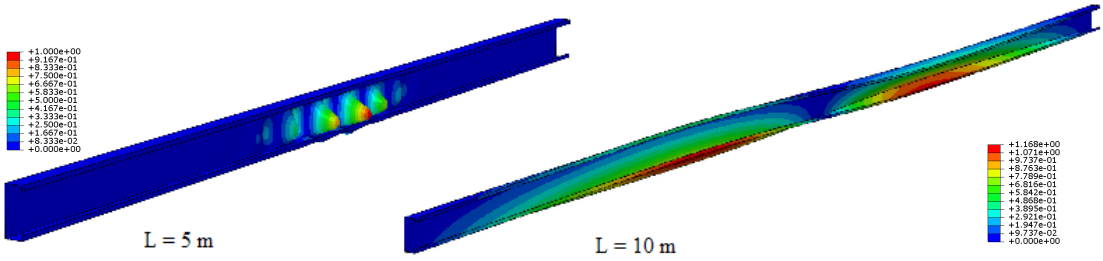

(b) C20720

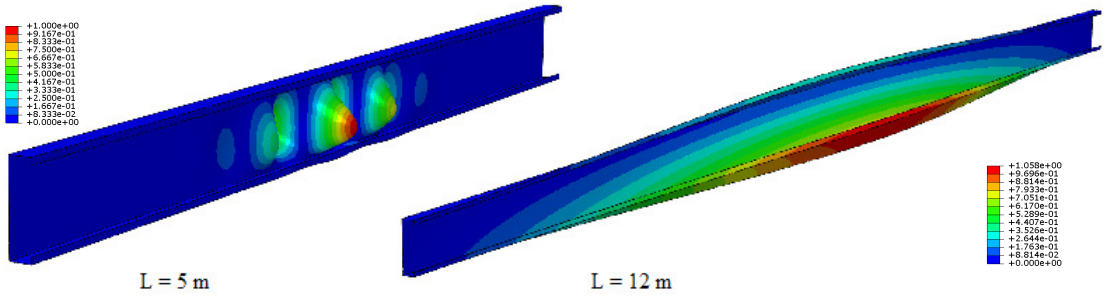

(c) C40132

Figure 4.14 Buckling modes of cold-formed steel members of different beam lengths, with different cross section dimensions (k_{ϕ} =750 N).

4.5 Summary

A numerical investigation into the buckling behaviour of cold-formed steel purlins has been conducted using linear finite element methods. The results have highlighted the buckling behaviour which occurs when the zed- and channel-section purlins are subjected to transverse distributed uplift loading with partial sheeting restraints. Some important conclusions drawn from the present study are summarised as follows:

1. A comparison of the finite element analysis and experimental measurement results is illustrated. The present finite element analysis model is in good agreement with the experimental data, which demonstrates that the buckling analysis can provide a good prediction of buckling behaviour for the partially or fully restrained zed- and channel-section purlin subjected to uplift loading.

2. For zed- and channel-sections, comparisons of the results of cleat bolted supported and web simply supported boundary conditions are verified. The idealised boundary condition proposed in the present study is able to represent the standard two-hole cleat support conditions used in practice.

3. For both zed- and channel-section purlins, the rotational spring has significant influence on the buckling behaviour of the purlins, including both the critical load and the corresponding buckling mode. The purlin length and section dimensions can also affect the buckling behaviour of the purlins.

4. The parametric distribution of different buckling modes obtained from the finite element analysis for zed-section purlins are presented. The distribution of buckling demonstrates that the buckling modes are effected not only by the rotational restraint but also by the geometric of purlin.

5. For purlin-sheeting systems, pre-buckling stress has a significant influence on buckling behaviour when the purlin reaches a certain length. In order to provide accurate results, consistent analysis models should be used for both pre-buckling stress and buckling analyses.

6. Secondary lateral-torsional buckling is found in partially rotationally restrained long length purlins. The half-wavelength of the secondary lateral-torsional buckling mode can be several times longer than the half-wavelength of distortional buckling. However, the half-wavelength is shorter than the beam length, which comprises more than two half-wavelengths rather than one half-wavelength in the lateral-torsional buckling mode.

CHAPTER 5 POST-BUCKLING ANALYSIS OF PURLIN-SHEETING SYSTEMS

5.1 Introduction

Cold-formed steel sections such as zed-, channel- and sigma-sections are widely used in buildings as purlins and rails to support corrugated sheeting. Roof purlins and cladding rails are considered to be the most popular products and account for a substantial proportion of cold-formed steel usage in buildings. In practice, the corrugated sheeting provides sufficient lateral restraint but limited rotational restraint. As is discussed in chapter three and four, the connection of sheeting to purlin has significant influence on the bending stresses and buckling loads of purlins.

In this chapter, nonlinear finite element analysis models are developed for cold-formed steel zed- and channel-section purlins subjected to transverse uniformly distributed uplift loading. In the model, the lateral and rotational restraints provided by the sheeting to the purlin are simplified as a lateral rigid restraint imposed at the upper flange-web junction, and a rotational spring restraint applied at the middle of the upper flange where the sheeting is fixed. The analyses are performed by considering both geometric and material nonlinearities. The load-displacement curves of the zed- and channel-section purlins of different dimensions subjected to uplift loading under the influence of rotational spring stiffness on the middle of upper flange are examined. Moreover, the design curves of zed-

and channel-section purlins are established. Furthermore, the comparisons of cleat bolted supported and web simply supported boundary conditions are presented and the results of finite element analysis are validated with available experimental data.

5.2 Finite element model and validation

5.2.1 Validation of the model

The present nonlinear finite element model is validated using the experimental data reported by Rousch and Hancock (1997), in which the dimensions of the zed-section purlin analysed are web depth h=202.8 mm, upper flange width b_1=80.7 mm, lower flange width b_2=72.5 mm, lip length c=21.5 mm, and thickness t=1.5 mm. The material properties are Young's modulus E=200 GPa, Poisson's ratio ν=0.3, and yield stress σ_y=350 MPa. The torsion restraint provided by the sheeting is taken as 0.023 N/mm^2, as described in the report of Rousch and Hancock (1997). The loading conditions and boundary conditions employed are exactly the same as those used in the previous sections. For the beam theory, the ratio of web depth to beam length is less than 1/10, as long as a member meets this requirement, this member works as a beam. It should be pointed out that the models mentioned in this thesis do not consider the initial imperfection, because it is believed that the eccentric loads will cause instantaneous movement, which will outweigh the effect of imperfection. Figure 5.1 shows the comparisons of the finite element analysis and experimental measurement results. It can be seen from the figure that for the lateral displacement at the lower flange-web junction the finite element analysis results compare closely with those obtained in the test. However, for the vertical displacement at the upper flange-web junction the finite element analysis results are a little higher than those obtained in tests. This is probably due to the influence of the sheeting bending stiffness, which is not taken into account in the FEA model, but in the test it may take some loading.

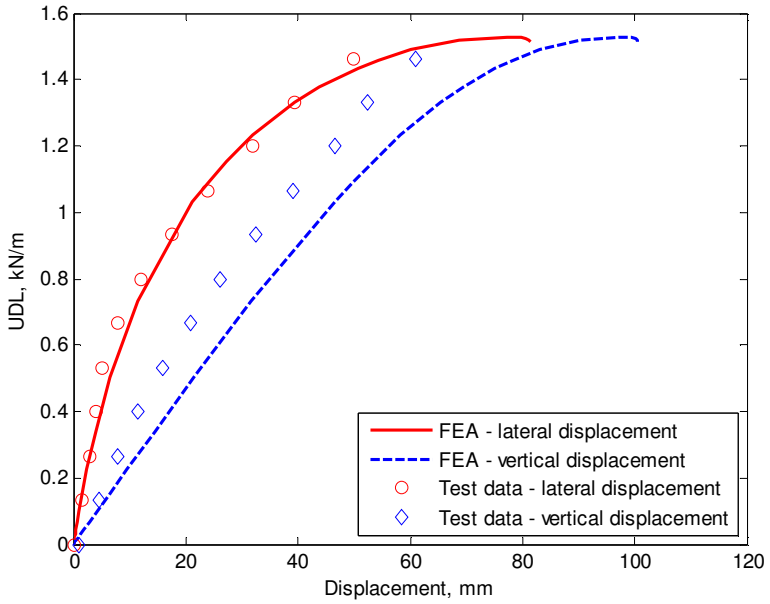

Figure 5.1 Comparison of FEA results with experimental data

(The test data for lateral displacement is from Rousch and Hancock, 1997.

The test data for vertical displacement is from Rousch and Hancock, 1996).

5.2.2 *Influence of boundary conditions*

To compare the practical and analytically/numerically used boundary conditions, the same model and analysis method used in chapter three are employed again in this chapter (see Figure 3.1). The models use the cleat bolted supported as the practical boundary condition and the web simply supported as the analytical boundary condition. However, in chapter three and four, only elasticity is considered, and material yield is neglected due to the use of linear analysis. In this chapter, for the purpose of ultimate state analysis, non-linear analysis is employed. For thin-walled structures this should include both geometric and material nonlinearities. For cold-formed steel sections the yield strength and ultimate strength are almost identical because of the cold-forming processes. Hence,

the stress-strain curve here is assumed to follow that of the elastic-perfectly plastic material, and the yield stress is taken as σ_y=390 MPa.

For a given purlin length, section dimensions and rotational spring stiffness, one can obtain the load-displacement curve from the finite element analysis. Figure 5.2 shows the load-displacement curves of a zed-section purlin (Z12515) of length L=7000 mm for two different rotational spring stiffness values (k_ϕ=0 N and k_ϕ=750 N), in which the load is the uniformly distributed uplift load acting on the middle line of the upper flange, and the displacements are the vertical displacement at the upper flange-web junction and the lateral displacement at the lower flange-web junction, both on the symmetric section of the purlin (middle of the beam). It can be seen from the figure that the load-displacement curves obtained from the two different boundary conditions are very close. The exception is the case of k_ϕ=0 N, where the ultimate load of the cleat bolted supported boundary condition is slightly higher than that of the web simply supported boundary condition. The explanation for this is that in the case of an extremely large deformation of the zed-section, the cleat bolted supported boundary condition is located at the hole in the web which is 29 mm away from its edge, therefore, the effective length of the cleat bolted supported boundary condition is slightly shorter than that of the web simply supported boundary condition. It can be seen in Figure 5.2a, when k_ϕ=0 N, the trend of lateral displacement indicates that the purlin is bent initially about its major axis, has had a lateral-torsional buckling. After the buckling, because the rotation of the section, the purlin is bent about its minor axis, and until the purlin becomes fully plastic. Figure 5.3 shows the load-displacement curves of a large section (Z40132) zed purlin of length

L=7000 mm for two different rotational spring stiffness values (k_ϕ=0 N and k_ϕ=750 N). It can be seen from this figure that, the load-displacement curves for both vertical and lateral displacements obtained from the two boundary conditions are again very close. It also can be seen in Figure 5.3a, when k_ϕ=0 N, the vertical displacement reduces when the load reach their ultimate values. The reason for the decreased displacement is that the shear buckling effects the moving direction of free flange and pulls the free flange down when the purlin begins to failure. Figure 5.4 and Figure 5.5 show the load-displacement curves of small and large channel-sections (C12515 & C40132) of length L=7000 mm, for two different rotational spring stiffness values (k_ϕ=0 N and k_ϕ=750 N). The load is the uniformly distributed uplift load acting on the middle line of the upper flange, and the displacements are the vertical displacement at the upper flange-web junction and the lateral displacement at the lower flange-web junction, both on the symmetric section of the purlin. From Figure 5.4 and Figure 5.5, it can be seen that for both small and large sections, the load-displacement curves obtained from the two boundary conditions are almost the same. It can be found that in Figure 5.4a, due to the purlin has severe twisting deformation, the flexural rigidity is reduced significantly in the loading direction while increased in the perpendicular direction, the lateral displacement increases only marginally when the increased load climbs rapidly.

The good agreement of the load-displacement curves between the two different boundary conditions for both the zed- and channel-section purlins demonstrates that the idealised web simply supported boundary condition proposed in the present study are able to represent the standard two-hole cleat support conditions used in practice.

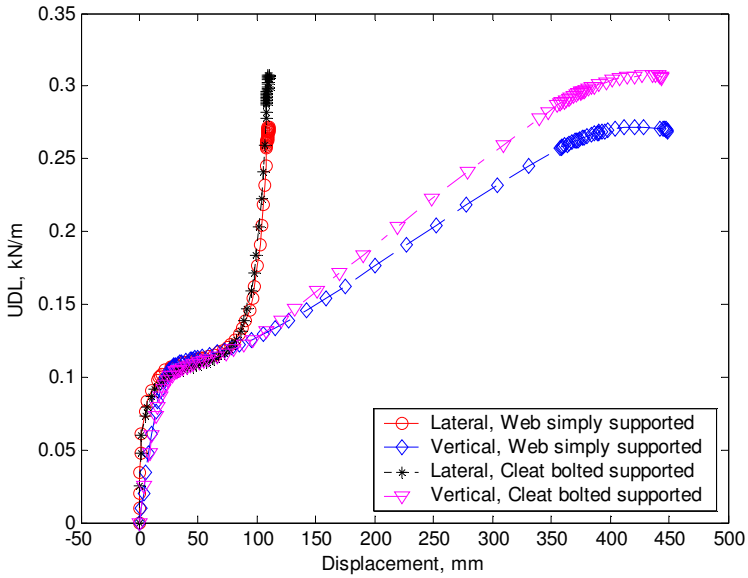

(a) k_{ϕ} =0 N

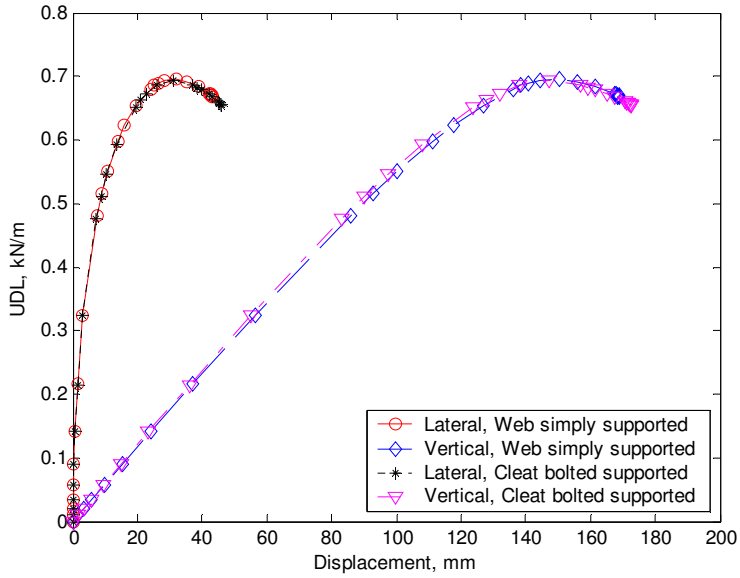

(b) k_{ϕ} =750 N

Figure 5.2 Load-displacement curves of purlin with different rotational spring constants (Z12515, L=7000 mm).

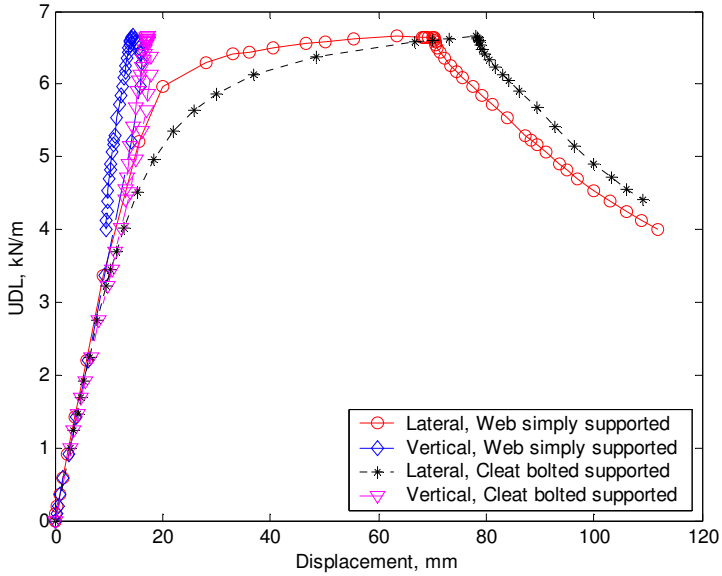

(a) k_{ϕ} =0 N

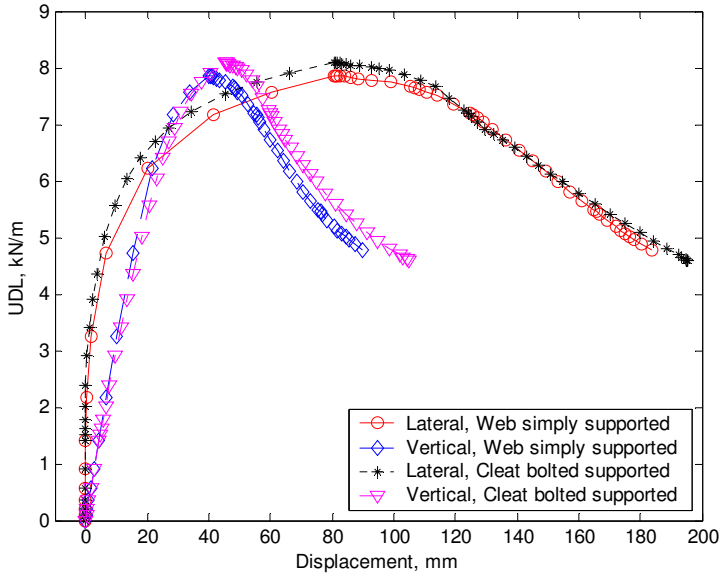

(b) k_{ϕ} =750 N

Figure 5.3 Load-displacement curves of purlin with different rotational spring constants (Z40132, L=7000mm).

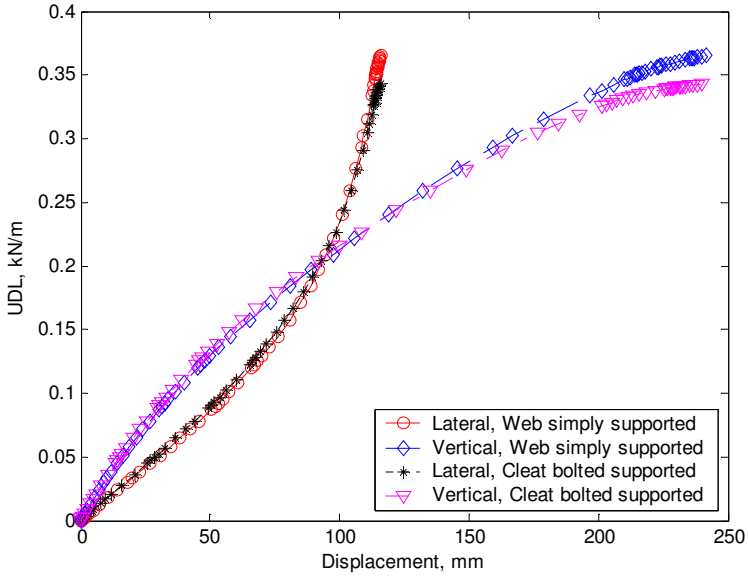

(a) k_{ϕ}=0 N

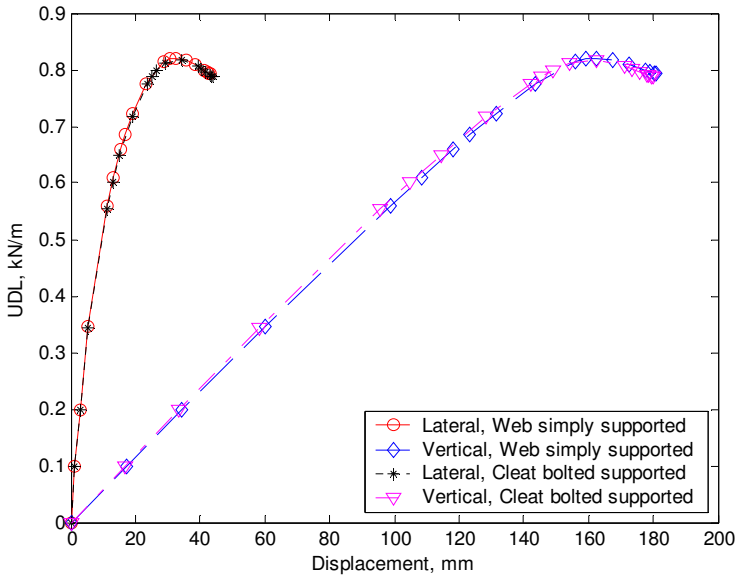

(b) k_{ϕ}=750 N

Figure 5.4 Load-displacement curves of purlin with different rotational spring constants (C12515, L=7000mm).

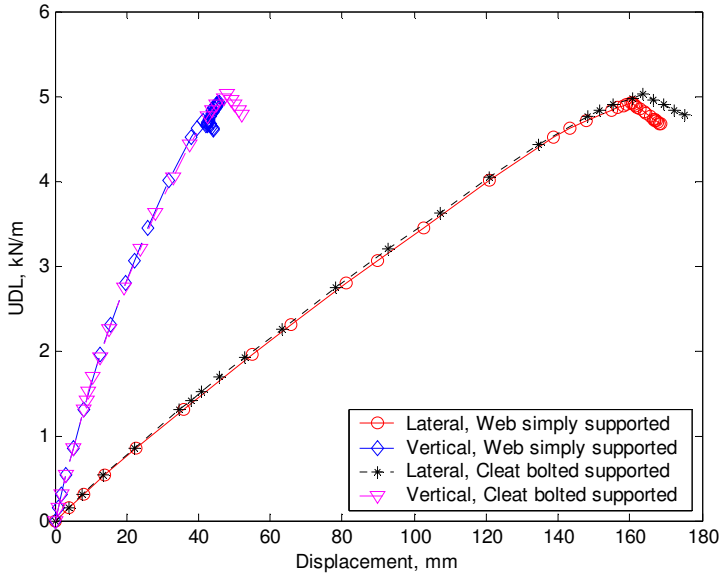

(a) k_{ϕ} =0 N

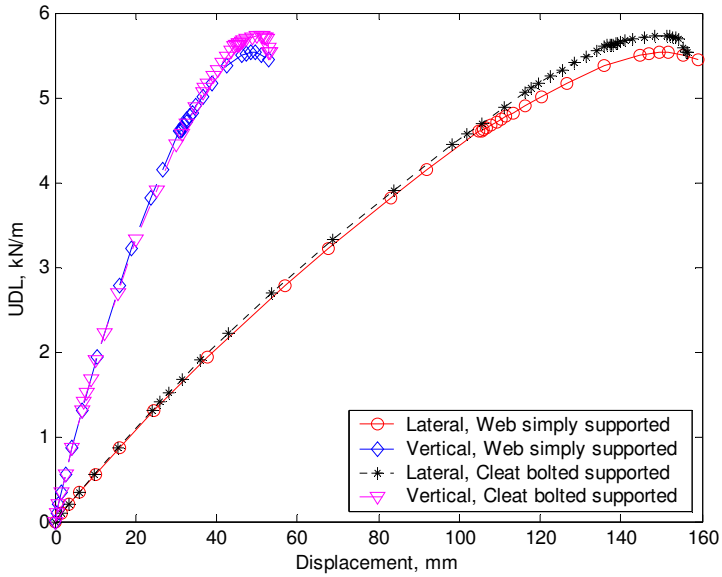

(b) k_{ϕ} =750 N

Figure 5.5 Load-displacement curves of purlin with different rotational spring constants (C40132, L=7000mm).

5.3 Post-Buckling analysis of zed-sections

5.3.1 Finite element model

The finite element models of post-buckling analysis for zed- and channel-sections are similar to the models used in chapter three. Geometry, loads, boundary conditions, restraints, element type, and corresponding element mesh used are all identical to the models used in the pre-buckling analysis shown in chapter three, the only differences are in their material properties. For the pre-buckling analysis elasticity is assumed, while for the post-buckling analysis the plasticity is considered. For thin-walled structures geometric nonlinearity need also be considered. Here, the stress-strain curve is assumed to follow that of the elastic-perfectly plastic material, the von Mises yield criteria is used and the yield stress σ_y=390 MPa (see Figure 5.6). The elastic-plastic nonlinear analysis is to determine the load-displacement response curve and also the limit load at which the member has a snap-through buckling. The modified Riks method built in ABAQUS is used, which employs the arc length along the static equilibrium path in load-displacement space. The load-displacement response curve for each member analysed is computed, and the limit load is determined from the peak point of the load-displacement curve.

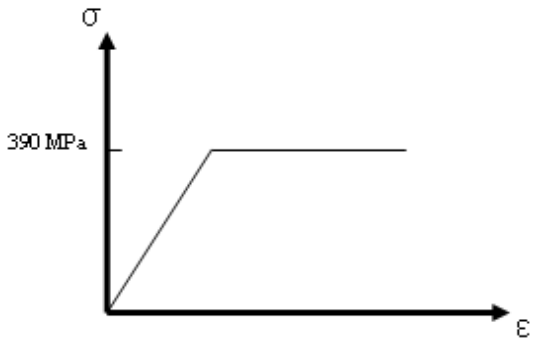

Figure 5.6 Stress–strain curve of the elastic-perfectly plastic material.

5.3.2 Influence of spring stiffness and the dimensions of cross section

For a given purlin length and rotational spring stiffness, one can obtain the load-displacement curve from the finite element analysis. Figure 5.7 shows the load-displacement curves of a small zed-section (Z12515) purlin of length L=4000 mm for four different rotational spring stiffness values (k_ϕ=0, k_ϕ=300 N, k_ϕ=750 N and k_ϕ=∞ N), in which the displacements are the vertical displacement at the upper flange-web junction and the horizontal displacement at the lower flange-web junction, both on the symmetric section of the purlin. It can be seen from this figure that the load-displacement curves for purlin with k_ϕ=0 are different from those for purlin with k_ϕ=300 N, k_ϕ=750 N or k_ϕ=∞ N. In the former, when k_ϕ=0, the load increases with the displacement until the load approaches its upper-limit value where a small increase in the load results in a rapid increase in displacement. This indicates that the failure of the purlin is a typical limiting failure of plasticity. In the latter, when k_ϕ=300 N, k_ϕ=750 N or k_ϕ=∞ N, the load increases with the displacement until it reaches the ultimate load point. After this point, the load decreases with further increased displacement, indicating that the failure of the purlin is a typical buckling failure. As would be expected, the failure load of the purlin increases with the rotational spring stiffness. This reveals that the rotational spring has significant influence on the performance.

The reason that the rotational spring not only increases the failure load but also alters the failure type of the purlin is that it provides some restraints on the purlin's pre-buckling twisting displacement. When a beam is subjected to a transverse load, it is initially bent

about its major axis. However, after the beam undergoes lateral-torsional buckling, the bending axis suddenly moves from its major axis to a minor axis. Therefore, the post-buckling curve is usually unstable when a purlin has lateral-torsional buckling, as shown in Figure 5.7 for the purlins with k_ϕ=300 N, k_ϕ=750 N and k_ϕ=∞ N. However, under conditions of free rotational restraint, if a beam is initially bent about its minor axis or is simultaneously subjected to bending and twisting, the beam deforms gradually towards its post-buckling mode and will eventually undergo a plastic failure, like what is shown in the figure for the purlin with k_ϕ=0.

Figure 5.8 shows the deformed shapes of a small zed-section (Z12515) purlin with four different k_ϕ values when the loads reach their ultimate load points. It can be seen from the figure that when k_ϕ=0 the purlin has severe twisting deformation, which significantly reduces the flexural rigidity in the loading direction but increases the flexural rigidity in the perpendicular direction. As a consequence of this, the bending stresses increase much more quickly than the actual load does. This leads the purlin eventually to have a plastic failure. The deformations of the purlin with k_ϕ=300 N, k_ϕ=750 N and k_ϕ=∞ N are very similar, but there is less twisting when compared to the purlin with k_ϕ=0. According to the distribution of compression area (coloured blue) shown in the deformed shapes, the main failure mode is characterized by the lateral-torsional buckling mode.

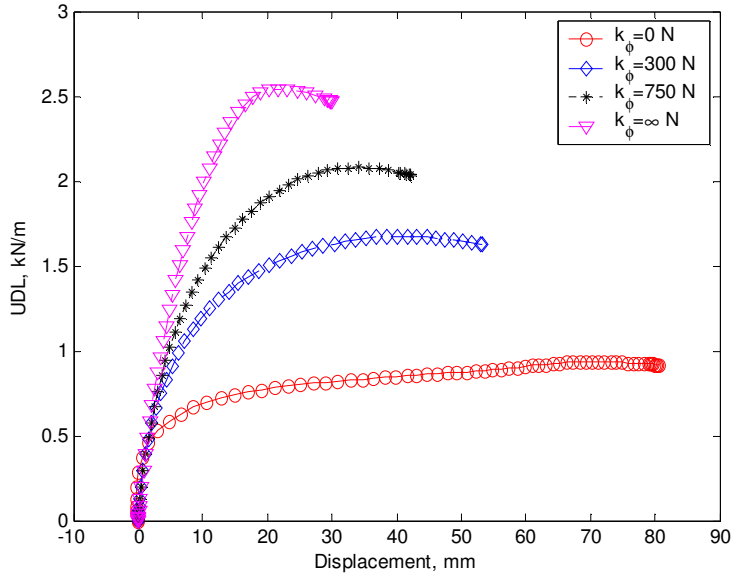

(a) Lateral displacement

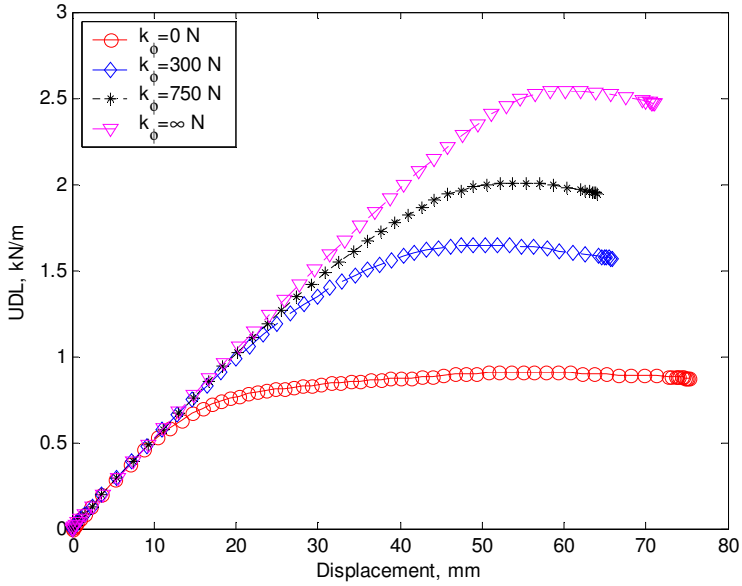

(b) Vertical displacement

Figure 5.7 Load-displacement curves of purlin with different rotational spring constants (Z12515, L=4000 mm).

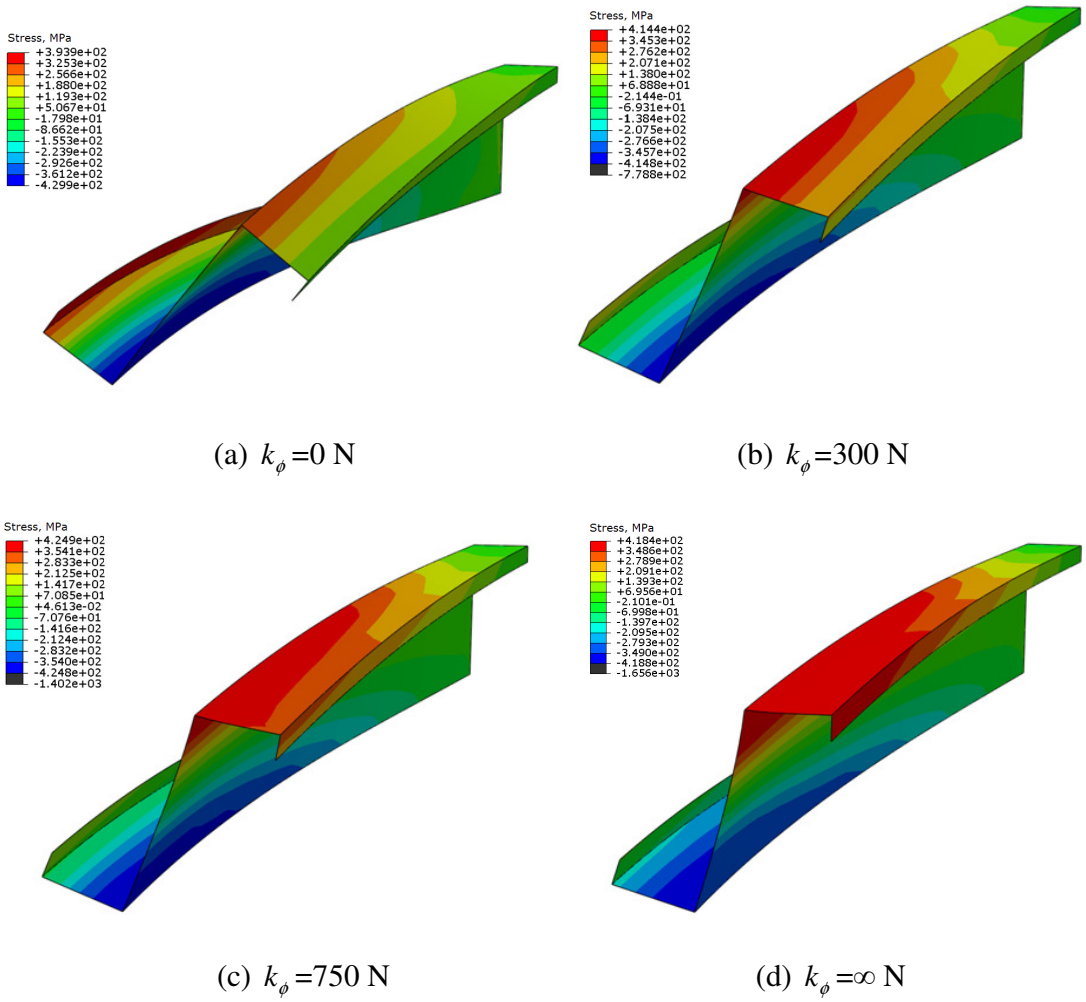

(a) k_ϕ =0 N (b) k_ϕ =300 N

(c) k_ϕ =750 N (d) k_ϕ =∞ N

Figure 5.8 Deformed shapes of purlin at failure point with longitudinal stress contours (Z12515, L=4000 mm).

Figure 5.9 shows the load-displacement curves of a small zed-section (Z12515) purlin of length L=7000 mm for four different rotational spring stiffness values (k_ϕ=0, k_ϕ=300 N, k_ϕ=750 N and k_ϕ=∞ N). It can be seen from the figure that the curves for k_ϕ=0, k_ϕ=300 N, k_ϕ=750 N and k_ϕ=∞ N are very similar to those shown in Figure 5.7, except that the loads are smaller as the purlin gets longer. It is observed from Figure 5.9 that the load-

displacement curves corresponding to k_ϕ=0 can be divided into three different segments. The first one is the initial part of the curves where both lateral and vertical displacements seem to increase linearly with the load. The second one is the mid part of the curves where both types of displacement increase rapidly while the load increases very slowly. The third segment is the last part of the curves where the vertical displacement increases with the load until it reaches the maximum load point, while the lateral displacement increases only marginally with the increased load. In order to find out why there is a flat part in the middle of the load-displacement curves, linear buckling analysis was also carried out, which shows the purlin to have a lateral-torsional buckling critical load of 0.13 kN/m. This critical load matches very well with the load in the mid part of the curves. This indicates that the purlin, which is bent initially about its major axis, has had a lateral-torsional buckling when the load reaches about 0.13 kN/m. After the buckling, the purlin is bent about its minor axis. However, since the plastic bending load about the minor axis is greater than the critical buckling load 0.13 kN/m, the load can increase continuously until the purlin becomes fully plastic. Thus, the final failure of the purlin is characterised by plastic bending failure. Figure 5.10 shows the deformed shapes of the purlins when the loads reach their ultimate values. Again, the deformed shapes are very similar, although the longitudinal stress contours are different. It should be pointed out that although the plastic failure load of the purlin with k_ϕ=0 is more than twice its critical buckling load, the purlin develops large vertical and horizontal deflections while it buckles. Therefore, in terms of serviceability, the purlin will fail when lateral-torsional buckling occurs, even though the post-lateral-torsional buckling of the purlin is actually stable.

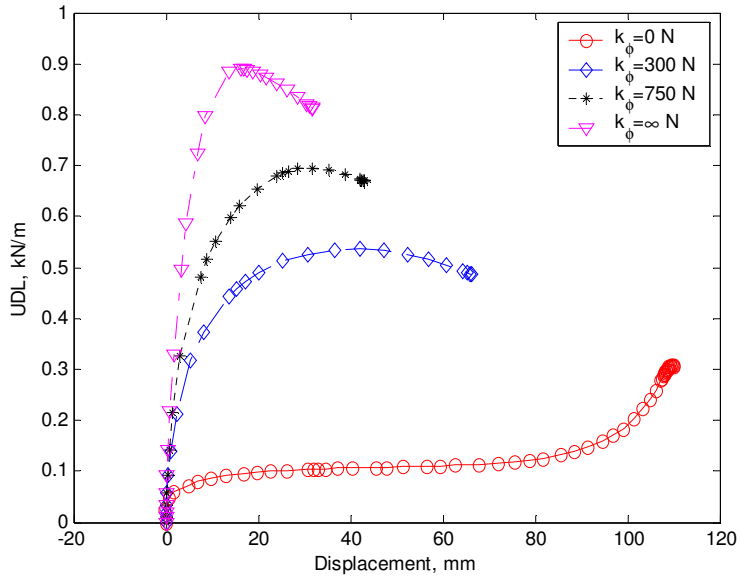

(a) Lateral displacement

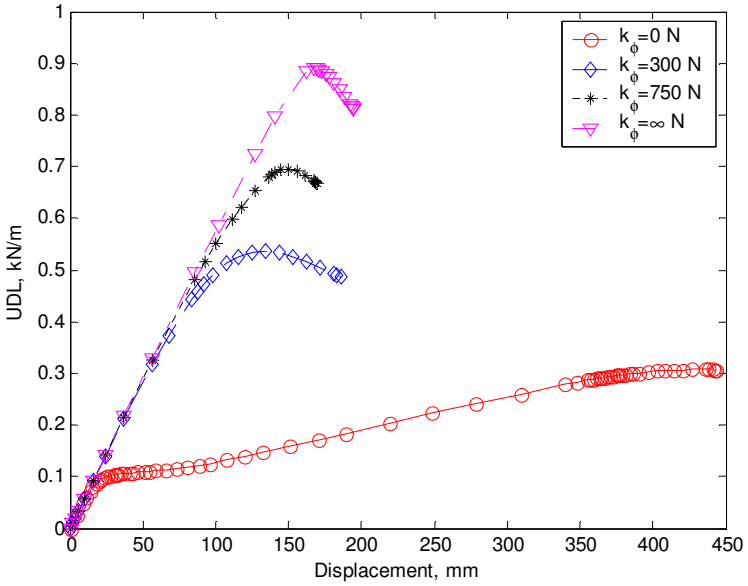

(b) Vertical displacement

Figure 5.9 Load-displacement curves of purlin with different rotational spring constants (Z12515, L=7000 mm).

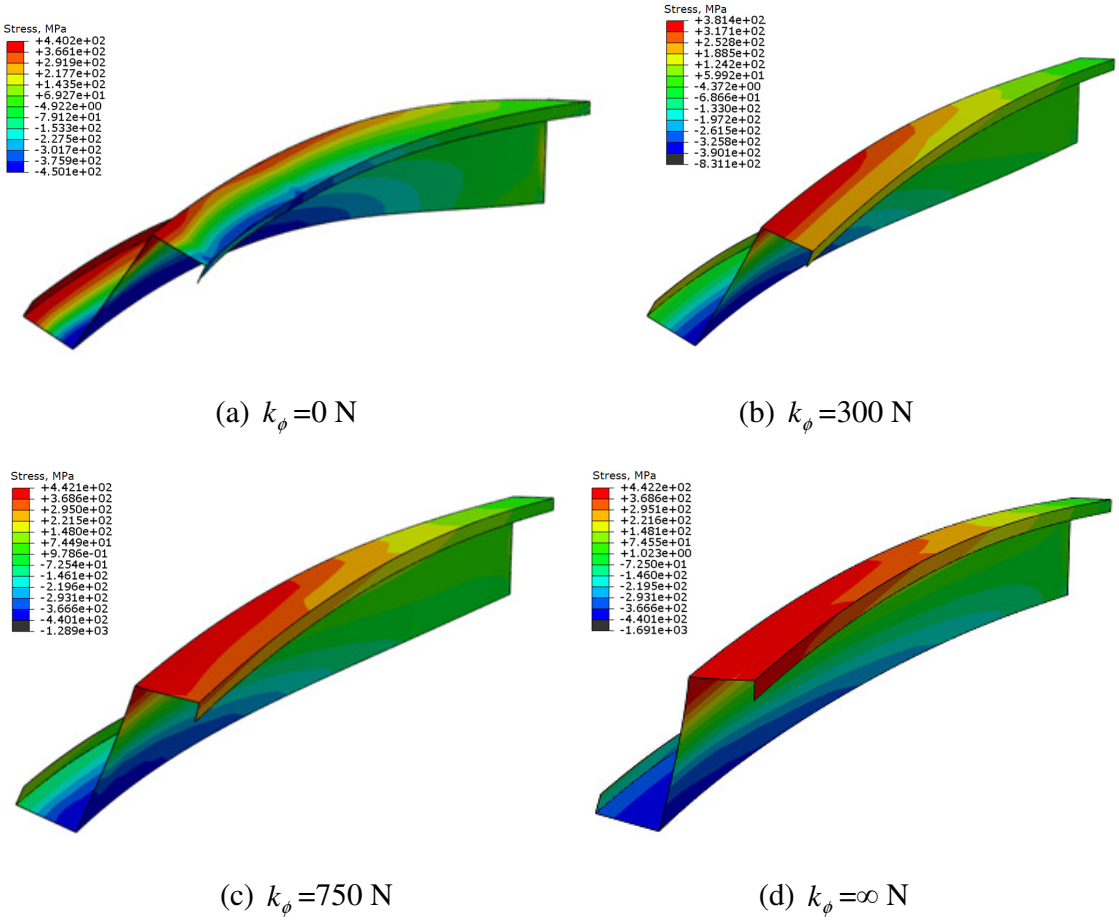

(a) k_ϕ =0 N (b) k_ϕ =300 N

(c) k_ϕ =750 N (d) k_ϕ =∞ N

Figure 5.10 Deformed shapes of purlin at failure point with longitudinal stress contours (Z12515, L=7000 mm).

Figure 5.11 shows the load-displacement curves of a small zed-section (Z12515) purlin of length, L=10000 mm for four different rotational spring stiffness values (k_ϕ=0, k_ϕ=300 N, k_ϕ=750 N and k_ϕ=∞ N). The corresponding deformed shapes of the purlins when the loads reach their ultimate values are shown in Figure 5.12. The main features of these figures are similar to those shown in Figures 5.9 and 5.10 and thus are not discussed further. To demonstrate the difference between the critical load of lateral-torsional buckling calculated from linear buckling analysis and the failure load obtained from the

nonlinear analysis, Table 5.1 provides a detailed comparison. For purlins with k_ϕ=300 N, k_ϕ=750 N and k_ϕ=∞ N, the critical bucking load is found to be higher than the plastic failure load. In design practice, the design formula by considering the nonlinear effect always refers to the linear buckling equations which have a closed-form solution. All design codes and previous research (EN1993-1-3, 2006) have confirmed that the nonlinear failure load is lower than the linear buckling load due to the effect of geometrical and material nonlinearity. However, due to catenary action, the linear elastic buckling load may be lower than the non-linear failure load, and this case is marked with a star as shown in the tables,. Due to the second order nonlinear membrane stress, the structure that have a stable post-buckling path and the member in the post-buckling period has extremely large deflection, and the large deflection will trig the catenary action and hence increase the stiffness (i.e. Z12515, L=7000mm, k_ϕ=0). In design practice, the serviceability requirement does not allow the structure to develop such a large deflection, and therefore they always set a failure limit before the catenary action is formed. In this case, the critical buckling without considering the imperfection and material yield will set an upper boundary for failure load. For short length purlins without rotational spring restraint, the critical buckling load is higher than the plastic failure load, whereas for medium and long length purlins, the critical buckling load is lower than the plastic failure load. This implies that the influence of the rotational spring on the failure mode of the purlin is also dependent on the purlin length.

Table 5.1 Comparison of critical buckling loads and plastic failure loads (Z12515).

L **(mm)**	k_ϕ**=0 N**		k_ϕ**=300 N**		k_ϕ**=750 N**		k_ϕ**=∞ N**	
	Failure Load (kN/m)	Buckling Load (kN/m)	Failure Load (kN/m)	Buckling Load (kN/m)	Failure Load (kN/m)	Buckling Load (kN/m)	Failure Load (kN/m)	Buckling Load (kN/m)
4000	0.91	0.933	1.65	2.8	2.01	3.52	2.54021	4.4495
7000	0.28*	0.13	0.533	0.722	0.676	0.935	0.889548	1.3167
10000	0.141*	0.042	0.25	0.324	0.331	0.42	0.447682	0.605

Note: * = The catenary action.

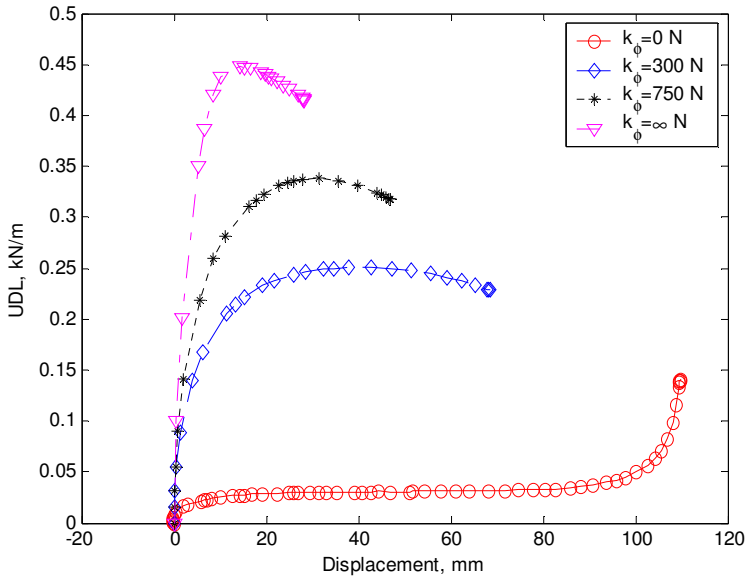

(a) Lateral displacement

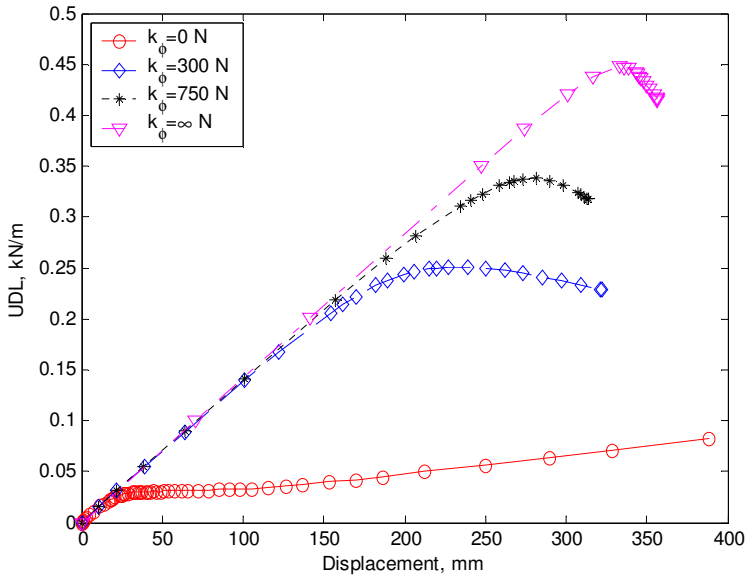

(b) Vertical displacement

Figure 5.11 Load-displacement curves of purlin with different rotational spring constants (Z12515, L=10000 mm).

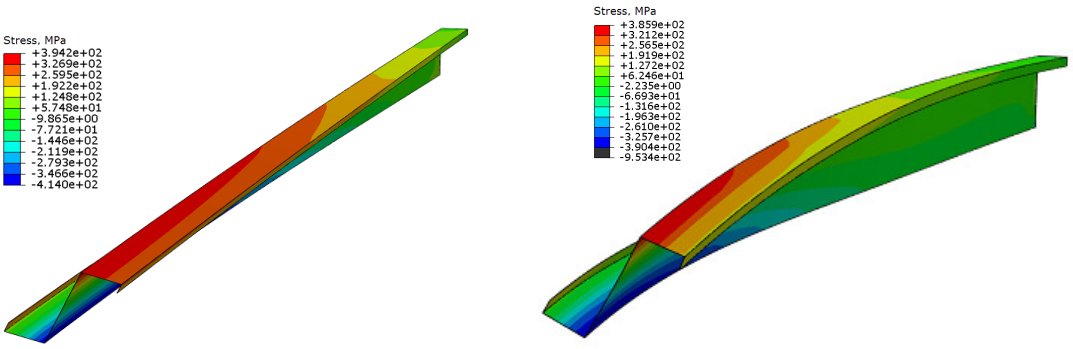

(a) k_{ϕ}=0 N (b) k_{ϕ}=300 N

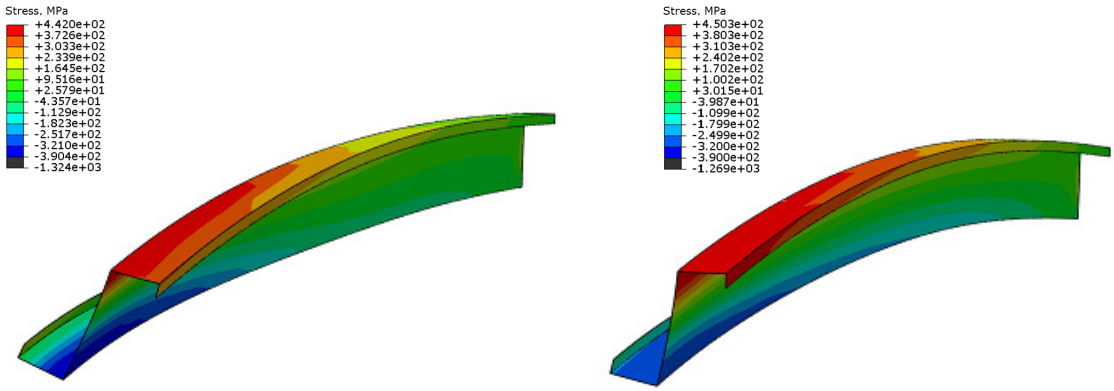

(c) k_ϕ =750 N (d) k_ϕ =∞ N

Figure 5.12 Deformed shapes of purlin at failure point with longitudinal stress contours (Z12515, L=10000 mm).

The load-displacement curves of an intermediate zed-section (Z20720) purlin of length, L=4000 mm for four different rotational spring stiffness values (k_ϕ=0, k_ϕ=300 N, k_ϕ=750 N and k_ϕ=∞ N) are plotted in Figure 5.13. As mentioned for the small zed-section (Z12515), the load is the uniformly distributed uplift load acting on the middle line of the upper flange, and the displacements are the vertical displacement at the upper flange-web junction and the horizontal displacement at the lower flange-web junction, both on the symmetric section of the purlin. It can be seen from this figure that for all rotational spring stiffness values, the load increases to reach the peak point with increasing displacement; after the peak point, the load drops rapidly with further increased displacement. This implies that the failures of the purlin are typical buckling failure and the failure load of the purlin increases with the rotational spring stiffness.

Figure 5.14 shows the deformed shapes of an intermediate zed-section (Z20720) purlin with four different k_ϕ values when they reach their ultimate loads. It is found from the figure that the deformations of the purlins for all values of rotational spring stiffness are very similar; compressive stress is located at the purlin's middle span of the lower web-flange junction and develops through the interaction of distortional and local buckling, and this is due to the wavelength of purlin which is dependent on the purlin's length and web depth. For short lengths of the member, the purlin is more likely to have distortional buckling rather than lateral-torsional buckling. However, when an element has distortional buckling it does not necessarily mean that this element will collapse or lose its ability to carry loads. In fact, a plate is able to take a considerably increased load beyond initial buckling before any danger of collapse occurs. This is because the deflections due to buckling are accompanied by stretching of the middle surface of the plate. Furthermore, the increased rotational restraint increases the compression at the lower flange which is responsible for local buckling being involved. The significance of the interaction between distortional and local buckling increases with increased rotational spring stiffness. From k_ϕ=0 to k_ϕ=∞ N, the effect of local buckling increases while the influence of distortional buckling decreases. This indicates that the rotational spring stiffness has important influence not only on the ultimate load but also on its failure mode.

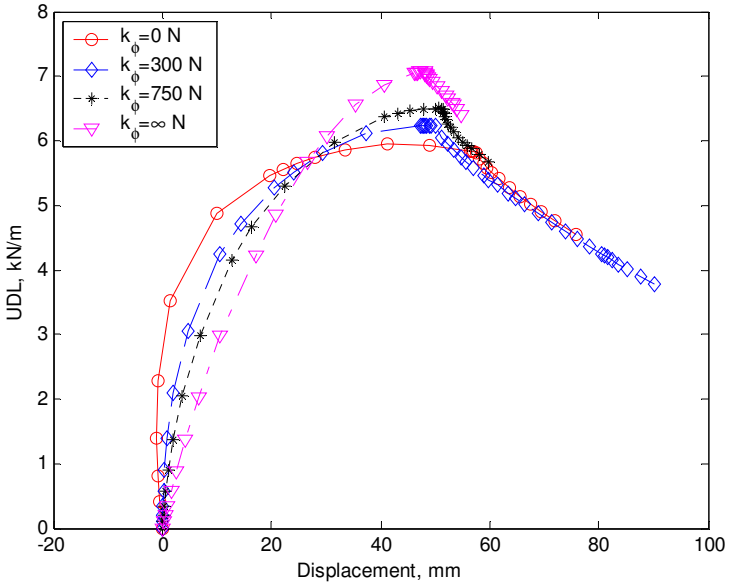

(a) Lateral displacement

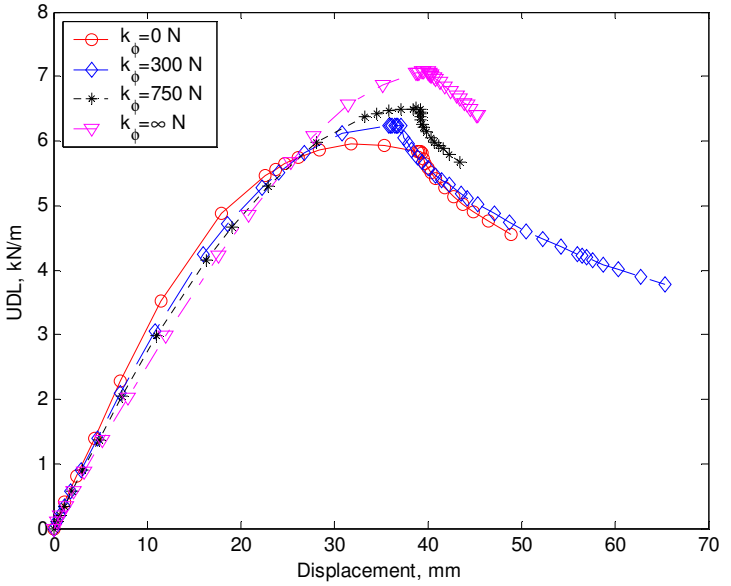

(b) Vertical displacement

Figure 5.13 Load-displacement curves of purlin with different rotational spring constants (Z20720, L=4000 mm).

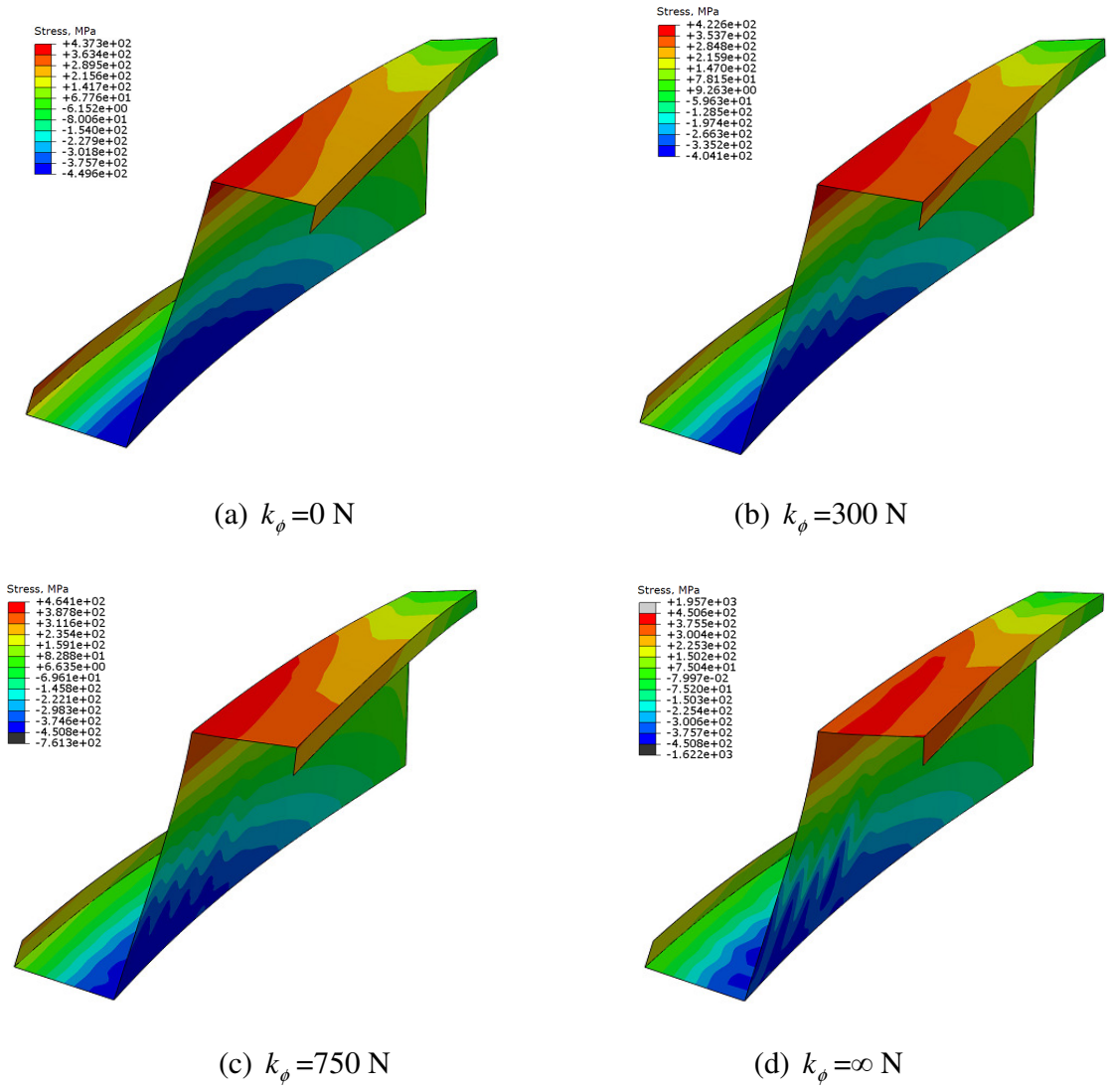

(a) k_ϕ =0 N (b) k_ϕ =300 N

(c) k_ϕ =750 N (d) k_ϕ =∞ N

Figure 5.14 Deformed shapes of purlin at failure point with longitudinal stress contours (Z20720, L=4000 mm).

The load-displacement curves of an intermediate zed-section (Z20720) purlin of length, L=7000 mm for four different rotational spring stiffness values (k_ϕ=0, k_ϕ=300 N, k_ϕ=750 N and k_ϕ=∞ N) are shown in Figure 5.15. The main features of this figure are similar to

those shown in Figure 5.7; the only differences being the increased ultimate load and lateral and vertical displacements, which are due to the increased dimensions of the cross section.

Figure 5.16 plots the deformed shapes of purlin at failure point with longitudinal stress contour for the zed-section (Z20720) purlin of length 7000 mm. It can be observed from this figure that for k_ϕ=300 N and k_ϕ=750 N, the failure mode is mainly determined by lateral-torsional buckling. However, when k_ϕ=∞ N, the failure mode is slightly different from that of k_ϕ=300 N and k_ϕ=750 N, due to the rotational restraint. One can see that the distortional buckling begins to combine with local buckling to dominate the buckling failure mode. The reason for the interaction of the distortional and local buckling is that the wavelength of the distortional buckling is dependent on the k_ϕ value. For high k_ϕ, the failure of the beam is dominated by distortional buckling, and for low k_ϕ, lateral-torsional buckling is the main failure mode. This can be found from the failure modes of purlins from k_ϕ=0 to k_ϕ =∞ N that, because the rotational restraint has an important impact on the distribution of wavelength; the effect is that distortional buckling becomes the dominant failure mode and the influence of lateral-torsional buckling is weakened. This indicates that the rotational spring stiffness of the member has significant influence on the failure mode of the member.

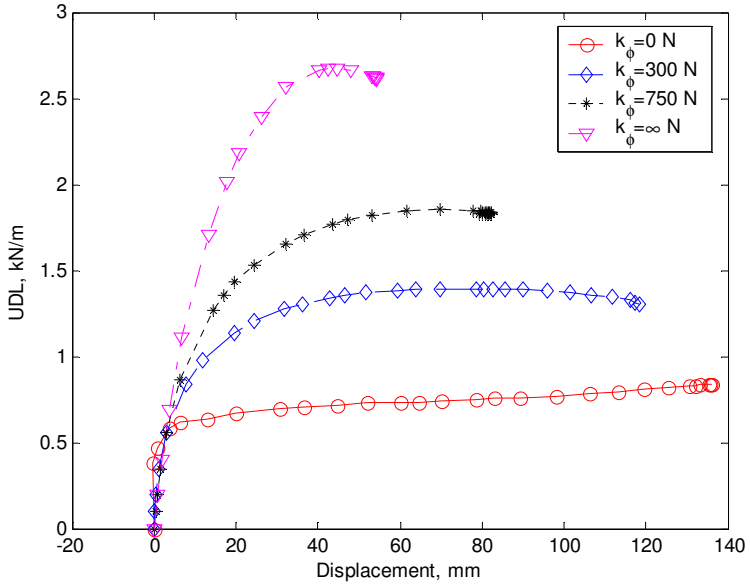

(a) Lateral displacement

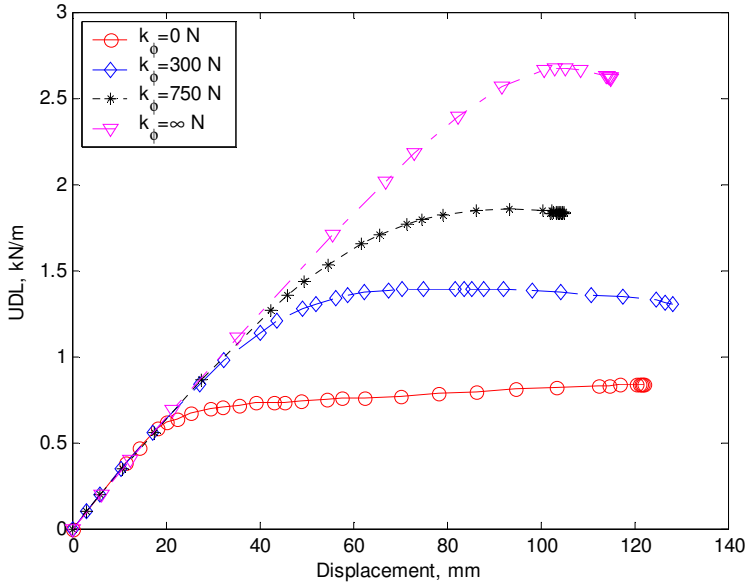

(b) Vertical displacement

Figure 5.15 Load-displacement curves of purlin with different rotational spring constants (Z20720, L=7000 mm).

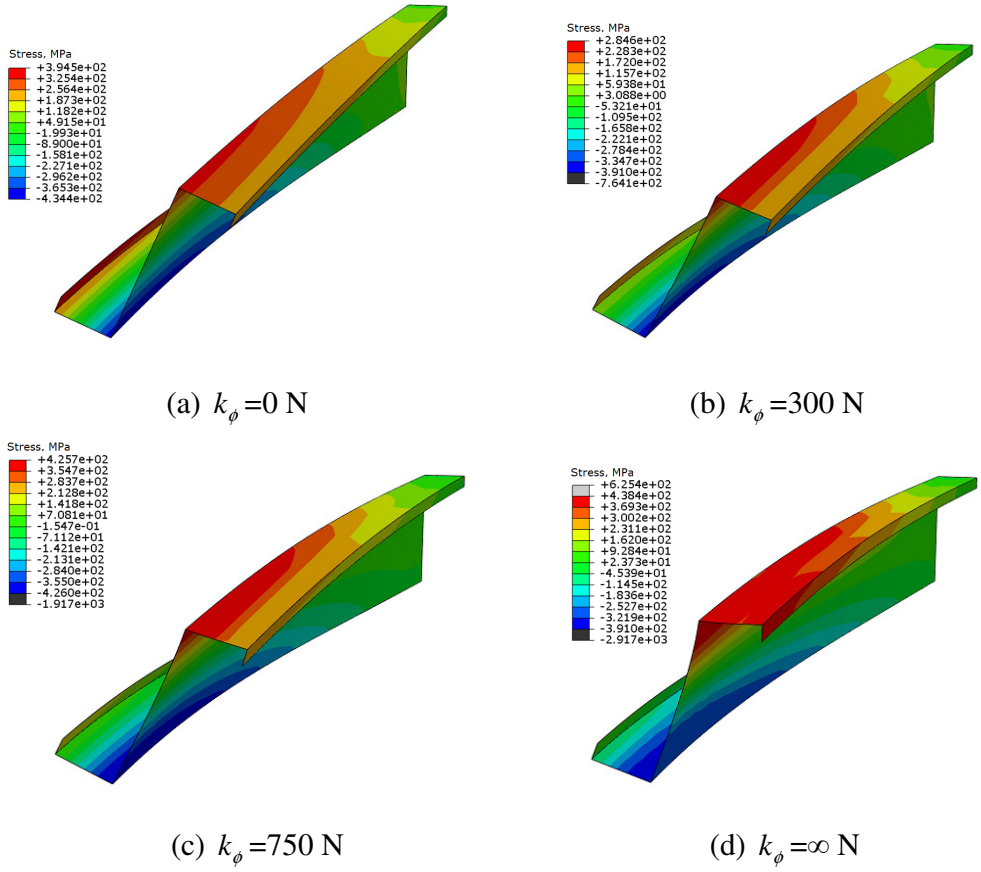

(a) k_ϕ =0 N (b) k_ϕ =300 N

(c) k_ϕ =750 N (d) k_ϕ =∞ N

Figure 5.16 Deformed shapes of purlin at failure point with longitudinal stress contours (Z20720, L=7000 mm).

Figures 5.17 and 5.18 show the load-displacement curves of an intermediate zed-section (Z20720) purlin, and the deformed shape of purlins at failure point with longitudinal stress contours when length, L=10000 mm, respectively. It can be seen in Figure 5.17 that the typical limiting failure of plasticity is found when k_ϕ=0 and the typical buckling failure is found when k_ϕ=300 N, k_ϕ=750 N, or k_ϕ=∞ N. It can also be seen from these two figures that the rotational spring stiffness has significant influence on the purlin performance; not only can it increase the failure load, but it can also alter the failure

mode of the purlin. Additionally, the investigation indicates that the lateral-torsional buckling essentially dominates the purlin with less rotational spring restraint (k_ϕ=300 N and k_ϕ=750 N), and the failure of the purlin is mainly controlled by the interaction of distortional and local buckling when the purlin has strong rotational spring restraint (k_ϕ=∞ N). For the purlin with no rotational restraint (k_ϕ=0), the failure of the purlin is mainly due to the plastic bending failure occurring in the plane of the minor axis. However, before failure, the purlin undergoes a lateral-torsional buckling. Furthermore, Table 5.2 presents the comparisons of critical buckling loads and ultimate failure loads for the intermediate zed-section (Z20720). It can be seen from this table that, the failure load is generally less than the critical load obtained directly from the linear buckling analysis, except for the purlins of length 7000 mm and 10000 mm with k_ϕ=0. Again, this is partly due to the influence of geometric nonlinearity and partly due to the influence of material nonlinearity before the buckling occurs. This indicates that for intermediate and long zed-section purlins subjected to uplift loading with no rotational restraint, the critical buckling load predicted using linear buckling analysis is very close to the limit load obtained from nonlinear analysis, which means that the bifurcation buckling is the weakest mode of failure for such purlins, and in this case linear buckling analysis can provide a very good prediction for the buckling behaviour as well as for the failure of the purlin. However, for the purlin with rotational restraint, the results that are obtained by linear buckling analysis are overestimated for most cases. This implies that the buckling interaction and the rotational spring stiffness have significant influence on the performance of the purlin, and the purlin length also has important impact on either the performance or failure mode of the purlin.

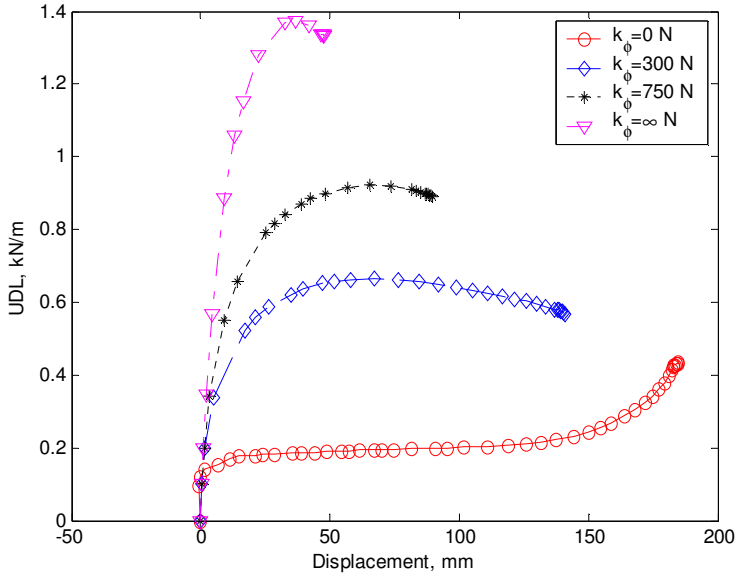

(a) Lateral displacement

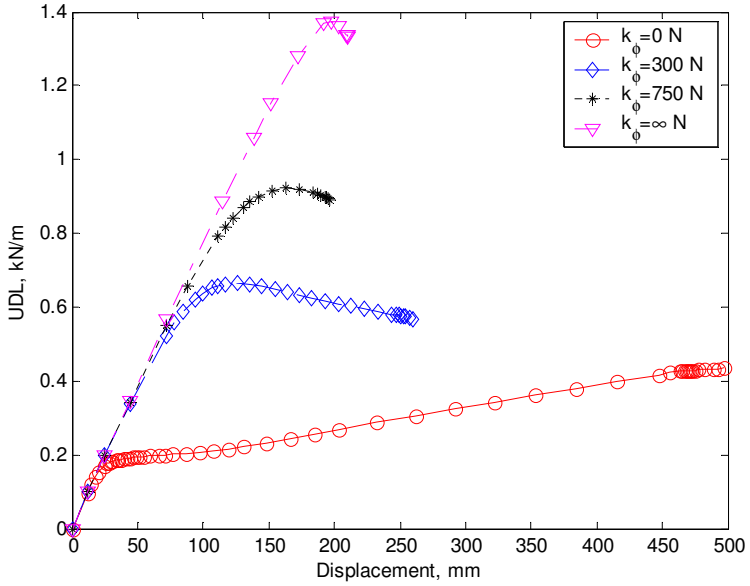

(b) Vertical displacement

Figure 5.17 Load-displacement curves of purlin with different rotational spring constants (Z20720, L=10000 mm).

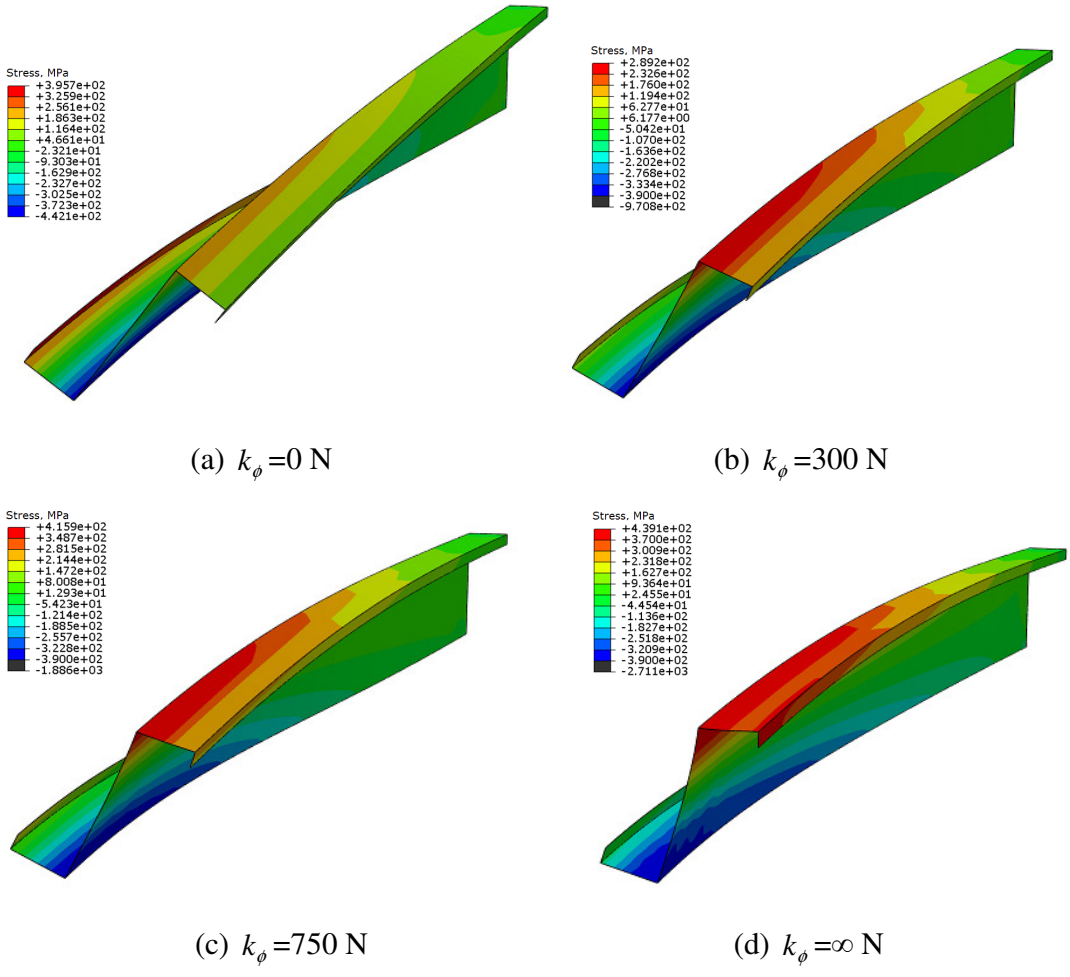

(a) k_ϕ =0 N (b) k_ϕ =300 N

(c) k_ϕ =750 N (d) k_ϕ =∞ N

Figure 5.18 Deformed shapes of purlin at failure point with longitudinal stress contours (Z20720, L=10000 mm).

Table 5.2 Comparison of critical buckling loads and plastic failure loads (Z20720).

L **(mm)**	k_ϕ**=0 N**		k_ϕ**=300 N**		k_ϕ**=750 N**		k_ϕ**=∞ N**	
	Failure Load (kN/m)	Buckling Load (kN/m)	Failure Load (kN/m)	Buckling Load (kN/m)	Failure Load (kN/m)	Buckling Load (kN/m)	Failure Load (kN/m)	Buckling Load (kN/m)
4000	5.951	6.132	6.245	7.52	6.504	8.85	7.076	10.03
7000	0.837*	0.762	1.394	2.107	1.855	2.798	2.670	3.636
10000	0.435*	0.211	0.664	0.859	0.921	1.123	1.371	1.681

Note: * = The catenary action.

The load-displacement curves of a large zed-section (Z40132) purlin of length L=4000 mm for four different rotational spring stiffness values (k_ϕ=0, k_ϕ=300 N, k_ϕ=750 N and k_ϕ=∞ N) and the corresponding deformed shapes of the purlins when the loads reach their ultimate values are not shown here. This is because for web depth of zed sections are greater than 400 mm, the ratio of beam length to web depth will be less than 1/10, in which case the member doesn't works as a beam. For extremely short beams the shear buckling is more dominant, in which case the load-displacement curves and the failure modes would be different from those of normal length beams.

Figure 5.19 shows the load-displacement curves of a large zed-section (Z40132) purlin of length, L=7000 mm for four different rotational spring stiffness values (k_ϕ=0, k_ϕ=300 N, k_ϕ=750 N and k_ϕ=∞ N). It is seen from this figure that for all stiffnesses of rotational spring, the typical buckling failure is defined by the load-displacement curves, in which the load raises to a peak point with increased displacement, and when the load passes the peak point, the load drops with further increased displacement. Furthermore, it also can be found that the failure load of the purlin increases with the stiffness value of the rotational spring.

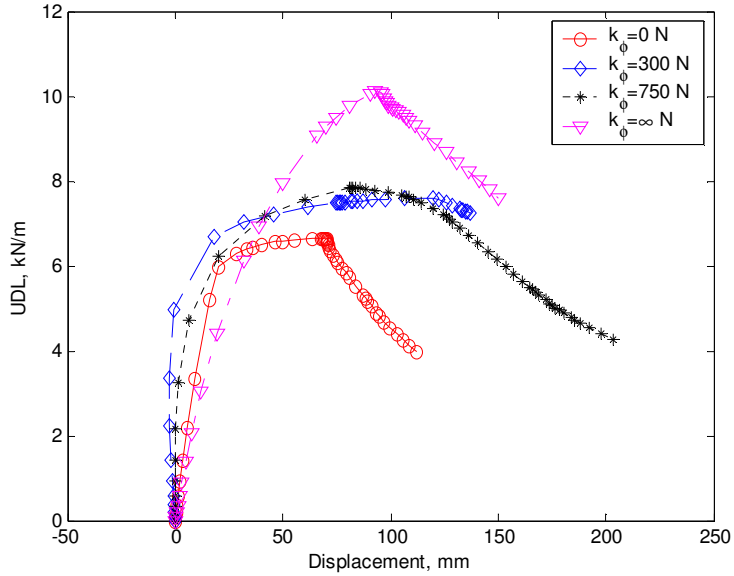

(a) Lateral displacement

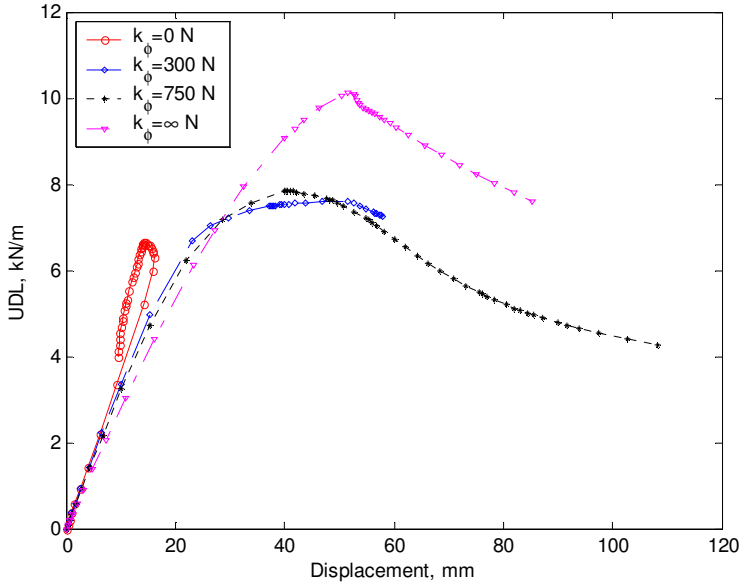

(b) Vertical displacement

Figure 5.19 Load-displacement curves of purlin with different rotational spring constants (Z40132, L=7000 mm).

Figure 5.20 shows the deformed shape of a large zed-section (Z40132) purlin at failure point with longitudinal stress contours for the beam length, L=7000 mm. It can be seen in the figure that when k_ϕ=0, the purlin is dominated by lateral-torsional buckling at the compression flange and lip system. However, because the torsion and lateral bending are dependent on the loading position and the web depth, in cases where the web is deeper, direction of movement of the free flange is in the opposite direction when the purlin is without rotational restraint at the upper flange. It can be seen that for other members with rotational spring, the failure mode is mainly controlled by the interaction of distortional and local buckling, which has varying wavelengths on the purlin dependent on different stiffnesses of rotational spring. The former reveals the significant influence of section dimensions. The latter implies that the rotational spring has significant influence on the failure mode and the wavelength of the distortional buckling. It is worth noting here that in the large zed-sections, the interaction of distortional and local buckling is located at the junction of the web and the lower flange, and the influence of the interaction increases with the increased stiffness of rotational spring. Additionally, compared with a smaller zed-section, the interaction in the large section has more influence, which is due to the ratio of length to web depth.

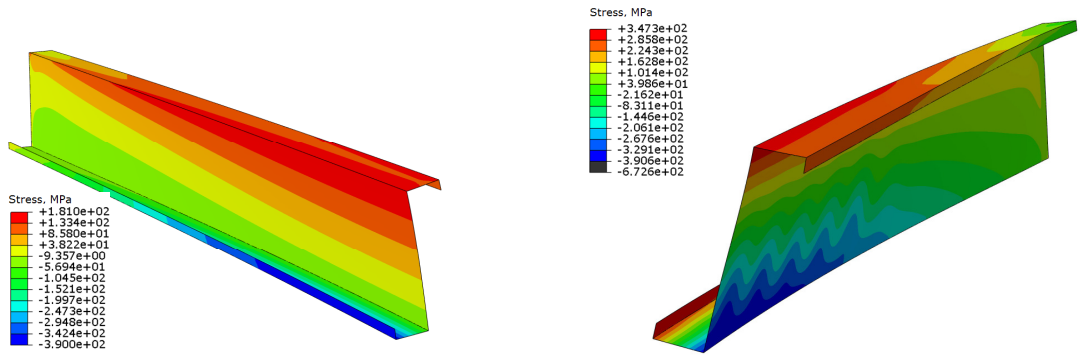

(a) k_ϕ =0 N (b) k_ϕ =300 N

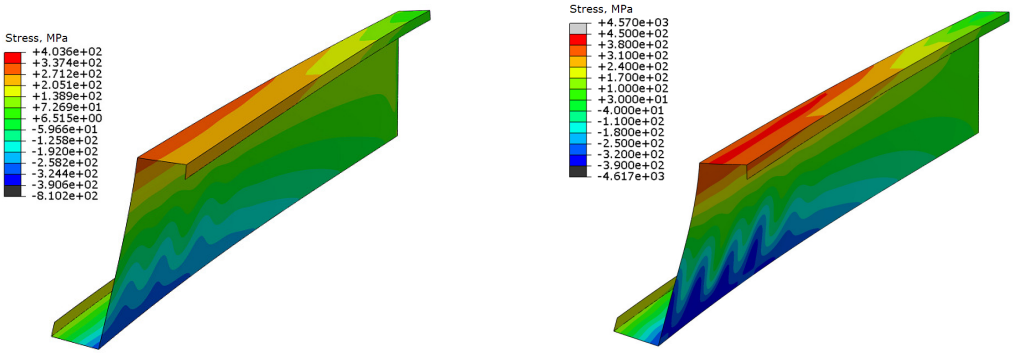

(c) k_ϕ =750 N (d) k_ϕ =∞ N

Figure 5.20 Deformed shapes of purlin at failure point with longitudinal stress contours (Z40132, L=7000 mm).

Figure 5.21 shows the load-displacement curves of the large zed-section (Z40132) purlin of length, L=10000 mm for four different rotational spring stiffness values (k_ϕ=0, k_ϕ=300 N, k_ϕ=750 N and k_ϕ=∞ N). It can be seen in this figure that the load increases with deflection until it reaches a limit point and after that it decreases with increasing deflection, indicating that for all stiffnesses of rotational spring, the failure mode of the purlins is typical buckling failure. However, it can also be observed from the figure that

the lateral displacements for k_ϕ=0, k_ϕ=300 N, and k_ϕ=750 N are much larger than the displacement when k_ϕ=∞ N, and in the post-buckling region, the increase of the load is very low with extremely large displacement. The reason for the stable post-buckling behaviour is that because of the ratio of purlin length to web depth, when a purlin is subjected to a transverse uplift load, the purlin rotates dramatically under no rotational restraint (or if the rotational restraint is not strong enough). This significantly reduces the flexural rigidity in the loading direction but increases the flexural rigidity in the perpendicular direction, and this in turn decreases its compression stress at the compression flange and thus postpones its distortional buckling and also increases its overall ultimate load. However, after an extremely large displacement, the purlin fails as a result of lateral-torsional buckling or the interaction of distortional and local buckling. Figure 5.22 reveals the deformed shapes of the large zed-section (Z40132) purlins with four different k_ϕ values when the loads reach their ultimate values. It is seen from this figure that when k_ϕ=0, due to the direction of lateral movement, the compressive stress is distributed at the middle junction of the lower flange and lip, and eventually there is a lateral-torsional buckling failure. The interaction of distortional and local buckling is found when k_ϕ=300 N, k_ϕ=750 N and k_ϕ=∞ N. Again, this shows that the rotational spring has significant influence on the failure mode of a large zed-section.

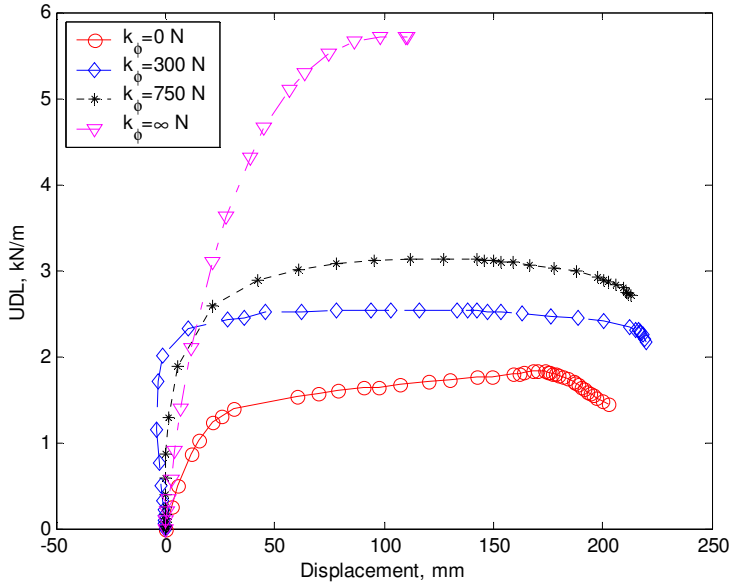

(a) Lateral displacement

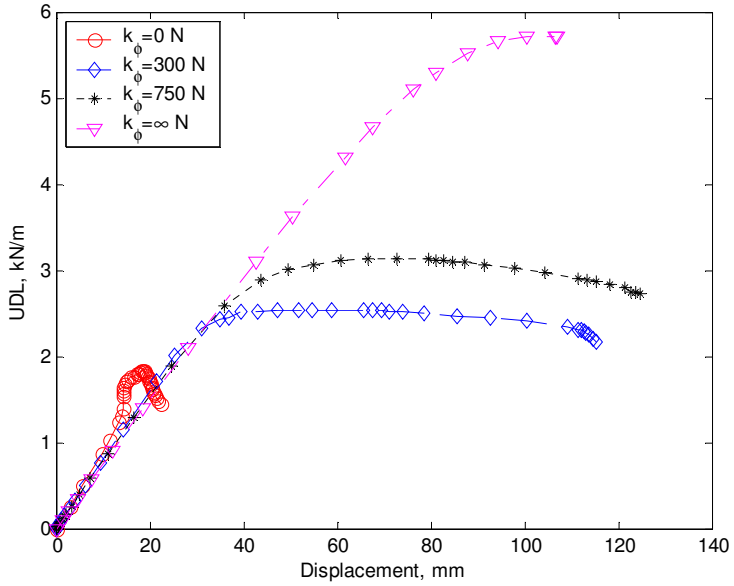

(b) Vertical displacement

Figure 5.21 Load-displacement curves of purlin with different rotational spring constants (Z40132, L=10000 mm).

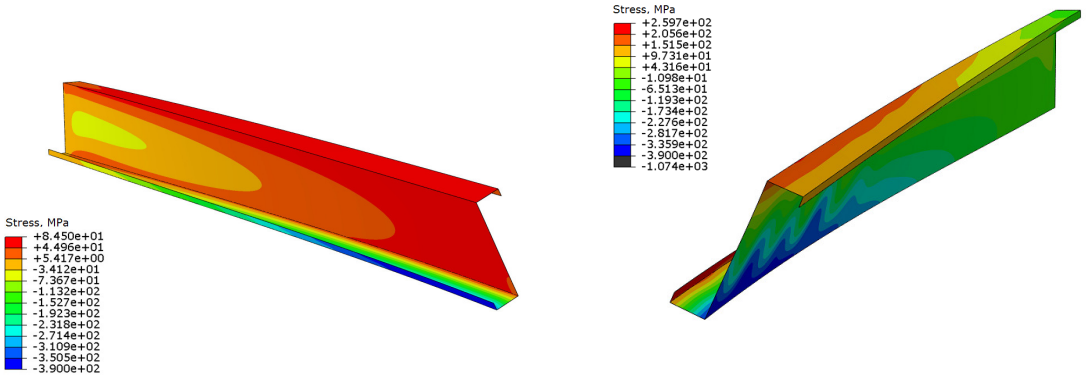

(a) k_ϕ =0 N (b) k_ϕ =300 N

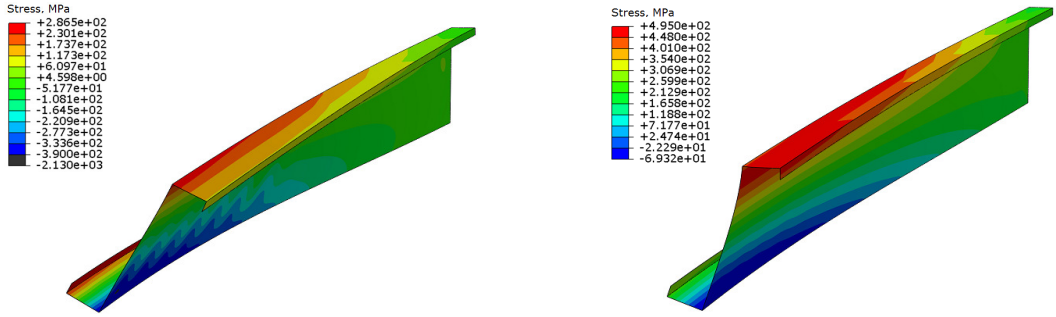

(c) k_ϕ =750 N (d) k_ϕ =∞ N

Figure 5.22 Deformed shapes of purlin at failure point with longitudinal stress contours (Z40132, L=10000 mm).

Table 5.3 presents comparisons of critical buckling loads and ultimate failure loads for large zed-section (Z40132). Only intermediate and long lengths of purlin are shown in this table, and it can be seen that for both lengths of purlin, when k_ϕ=0, the ultimate loads obtained from nonlinear analysis are higher than the critical buckling loads predicted by linear buckling analysis. But for other stiffnesses of rotational spring, the ultimate load is lower than the critical buckling load. This reveals that the rotational spring has important effect on the performance of large zed-section.

Table 5.3 Comparison of critical buckling loads and plastic failure loads (Z40132).

L (mm)	**k_ϕ=0 N**		**k_ϕ=300 N**		**k_ϕ=750 N**		**k_ϕ=∞ N**	
	Failure Load (kN/m)	Buckling Load (kN/m)	Failure Load (kN/m)	Buckling Load (kN/m)	Failure Load (kN/m)	Buckling Load (kN/m)	Failure Load (kN/m)	Buckling Load (kN/m)
7000	6.6512*	6.464	7.6112	7.9892	7.8509	8.2716	10.11	12.121
10000	1.8316*	1.7424	2.5551	2.6512	3.1316	6.6589	5.715	7.0431

Note: * = The catenary action.

Figure 5.23 illustrates a comparison of normalised moment capacities obtained from different lengths of small zed-section (Z12515) with various stiffnesses of rotational spring. The M_{Ed} is calculated based on the obtained critical load in terms of the following formula,

$$M_{Ed} = \frac{\omega_{cr} L^2}{8} \tag{5-1}$$

where ω_{cr} = the ultimate load obtained from the nonlinear finite element analysis.

Figure 5.23 shows that for small zed-section (Z12515), the moment capacity of three different lengths of purlin are very similar, and the moment capacities increase rapidly until k_ϕ=4000N. After that, the moment capacities rise slightly to reach the point of full restraint. This indicates that for all lengths of small zed-section, the rotational spring has noticeable effect on the performance when the purlin is partially restrained, but when the purlin approaches full restraint, the influence of the rotational spring is insignificant. It can also be found that for a high k_ϕ, the moment capacity increases with the purlin length.

This is because for a high $k_{\phi,}$ the failure of the beam is dominated by distortional buckling. The wavelength of the distortional buckling however is dependent on the k_{ϕ} value.

Figure 5.24 shows the normalised moment capacity against the rotational spring stiffness for intermediate zed-section (Z20720) of three different lengths. When the length of the purlins is 4000 mm, the moment capacity increases slightly with increased rotational spring stiffness, which implies that the rotational spring stiffness has almost no influence on the performance of moment capacity. However, for intermediate and long length purlins (L=7000 mm & 10000 mm), the moment capacities increase rapidly and closely with rotational spring stiffness, particularly, when k_{ϕ} increases from 100N to 4000N. This reveals that, for intermediate and long members, the rotational spring stiffness has a considerable influence on the performance of moment capacity.

Figure 5.25 presents the normalised moment capacities obtained from different lengths against rotational spring stiffness for large zed-section (Z40132). Due to beam theory, the ratio of beam web depth to beam length should be less than 1/10. For large zed section, because of deep depth of web (400mm), therefore, the length of 4000mm should not be considered as a beam and the result for 4000mm is not considered in large sections, only 7000mm and 10000mm are remained. When the length is 7000 mm or 10000 mm, the moment capacity increases with increased stiffness of rotational spring; however, the difference between these two lengths is that the moment capacity increases gently when L=7000 mm, but rises strikingly at the region of 100N to 10000N when L=10000 mm.

This implies that the length of the purlin has significant influence on the performance of the large zed-section.

It should be mentioned that the rotational spring has significant influence on the performance of the purlin, and the level of significance is dependent on the stiffness value of the rotational spring, in the range of k_ϕ=100 N to k_ϕ=4000 N. Additionally, it can be shown from these figures that the longer beam is more affected by the rotational spring, and the section dimensions also have considerably more impact on the performance of the purlin.

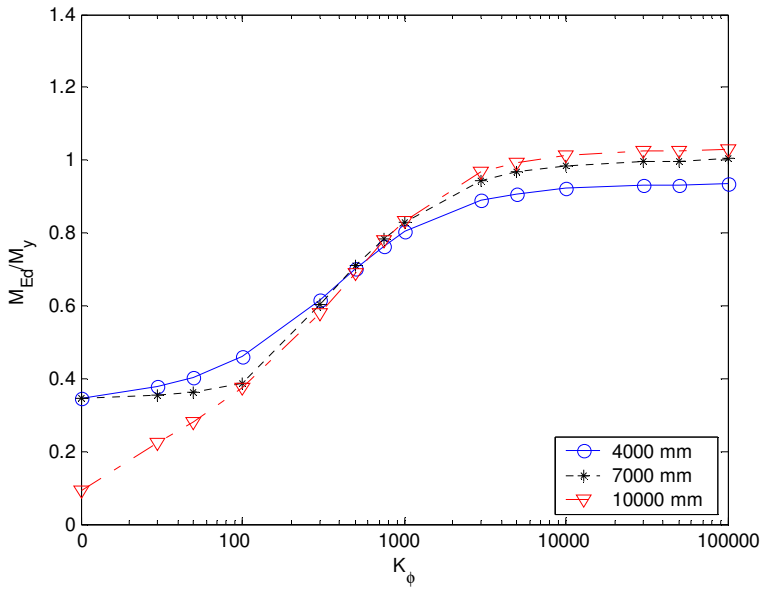

Figure 5.23 Moment capacity against rotational spring stiffness for small zed-section (Z12515).

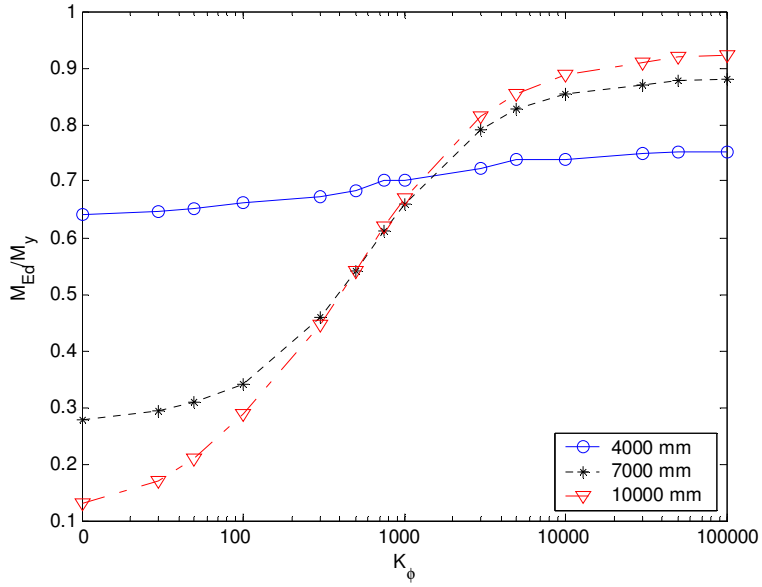

Figure 5.24 Moment capacity against rotational spring stiffness for intermediate zed-section (Z20720).

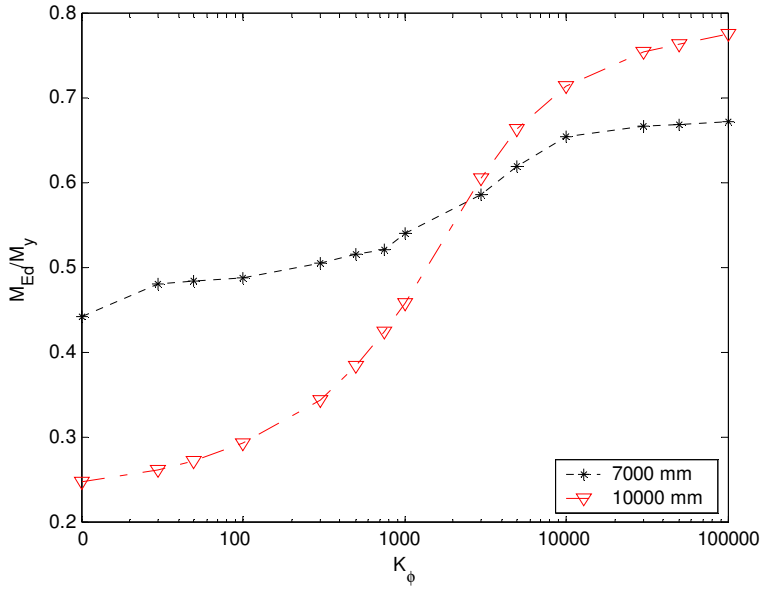

Figure 5.25 Moment capacity against rotational spring stiffness for large zed-section (Z40132).

5.3.3 Design curve of zed-sections

Figures 5.26 to 5.28 illustrate the comparison of the normalised moment capacities obtained from different rotational spring stiffnesses (k_ϕ=0, k_ϕ=300 N, k_ϕ=750 N and k_ϕ=∞ N) and varying length for small (Z12515), intermediate (Z20720) and large (Z40132) zed-sections, respectively. The M_{Ed} and M_y values are calculated using the same method as used in section 5.3.2, with the yield strength of 390MPa. It can be seen from Figure 5.26 that the moment capacities of small zed-sections are divided into four levels by the four different stiffnesses of rotational spring, in which the moment capacity increases with rotational spring stiffness. For each individual value of rotational spring stiffness, the amount of moment capacity affected by the length is not significantly different. This indicates that, for small zed-sections, the rotational spring has very important influence on the performance of the purlin, but the effect of the length is not significant. It also can be seen in Figure 5.27 that for intermediate zed-sections, when k_ϕ=0, k_ϕ=300 N and k_ϕ=750 N, the moment capacity reduces with increased length for each individual rotational spring stiffness. As is to be expected, the moment capacity rises with increased rotational spring stiffness. However, when k_ϕ=∞ N, the moment capacity increases with length and still rises with increased rotational spring stiffness. The former shows that length has considerable impact on moment capacity of the purlin. The latter also suggests that the rotational spring stiffness has important influence on purlin performance. The main features of Figure 5.28 are similar to those shown in Figure 5.27, but the key difference is the amount of increased moment capacities are reduced. This implies that greater rotational spring stiffness has more significant influence on the moment capacity of the large zed-section than the does lesser rotational spring stiffness.

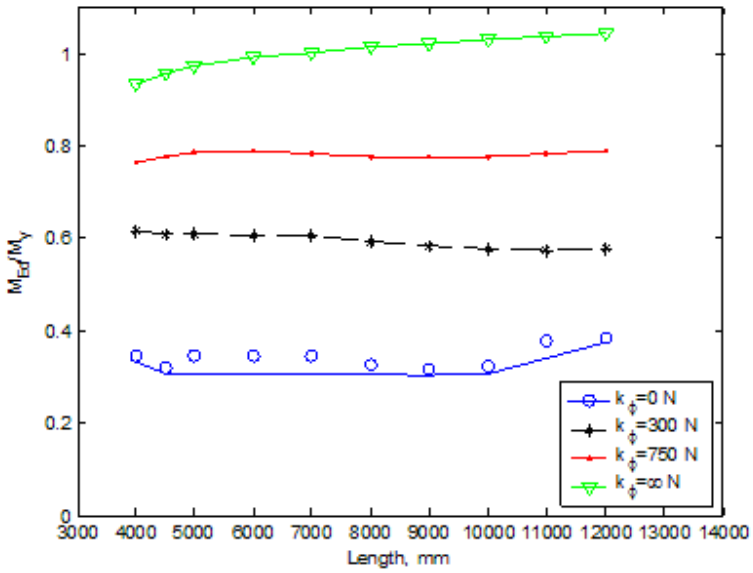

Figure 5.26 Design curves of moment capacity against length for small zed-section (Z12515).

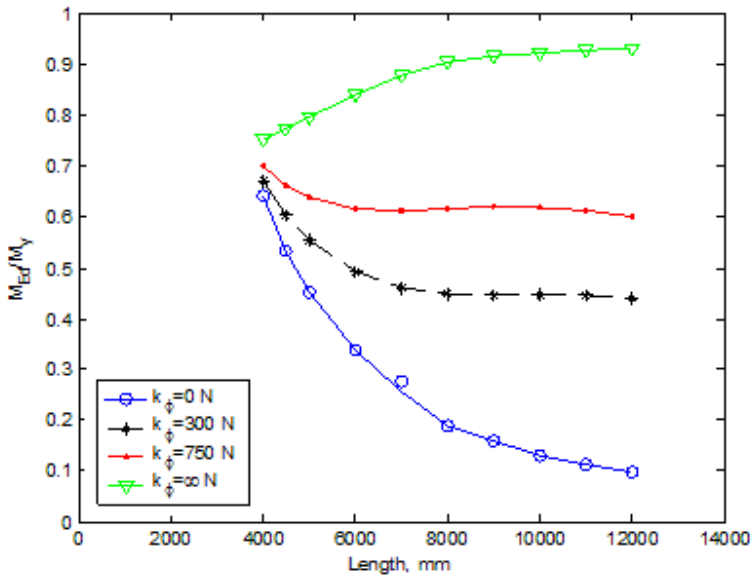

Figure 5.27 Design curves of moment capacity against length for intermediate zed-section (Z20720).

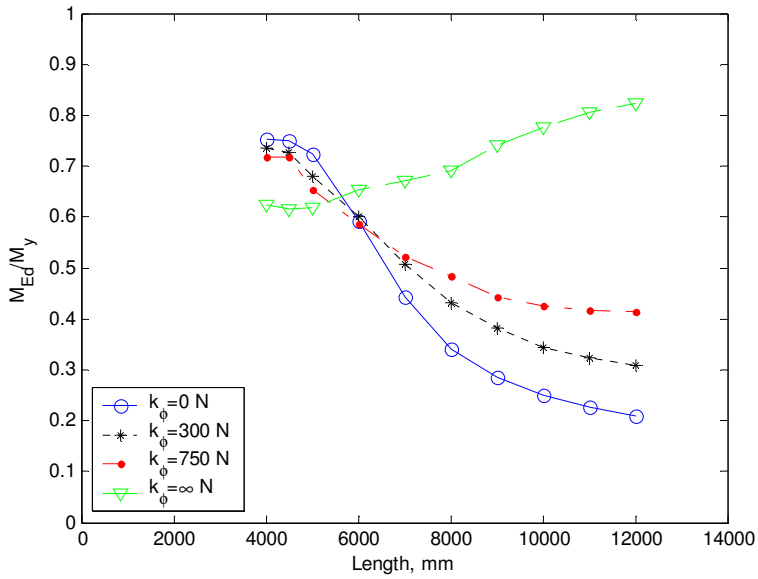

Figure 5.28 Design curves of moment capacity against length for large zed-section (Z40132).

Figures 5.29 to Figure 5.31 show the comparison of the Direct Strength Method (DSM) and the present finite element analysis (FEA) for small (Z12515), intermediate (Z20720) and large (Z40132) zed-sections beams under various rotational spring stiffnesses (k_ϕ=0, k_ϕ=300 N, k_ϕ=750 N and k_ϕ=∞ N). The slenderness of the beam is represented by $(M_y/M_{cr})^{0.5}$, where M_{cr} is the critical moment of buckling which is calculated using the first eigen-value of lateral-torsional buckling. From Figure 5.29, it can be seen that when k_ϕ=0 in the small zed-section (Z12515), the FEA results are compared with predictions by DSM and indicate that the latter provides a very good estimate for lateral-torsional buckling in the pure bending condition but the predictions can be rather conservative when a moment gradient is present. However, it can be seen in Figures 5.30 and 5.31 that the predictions show good agreement between the DSM and FEA when k_ϕ=0 in the

intermediate zed-section (Z20720) and large zed-section (Z40132). This indicates the DSM (which is based on pure bending to estimate the lateral-torsional buckling) can be used for the intermediate and large zed-section beam under uniformly distributed load if these members have no rotational restraint. It should be pointed out that the prediction lines of the purlin with rotational restraint are above the DSM line, which indicates that the limit stress related to the failure mode is dominated by the interaction of distortional and local buckling. Consequently, when the DSM is applied to beams with uniformly distributed load with rotational restraint, the moment prediction will be overly conservative. Another feature found from Figure 5.31 is that the FEA results are below the DSM line. This can be explained by the shear buckling which is occurring in the short length purlins, particularly in the large zed-section due to the lower ratio of length to web depth.

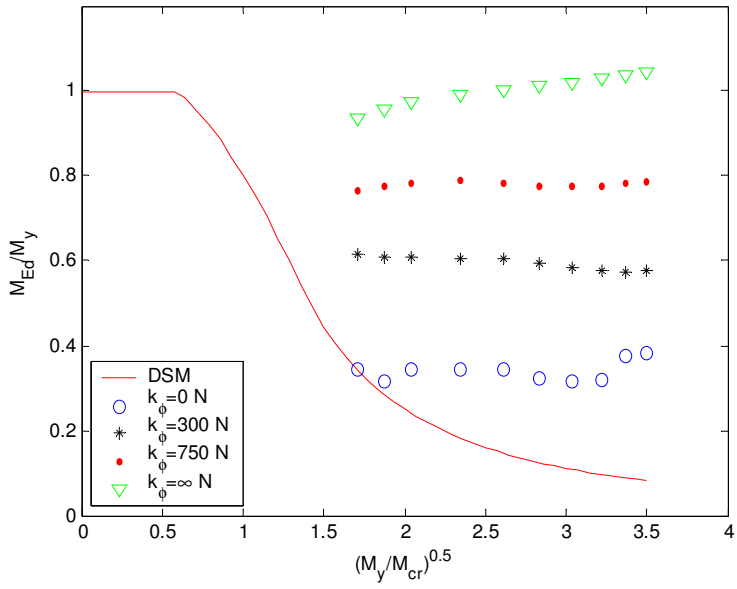

Figure 5.29 Design curves of moment capacity against slenderness for small zed-section (Z12515).

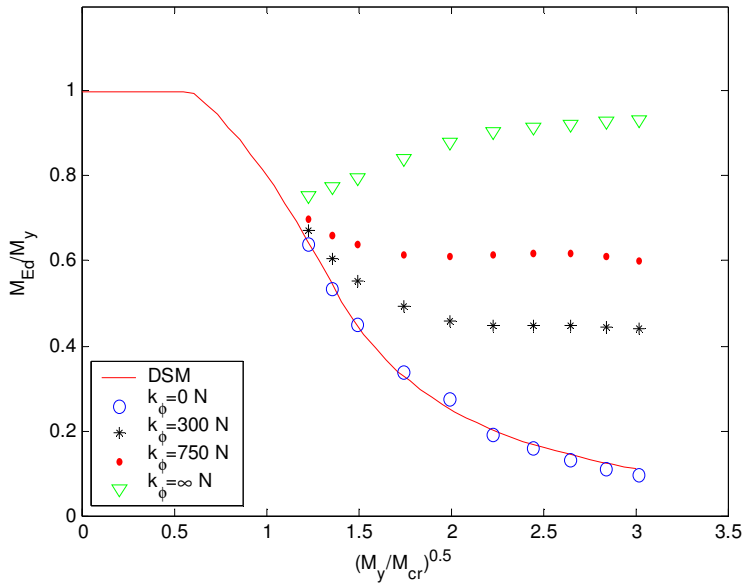

Figure 5.30 Design curves of moment capacity against slenderness for intermediate zed-section (Z20720).

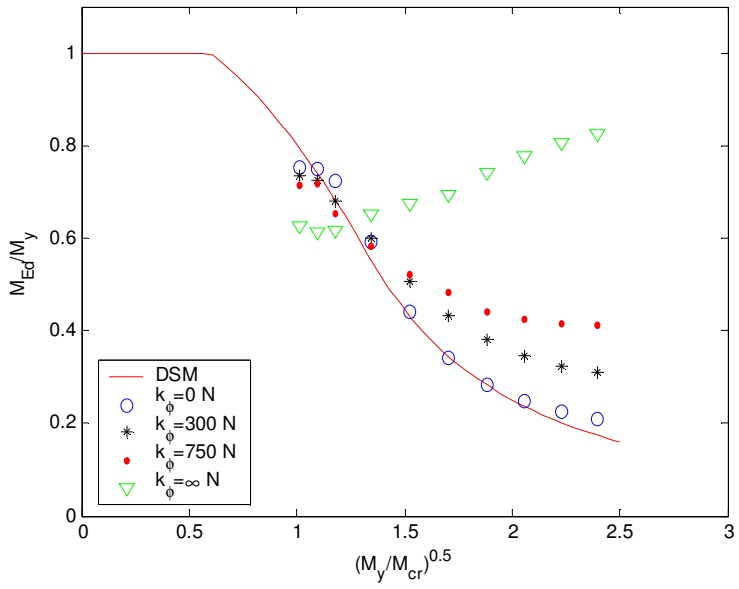

Figure 5.31 Design curves of moment capacity against slenderness for large zed-section (Z40132).

5.4 Post-Buckling analysis of channel-sections

5.4.1 Influence of spring stiffness and the dimensions of cross section

For a given purlin length and rotational spring stiffness, the load-displacement curves of the purlin can be obtained from the geometric and material nonlinear finite element analysis. Figure 5.32 shows the load-displacement curves of a small channel-section (C12515) purlin of length, L=4000 mm for four different rotational spring stiffness values (k_ϕ=0, k_ϕ=300 N, k_ϕ=750 N and k_ϕ =∞ N). The displacements are the vertical displacement at the upper flange-web junction and the horizontal displacement at the lower flange-web junction, both on the symmetric section of the purlin. It can be seen from this figure that the load increases with the displacement until it reaches the peak point, afterwards it decreases with further increased displacement. This indicates that the failure of the purlin is a typical buckling failure. The failure load of the purlin increases with the rotational spring stiffness and the lateral displacement reduces with increased rotational spring stiffness. This implies that the rotational spring stiffness not only increases the failure load but also varies the failure type of the purlin. Figure 5.33 shows the deformed shapes of the small channel-section (C12515) purlins with four different k_ϕ values when the loads reach their ultimate points. It can be seen in this figure that the dominated buckling at failure point changes from local buckling to the interaction of distortional and local buckling as the rotational spring stiffness increases. When k_ϕ=0, the purlin has severe twisting deformation, and the interaction of distortional and local buckling can be found at the lower web. The results shown in the figure demonstrate that the rotational spring has significant influence on its failure mode.

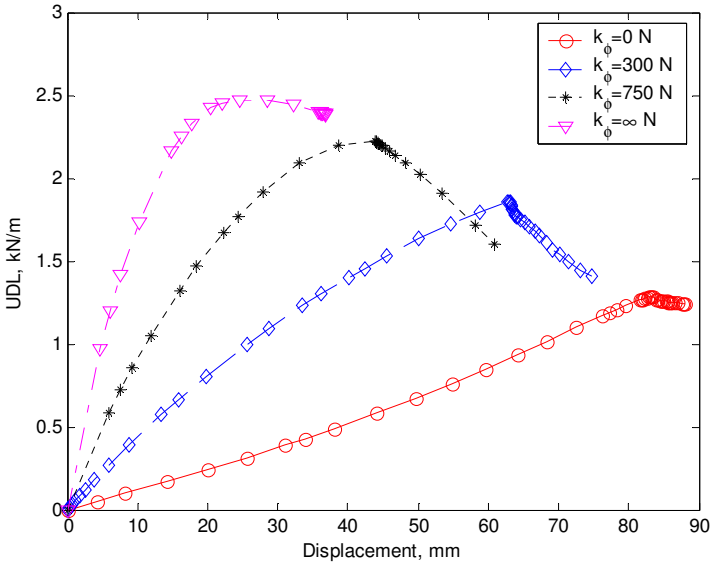

(a) Lateral displacement

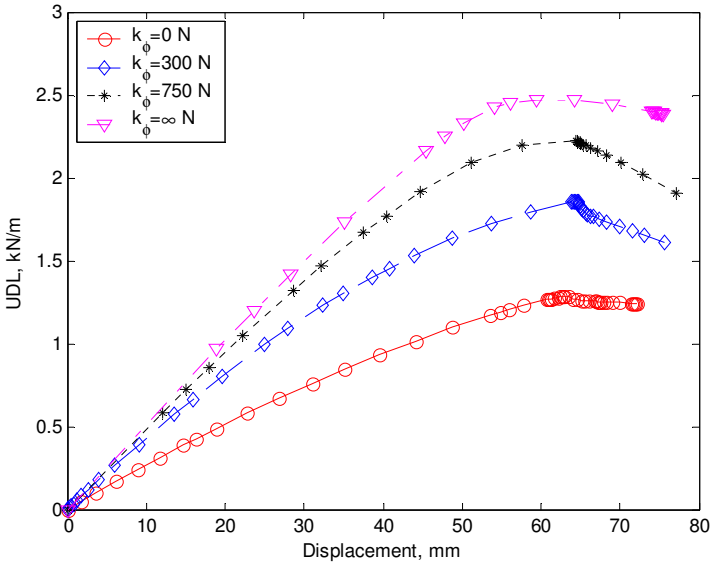

(b) Vertical displacement

Figure 5.32 Load-displacement curves of purlin with different rotational spring constants (C12515, L=4000 mm).

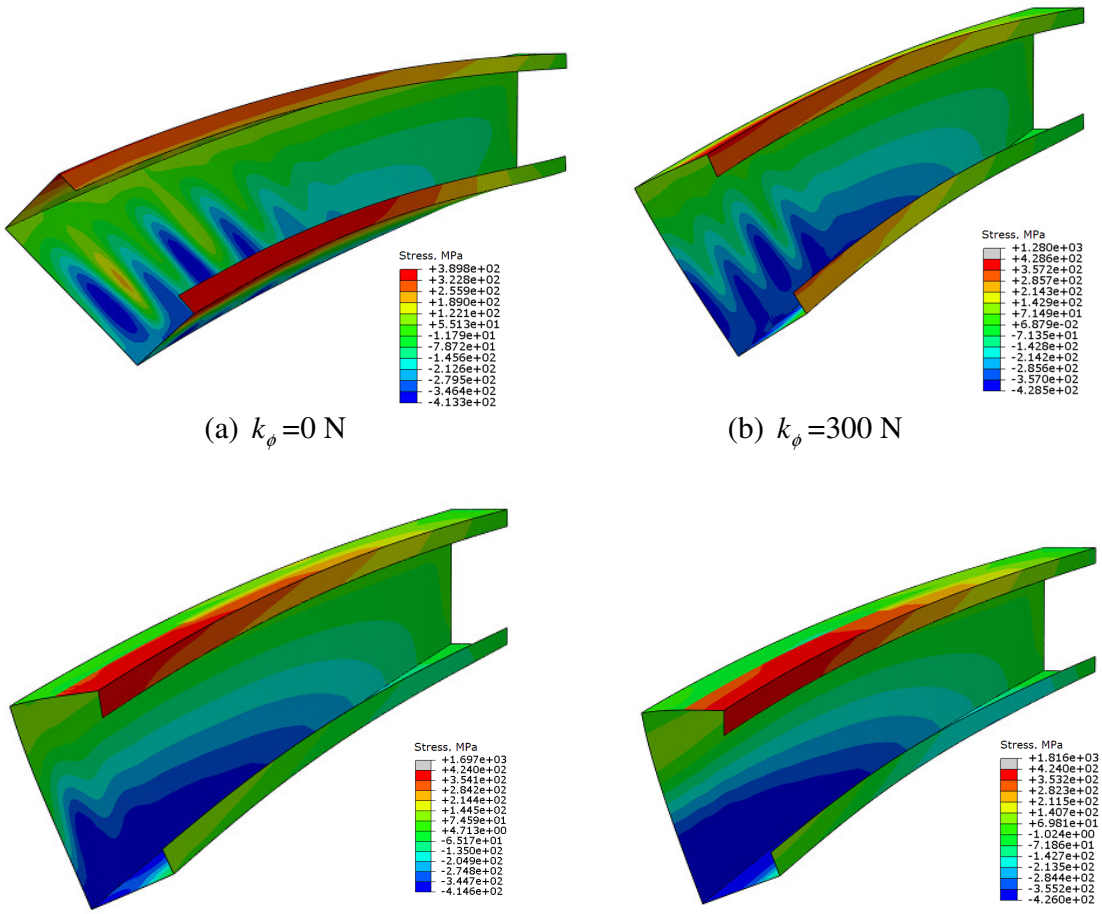

(a) k_ϕ =0 N (b) k_ϕ =300 N

(c) k_ϕ =750 N (d) k_ϕ =∞ N

Figure 5.33 Deformed shapes of purlin at failure point with longitudinal stress contours (C12515, L=4000 mm).

Figure 5.34 shows the load-displacement curves of small channel-section (C12515) with length of purlin, L=7000 mm for four different rotational spring stiffness values (k_ϕ=0, k_ϕ=300 N, k_ϕ=750 N and k_ϕ=∞ N). When k_ϕ=0, the typical plasticity failure is found from the load-displacement curve, in which the displacement rises dramatically while the load

increases gradually in the first part. In the second part of the curve, the vertical displacement increases with the load until it reaches the maximum load point, while the lateral displacement increases only marginally when the increased load climbs rapidly. When k_ϕ=300 N, k_ϕ=750 N or $k_\phi = \infty$ N, the load increases with displacement until the load reaches the peak point. After the peak point, the load reduces with further increased displacement. This again shows typical buckling failure. The resultant deformed shapes of the purlins when the loads reach their ultimate values are shown in Figure 5.35. It can be seen from the figure that, when k_ϕ=0, the flexural rigidity is reduced significantly in the loading direction due to the purlin twisting considerably, which increases the flexural rigidity in the perpendicular direction. This leads the bending stresses to increase at a higher rate than the actual load, and eventually causes the purlin to have a plastic failure. The deformations of the purlins with k_ϕ=300 N, k_ϕ=750 N and $k_\phi = \infty$ N are very similar and the compression stresses are distributed at the lower flange-web junction of the middle of the purlin and lead to distortional buckling being the main failure mode for spring stiffnesses, k_ϕ=300 N, k_ϕ=750 N or $k_\phi = \infty$ N. These figures again show that rotational spring stiffness has significant influence on the performance and failure mode of the section.

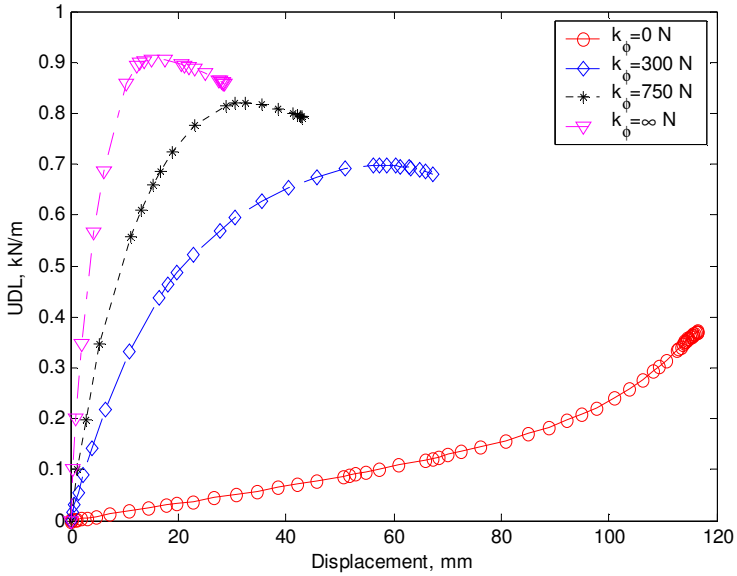

(a) Lateral displacement

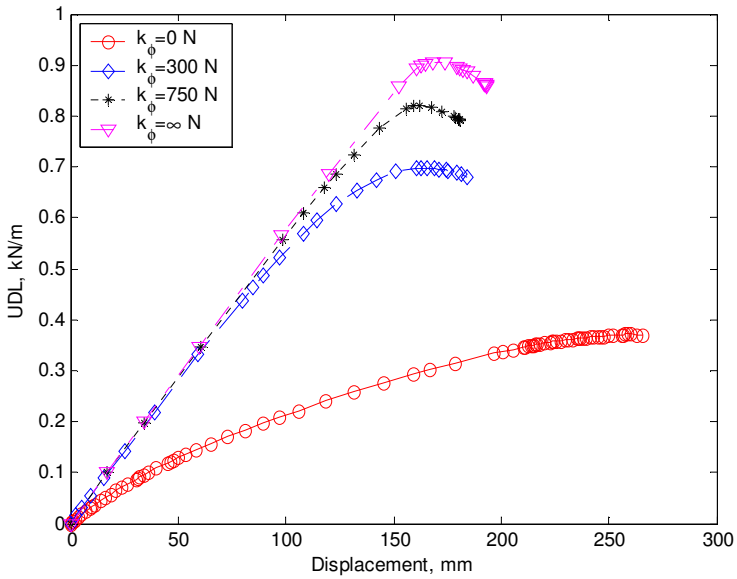

(b) Vertical displacement

Figure 5.34 Load-displacement curves of purlin with different rotational spring constants (C12515, L=7000 mm).

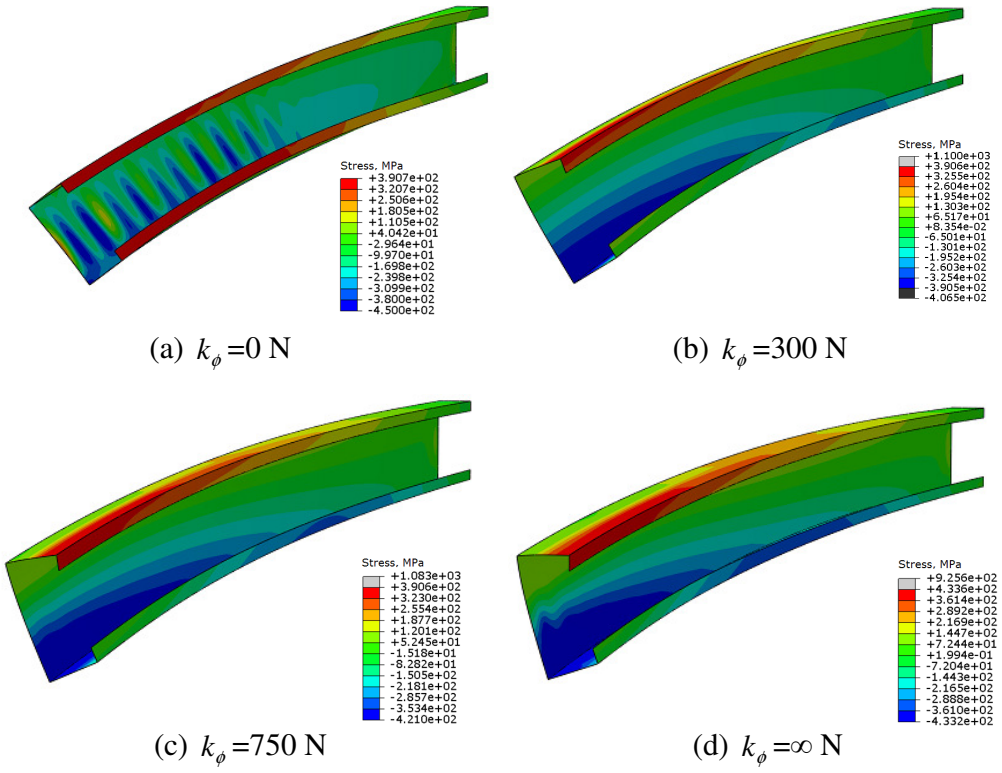

(a) k_ϕ =0 N (b) k_ϕ =300 N

(c) k_ϕ =750 N (d) k_ϕ =∞ N

Figure 5.35 Deformed shapes of purlin at failure point with longitudinal stress contours (C12515, L=7000 mm).

Figure 5.36 shows the load-displacement curves of the small channel-section (C12515) with length of purlin, L=10000 mm for four different rotational spring stiffness values (k_ϕ=0, k_ϕ=300 N, k_ϕ=750 N and k_ϕ=∞ N). The related deformed shapes of the purlins for different rotational spring stiffnesses are shown in Figure 5.37. The main features of these figures are similar to those shown in the figures for length, L=7000 mm. The typical plasticity and buckling failure modes are distinguished. Due to compression stress at the lower flange-web junction in the middle of the purlin and also in the compression flange and lip system, the interaction of distortional and local buckling is expected when k_ϕ=300 N, and distortional buckling is present when k_ϕ=750 N and k_ϕ=∞ N.

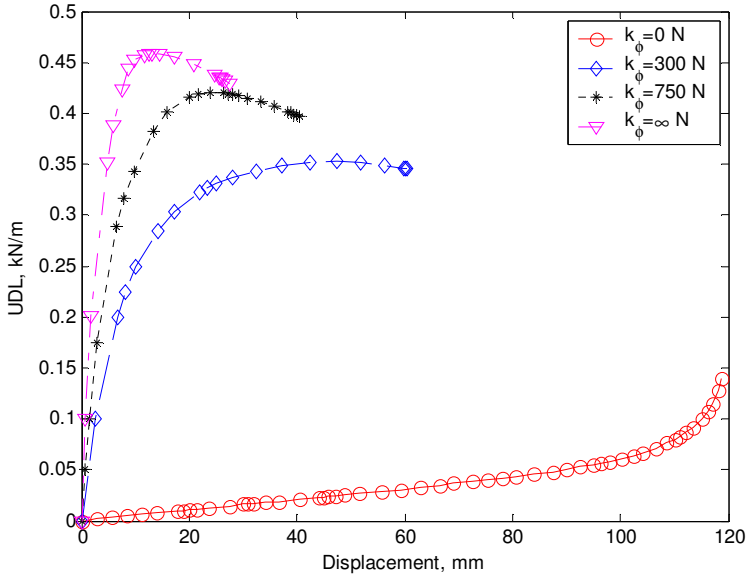

(a) Lateral displacement

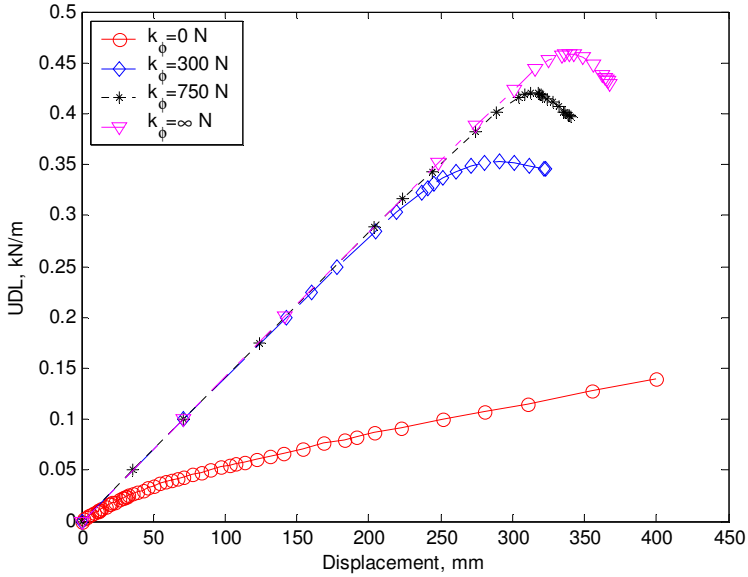

(b) Vertical displacement

Figure 5.36 Load-displacement curves of purlin with different rotational spring constants (C12515, L=10000 mm).

Table 5.4 provides a detailed comparison of the difference between the critical load calculated from linear buckling analysis and the failure load obtained from nonlinear analysis. The difference is partially due to the influence of geometric nonlinearity and partially caused by the influence of material nonlinearity before the buckling occurs. For short length purlins with no rotational spring restraint, the critical buckling load is higher than the plastic failure load, whereas for medium and long length purlins, the critical buckling load is lower than the plastic failure load. This implies that the influence of the rotational spring on the failure mode of the purlin is also dependent on the purlin length.

Table 5.4 Comparison of critical buckling loads and plastic failure loads (C12515).

L **(mm)**	k_ϕ**=0 N**		k_ϕ**=300 N**		k_ϕ**=750 N**		k_ϕ**=∞ N**	
	Failure Load (kN/m)	Buckling Load (kN/m)	Failure Load (kN/m)	Buckling Load (kN/m)	Failure Load (kN/m)	Buckling Load (kN/m)	Failure Load (kN/m)	Buckling Load (kN/m)
4000	1.2862	1.6072	1.8578	3.8379	2.2216	4.0858	2.4717	4.5602
7000	0.3718*	0.2699	0.6970	0.8342	0.8200	1.0315	0.9062	1.3322
10000	0.1395*	0.0764	0.3524	0.3672	0.4205	0.4610	0.4585	0.6176

Note: * = The catenary action.

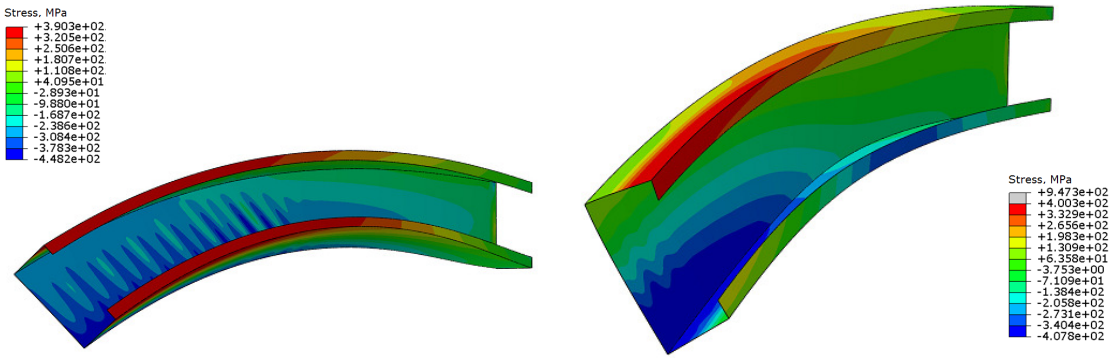

(a) k_ϕ =0 N (b) k_ϕ =300 N

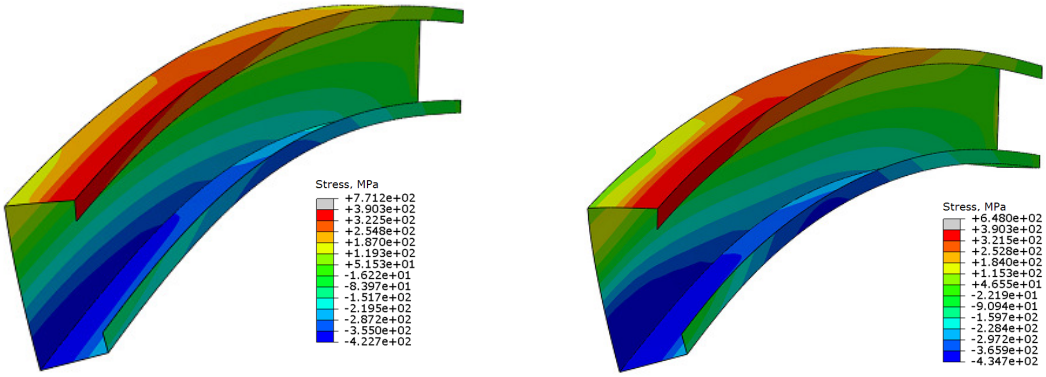

(c) k_ϕ =750 N (d) k_ϕ =∞ N

Figure 5.37 Deformed shapes of purlin at failure point with longitudinal stress contours (C12515, L=10000 mm).

Figures 5.38 and 5.39 show the influence of rotational spring stiffness (k_ϕ=0, k_ϕ=300 N, k_ϕ=750 N and k_ϕ=∞ N) on intermediate channel-section (C20720) with length of purlin, L=4000 mm when it is subjected to transverse uniformly distributed uplift loading. Figure 5.38 shows the load-displacement curves of the geometric and material nonlinear analysis for the vertical displacement at the upper flange-web junction and the lateral displacement at the lower flange-web junction. It is clear that when k_ϕ=0, k_ϕ=300 N, k_ϕ=750 N or k_ϕ=∞ N, the typical buckling failure is illustrated by the load-displacement curves, in which the load increases to reach peak point with increasing displacement and decreases with further increased displacement. The ultimate load increases and the lateral displacement decreases with increased stiffness of the rotational spring. This indicates the rotational spring has important effect on the purlin performance.

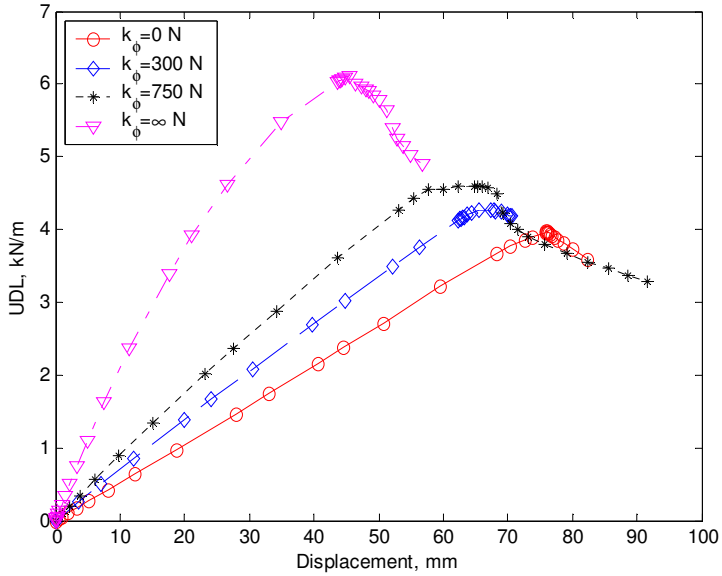

(a) Lateral displacement

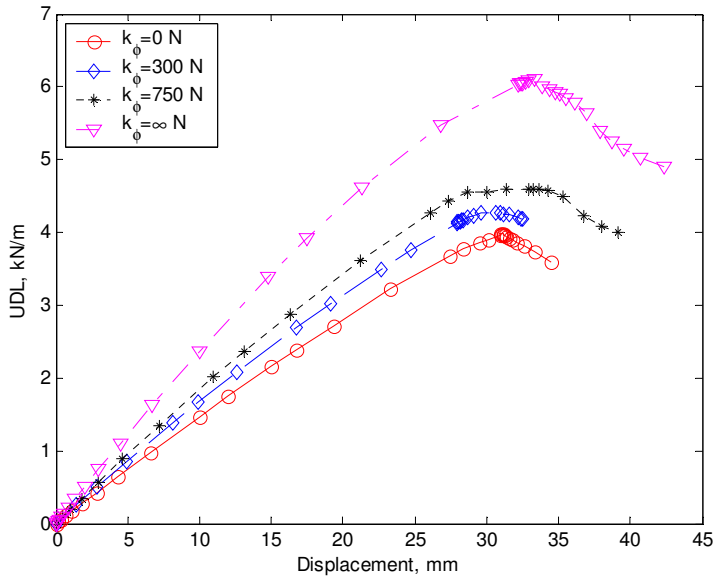

(b) Vertical displacement

Figure 5.38 Load-displacement curves of purlin with different rotational spring constants (C20720, L=4000 mm).

Figure 5.39 shows the deformed shapes and longitudinal stress distribution in intermediate channel-section (C20720) purlins with four different k_ϕ values when the loads reach their ultimate points. It is seen from this figure that the buckling failure mode is affected due to varying half-wavelength when the purlin is under the influence of a rotational spring. The buckling mode varies with spring constant. For example, it is distortional buckling for k_ϕ=0, and the interaction of distortional and local buckling for k_ϕ=300 N, k_ϕ=750 N or k_ϕ=∞ N. These two figures not only reveal the significance of rotational spring stiffness on the performance of the purlin but also on its failure mode.

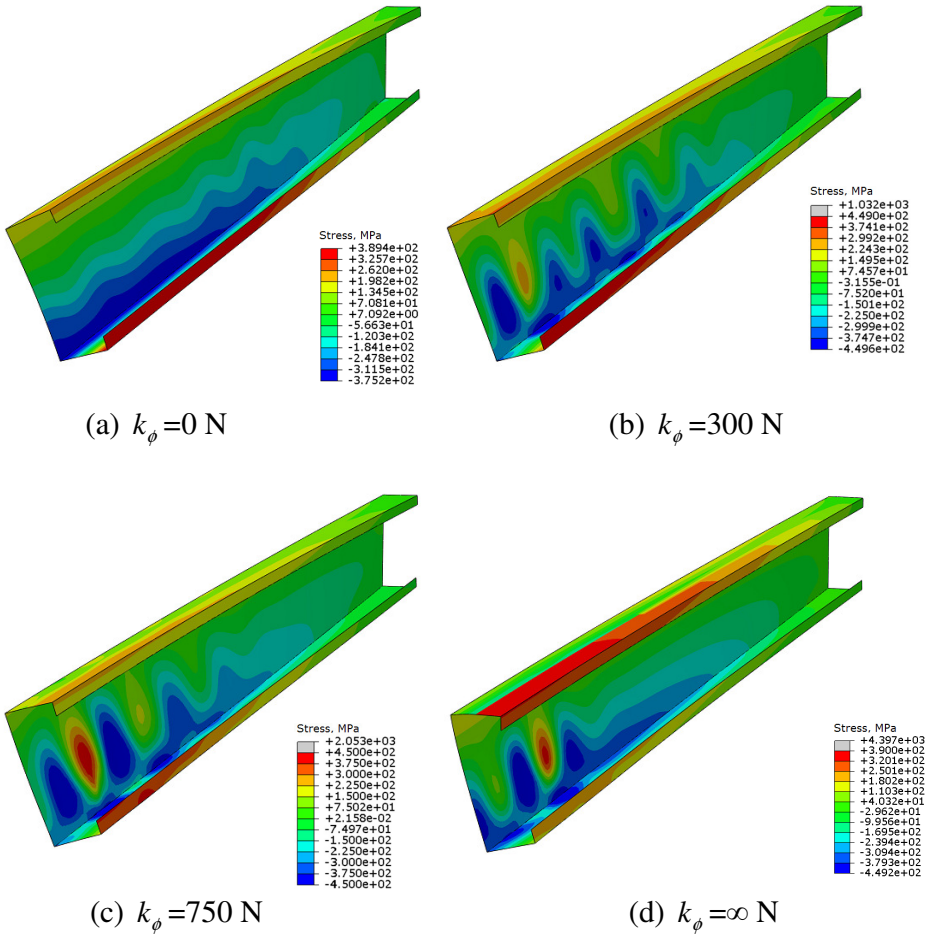

(a) k_ϕ=0 N (b) k_ϕ=300 N

(c) k_ϕ=750 N (d) k_ϕ=∞ N

Figure 5.39 Deformed shapes of purlin at failure point with longitudinal stress contours (C20720, L=4000 mm).

The load-displacement curves of the intermediate channel-section (C20720) purlin of length, L=7000 mm for four different rotational spring stiffness values (k_ϕ=0, k_ϕ=300 N, k_ϕ=750 N and k_ϕ=∞ N) are shown in Figure 5.40. The main feature of this figure is similar to those shown in Figure 5.38 and thus is not discussed further. The deformed shapes of the purlin at failure point are shown in Figure 5.41. It can be seen that the intermediate channel-section has an extremely large displacement when k_ϕ=0 and k_ϕ=300 N, and the failure mode is local buckling, which is located within the web. However, for the higher rotational spring stiffness, the half-wavelength is increased which results in the failure mode being more complicated when the rotational spring stiffness is increased. The interaction of distortional and local buckling can be found when k_ϕ=750 N and k_ϕ=∞ N. These consequences reveal that the rotational spring is important, as explained in chapter three, the channel-section is complicated due to the shear centre being far away from the centroid centre.

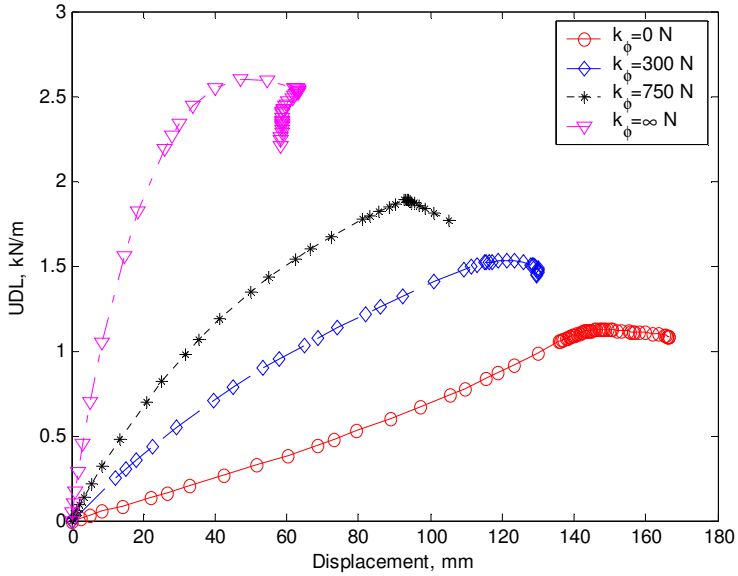

(a) Lateral displacement

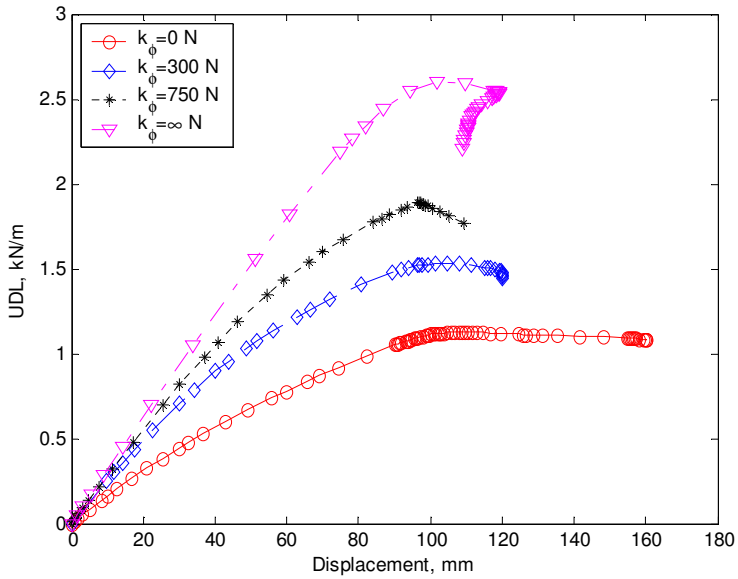

(b) Vertical displacement

Figure 5.40 Load-displacement curves of purlin with different rotational spring constants (C20720, L=7000 mm).

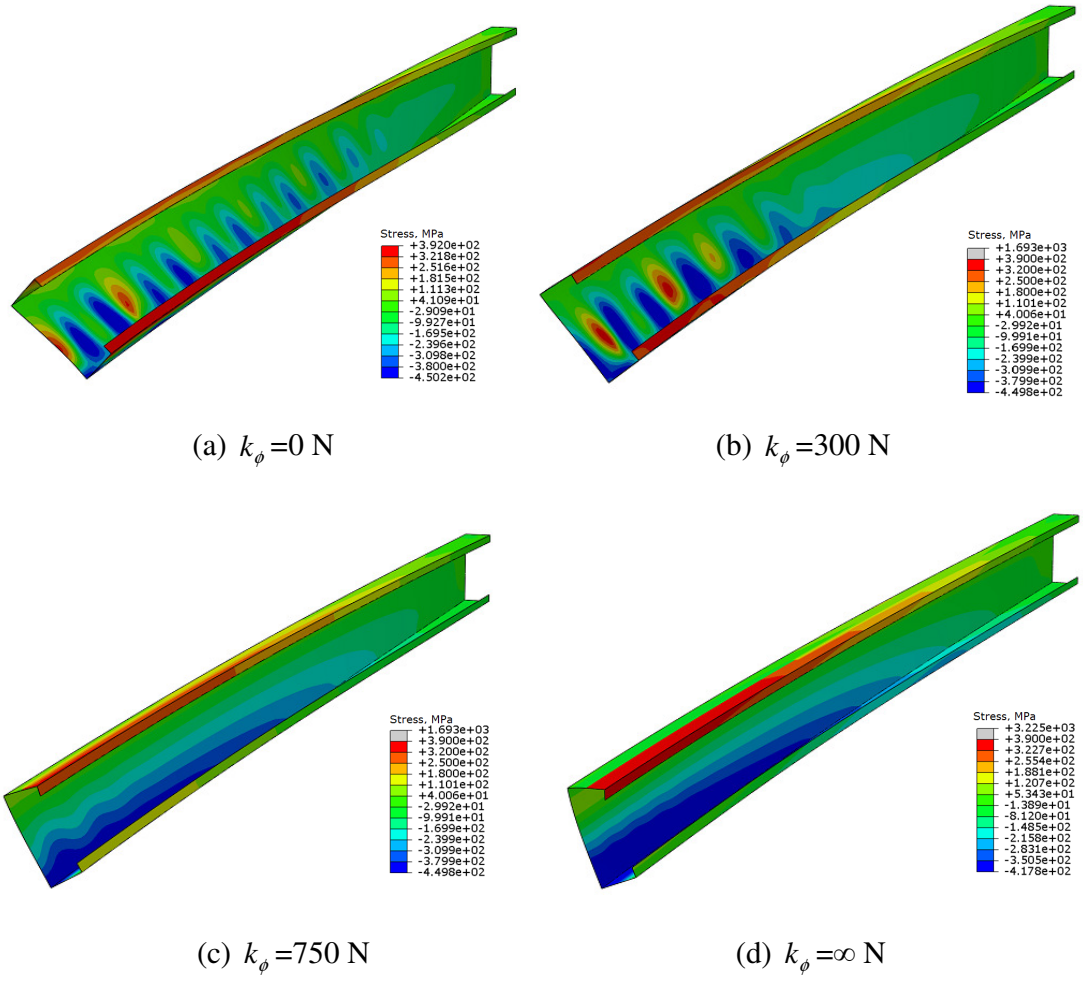

(a) k_ϕ =0 N (b) k_ϕ =300 N

(c) k_ϕ =750 N (d) k_ϕ =∞ N

Figure 5.41 Deformed shapes of purlin at failure point with longitudinal stress contours (C20720, L=7000 mm).

The load-displacement curves of intermediate channel-section (C20720) purlin of length, L=10000 mm for four different rotational spring stiffness values (k_ϕ=0, k_ϕ=300 N, k_ϕ=750 N and k_ϕ=∞ N) and the corresponding deformed shapes of the purlins when the loads reach their ultimate values are shown in Figures 5.42 and 5.43, respectively. Unlike the results for k_ϕ=0 in Figures 5.40 and 5.41, the purlin has severe twisting deformation,

which significantly reduces the flexural rigidity in the loading direction but increases the flexural rigidity in the perpendicular direction. As a consequence of this, when k_ϕ=0, the typical limiting failure of plasticity is the main failure mode. This indicates that the length has significant influence not only on the performance but also on the failure type when the rotation is unrestrained. Additionally, it can be seen that under the influence of a rotational spring, the wavelength of the distortional buckling is dependent on the k_ϕ value. This leads the interaction of distortional and local buckling to be the main failure mode when k_ϕ=750 N and distortional buckling to be the main failure mode when k_ϕ=∞ N. Furthermore, a comparison of critical buckling loads and ultimate failure loads for the intermediate channel-section (C20720) as shown in Table 5.5 implies that the performance for an intermediate channel-section is dependent not only on the influence of rotational spring but also on the length of the purlin.

Table 5.5 Comparison of critical buckling loads and plastic failure loads (C20720).

L **(mm)**	k_ϕ**=0 N**		k_ϕ**=300 N**		k_ϕ**=750 N**		k_ϕ**=∞ N**	
	Failure Load (kN/m)	Buckling Load (kN/m)	Failure Load (kN/m)	Buckling Load (kN/m)	Failure Load (kN/m)	Buckling Load (kN/m)	Failure Load (kN/m)	Buckling Load (kN/m)
4000	3.9758*	3.3419	4.2761	4.2806	4.6001	5.2205	6.1194	8.7526
7000	1.1248*	1.1751	1.5294	2.6811	1.8911	3.2110	2.6008	3.7044
10000	0.5143*	0.4105	0.8002	0.9860	1.0750	1.2410	1.3917	1.6838

Note: * = The catenary action.

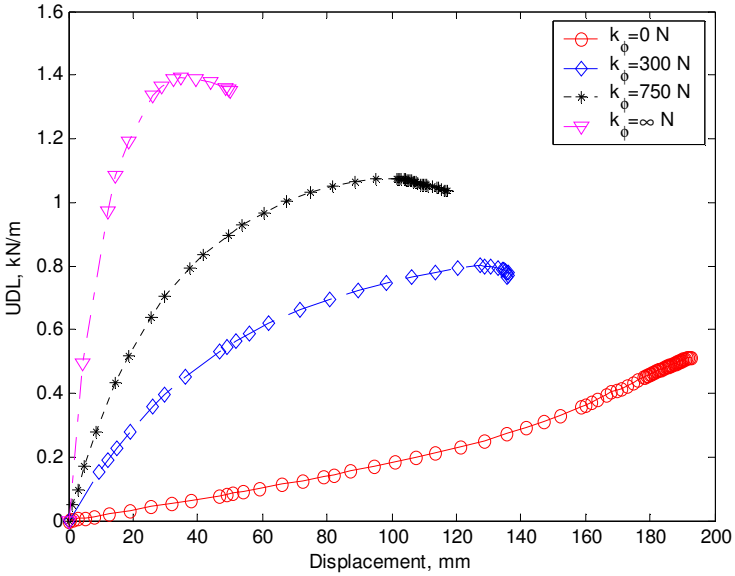

(a) Lateral displacement

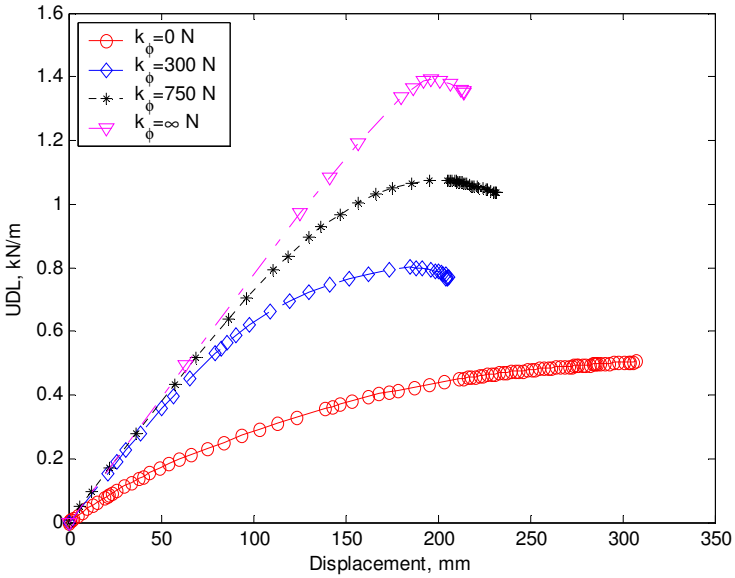

(b) Vertical displacement

Figure 5.42 Load-displacement curves of purlin with different rotational spring constants (C20720, L=10000 mm).

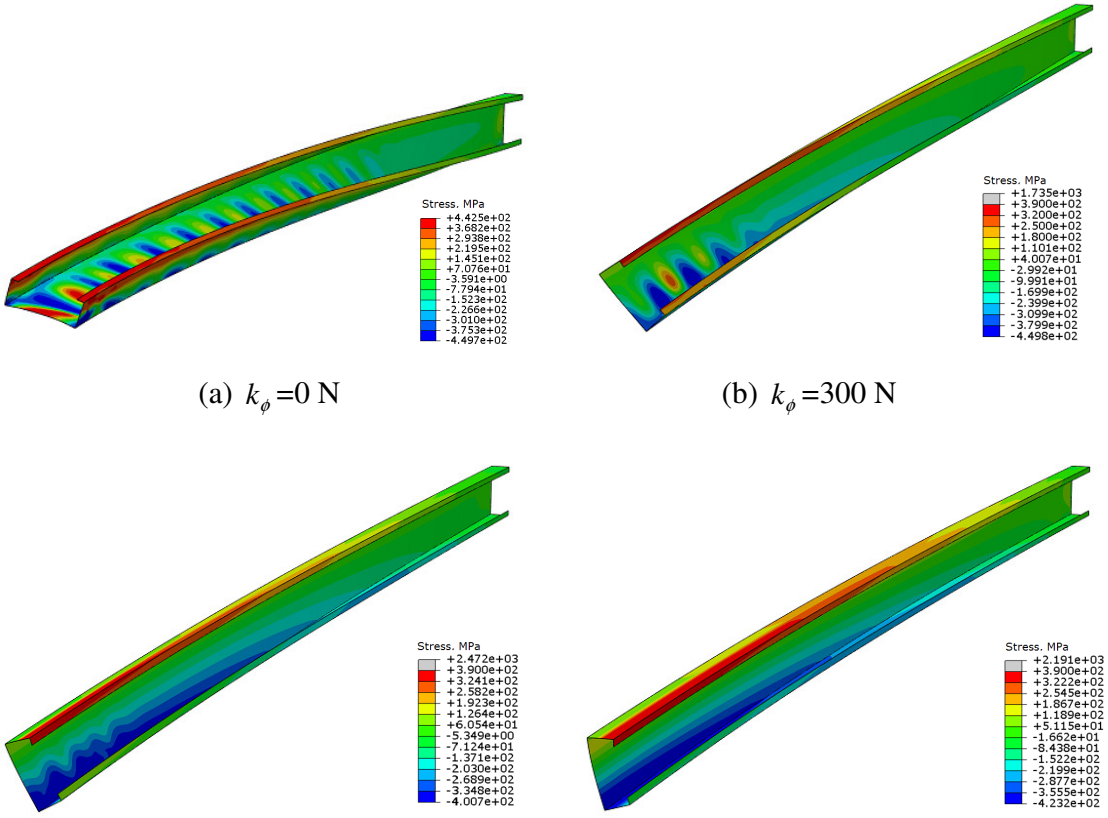

(a) k_ϕ =0 N (b) k_ϕ =300 N

(c) k_ϕ =750 N (d) k_ϕ =∞ N

Figure 5.43 Deformed shapes of purlin at failure point with longitudinal stress contours (C20720, L=10000 mm).

The load-displacement curves of a large channel-section (C40132) purlin of length, L=4000 mm for four different rotational spring stiffness values (k_ϕ=0, k_ϕ=300 N, k_ϕ=750 N and k_ϕ=∞ N) and the corresponding deformed shapes of the purlins when the loads reach their ultimate values are not provided here. This is because for 400 mm web depth channel-sections, due to the ratio of depth to length being less than 1/10, the member

does not behave like a beam. For an extremely short beam shear buckling would be the main failure mode, in which case the failure mode would be different from those of normal length beams and thus is not discussed herein.

Figures 5.44 and 5.45 illustrate the load-displacement curves of the large channel-section (C40132) purlin of length, L=7000 mm for four different rotational spring stiffness values (k_ϕ=0, k_ϕ=300 N, k_ϕ=750 N and k_ϕ=∞ N) and the corresponding deformed shapes of the purlins when the loads reach their ultimate values, respectively. It can be seen in Figure 5.44, for all rotational spring stiffnesses, the load rises with displacement until it reaches a peak point, which is the ultimate load for nonlinear analysis. After the peak point, the load drops with further increased displacement. These kinds of load-displacement curves represent typical buckling failure. Interestingly, when k_ϕ=0, k_ϕ=300 N and k_ϕ=750 N, the ultimate loads of these beams are very close. However, when k_ϕ=∞ N, the purlin has a much higher ultimate load but less lateral displacement than the other three cases. This demonstrates that only large values of rotational spring stiffness have an impact on load capacity of a large channel-section, and may lead the section to have different failure modes. Moreover, it can be found in the deformed shapes that the buckling failure at the ultimate value is the interaction of distortional and local buckling, in which the influence of local buckling increases with increased stiffness of rotational spring. Figures 5.44 and 5.45 highlight the noticeable rotational spring effect on the performance and failure mode of large channel-section purlin of length, L=7000 mm.

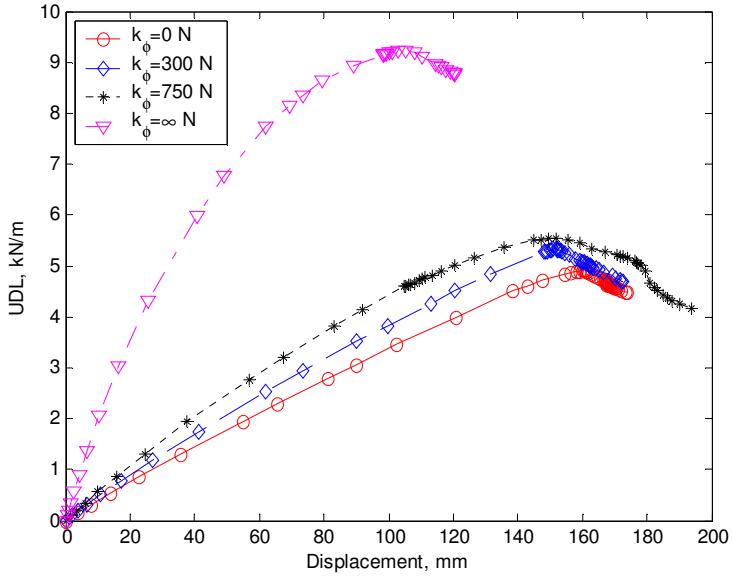

(a) Lateral displacement

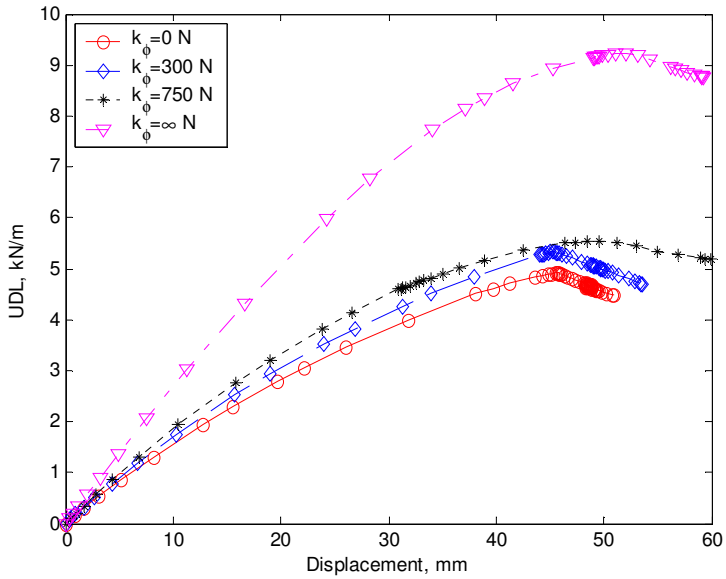

(b) Vertical displacement

Figure 5.44 Load-displacement curves of purlin with different rotational spring constants (C40132, L=7000 mm).

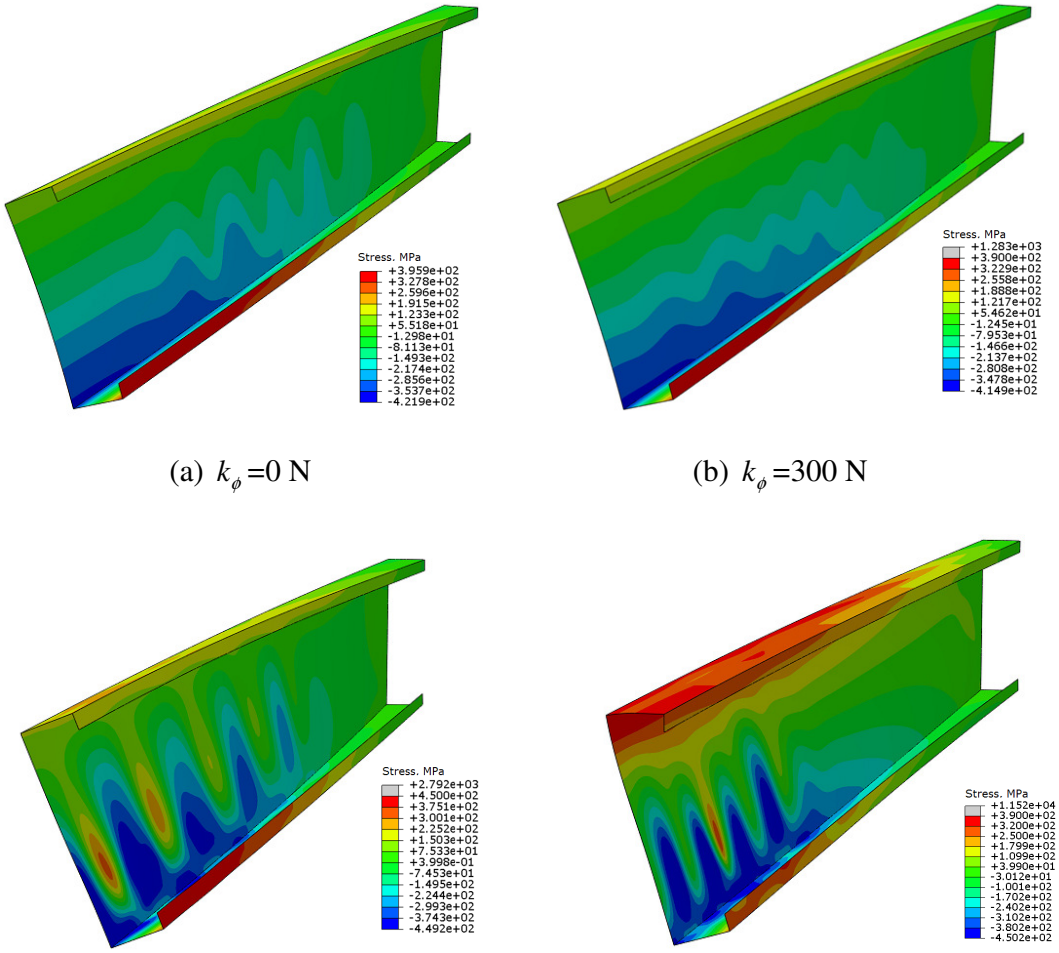

(a) k_ϕ =0 N (b) k_ϕ =300 N

(c) k_ϕ =750 N (d) k_ϕ =∞ N

Figure 5.45 Deformed shapes of purlin at failure point with longitudinal stress contours (C40132, L=7000 mm).

Figure 5.46 shows the load-displacement curves of a large channel-section (C40132) purlin of length, L=10000 mm for four different rotational spring stiffness values (k_ϕ=0, k_ϕ=300 N, k_ϕ=750 N and k_ϕ=∞ N). The corresponding deformed shapes of the purlins when the loads reach their ultimate values are shown in Figure 5.47. It can be seen in

Figure 5.46 that the main features of this figure are similar to those shown in Figures 5.44 and thus are not discussed further. As is to be expected, the failure load of the purlin with k_ϕ=∞ N is several times that of the purlins with k_ϕ=0, k_ϕ=300 N or k_ϕ=750 N, which indicates that for a large channel-section (C40132), only a large value of rotational spring stiffness has significant influence on the performance of the purlin. Figure 5.47 shows the deformed shapes of the purlins when k_ϕ=0, k_ϕ=300 N, k_ϕ=750 N and k_ϕ=∞ N and the failure modes for these purlins are the interaction of distortional and local buckling at the lower web-flange junction. Table 5.6 shows a comparison of critical buckling loads and plastic failure loads for large channel-section (C40132).

Table 5.6 Comparison of critical buckling loads and plastic failure loads (C40132).

L **(mm)**	k_ϕ**=0 N**		k_ϕ**=300 N**		k_ϕ**=750 N**		k_ϕ**=∞ N**	
	Failure Load (kN/m)	Buckling Load (kN/m)	Failure Load (kN/m)	Buckling Load (kN/m)	Failure Load (kN/m)	Buckling Load (kN/m)	Failure Load (kN/m)	Buckling Load (kN/m)
7000	4.6984*	4.2882	5.3366*	4.9249	5.5269	5.6934	9.2255	11.075
10000	2.1906*	2.1879	2.3847	3.1425	2.7793	4.4072	6.0050	6.8479

Note: * = The catenary action.

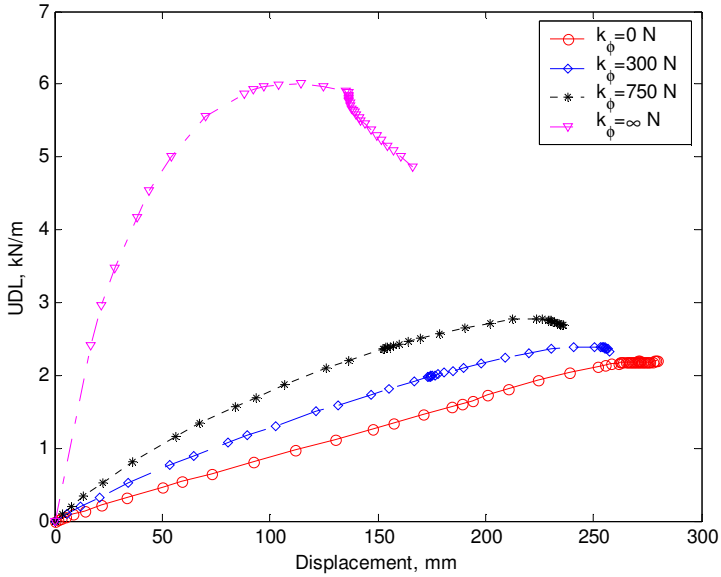

(a) Lateral displacement

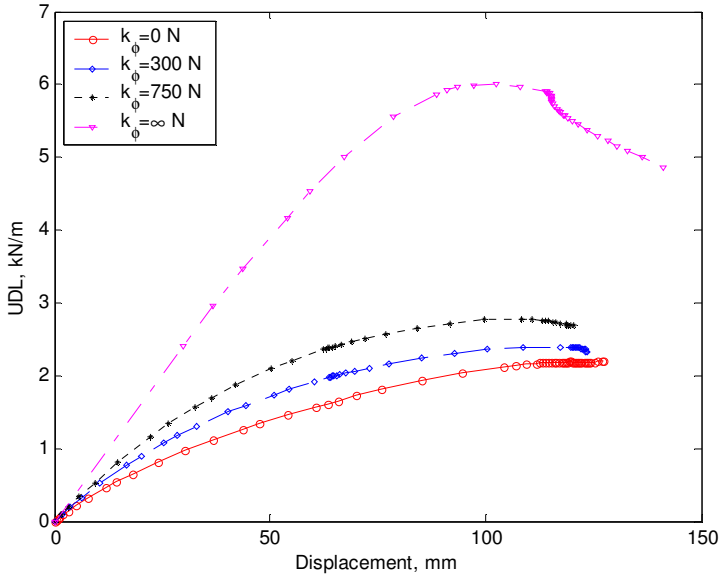

(b) Vertical displacement

Figure 5.46 Load-displacement curves of purlin with different rotational spring constants (C40132, L=10000 mm).

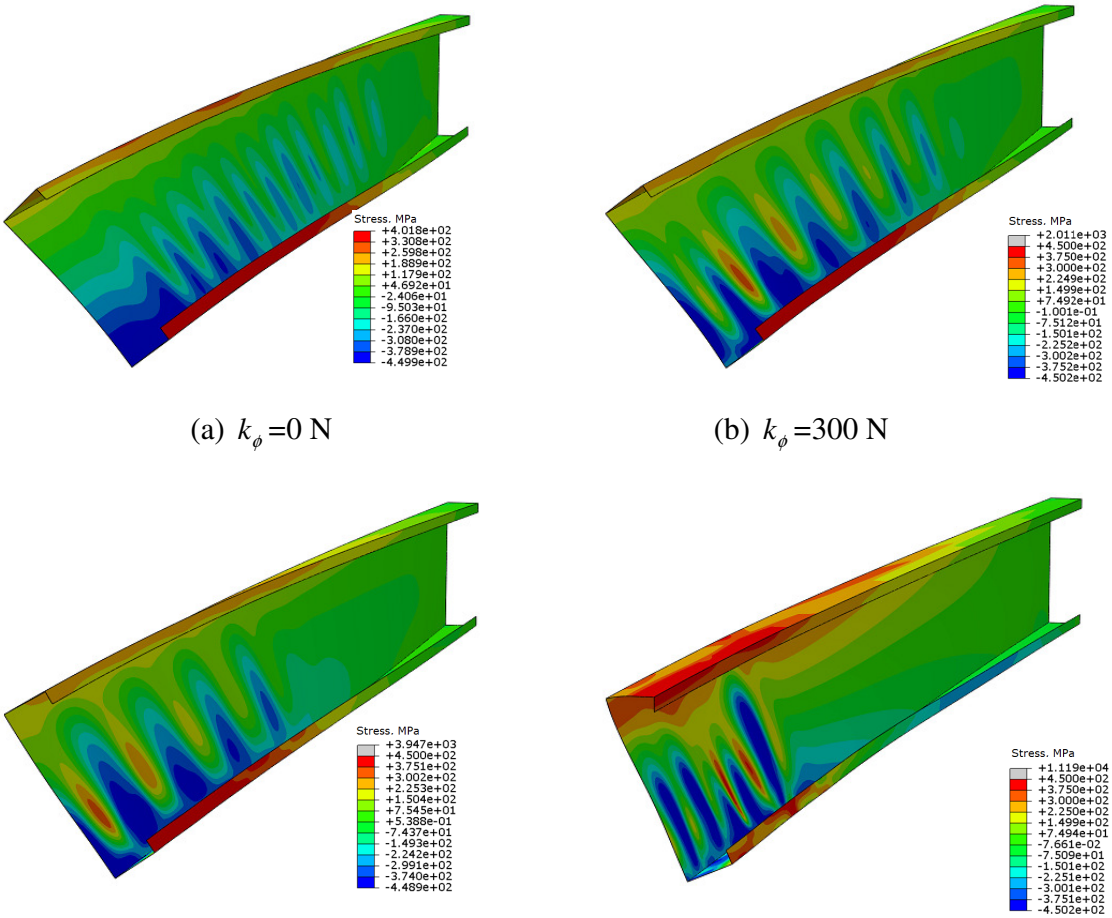

(a) k_{ϕ}=0 N (b) k_{ϕ}=300 N

(c) k_{ϕ}=750 N (d) k_{ϕ}=∞ N

Figure 5.47 Deformed shapes of purlin at failure point with longitudinal stress contours (C40132, L=10000 mm).

Figure 5.48 shows the comparison of normalised moment capacities obtained from different lengths for small channel-section (C12515) of various stiffnesses of rotational spring. It can be seen in this figure that for the small section (C12515) purlin, the moment capacity increases with spring stiffness. However, after k_{ϕ}=3000 N, the capacity increases gradually compared to the steep increase shown before k_{ϕ}=3000 N. This

indicates that, for small channel-sections, the rotational spring has significant influence on moment capacity when the purlin is partially restrained and minor effect when the restraint becomes fully restrained. Additionally, it can be found that the moment capacities for a rotational spring larger than 3000N are higher than the yield moment when the length of the purlin is 7000 mm or 10000 mm. Note that when the beam reaches a yield moment, it is only the maximum stress in the beam reaches its yield stress. The stresses in other parts of the beam are still below the yield stress and thus they can take load until the purlin fails totally. It is known that for a rectangular cross-section beam if all stresses reach yield stress, the fully plastic moment will be $1.5M_y$. This will also apply to channel-section, although the maximum moment will be slightly different. Again, as in the zed-section, it can be found that for high k_ϕ, the moment capacity increases with length. Figure 5.49 shows a comparison of normalised moment capacities obtained from different lengths for intermediate channel-sections (C20720) of varying stiffness of rotational spring. Overall, the purlins have a similar behaviour to the small section. However, due to the increased section dimensions, the magnitude of moment capacity for all lengths is slightly reduced, and the moment capacity increases dramatically with rotational spring stiffness until the rotational spring stiffness reaches 10000N. This reveals that the rotational spring stiffness still has significant influence on the moment capacity, but for larger cross sections, the significance is dependent on the higher stiffness of rotational spring. For the large section purlins (C40132), Figure 5.50 shows a comparison of normalised moment capacities against various stiffnesses of rotational spring for three different lengths. For a purlin of length, L=4000 mm, the difference between maximum and minimum moment capacity is only 0.1, which is unremarkable.

For a purlin of length, L=7000 mm, a dramatic increase of moment capacity starts from k_{ϕ}=1000 N when the purlin is fully restrained, and for a purlin of length, L=10000 mm, a dramatic increase of moment capacity starts from k_{ϕ}=100N when the purlin is fully restrained. This reveals that for the large sections, the length and rotational spring have an important effect on the performance of the purlins. The rotational spring has an insignificant influence on the moment capacity in short length purlins and a significant influence on the moment capacity in long length purlins. It is worth noting here that overall, for these three different section sizes, the moment capacity increases with rotational spring stiffness. However, sensitivity of the amount of influence on the moment capacity is dependent not only on the section dimensions but also on the stiffness of rotational spring. The length, section dimensions and the rotational spring stiffness are all related to the performance and failure mode of the purlin.

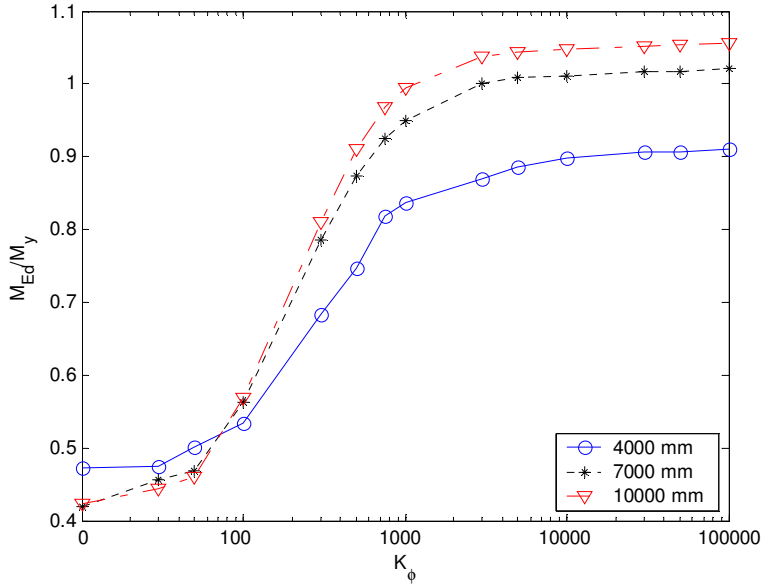

Figure 5.48 Moment capacity against rotational spring stiffness for small channel-section (C12515).

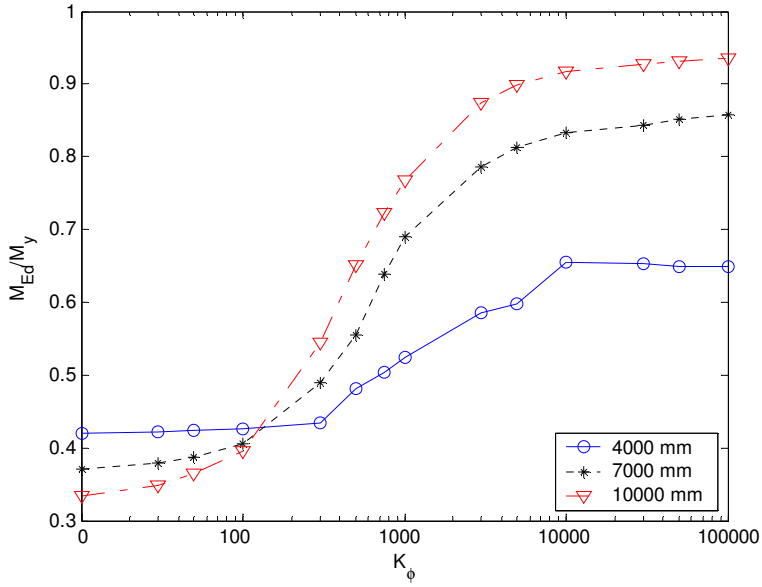

Figure 5.49 Moment capacity against rotational spring stiffness for intermediate channel-section (C20720).

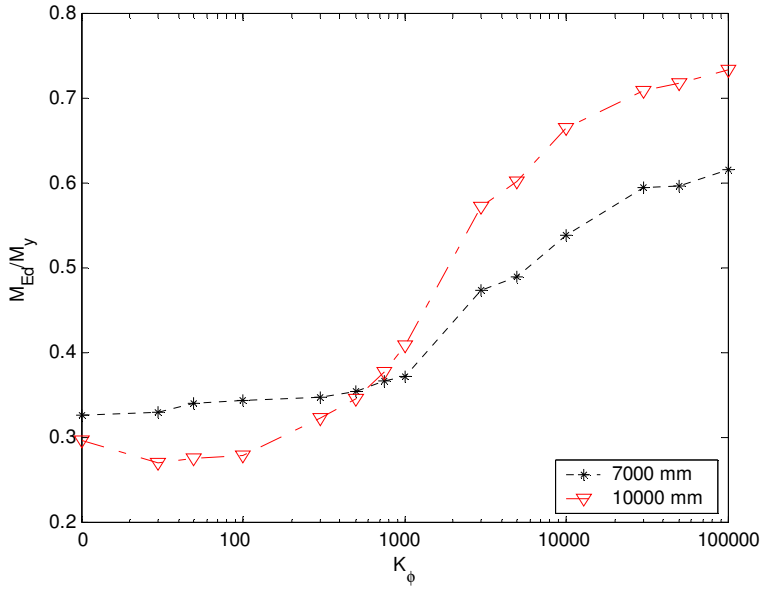

Figure 5.50 Moment capacity against rotational spring stiffness for large channel-section (C40132).

5.4.2 Design curve of channel-sections

In practical design, one is more interested in the moment capacity rather than the failure load. Figures 5.51 to 5.53 show a comparison of the normalised moment capacities (M_{Ed}/M_y) obtained from different rotational spring stiffnesses for small (C12515), intermediate (C20720) and large (C40132) channel-sections of various lengths. Here the moment capacity is calculated directly based on the failure load and purlin length using the simple formula for beams, $M = \frac{q_z l^2}{8}$. For the beam data in these figures, all of the M_{Ed} values are normalised against the moment at first yield, M_y is yield moment (which is $2\sigma_y I_z/d$, where the yield strength σ_y is 390 N/mm) and I_z is the second moment of the gross cross section area about the z-axis. It can be seen in Figure 5.51 that when k_ϕ=0, the normalised moment capacities decrease with increased length, and above 10000 mm, the moment capacity rises with length. In the cases of k_ϕ=300 N, k_ϕ=750 N or k_ϕ=∞ N, the normalised moment capacities rises with an increase in purlin length. It also can be found from the figure that the influence of rotational spring stiffness on the moment capacity increases with increased rotational spring stiffness. The former reveals that in small channel-section, the length of the purlin has a slight influence on its performance if the rotational restraint is applied, but it has a significant impact on its performance if the purlin has no rotational restraint. The latter implies that the rotational spring stiffness has significant influence on the performance of small channel-section. The main features of Figure 5.52 are similar to those shown in Figure 5.51; the difference is that the moment capacity reduces with increased length above 10000 mm. The reason for this is that the typical limiting failures of plasticity, obtained from the small channel-section, and the typical buckling failures, obtained from the intermediate channel-section, represent two

different failure modes. The former represents that yield is the main failure mode in the small channel-section and the latter shows the main failure mode in the intermediate channel-section is lateral-torsional buckling. However, compared with large channel-sections, it can be seen in Figure 5.53 that the moment capacity for k_ϕ=∞ N increases with length from 4000 mm to 12000 mm. When k_ϕ=0 N, k_ϕ=300 N or k_ϕ=750 N, due to the complex interaction buckling failure modes at different lengths, the large channel-section has moment capacity fluctuates, indicating the stronger influence of wavelength of buckling modes of the failure load.

Figure 5.54 illustrates the design curves of the moment capacity (M_{Ed}) with different rotational spring stiffnesses, which are obtained from the non-linear finite element analysis in the small (C12515) channel-sections when these members act as beams. The slenderness of the beam is represented by $(M_y/M_{cr})^{0.5}$, where M_{cr} is the critical moment of buckling which is calculated by using the first eigen-value of lateral-torsional buckling. It can be seen from Figure 5.54 that the tendency of moment capacity against slenderness is similar to that of moment capacity against length as shown in Figure 5.51, which indicates that the rotational spring has significant influence on the performance of the purlins. It should be pointed out that, the moment capacity against slenderness for a channel-section is not compared with DSM, because channel-section purlins are assumed to be simply supported on both its ends and subjected to a uniformly distributed uplift load acting on the middle line of the upper flange, in which the distance between the shear centre to the loading position is not negligible. Consequently, the purlin exhibits not only bending but also torsion, which may change the failure modes from lateral-

torsional buckling to local or distortional buckling and provides an undesirable comparison with DSM. Figures 5.55 and 5.56 show the design curves of moment capacity against slenderness for intermediate (C20720) and large (C40132) channel-sections. The main features of these figures are similar to those shown in Figures 5.52 and 5.53 and thus are not discussed further. It can be found in these figures that, the rotational spring has important influence on the performance of purlin.

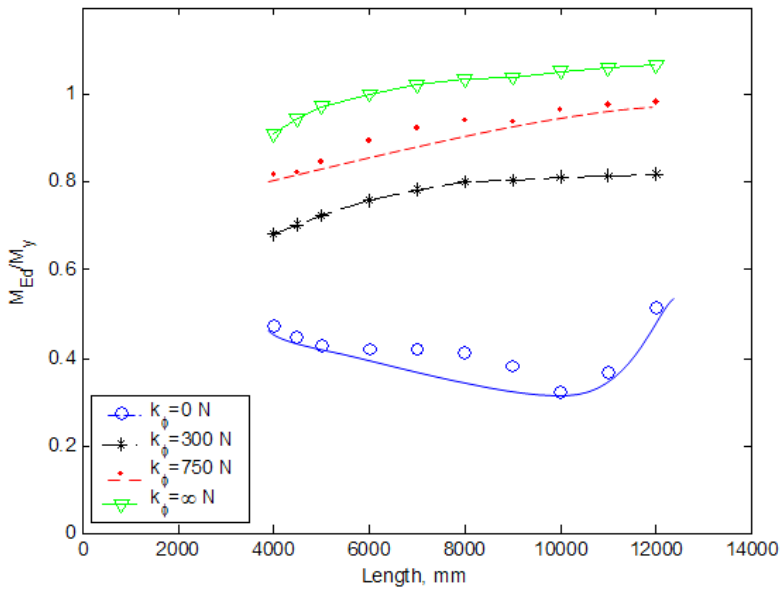

Figure 5.51 Design curves of moment capacity against length for small channel-section (C12515).

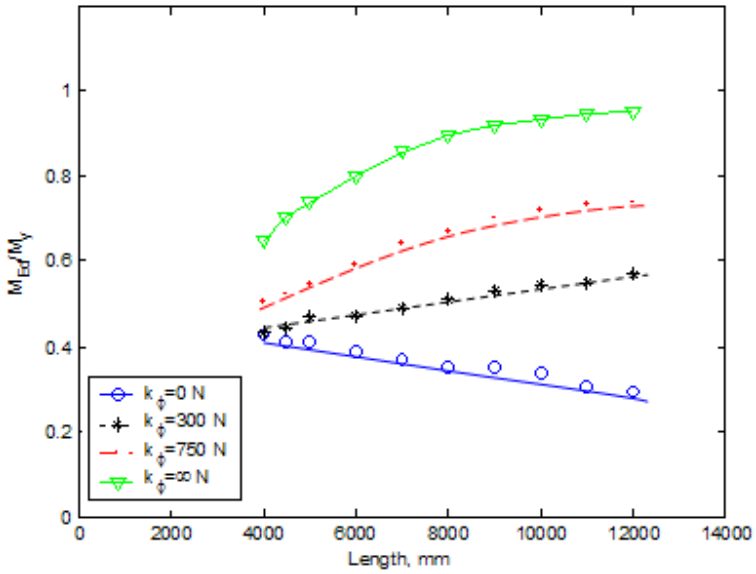

Figure 5.52 Design curves of moment capacity against length for intermediate channel-section (C20720).

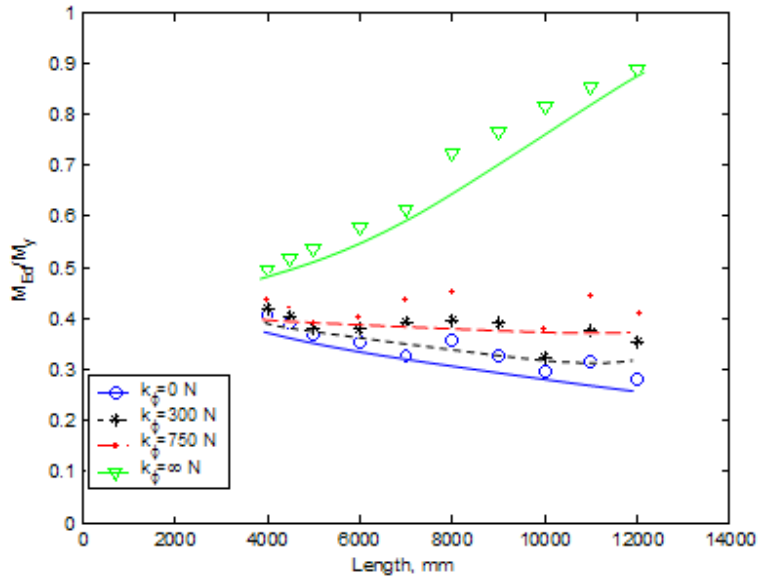

Figure 5.53 Design curves of moment capacity against length for large channel-section (C40132).

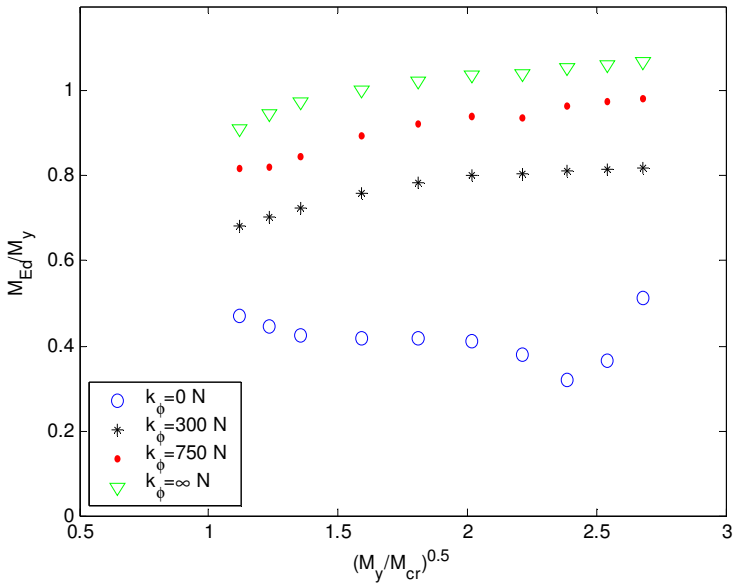

Figure 5.54 Design curves of moment capacity against slenderness for small channel-section (C12515).

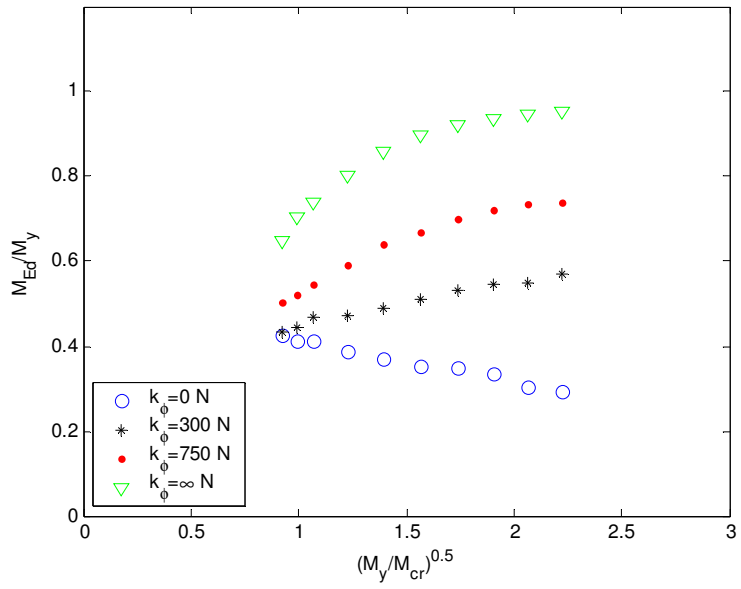

Figure 5.55 Design curves of moment capacity against slenderness for intermediate channel-section (C20720).

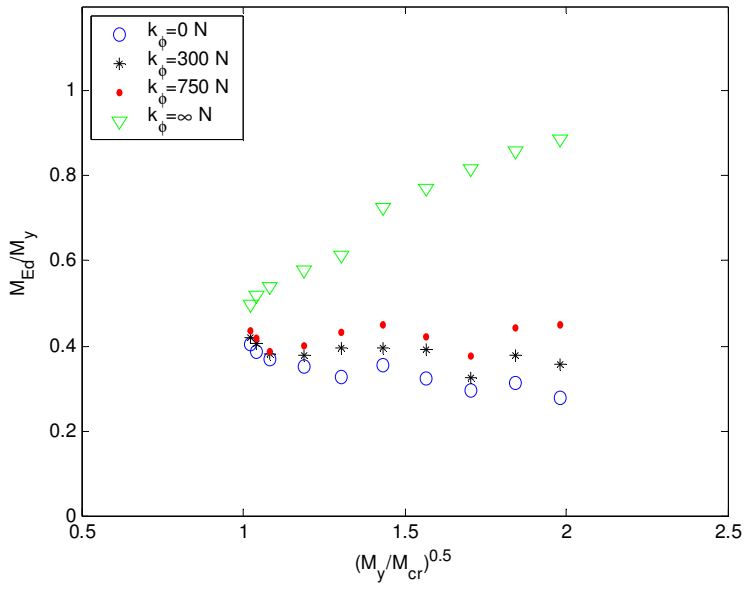

Figure 5.56 Design curves of moment capacity against slenderness for large channel-section (C40132).

5.5 Summary

This chapter has presented a numerical investigation into the influence of the rotational spring stiffness on the performance of cold-formed steel purlins under the action of uplift loading using geometric and material nonlinear finite element analysis methods. The following major conclusions can be drawn based on the investigated examples:

1. The comparison of the finite element analysis and experimental measurement results has provided. Good agreement of the present finite element analysis model with the experimental data demonstrates that the geometric and material nonlinear finite element analysis methods can provide a good prediction of the ultimate load and displacements in the lateral and vertical direction for the partially or fully restrained zed- and channel-section purlins subjected to uplift loading.

2. For both zed- and channel-sections, the comparison results of cleat bolted supported and web simply supported boundary conditions have demonstrated that the idealised boundary condition proposed in the present study are able to represent the standard two-hole cleat support conditions used in practice. This means that the web simply supported boundary can be employed for geometric and material nonlinear finite element analysis.

3. The rotational spring stiffness has significant influence on the performance of the zed- and channel-section purlins. Not only can it affect the performance but it can

also alter the failure mode of the purlin.

4. Buckling interactions of zed- and channel purlins exist and have considerable influence not only on performance but also on failure mode.

5. For the zed- and channel-section purlins with strong rotational spring restraint, the failure of the purlin is mainly controlled by buckling. For most cases of zed- and channel-section purlins with no rotational restraint, plastic bending occurring in the plane of minor axis is the main reason for failure.

6. Due to the length to web depth ratio affecting the half-wavelength distribution of the buckling mode in the purlin, the failure mode of large zed- or channel-sections are mostly dominated by the interaction of distortional and local buckling, and the failure load of large zed- or channel-sections are much greater than small or intermediate sections.

7. For different lengths of zed- and channel-section purlins, the comparison of moment capacity with various stiffnesses of rotational spring reveals that the purlin length and section dimensions can also affect the performance of the purlins.

8. For intermediate and large zed-sections, good agreement of the present finite element analysis model with DSM means that the DSM, which is based on pure

ending, can be used for zed-section beams under uniformly distributed load if they are not rotationally restrained.

9. When the DSM is applied to small zed-section purlins with no rotational restraint, the predicted results will be over conservative. The DSM cannot predict the behaviour of beams with rotational restraint.

CHAPTER 6 CONCLUSIONS AND FUTURE RESEARCH

6.1 General

This thesis has investigated the structural behaviour of cold-formed steel zed- and channel-section purlins with partial restraints from sheeting when subjected to transverse uniformly distributed uplift loading. The investigations cover pre-buckling, buckling and post-buckling stress analysis of purlin-sheeting systems. Additionally, comparisons of cleat bolted supported and web simply supported boundary conditions have also been presented for all buckling stress analyses and the results obtained have been validated with available experimental data.

6.2 Pre-buckling stress analysis of purlin-sheeting systems

For pre-buckling stress analysis of purlin-sheeting systems, the investigation has developed an analytical method to describe the bending and twisting behaviour of partially restrained cold-formed steel purlins when subjected to uplift loading for zed- and channel-sections. Formulae used to calculate the bending stresses of the roof purlins were derived using the classical bending theory of thin-walled beams. Detailed comparisons were made between the present model and the simplified model proposed in Eurocode (EN1993-1-3). Finite element analysis was employed to provide comparison

and validation. Some important conclusions drawn from the present study are summarised as follows:

1. Detailed comparisons of zed- and channel-sections have been made between the present model and the simplified model proposed in Eurocode (EN1993-1-3), and have shown that, although the bending stresses in the compression flange for lateral bending are over-predicted by EN1993-1-3, the total bending stresses are still accurate enough as they are being dominated by the bending in the plane of the web rather than the lateral bending.

2. For zed-sections, the finite element analysis results have demonstrated that the total bending stresses predicted using the present and EN1993-1-3 models are accurate for intermediate and long beams. Only for short beams with the large stiffness of rotational spring, the bending stresses in the lip and part of the flange are over-predicted by the two analytical models.

3. The results obtained from the present model have also shown that the longitudinal stresses induced by the lateral bending are significant for channel-section purlins. This additional stress may change the failure modes from lateral-torsional buckling to local or distortional buckling.

4. For channel-sections, detailed comparisons of bending stresses obtained from finite element analysis, available experimental data, the present model and the EN1993-1-3 model are provided. This demonstrates that the linear bending

model, while taking into account warping torsion, can provide a good prediction of the bending stresses in the purlin-sheeting system. For most cases, the results provided by the EN1993-1-3 model are over conservative, particularly when the stiffness of the rotational spring is very low.

6.3 Buckling stress analysis of purlin-sheeting systems

For buckling stress analysis of purlin-sheeting systems, the investigation was performed numerically using linear finite element methods to discover the buckling behaviour of partially restrained cold formed steel zed- and channel-section purlins when subject to transverse distributed uplift loading. The significant findings drawn from buckling stress analysis of purlin-sheeting systems are as follows:

1. For both zed- and channel-section purlins, the rotational spring has a significant influence on the buckling behaviour, including both the critical load and the corresponding buckling mode. The purlin length and section dimensions can also affect the buckling behaviour of the purlins.

2. For purlin-sheeting systems, pre-buckling stress has a significant influence on buckling behaviour when the purlin reaches a certain length. In order to provide accurate results, consistent analysis models should be used for both pre-buckling stress and buckling analyses.

3. The parametric distribution of different buckling modes obtained from the finite element analysis for zed-section purlins are presented. The distribution of buckling demonstrate that the buckling modes are influenced not only by the rotational restraint but also by the geometric of purlin.

4. Secondary lateral-torsional buckling is found in partial rotationally restrained long length purlins. The half-wavelength of the secondary lateral-torsional buckling mode can be several times longer than the half-wavelength of distortional buckling. However, it is shorter than the beam length, which comprises more than two half-wavelengths rather than one half-wavelength in lateral-torsional buckling.

6.4 Post-buckling analysis of purlin-sheeting systems

For post-buckling stress analysis of purlin-sheeting systems, nonlinear finite element analysis models were created for cold-formed steel zed- and channel-section purlins subjected to transverse uniformly distributed uplift loading. The analyses were performed by considering both geometric and material nonlinearities. The load-displacement curves of different sized zed- and channel-section purlins subjected to uplift loading under the influence of rotational spring stiffness on the middle of the upper flange were examined, and the design curves of zed- and channel-section purlins were established. The following major conclusions drawn based on the investigation of post-buckling analysis of purlin-sheeting systems are summarised as follows:

1. The rotational spring stiffness has significant influence on the performance of the zed- and channel-section purlins. It can also alter the failure mode of the purlin. Additionally, buckling interactions exist and have significant influence on either the performance or the failure mode.

2. For the zed- and channel-section purlins with strong rotational spring restraint, the failure of the purlin is mainly controlled by buckling. For most cases of zed- and channel-section purlins without rotational restraint, the main cause of failure is plastic bending occurring in the plane of minor axis.

3. For zed- and channel-sections, due to the influence of the deformations and material yielding prior to buckling, the failure load is generally less than the critical load obtained directly from linear buckling analysis.

4. For different lengths of zed- and channel-section purlins, a comparison of moment capacity with varying stiffness of rotational spring reveals that the purlin length and section dimensions can also affect the performance of the purlins.

5. For intermediate and large zed-sections, there is good agreement of the present finite element analysis model with the DSM meaning that the DSM, which is based on pure bending, can be used for zed-section beams under uniformly distributed load if this member without rotational restraint. Furthermore, when the DSM is applied to small zed-section purlins with no rotational restraint, the

predicted results will be over-conservative. The DSM cannot predict the behaviour of beams with rotational restraint.

6.5 Recommendations for future research

This thesis has addressed some important problems by using numerical and analytical methods. However, many issues still remain to be studied further. These issues are as follows:

1. Due to financial and facility limitation problems, experimental tests have not been carried out in this study; only numerical and analytical methods have been used for investigating the structural behaviour of cold-formed steel purlins. It is suggested to undertake experimental tests of UDL gravity and uplift loading to investigate the structural behaviour of purlin-sheeting systems.

2. In this study, only zed- and channel-section purlins have been investigated and reported, indicating different structural behaviour between zed- and channel-section purlins. Therefore, cold-formed steel purlins with other types of cross sections (sigma section) are recommended for further study. By using the same methodology described in this thesis, the structural behaviour of cold-formed steel sigma section purlin with partial restraints from sheeting when subjected to transverse uniformly distributed uplift loading may also be investigated in future research.

3. Buckling interactions have significant influence on both performance and buckling behaviour, and have been investigated and reported in this study. However, the interaction is complex, and affected by many parameters, although some findings were highlighted in the study. Thus, comprehensive investigation of buckling interactions is recommended for further research.

4. Purlin-sheeting systems have been studied and analysed by using analytical and numerical methods, in which only a single-span purlin with lateral rigid restraint and rotational spring restraint was examined. However, in practical terms, roof sheeting purlin systems also use continuous purlins and it is thus recommended that future studies investigate continuous purlin-sheeting systems.

5. Static analysis has been carried out to investigate the structural behaviour of cold-formed steel purlins. The parameters were chosen to simulate static situation rather than dynamic one. In any further study, the influence of dynamic analysis on cold-formed steel, including simulated earthquake investigations, is suggested.

6. The structural behaviour of cold-formed steel can be affected by temperature, which was not considered in this study. Fire resistance of cold-formed steel sections is proposed as a topic for further research.

7. In addition to the numerical and analytical methods investigated in this thesis, it is always worth considering industrial input, such as failure case studies, new

technology and the direction of development. Industry collaboration can offer new insights and perspectives thus it has the potential to make a valuable contribution to this study. It is suggested that liaison with industry will be encouraged in future research.

8. In this thesis, only transverse uniformly distributed uplift loading has been investigated and reported. The effect of loading distribution pattern such as non-uniform distributed loads should be a subject of future research.

REFERENCE

ABAQUS standard user's manual—version 6.3 (2002). Hibbitt, Karlsson and Sorenson, Inc. page 15.6.1-1 to 15.6.3-3.

Ádány, S. and Schafer, B. W. (2006a). Buckling mode decomposition of single-branched open cross-section members via finite strip method: Derivation. Thin-Walled Structures 44(5), 563-584.

Ádány, S. and Schafer, B. W. (2006b). Buckling mode decomposition of single-branched open cross-section members via finite strip method: Application and examples. Thin-Walled Structures 44(5), 585-600.

Ádány, S. and Schafer, B. W. (2008). A full modal decomposition of thin-walled, single-branched open cross-section members via the constrained finite strip method. Journal of Constructional Steel Research 64(1), 12-29.

AISI (1946). Specification for the design of light gage steel structural members. American Iron and Steel Institute. Washington, D.C.

AISI (1986). Specification for the design of light gage steel structural members. American Iron and Steel Institute. Washington, D.C.

AISI (2005). Supplement 2004 to the North American Specification for the Design of Cold-Formed Steel Structural Members. American Iron and Steel Institute, Washington, D.C.

Albion Sections Ltd (2008). Albion Sections Zed Purlin and Rail Technical Manual. Birmingham, UK (http://www.albionsections.co.uk).

AS/NZS (2005). Australian/New Zealand Standard on Cold-formed Steel Structures – AS/NZS-4600 (second edition). Standards of Australian and Standards of New Zealand, Sydney-Wellington.

Becque, J., and Rasmussen, K. J. R. (2006). Experimental investigation of the interaction of local and overall buckling of cold-formed stainless steel columns. Research report R887, School of Civil Engineering, University of Sydney.

Beshara, B. and LaBoube, R.A. (2001). Pilot study: lateral braced C-sections under bending. Thin-Walled Structures 39, 827-839.

BSI (1959). Specification for the use of cold-formed steel sections in building. Addendum No.1 to BS 449.

Camotim, D., Basaglia, C. and Silvestre, N. (2008a). GBT buckling analysis of thin-walled steel frames. Fifth International Conference on Coupled Instabilities in Metal Structures, Sydney, Australia, 23-25 June 2008.

Camotim, D., Silvestre, N., Basaglia, C. and Bebiano, R. (2008b). GBT-based buckling analysis of thin-walled members with non-standard support conditions. Thin-Walled Structures 46, 800–815.

Cheung, Y. K. (1976). Finite Strip Method in Structural Analysis, Pergramon Press.

Chilver, A. H. (1953a). The stability and strength of thin-walled steel struts. The Engineer 12, 180-188.

Chilver, A. H. (1953b). The maximum strength of the thin-walled channel strut. Civil Engineering and Public Works Review 48, 576-586.

Chin, C.K., Al-Bermani, F.G.A. and Kitipornchai, S. (1993). Finite element method for buckling analysis of plate structures. J Struct Eng ASCE; 119:1048–68.

Chu, X. T., Ye, Z. M., Kettle, R. and Li, L. Y. (2005). Buckling behaviour of cold-formed channel sections under uniformly distributed loads. Thin-Walled Structures 43(4), 531-542.

Chu, X. T., Ye, Z. M., Li, L. Y. and Kettle, R. (2006). Local and distortional buckling of cold-formed zed section beams under uniformly distributed transverse loads. International Journal of Mechanical Sciences 48(8), 378–388.

Davies, J. M. (2000). Recent research advances in cold-formed steel structures. Journal of Constructional Steel Research 5, 1–3, 267–288.

Davies, J. M. and Jiang, C. (1996). Design of thin-walled beams for distortional buckling. In: 13th International specialty conference on cold-formed steel structures, St Louis, Missouri, October 1996.

Davies, J. M. and Jiang, C. (1998). Design for distortional buckling, Journal of Constructional Steel Research 46 (1-3), 174-175.

Davies, J. M. and Leach, P. (1994a). First-Order Generalised Beam Theory, Journal Construction Steel Research 31, 187-220.

Davies, J. M. and Leach, P. (1994b). Second-Order Generalised Beam Theory, Journal Construction Steel Research 31, 221-241.

Davies, J. M., Leach, P. and Taylor, A. (1997). The design of perforated cold-formed steel sections subject to axial load and bending. Thin-Walled Structures 29(1-4), 141-157.

Desmond, T. P. (1977). The behavior and strength of thin-walled compression elements with longitudinal stiffeners. PhD Thesis, Cornell University. Ithaca, New York.

Desmond, T. P., Pekoz, T. and Winter, G. (1981a). Edge stiffeners for thin-walled members. Journal of Structural Engineering (ASCE), 107(2), 329-353.

Desmond, T. P., Pekoz, T. and Winter, G. (1981b). Intermediate stiffeners for thin-walled members. Journal of Structural Engineering (ASCE), 107(4), 627-648.

Dinar, P. B. and Camotim, D. (2008). Local-plate/Distortional mode interaction in cold-formed steel lipped channel beams. Fifth international conference on coupled instabilities in metal structures, Sydney, Australia, 23-25 June 2008.

Dinis, P. B., Camotim, D. and Silvestre, N. (2007). FEM-based analysis of the local-plate/distortional mode interaction in cold-formed steel lipped channel columns. Computers and Structures 85, 1461–1474.

Dwight, J. B. (1963). Aluminum sections with lipped flanges and their resistance to local buckling. In: Proc. of Symposium on Aluminum in Structural Engineering, London, England.

EN 1993-1-3 (2006). Design of Steel Structures – Cold-Formed Structures. BSI.

Friedrich, R. (2000). Finite strip method: 30 years A bibliography (1968-1998), Engineering Computations, Vol. 17 Iss: 1, pp.92 – 111.

Gallaher, G. L. and Boughan, R. B. (1947). A method of calculating the compressive strength of z-stiffened panels and that develop local instability. NACA Report TN-1482, Langley Memorial Aeronautical Laboratory.

Hancock, G. J. (1978). Local, distortional, and lateral buckling of I-beams. Journal of Structural Division (ASCE), 104(11), 1787-1798.

Hancock, G. J. (1985). Distortional Buckling of Steel Storage Rack Columns. Journal of Structural Engineering (ASCE), 111(12), 2770-2783.

Hancock, G. J. (1995). Design for distortional buckling of flexural members. In: Proceedings of the third international conference on steel and aluminium structures, Istanbul.

Hancock, G. J. (1997). Design for distortional buckling of flexural members. Thin-Walled Structures, 27(1), 3–12.

Hancock, G. J. (2003). Cold-formed steel structures. Journal of Constructional Steel Research 59, 473–487.

Hancock, G. J. (2008). Design of cold-formed steel structures to AS/NZS 4600:2005 (4th edition). Australia Steel Institute.

Hancock, G. J., Celeban, M., Healy C., Georgiou, P. N. and Ings, N. L. (1990). Tests of purlins with screw fastened sheeting under wind uplift. Tenth International Speciality Conference on Cold-formed Steel Structures, St. Louis, Missouri, USA.

Harvey, J. M. (1952). Studies on the interactions of plate components of structural sections under selected load conditions. PhD thesis, University of Glasgow.

Harvey, J. M. (1953). Structural strength of thin-walled channel sections. Engineering CLXXV.

Ings, N. L. and Trahair, N. S. (1984) 'Lateral buckling of restrained roof purlins', Thin-Walled Structures, Vol. 2, pp.285–306.

Jiang, C. and Davies, J. M. (1997). Design of thin-walled purlins for distortional buckling. Thin-Walled Structures, 29(1–4), 189–202.

Katnam, K. B., van Impe, R., Lagae, G. and De Strycker, M. (2007a). A theoretical numerical study of the rotational restraint in cold-formed steel single skin purlin-sheeting systems. Computers and Structures, 85, 1185-1193.

Katnam, K. B., van Impe, R., Lagae, G. and De Strycker, M. (2007b). Modelling of cold-formed steel sandwich purlin-sheeting systems to estimate the rotational restraint. Thin-Walled Structures, 45, 584-590.

Kenedi, R. M. and Harvey, J. M. (1951). The use of equal strength sections in structural design. Trans Institution of Engineers and Shipbuilders in Scotland, Institution of Engineers and Shipbuilders, Glasgow.

Kwon, Y. B., Kim, B. S. and Hancock, G. J. (2009). Compression tests of high strength cold-formed steel channels with buckling interaction. Journal of Constructional Steel Research 65(2), 278-289.

LaBoube, R. A. (1986). Literature survey of cold-formed sections. Proc. Eighth Int. Specialty Conference on Cold Formed Steel Structures. St. Louis, USA. University of Missouri-Rolla, Missouri.

Laine, M. and Tuomala, M. (1999). Testing and design of gravity-loaded steel purlins restrained by sheeting. Journal of Constructional Steel Research, 49, 129-138.

Lau, S. C. W. and Hancock, G. J. (1986). Buckling of thin flat-walled structures by a spline finite strip method. Thin-Walled Structures, 4(4), 269-294.

Lau, S. C. W. and Hancock, G. J. (1987). Distortional buckling formulas for channel columns. . Journal Structures Eng ASCE, 113, 1063–78.

Lau, S. C. W. and Hancock, G. J. (1988). Inelastic buckling of channel columns in the distortional mode. Research Report – University of Sydney, Department of Civil and Mining Engineering (R578), Var paping.

Lau, S. C. W. and Hancock, G. J. (1989). Inelastic buckling analyses of beams, columns and plates using the spline finite strip method. Thin-Walled Structures, 7(3-4), 213-238.

Lau, S. C. W. and Hancock, G. J. (1990). Inelastic buckling of channel columns in the distortional mode. Thin-Walled Structures, 10(1), 59-84.

Laurence, H. M. and Purkiss, J. A. (2007). Structural design of steelwork to EN 1993 and EN 1994. A Butterworth-Heinemann Title, 3rd Edition.

Leach, P., and Davies, J. M. (1996). An experimental verification of the generalized beam theory applied to interactive buckling problems. Thin-Walled Structures, Volume 25, Issue 1, Pages 61-79.

Li, L. Y. (2004). Lateral–torsional buckling of cold-formed zed-purlins partial-laterally restrained by metal sheeting. Thin-Walled Structures 42(7), 995-1011.

Li, L. Y. (2011). Calculation of moment capacity of cold-formed steel members. International Journal of Structural Engineering 2(2), 101-115.

Li, L. Y. and Chen, J. K. (2008). An analytical model for analyzing distortional buckling of cold-formed steel sections. Thin-Walled Structures 46, (12)1430-1436.

Li, L. Y. and Chu, X. T. (2007). Cold-formed Steel Sections. In: Martin LH and Purkiss JA, editors, Structural Design of Steelwork. Oxford: Elsevier, Chapter 11, p.411-457.

Li, L. Y., Ren, C. and Yang, J. (2012). Theoretical analysis of partially restrained zed-purlin beams subjected to up-lift loads. Journal of Constructional Steel Research 70, 273-279.

Lindner, J. and Guo, Y. L. (1994). Buckling behaviour of cold-formed thin-walled members by spline finite strip analysis. International Specialty Conference on Cold-formed Steel Structures: Recent Research and Cold-formed Steel Design and Construction, 229-249.

Liu, Q. Yang, J. and Li, L.Y. (2011) Pseudo-plastic moment resistance of continuous beams with cold-formed Sigma sections at internal supports: Experimental study. Engineering Structures, 33, 947-957.

Liu, Q. Yang, J. Chan, A.H.C. and Li, L.Y. (2011) Pseudo-plastic moment resistance of continuous beams with cold-formed Sigma sections at internal supports: A numerical Study. Thin-Walled Structures, 49, 1592-1604.

Loughlan, J. (1993). Thin-walled cold-formed sections subjected to compressive loading, Thin-Walled Structures, 16(1–4), 65–109.

Lucas, R. M., Al-Bermani, G. A. and Kitiporchai, S. (1997a). Modelling of cold-formed purlin-sheeting systems – Part 1: Full model, Thin-Walled Structures 27(3), 223-243.

Lucas, R. M., Al-Bermani, G. A. and Kitiporchai, S. (1997b). Modelling of cold-formed purlin-sheeting systems – Part 2: Simplified model. Thin-Walled Structures, 27(4), 263-286.

Lundquist, E. E. and Stowell, E. Z. (1943). Principles of moment distribution applied to the stability of structures composed of bars or plates. NACA, L-326.

Mahendran, M. and Avery, P. (1997). Buckling experiments on hollow flange beams with web stiffeners, Journal of Structural Engineering 123 (9), 1130-1134.

Moen, C.D. Igusa, T. and Schafer, B.W. (2008a) Prediction of residual stresses and strains in cold-formed steel members. Thin-Walled Structures, 46, 1274-1289.

Moen, C. D. and Schafer, B. W. (2008b). Experiments on cold-formed steel columns with holes, Thin-Walled Structures 46 (10), 1164-1182.

Nandini, P. and Kalyanaraman, V. (2008). Interaction of local and distortional buckling with lateral torsional buckling of cold-formed steel beams. Fifth International Conference on Coupled Instabilities in Metal Structures, Sydney, Australia, 23-25 June 2008.

Pekoz, T. and Soroushian, P. (1982) 'Behaviour of C- and Z-purlins under wind uplift', Proc. Sixth International Specialty Conference on Cold-formed Steel Structures, University of Missouri-Rolla, St. Louis, pp.409–429.

Pi, Y. L., Put, B. M. and Trahair, N. S. (1997). Lateral buckling strengths of cold-formed channel section. Research Report – University of Sydney, Department of Civil Engineering 748, 1-65.

Pi, Y. L., Put, B. M. and Trahair, N. S. (1999). Lateral buckling strengths of cold-formed Z-section beams. Thin-Walled Structures 34(1), 65-93.

Put, B. M. Pi, Y. L. and Trahair, N. S. (1999a) Lateral buckling tests on cold-formed channel beams. Journal of Structural Engineering, 125, 532-539.

Put, B. M. Pi, Y. L. and Trahair, N. S. (1999b) Lateral buckling tests on cold-formed Z-beams. Journal of Structural Engineering, 125, 1277-1283.

Ren, C., Li, L. Y. and Yang, J. (2012). Bending analysis of partially restrained channel-section purlins subjected to up-lift loadings. Journal of Constructional Steel Research 72. 254-260.

Rhodes, J. (1991). Design of cold formed steel members. Elsevier Applied Science, London.

Rhodes, J. and Lawson, R. M. (1992). Design of Structures Using Cold-formed Steel Sections. SCI Publication, 089. The Steel Construction Institute.

Roger, C. A. and Schuster, R. M. (1997). Flange/web distortional buckling of cold-formed steel sections in bending. Thin-Walled Structures 27(1), 13-29.

Rondal, J. (2000). Cold formed steel members and structures – general report. Journal of Constructional Steel Research 55, 1–3, 155–158.

Rousch, C.J. and Hancock, G. J. (1996). Purlin-sheeting connection tests. Research report R724, School of Civil and Mining Engineering, The University of Sydney, Australia.

Rousch, C. J. and Hancock, G. J. (1997). Comparison of tests of bridged and unbridged purlins with a nonlinear analysis model. Journal of Constructional Steel Research 41(2/3), 197-220.

Schafer, B. W. (1997). Cold-formed Steel Behaviour and Design: Analytical and Numerical Modelling of Elements and Members with Longitudinal Stiffeners. Ph.D. Thesis. Cornell University.

Schafer, B. W. (2001). Thin-walled column design considering local, distortional and euler buckling. Structural Stability Research Council, Annual Technical Session and Meeting.

Schafer, B. W. (2003). Elastic buckling analysis of thin-walled members using the classical finite strip method, CUFSM Version 2.6 Johbs Hopkins University.

Schafer, B. W. (2008). Review: the direct strength method of cold-formed steel member design. Journal of Constructional Steel Research 64, 7/8, 766–778.

Schafer, B. W. and Pekoz, T. (1998). Direct strength prediction of cold-formed steel members using numerical elastic buckling solutions. In Proceedings, 2nd International Conference on Thin-Walled Structures, Research and Development, Singapore, Elsevier Science Ltd., Oxford, pp.137–144.

Schardt, R. (1989). Verallgemeinerte Technische Biegetheorie, Springer Verlag, Berlin, 1989.

Schardt, R. (1994). Lateral torsional and distortional buckling of channel- and hat-sections. Journal of Constructional Steel Research, 31(2-3),243-265.

Sharp, M. L. (1966). Longitudinal stiffeners for compression members. Journal of Structural Division (ASCE), 92(ST5), 187-211.

Shearer, S.W. (1951). Cold-formed sections in structural practice with a proposed design specification. Structural Engineer 29, 165-167.

Silvestre, N. and Camotim, D. (2002a). First-order generalised beam theory for arbitrary orthotropic materials, Thin-Walled Structures 40, 755-789.

Silvestre, N. and Camotim, D. (2002b). Second-order generalised beam theory for arbitrary orthotropic materials, Thin-Walled Structures 40, 791-820.

Silvestre, N. and Camotim, D. (2002c). GBT-based distortional buckling formulae for thin-walled channel columns and beams, International Specialty Conference on Cold-Formed Steel Structures: Recent Research and Developments in Cold-Formed Steel Design and Construction, 68-83.

Silvestre, N. and Camotim, D. (2003). GBT-based approach to develop distortional buckling formulae for cold-formed steel members, Proceedings –Annual Technical Session, Structural Stability Research Council, 493-518.

Silvestre, N. and Camotim, D. (2004). Distortional buckling formulae for cold-formed steel C and Z-section members: Part I –Derivation, Thin-Walled Structures 42 (11), 1599-1629.

Silvestre, N. AND Camotim, D. (2005). Second-order analysis and design of pitched-roof steel frames. Fourth International Conference on Advances in Steel Structures, 225-232.

Silvestre, N. and Camotim, D. (2006). Vibration behaviour of axially compressed cold-formed steel members, Steel and Composite Structures 6(3), 529-540.

Sokol, L. (1996). Stability of cold formed purlins braced by steel sheeting. Thin-Walled Structures 25(4), 247-268.

Teng, J. G., Yao, J. and Zhao, Y. (2003). Distortional buckling of channel beam-columns. Thin-Walled Structures, 41(7), 595-617.

Thomasson, P. (1978). Thin-walled C-shaped panels in axial compression. Swedish Council for Building Research. D1:1978, Stockholm, Sweden.

Timoshenko, S. P. (1953). History of Strength of Materials. McGraw Hill, New York.

Timoshenko, S. P. and Gere, J. M. (1961). Theory of Elastic Stability. New York, McGraw-Hill.

Toma T. and Wittemann K. (1994). Design of cold-formed purlins and rails restrained by sheeting. Journal of Constructional Steel Research 31, 149-168.

Van der Maas, C. J. (1954). Charts for the calculation of the critical compressive stress for local instability of columns with hat sections. Journal of the Aeronautical Science, 21(6), 399-403.

Vieira, Jr. L. C. M., Malite, M., Schafer, B. W. (2010). Simplified models for cross-section stress demands on C-section purlins in uplift. Thin-Walled Structures 48, 33-41.

Von Karman, T., Sechler, E. E. and Donnell, L. H. (1932). The strength design of thin plates in compression. Transactions ASME 54, 53-55.

Walker, A. C. (1975). Design and analysis of cold-formed sections. International Textbook Company Ltd, London.

Willis, C. T. and Wallace, B. (1990). Behaviour of cold-formed steel purlins under gravity loading. Journal of Structural Engineering, 116 (8), 2061–2069.

Winter, G. (1947). Strength of thin steel compression flanges. Connell University, Engineering Experiment Station Reprint No. 32.

Winter, G. (1949). Light gage steel – a new technique in building construction. The Cornell Engineer 14, (6).

Winter, G. (1968). Thin walled structures – theoretical solutions and test results. Preliminary Publications 8th Congress IABSE, 101-112.

Yap, D. C. Y. and Hancock, G. J. (2006). Compression tests of high strength cold-formed corss-shaped steel columns, Research Report – University of Sydney, Department of Civil Engineering (869), 1-115.

Yap, D. C. Y. and Hancock, G. J. (2008). Experimental study of complex high-strength cold-formed cross-shaped steel section. Journal of Structural Engineering, 134(8), 1322-1333.

Ye, Z. M., Kettle, R. and Li, L. Y. (2004). Analysis of cold-formed zed-purlins partially restrained by steel sheeting. Computer and Structures, 82, 731-739.

Ye, Z. M., Kettle, R., Li, L. Y. and Schafer, B. (2002). Buckling behaviour of cold-formed zed-purlins partially restrained by steel sheeting, Thin-Walled Structures, 40, 853–864.

Yin, J., Zha, X. X. and Li, L. Y. (2011) Interaction between local and distortional buckling modes in cold-formed steel members subjected to pure bending. International Journal of Computer Applications in Technology (IJCAT), Vol. 42, No. 4

Young, B., Kwon, B. and Hancock, G. J. (1992). Tests of cold-formed channels with local and distortional buckling. Journal of structural engineering, Vol. 117, No. 7.

Yu, C. and Schafer, B. W. (2003). Local buckling tests on cold formed steel beams. Journal of Structural Engineering, 129, 1596-1606.

Yu, C. and Schafer, B. W. (2006). Distortional buckling tests on cold-formed steel beams. Journal of Structural Engineering, 132, 515-528.

Yu, C. and Schafer, B. W. (2007). Simulation of cold-formed steel beams in local and distortional buckling with applications to the direct strength method. Journal Constructional Steel Research 63(5), 581-590.

Yu, W. W. (2000). Cold-Formed Steel Design. John Wiley and Sons, New-York.

Zhu, J., Chen, J. K., Ren, C. and Li, L. Y. (2012). Numerical study on the moment capacity of zed-section purlin under uplift loading. Journal of Constructional Steel Research (submitted).

Zhao, C., Yang, J. and Liu, Q. (2012). 10th International Conference on Advances in Steel Concrete Composite and Hybrid Structures, Singapore.

Appendix A has been removed from the electronic version of this thesis due to copyright restrictions

Appendix B

Journal of Constructional Steel Research 70 (2012) 273–279

Contents lists available at SciVerse ScienceDirect

Journal of Constructional Steel Research

Theoretical analysis of partially restrained zed-purlin beams subjected to up-lift loads

Long-yuan Li *, Chong Ren, Jian Yang

School of Civil Engineering, University of Birmingham, Birmingham, UK

ARTICLE INFO

Article history:
Received 17 January 2011
Accepted 25 August 2011
Available online 23 September 2011

Keywords:
Cold-formed steel
Purlin
Bending
Uplift loading
Roof-purlin system

ABSTRACT

Cold-formed steel section beams are usually used as the secondary structural members in buildings to support roof and side cladding or sheeting. Thus these members are commonly treated as the restrained beams either fully or partially in its lateral and rotational directions. In this paper an analytical model is presented to describe the bending and twisting behaviour of partially restrained cold-formed steel purlins when subjected to uplift loading. Formulae used to calculate the bending stresses of the roof purlins are derived by using the classical bending theory of thin-walled beams. Detailed comparisons are made between the present model and the simplified model proposed in Eurocodes (EN1993-1-3). To validate the accuracy of the present model, finite element analysis is also conducted and the bending stress distribution along the lip, flange and web lines obtained from the finite element analysis is compared with those obtained from the present and EN1993-1-3 models.

1. Introduction

Thin-walled, cold-formed steel sections are widely used as purlins and rails, the intermediate members between the main structural frame and the corrugated roof or wall sheeting in farming and industrial buildings. Trapezoidal sheeting is usually fixed to these members in order to enclose the building. The most common sections are the zed, channel and sigma shapes, which may be plain or have lips. The lips are small additional elements provided to a section to improve its efficiency under compressive loads. The main benefits of using a cold-formed section are not only its high strength-to-weight ratio but also its lightness, which can save costs on transport, erection and the construction of foundation, and flexibility that the members can be produced in a wide variety of sectional profiles, which can result in more cost-effective designs.

The prime difference between the behaviour of cold-formed sections and hot rolled structural sections is that the cold-formed members involve thin-walled plate elements which tend to buckle locally under compression. Cold-formed cross-sections are therefore usually classified as slender sections because they cannot generally reach their full strength based on the amount of material in the cross-section due to the premature buckling failure [1,2]. The secondary difference is that the cold-formed members have low lateral bending stiffness and low torsional stiffness because of their open, thin, cross-sectional geometry, which gives great flexural rigidity about one axis at the expense of low torsional rigidity and low flexural rigidity about a perpendicular axis. This leads the cold-formed members also to be susceptible to distortional buckling [3] and lateral-torsional buckling [4].

Roof purlins and sheeting rails are usually restrained against lateral movement by their supported roof or wall cladding. Such restraints reduce the potential of lateral buckling of the whole section, but do not necessarily eradicate the problem [5]. For example, roof purlins are generally restrained against lateral displacement by the cladding, but under wind uplift, which induces compression in the unrestrained flange, lateral-torsional buckling is still a common cause of failure [6]. This occurs due to the flexibility of the restraining cladding and to the distortional flexibility of the section itself which permits lateral movement to occur in the compression flange even if the other flange is restrained.

Several researchers have investigated the behaviour of the roof purlins with partial restraints provided by their supported cladding or sheeting. For example, Ye et al. studied the influence of sheeting on the bending [7], local and distortional buckling [8] behaviour of roof purlins. Lucas et al. studied the interaction between the sheeting and purlins using finite element methods [9,10]. The lateral-torsional buckling of purlins subjected to downwards and/or upwards loads has also been discussed by several researchers [4,11–14]. Analytical models have been developed to predict the critical loads of lateral-torsional buckling and the influence of sheeting on the lateral-torsional buckling behaviour of roof purlins [13–15]. Experimental tests have also been performed on both bridged and unbridged zed- and channel-section purlins under uplift loads [16,17]. Calculation models for predicting the rotational restraint stiffness of the sheeting have also been

* Corresponding author. Tel.: +44 121 4144166; fax: +44 121 4143675.
E-mail address: long-yuan.li@plymouth.ac.uk (L. Li).

0143-974X/$ – see front matter © 2011 Elsevier Ltd. All rights reserved.
doi:10.1016/j.jcsr.2011.08.014

Appendix C

Journal of Constructional Steel Research 72 (2012) 254–260

Contents lists available at SciVerse ScienceDirect

Journal of Constructional Steel Research

Bending analysis of partially restrained channel-section purlins subjected to up-lift loadings

Chong Ren [a], Long-yuan Li [b,*], Jian Yang [a]

[a] School of Civil Engineering, University of Birmingham, Birmingham, UK
[b] School of Marine Science and Engineering, University of Plymouth, Plymouth, UK

ARTICLE INFO

Article history:
Received 14 October 2011
Accepted 3 January 2012
Available online 28 January 2012

Keywords:
Cold-formed steel
Channel
Bending
Uplift loading
Roof-purlin system

ABSTRACT

Cold-formed steel section beams are widely used as the secondary structural members in buildings to support roof and side cladding or sheeting. These members are thus commonly treated as the restrained beams either fully or partially in its lateral and rotational directions. In this paper an analytical model is presented to describe the bending and twisting behaviour of partially restrained channel-section purlins when subjected to uplift loading. Formulae used to calculate the bending stresses of the roof purlins are derived by using the classical bending theory of thin-walled beams. Detailed comparisons are made between the present model and the simplified model proposed in Eurocodes (EN1993-1-3). To validate the accuracy of the present model, both available experimental data and finite element analysis results are used, from which the bending stress distributions along the lip, flange and web lines are compared with those obtained from the present and EN1993-1-3 models.

1. Introduction

Thin-walled, cold-formed steel sections are widely used in buildings as sheeting, decking, purlins, rails, mezzanine floor beams, lattice beams, wall studs, storage racking and shelving. Among these products, purlins and rails are the most common members, widely used in buildings as the secondary members supporting the corrugated roof or wall sheeting and transmit the force to the main structural frame. Roof purlins and cladding rails have been considered to be the most popular products and account for a substantial proportion of cold-formed steel usage in buildings.

In the UK, most common sections are the zed, channel and sigma shapes, which may be plain or have stiffened lips. The lips are small additional elements at free edges in a cross section, and so added to provide the structural efficiency under compressive loads [1]. Roof purlins and sheeting rails are usually restrained against lateral movement by their supported roof or wall cladding. Such restraints reduce the potential of lateral buckling of the whole section, but do not necessarily eradicate the problem [2]. For example, roof purlins are generally restrained against lateral displacement by the cladding, but under wind uplift, which induces compression in the unrestrained flange, lateral-torsional buckling is still a common cause of failure [3]. This occurs due to the flexibility of the restraining cladding and to the distortional flexibility of the section itself, which permits lateral movement to occur in the compression flange even if the other flange is restrained.

Several researchers have investigated the behaviour of the roof purlins with partial restraints provided by their supported cladding or sheeting. For example, Lucas et al. investigated the interaction between the sheeting and purlins using finite element analysis methods [4,5]. Ye et al. presented several examples to demonstrate the influence of sheeting on the bending [6], local and distortional buckling behaviour [7] of roof purlins. Vieira et al. provided simplified models to predict the longitudinal stresses when the channel-section purlin is subjected to uplift loading [8]. The lateral-torsional buckling of purlins subjected to downwards and/or upwards loadings has also been discussed by several researchers [9–13]. Analytical models have been developed to predict the critical loads of lateral-torsional buckling and the influence of sheeting on the lateral-torsional buckling behaviour of roof purlins [12–14]. Experimental tests have also been performed on both bridged and unbridged zed- and channel-section purlins under uplift loads [15,16]. Calculation models for predicting the rotational restraint stiffness of the sheeting have been proposed recently [17,18]. Design specifications for the purlin-sheeting system have been provided in Eurocodes [3].

In this paper an analytical model is presented to describe the bending and twisting behaviour of the partially restrained channel-section purlins when subjected to uplift loading. The classical bending theory of thin-walled beams is used to calculate the bending stresses of the roof purlins. In order to validate the model, both available experimental data and finite element analysis results are used, from which the bending stress distributions along the lip, flange and

* Corresponding author. Tel.: +44 1752 586 180; fax: +44 1752 586 101.
E-mail address: long-yuan.li@plymouth.ac.uk (L. Li).

0143-974X/$ – see front matter © 2012 Elsevier Ltd. All rights reserved.
doi:10.1016/j.jcsr.2012.01.001